Aircraft Flight Mechanics Lecture Notes

ME EN 5960/6960 – Aircraft Flight Mechanics
Department of Mechanical Engineering
University of Utah

Fall 2025

Instructor: Xiaowei He*

Copyright © 2025 Xiaowei He

*Assistant Professor, Department of Mechanical Engineering, University of Utah; xiaowei.he@utah.edu.

Contents

1 Introduction and Review **1**
- 1.1 Overview . . . 1
- 1.2 Course objectives . . . 3
- 1.3 Review . . . 3
  - 1.3.1 Dynamics . . . 3
  - 1.3.2 Aircraft anatomy . . . 7
  - 1.3.3 Aerodynamics . . . 10
  - 1.3.4 Classical control systems . . . 16

2 Definitions **24**
- 2.1 Aircraft axis systems . . . 24
  - 2.1.1 Earth axes . . . 24
  - 2.1.2 Aircraft body-fixed axes . . . 25
  - 2.1.3 Quantities in different axes . . . 27
  - 2.1.4 Euler angles and aircraft attitude . . . 28
  - 2.1.5 Axis transformation . . . 29
  - 2.1.6 Angular body rates . . . 33
  - 2.1.7 Velocity in Earth and body axes . . . 34
- 2.2 Controls notation . . . 35
  - 2.2.1 Aerodynamic controls . . . 35
  - 2.2.2 Engine control . . . 36
- 2.3 Attitude indicator . . . 36

3 Aircraft Performance **39**
- 3.1 Airspeed . . . 39
- 3.2 Steady and level flight . . . 42
  - 3.2.1 Equations of motion . . . 44
  - 3.2.2 Vertical force . . . 45
  - 3.2.3 Longitudinal force . . . 45
- 3.3 Thrust and power curves . . . 46
  - 3.3.1 Thrust required . . . 46
  - 3.3.2 Minimum drag speed . . . 46
  - 3.3.3 Thrust curve . . . 46
- 3.4 Thrust-to-weight ratio and wing loading . . . 47
  - 3.4.1 Thrust-to-weight ratio . . . 47
  - 3.4.2 Wing loading . . . 48
- 3.5 Takeoff . . . 49
  - 3.5.1 Takeoff phases and ground roll distance . . . 50
  - 3.5.2 Forces during takeoff . . . 50
  - 3.5.3 Average acceleration method . . . 52
  - 3.5.4 Numerical method . . . 54
- 3.6 Landing . . . 57
  - 3.6.1 Landing phases . . . 57
  - 3.6.2 Forces and acceleration . . . 57
- 3.7 Gliding and climbs . . . 58

Copyright © 2025 Xiaowei He

3.7.1 Gliding flight . . . 58
3.7.2 Climbs . . . 59
3.8 Turns and V-n diagrams . . . 61
3.8.1 Acceleration and load factor . . . 61
3.8.2 Level turns . . . 62
3.8.3 Pull-ups . . . 65
3.8.4 Pull-downs . . . 66
3.8.5 V-n diagrams . . . 68
3.9 Energy maneuverability . . . 70
3.9.1 Energy height . . . 71
3.9.2 Weight specific excess power . . . 72
3.9.3 Energy control . . . 73
3.9.4 Minimum time-to-climb trajectory . . . 74

4 Aircraft Static Stability 76
4.1 Static stability overview . . . 76
4.1.1 Trim equilibrium . . . 76
4.1.2 Static stability . . . 76
4.2 Longitudinal static stability . . . 78
4.2.1 Conditions of stability . . . 78
4.2.2 Degree of longitudinal stability . . . 79
4.2.3 Power effects . . . 80
4.2.4 The pitch moment equation . . . 81
4.2.5 Controls-fixed stability . . . 84
4.3 Lateral-directional static stability . . . 87
4.3.1 Lateral static stability . . . 89
4.3.2 Directional static stability . . . 92

5 Aircraft Equations of Motion 94
5.1 Aircraft force equations . . . 94
5.1.1 Aircraft response of force equations . . . 94
5.1.2 Applied forces . . . 95
5.2 Aircraft moment equations . . . 96
5.2.1 Aircraft response of moment equations . . . 97
5.2.2 Applied moments . . . 99
5.3 Decoupled equations of motion . . . 99
5.3.1 Longitudinal equations of motion . . . 99
5.3.2 Lateral-directional equations of motion . . . 99
5.3.3 Kinematic equations . . . 100

6 Linearized Equations of Motion 101
6.1 Linearization theory . . . 101
6.1.1 Small perturbations . . . 101
6.1.2 Fundamentals of linearization . . . 101
6.2 Linearized aircraft equations of motion . . . 103
6.2.1 Trim state assumptions . . . 103
6.2.2 Gravitational terms . . . 104

Copyright © 2025 Xiaowei He

6.2.3 Aerodynamic terms . . . 105
6.2.4 Aerodynamic control terms . . . 106
6.2.5 Power terms . . . 107
6.2.6 Equations of motion for small perturbations . . . 107
6.3 Linearized longitudinal equations of motion . . . 108
6.4 Linearized lateral-directional equations of motion . . . 109
6.5 The dimensionless equations of motion . . . 110
6.6 Equations of motion in state space form . . . 112

7 Aircraft Dynamics 115
7.1 Cramer's rule . . . 115
7.1.1 General case . . . 115
7.1.2 Explicit formulas for small systems . . . 115
7.2 Aircraft transfer functions . . . 117
7.2.1 Aircraft input-output relations . . . 117
7.2.2 The longitudinal response transfer functions . . . 118
7.2.3 The lateral-directional response transfer functions . . . 120
7.2.4 Units of transfer functions . . . 120
7.2.5 Response to controls . . . 121
7.2.6 Acceleration response transfer functions . . . 122
7.3 The state-space method . . . 123
7.3.1 The transfer function matrix . . . 123
7.3.2 The longitudinal transfer function matrix . . . 124
7.3.3 The lateral-directional transfer function matrix . . . 124
7.4 Longitudinal dynamics . . . 125
7.4.1 Longitudinal transfer functions and response to controls . . . 125
7.4.2 Longitudinal characteristic equation . . . 128
7.4.3 The short-period oscillation mode . . . 128
7.4.4 The phugoid mode . . . 129
7.5 Lateral-directional dynamics . . . 130
7.5.1 Lateral-directional transfer functions and response to controls . . . 131
7.5.2 Lateral-directional characteristic equation . . . 135
7.5.3 The roll subsidence mode . . . 136
7.5.4 The spiral mode . . . 137
7.5.5 The Dutch roll mode . . . 138
7.6 Summary of aircraft dynamic modes . . . 141
7.7 Aerodynamic stability and control derivatives . . . 141
7.7.1 Longitudinal aerodynamic stability derivatives . . . 142
7.7.2 Lateral-directional aerodynamic stability derivatives . . . 147
7.7.3 Aerodynamic control derivatives . . . 149

8 Introduction to Aircraft Feedback Control 153
8.1 Time response . . . 153
8.1.1 Step input . . . 153
8.1.2 Poles and zeros of transfer functions . . . 153
8.1.3 Time response of first-order systems . . . 156
8.1.4 Time response of second-order systems . . . 157

Copyright © 2025 Xiaowei He

8.2 Frequency response . . . 160
8.2.1 The bode diagram . . . 161
8.2.2 Interpretation of the Bode diagram . . . 163
8.3 Closed-loop system analysis . . . 164
8.3.1 The control law . . . 165
8.3.2 Safety . . . 166
8.3.3 Augmentation system architecture . . . 166
8.3.4 Longitudinal stability augmentation . . . 169
8.3.5 Lateral-directional stability augmentation . . . 170

References **171**

Copyright © 2025 Xiaowei He

1 Introduction and Review

1.1 Overview

What is Flight Mechanics? A study of the kinematics and kinetics of flying vehicles, particularly of those that fly in the atmosphere. We are interested in the *forces* and *moments* acting on aircraft and the *motion* of the aircraft in response to the kinetics.

Flight mechanics is often called *flight dynamics* since it is concerned with the active interactions between the vehicle status and the forcing. We are mostly interested in the relatively *short-term* motion of the aircraft in response to external disturbances or controls. The external disturbances often come from the atmosphere, whereas controls are achieved through propulsion and flight control surfaces (recent developments in active flow control replace some of the control surfaces with fluidic or plasma devices in advanced flight control systems). These *inputs* influence the aircraft in terms of thrust and aerodynamic loads such as lift, drag, roll, pitch, and yaw moments. The aircraft's response includes the displacement, velocity, and acceleration changes, which are viewed as the *outputs* of the system. In this course, we treat the dynamics of the aircraft as an input-output control system, of which we use mathematical models to describe the control-response relationships between the forcing and the motion.

How does flight mechanics affect flying? The dynamic characteristics of an aircraft impact its flying qualities through the stability and control properties rooted in the aerodynamic and structural design of the aircraft.

Modern aircraft are often developed with autopilot and fly-by-wire (FBW) flight control to handle complex environmental disturbances and interactions between the airframe and control systems comprising sensors, actuators, flight computers, etc. From a control perspective, the airframe is treated as a component of the entire flight control system and can be modeled as *transfer functions* which describe the relationship between the input and output of the dynamic system of an aircraft. Therefore, we may utilize mathematical tools to analyze and modify the stability, control, and dynamic characteristics that influence the *flying and handling qualities* of the aircraft.

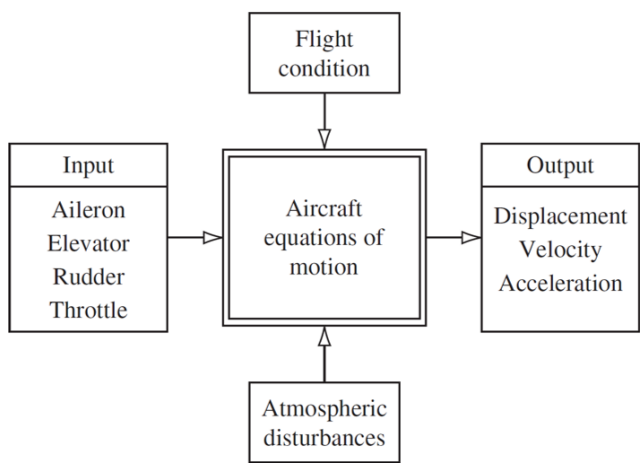

Figure 1.1: Aircraft control-response relationships [1].

The flying and handling qualities of an aircraft regard the effectiveness and efficiency of the aircraft in response to pilot commands or in compliance with the mission task requirements. The pilot commands and evaluations involve pilots' perception of the flying and handling qualities, which are often subjective or qualitative descriptions. The latter instance, in terms of mission requirements, may utilize sensors,

Copyright © 2025 Xiaowei He

FBW systems, and flight computers to provide observable quantities of the aircraft's response. In general, flying qualities refer to how well the aircraft carries out the commanded task, whereas handling qualities are considered the adequacy of the (short-term) dynamic response to controls. In other words, the flying qualities are task-related; the handling qualities are response-related, on the other hand.

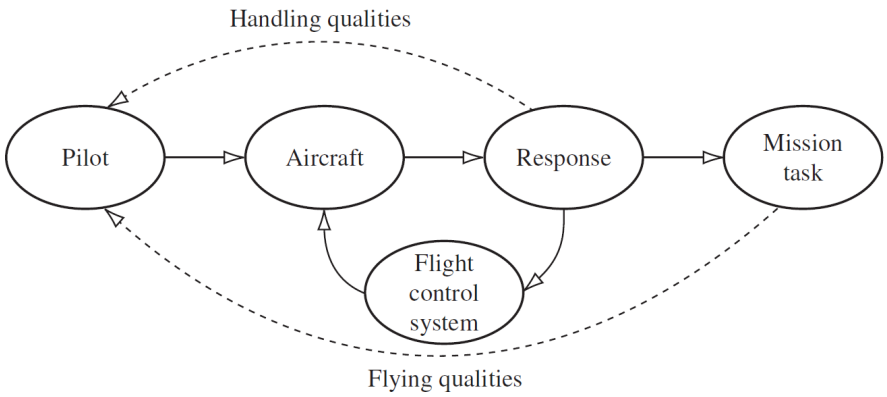

Figure 1.2: Flying and handling qualities of conventional aircraft [1].

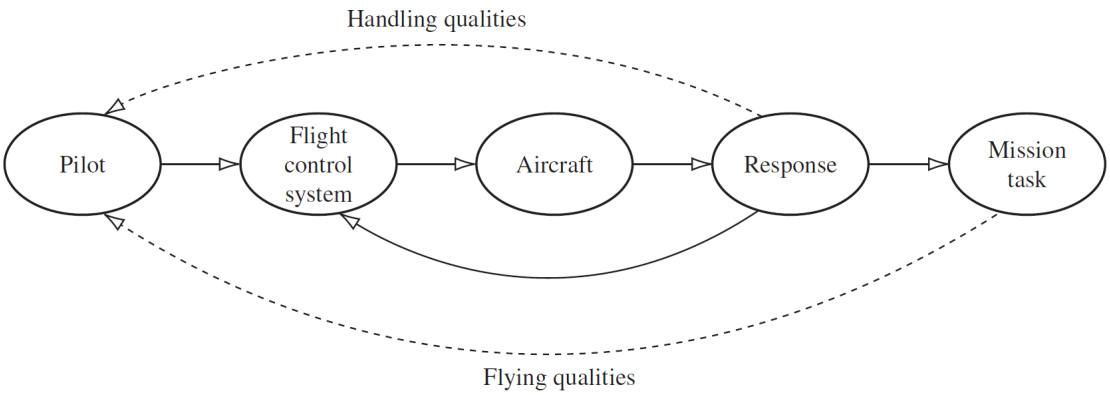

Figure 1.3: Flying and handling qualities of FBW aircraft [1].

To prevent us from being overwhelmed by and lost in mathematics and theories, it is not a bad idea to ask ourselves the following questions [1] at the beginning of the course and revisit them from time to time as reminders of building up physical interpretations and intuitive understanding of what happens during real flights.

- How are the stability and control characteristics of aircraft determined, and how do they influence flying qualities?
- What are acceptable flying qualities; how are the requirements defined, interpreted, and applied; and how do they limit flight characteristics?
- How may its dynamic characteristics be improved when an aircraft has unacceptable flying qualities?

The answers to these questions will be revealed as we establish a suitable mathematical framework, derive the equations of motion, investigate the control-response relations, and interpret the math with physical phenomena. They also require a good understanding of flying quality requirements regarding stability and control characteristics, as well as rudiments of feedback control as the means of modifying the basic airframe.

Copyright © 2025 Xiaowei He

1.2 Course objectives

In this course, we study intro to intermediate-level flight mechanics, which deals with small perturbations about steady flight (trim) conditions from a linearized point of view. With the concepts and mathematical tools taught, for a given aircraft, students can expect to

- derive equations of motion;
- evaluate general flight performance;
- analyze static and dynamic stability;
- characterize and modify the dynamic response;
- analyze and simulate flight control systems using a linear approach.

To help us achieve these outcomes, we will go through topics including

- **aircraft performance**: takeoff and landing, gliding and climbs, and turns;
- **aircraft equations of motion**: kinematics and dynamics of airplanes, and stability derivatives;
- **aircraft static stability**: longitudinal stability, directional stability, and roll stability;
- **linearized equations of motion**: small perturbations, transfer functions, and state variables;
- **aircraft dynamics**: dynamic stability, characteristic equation, longitudinal modes of motion, lateral modes of motion, and control derivatives;
- introduction to **aircraft feedback control**.

1.3 Review

Students should have a certain level of knowledge when taking this course, which includes undergraduate dynamics, basic aerodynamics and propulsion, concepts about aircraft components, fundamental ordinary differential equations, and sufficient numerical skills in MATLAB or other programming languages one may prefer (e.g., Python, C, Julia, etc.). Although we will not formally teach them in class, it should be worth the effort to briefly review some assumed knowledge that will be frequently used throughout the course at this juncture.

1.3.1 Dynamics

Dynamics includes kinematics and kinetics—motion and force. We only use rigid body dynamics where we do not consider aeroelasticity or deformation of the aircraft. Aircraft *Equations of motion* (EOM) are derived from Newton's Laws of Motion and are the basis of aircraft performance evaluation and flight control system analysis. The EOM of an aircraft concerns all 6 degrees of freedom, where the rotational degrees of freedom—longitudinal (pitch), lateral (roll), and directional (yaw)—are the critical ones that impact the stability and flying quality. The external forces and moments in the aircraft EOM are the net effects of the aerodynamic loads, propulsion, and inertia (gravity).

Rigid body kinematics. The motion of a rigid body contains *translation* and *rotation*. We first look at a pure translating case, in which any two points in the body move along parallel straight lines or congruent curves such that every line in the body, e.g., $\overline{AB}$ in figure 1.4, remains parallel to its original position. In this case, the relative positions among all points remain constant, and the velocities and accelerations of every point in the body are the same in a fixed reference frame

$$\boldsymbol{r}_A = \boldsymbol{r}_B + \boldsymbol{r}_{A/B}, \qquad \boldsymbol{v}_A = \boldsymbol{v}_B, \qquad \boldsymbol{a}_A = \boldsymbol{a}_B. \tag{1.1}$$

Copyright © 2025 Xiaowei He

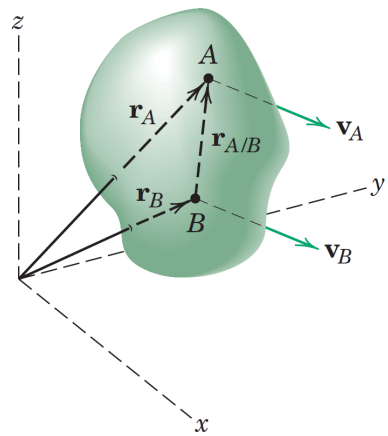

Figure 1.4: Rigid body translation [2].

The rotation of a rigid body involves the angular velocity vector $\boldsymbol{\omega}$ and the angular acceleration vector $\boldsymbol{\alpha} = \dot{\boldsymbol{\omega}}$. A fixed-axis rotation case is shown in figure 1.5. The velocity of any point moves in a circular arc in a plane normal to the axis and has a velocity

$$\boldsymbol{v} = \boldsymbol{\omega} \times \boldsymbol{r} \tag{1.2}$$

and an acceleration

$$\boldsymbol{a} = \dot{\boldsymbol{\omega}} \times \boldsymbol{r} + \boldsymbol{\omega} \times \dot{\boldsymbol{r}} = \dot{\boldsymbol{\omega}} \times \boldsymbol{r} + \boldsymbol{\omega} \times (\boldsymbol{\omega} \times \boldsymbol{r}), \tag{1.3}$$

in which $\dot{\boldsymbol{\omega}} \times \boldsymbol{r}$ is the tangential component and $\boldsymbol{\omega} \times (\boldsymbol{\omega} \times \boldsymbol{r})$ is the normal component of the acceleration.

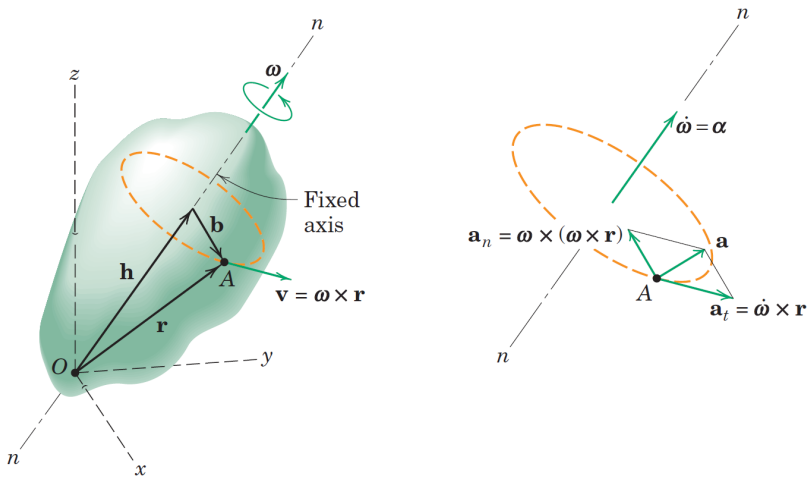

Figure 1.5: Rigid body fixed-axis rotation [2].

When a body rotates about a fixed point, the angular velocity vector no longer remains fixed in direction, and this change calls for a more general concept of rotation. In general, the order of rotation matters. As figure 1.6 shows, two sets of successive 90° rotations of the sphere about the x-axis and the y-axis in opposite orders do not produce the same final position in a fixed reference frame. Therefore,

Copyright © 2025 Xiaowei He

finite rotations do not generally obey the parallelogram law of vector addition and are not commutative. However, if the rotation is *infinitesimal*, it does obey the parallelogram law of vector addition as illustrated in figure 1.7. Either order of addition of these infinitesimal displacements produces the same resultant displacement, which is $\mathrm{d}\boldsymbol{\theta}_1 \times \boldsymbol{r} + \mathrm{d}\boldsymbol{\theta}_2 \times \boldsymbol{r} = (\mathrm{d}\boldsymbol{\theta}_1 + \mathrm{d}\boldsymbol{\theta}_2) \times \boldsymbol{r}$. Thus, the two rotations are equivalent to the single rotation $\mathrm{d}\boldsymbol{\theta} = \mathrm{d}\boldsymbol{\theta}_1 + \mathrm{d}\boldsymbol{\theta}_2$.

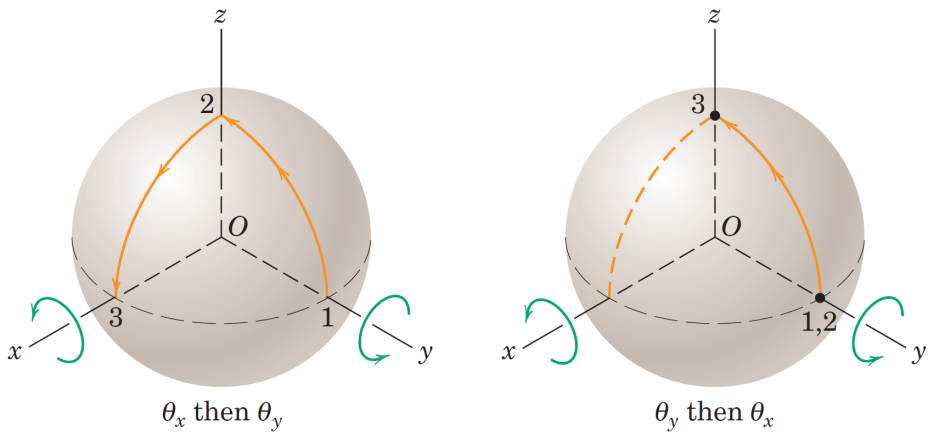

Figure 1.6: Rigid body rotation about a fixed point[2].

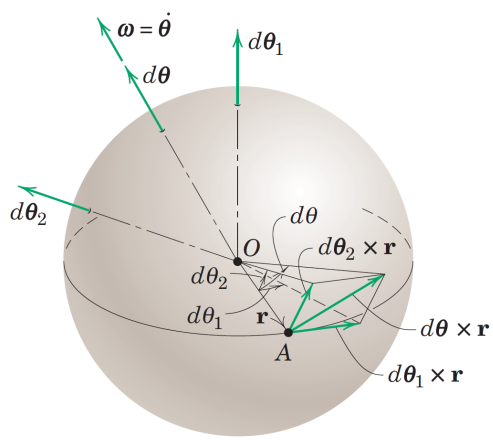

Figure 1.7: Rigid body infinitesimal rotation about a fixed point [2].

General motion. A general formulation of the motion of a rigid body in space uses the reference axes that rotate and translate. Figure 1.8 shows reference axes whose origin is attached to the reference point B rotates with an absolute angular velocity $\boldsymbol{\Omega}$ which may be different from the absolute angular velocity $\boldsymbol{\omega}$ of the body. The expressions for the velocity and acceleration of point A become

$$\boldsymbol{v}_A = \boldsymbol{v}_B + \boldsymbol{\Omega} \times \boldsymbol{r}_{A/B} + \boldsymbol{v}_{\mathrm{rel}},$$
$$\boldsymbol{a}_A = \boldsymbol{a}_B + \dot{\boldsymbol{\Omega}} \times \boldsymbol{r}_{A/B} + \boldsymbol{\Omega} \times (\boldsymbol{\Omega} \times \boldsymbol{r}_{A/B}) + 2\boldsymbol{\Omega} \times \boldsymbol{v}_{\mathrm{rel}} + \boldsymbol{a}_{\mathrm{rel}},$$

where $\boldsymbol{v}_{\mathrm{rel}} = \dot{x}\boldsymbol{i} + \dot{y}\boldsymbol{j} + \dot{z}\boldsymbol{k}$ and $\boldsymbol{a}_{\mathrm{rel}} = \ddot{x}\boldsymbol{i} + \ddot{y}\boldsymbol{j} + \ddot{z}\boldsymbol{k}$ are the velocity and acceleration of point A measured relative to x-y-z by an observer attached to x-y-z, respectively. Note that $\boldsymbol{\Omega}$ is the angular velocity of the axes and may be different from the angular velocity $\boldsymbol{\omega}$ of the body. Also note that $\boldsymbol{r}_{A/B}$ remains

Copyright © 2025 Xiaowei He

constant in magnitude for points A and B fixed to a rigid body, but it will change direction with respect to x-y-z when the angular velocity $\boldsymbol{\Omega}$ of the axes is different from the angular velocity $\boldsymbol{\omega}$ of the body.

Similar to equation (1.3), $\dot{\boldsymbol{\Omega}} \times \boldsymbol{r}_{A/B}$ and $\boldsymbol{\Omega} \times (\boldsymbol{\Omega} \times \boldsymbol{r}_{A/B})$ are the tangential and normal components of the angular acceleration, respectively, but of the reference frame x-y-z relative to the X-Y-Z frame. The additional term $\boldsymbol{a}_{\text{rel}}$ is the acceleration measured relative to the moving reference frame x-y-z. $2\boldsymbol{\Omega} \times \boldsymbol{v}_{\text{rel}}$ is the *Coriolis acceleration* representing the difference between the acceleration of A as measured from nonrotating axes and from rotating axes (in order to write Newton's law in an *inertial frame*). Its direction is always normal to the vector $\boldsymbol{v}_{\text{rel}}$ and $\boldsymbol{\Omega}$, established by the right-hand rule for the cross product.

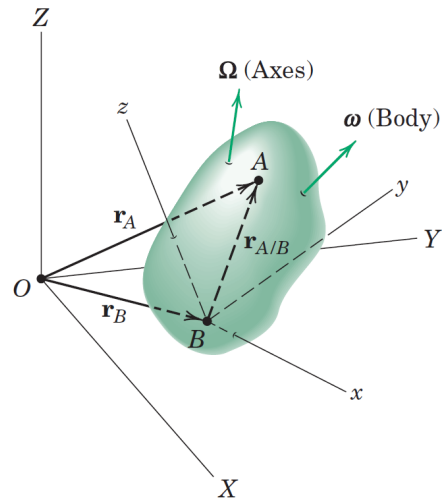

Figure 1.8: Rigid body general motion [2].

Kinetics and equations of motion. Kinetics is the forcing condition of the system of interest. We use free-body diagrams to analyze the external forces acting on the body and replace them with the resultant force acting through the center of mass, thus obtaining the kinetics of the force-coupled system as shown in figure 1.9.

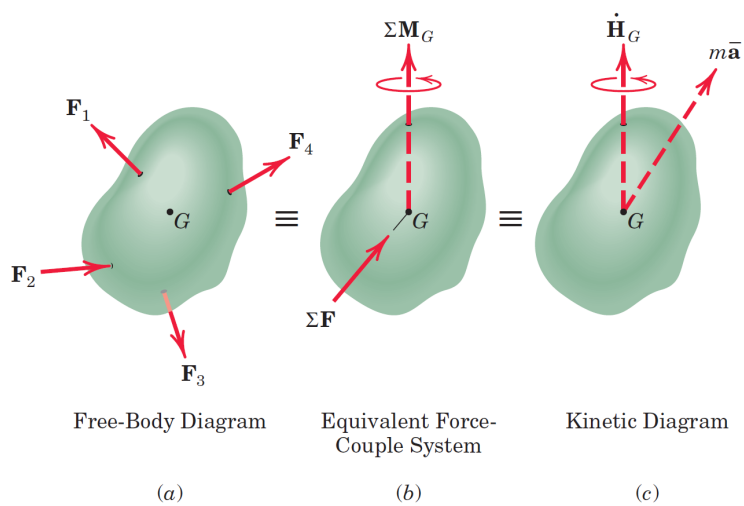

Figure 1.9: Free-body diagram and kinetic diagram [2].

Copyright © 2025 Xiaowei He

The equations of motion are the mathematical models that describe the dynamics of the system by connecting motion and forcing through Newton's Second Law. We have the force and moment equations in general

$$\begin{aligned} \Sigma \boldsymbol{F} &= m\boldsymbol{a}, \\ \Sigma \boldsymbol{M}_G &= \dot{\boldsymbol{H}}_G = \boldsymbol{I}\boldsymbol{\alpha} = \boldsymbol{I}\dot{\boldsymbol{\omega}}, \end{aligned} \tag{1.4}$$

in which $\boldsymbol{H}_G$ is the angular momentum which is determined by the angular acceleration and the moment of inertia $\boldsymbol{I}$. Just as the mass m of a body is a measure of the resistance to translational acceleration, the moment of inertia $\boldsymbol{I}$ is a measure of resistance to rotational acceleration of the body.

1.3.2 Aircraft anatomy

Aircraft components. The major components of a fixed-wing airplane are shown in figure 1.10. The basic components are cockpit, fuselage, wings, engine, stabilizers, landing gears, and control surfaces.

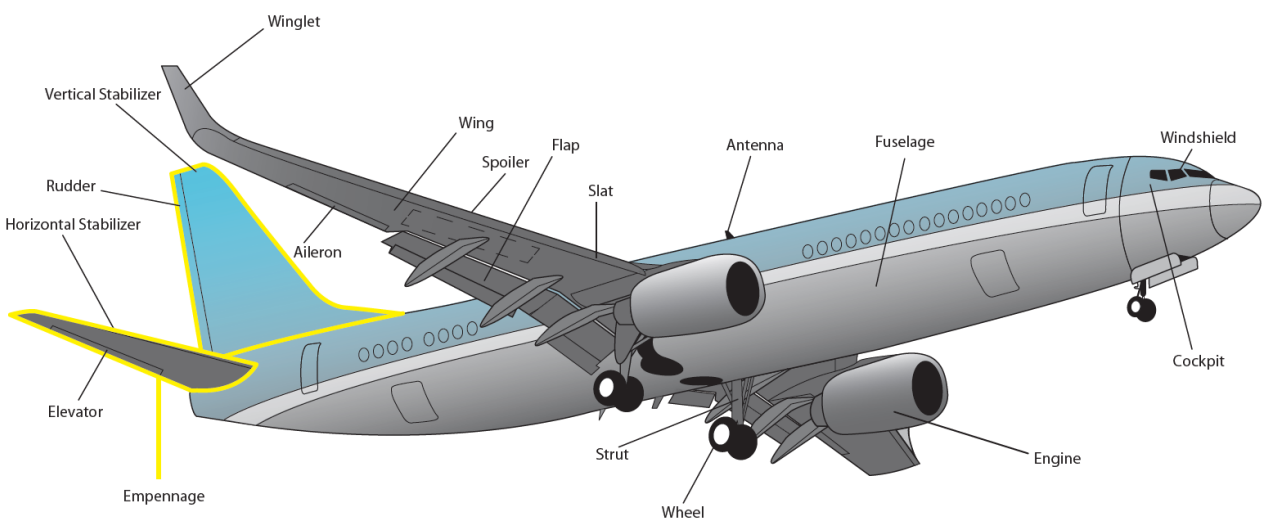

Figure 1.10: Major components of aircraft.

Control surfaces. Flight is controlled through the movement of control surfaces of the aircraft, and by adjusting the propulsion. The conventional control surfaces are the movable parts attached to the wings and stabilizers, including ailerons, elevators, and rudder, shown in red in figure 1.11. During takeoff and landing, aircraft usually use high-lift devices such as flaps and slats, as well as spoilers for different flow control purposes.

The functions of the control surfaces are mostly tied into the directional control of flight.

- **Ailerons**—are outboard on each wing, and operate in differential mode, meaning if one goes up, the other goes down. These are controlled via a sideways stick/yoke movement. This increases lift on one wing, and decreases it on the other, affecting a roll rate p which changes the roll angle ϕ.
- **Elevators**—usually situated on the horizontal stabilizer, and move in parallel mode for most cases, which increases/decreases the tail lift, and changes the aircraft pitch rate q and pitch angle θ. This is controlled by moving the stick/yoke forward/aft.
- **Rudder**—is on the vertical tail and is a single control surface. If the rudder moves to the port (left), it creates a sideways aerodynamic force on the tail towards the starboard (right), which moves the

Copyright © 2025 Xiaowei He

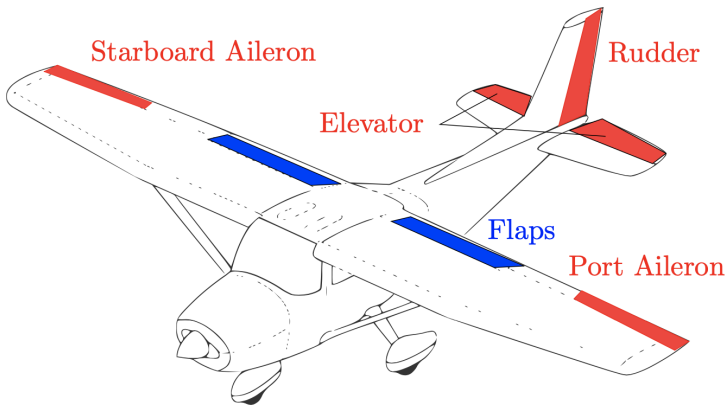

Figure 1.11: Control surfaces of aircraft [3].

aircraft's nose to a yaw angle ψ at a yaw rate r. This is controlled using pedals in the cockpit.

Wing geometry. Wing parameters are usually defined in terms of the gross wing as shown in figure 1.12a. As a measure of how far back the tip is compared to the root, *wing sweep* is measured by the sweep of the quarter-chord line. The *chord* is the length of the wing in the direction of travel (hence vertical in the image). The *root chord* is usually defined on the aircraft centerline, and not at the actual aircraft root.

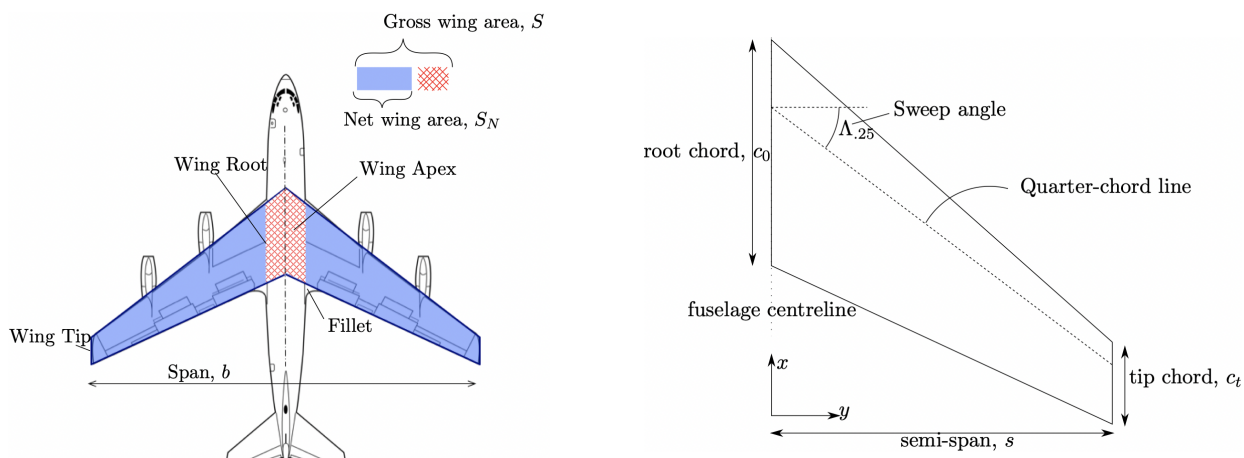

(a) Aircraft wing areas

(b) Aircraft trapezoidal wing

Figure 1.12: Aircraft wing geometry [3].

The main dimensional reference parameters of aircraft geometry are

- **Wing area**—also called the *planform area*. As mentioned above, it is the gross plan area of the wing, including the part within the fuselage. Defined as

$$S = b\bar{c} = b\frac{c_\mathrm{r} + c_\mathrm{t}}{2}, \tag{1.5}$$

  where b is the wing span, and $\bar{c}$ is the standard mean chord of the wing.

- **Standard mean chord**—is effectively the same as the geometric mean chord. For a wing of

Copyright © 2025 Xiaowei He

symmetric planform

$$\bar{c} = \frac{\int_{-s}^{s} c_y \mathrm{d}y}{\int_{-s}^{s} \mathrm{d}y} = \frac{c_\mathrm{r} + c_\mathrm{t}}{2}, \tag{1.6}$$

where $s = b/2$ is the semi-span and c_y is the local chord at spanwise coordinate y.

- **Aspect ratio**—is a measure of the spanwise slenderness of the wing, and is defined as

$$AR = \frac{b^2}{S} = \frac{b}{\bar{c}}. \tag{1.7}$$

- **Taper ratio**—the ratio of the tip and root chord lengths. It can also refer to a decrease in wing thickness from the root to the tip, as the thickness is usually proportional to the chord length.

$$\lambda = \frac{c_\mathrm{t}}{c_\mathrm{r}}. \tag{1.8}$$

- **Mean aerodynamic chord**—can be interpreted as the representative chord length for the forces and moments acting on a wing, and is defined as

$$mac = \bar{\bar{c}} = \frac{\int_{-s}^{s} c_y^2 \mathrm{d}y}{\int_{-s}^{s} c_y \mathrm{d}y}. \tag{1.9}$$

The reference *mac* is located on the centerline of the aircraft by projecting $\bar{\bar{c}}$ from its spanwise location as shown in figure 1.13. The *mac* represents the location of the root chord of a rectangular wing that has the same aerodynamic influence on the aircraft as the actual wing. Traditionally, the *mac* is used in stability and control studies since a number of important aerodynamic reference centers are located on it.

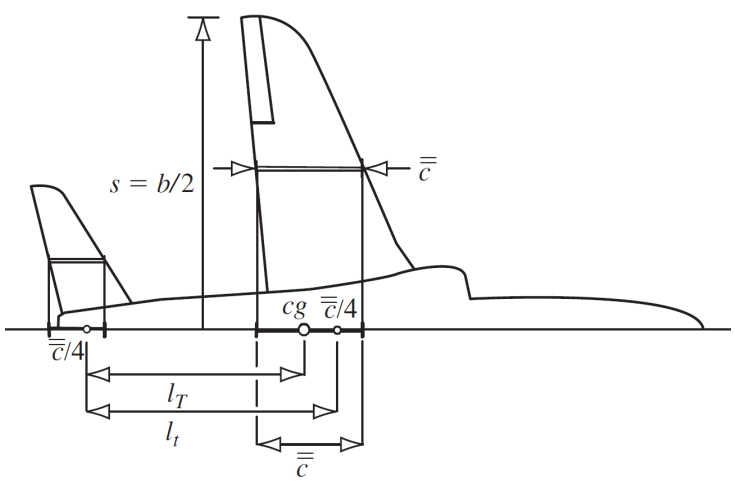

Figure 1.13: Longitudinal reference geometry [1].

- **Center of gravity**—denoted by *cg*, is usually located on the reference chord as indicated in figure 1.13. Its position is quoted as a fraction of $\bar{\bar{c}}$, and is measured from the leading edge of the reference chord as shown. The cg position varies as a function of aircraft loading; the typical variation is in the range of 10% to 40% of $\bar{\bar{c}}$.

Copyright © 2025 Xiaowei He

1.3.3 Aerodynamics

Airfoils. An airfoil is an infinitesimal cross-section of a wing, which can be represented in two dimensions. One of the simplest airfoils is a symmetric NACA 4-digit airfoil. This series of airfoils is denoted in the format "NACA $00XX$", where the first two zeros indicate that the airfoil has no chamber, and the last two digits indicate the airfoil thickness as a percentage of its chord length. For example, a NACA 0012 airfoil is symmetric about its chord with a maximum thickness of $12\%c$ at 30% of the chord from the leading edge (by default of the symmetrical 4-digit series airfoils) as shown in figure 1.14a. The thickness distribution with respect to the chordwise coordinates of a symmetric NACA 4-digit airfoil is defined by a 4th-order polynomial

$$y_t = 5t(0.2969x^{1/2} - 0.1260x - 03516x^2 + 0.2843x^3 - 0.1015x^4), \tag{1.10}$$

in which x is the chordwise coordinate between 0 to 1, y_t is the half thickness at a given value of x (centerline to surface), and t is the maximum thickness as a fraction of the chord ($t = XX/100$).

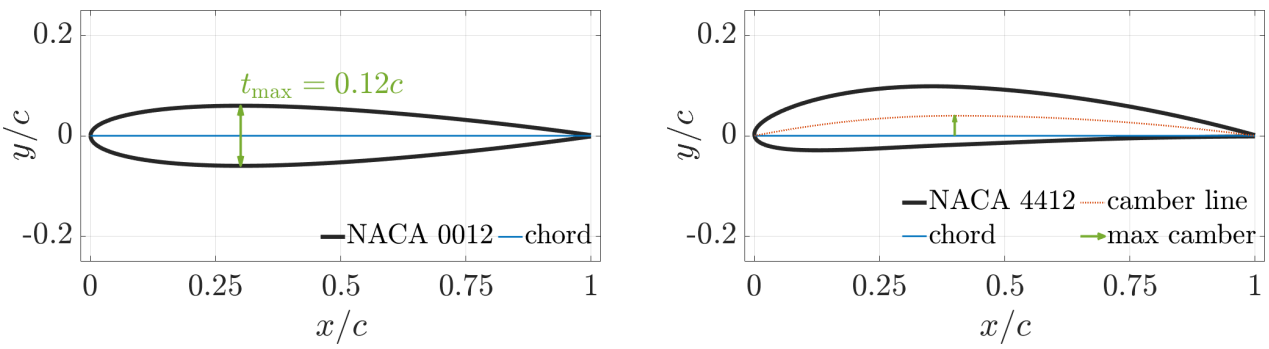

(a) NACA 0012 airfoil (b) NACA 4412 airfoil

Figure 1.14: NACA 4-digit airfoils.

For a cambered airfoil, the NACA number format becomes "NACA $MPXX$", where M is the maximum camber as a percentage of the chord and P is the position of the maximum camber from the leading edge in the chordwise direction in tenths of the chord length. A NACA 4412 airfoil based on a NACA 0012 thickness is shown in figure 1.14b, of which the maximum camber is $40\%c$ and is located at $0.4c$ from the leading edge. A cambered airfoil produces more lift than a symmetric one for the same angle of attack (before stall). The camber line is defined as the locus of points midway between the upper and lower surface, i.e., the midpoint between the upper and lower surface at all chordwise coordinates. The formula used to calculate the y-coordinates of the mean camber line is

$$y_c = \begin{cases} \dfrac{M}{P^2}(2Px - x^2), & 0 \leqslant x \leqslant P, \\ \dfrac{M}{(1-P)^2}(1 - 2P + 2Px - x^2), & P \leqslant x \leqslant 1. \end{cases} \tag{1.11}$$

because the thickness needs to be applied perpendicular to the camber line, the upper surface coordinates (x_u, y_u) and lower surface (x_l, y_l), become

$$\begin{aligned} x_\mathrm{u} &= x - y_t \sin\theta, \quad & y_\mathrm{u} &= y_c + y_t \cos\theta, \\ x_\mathrm{l} &= x + y_t \sin\theta, \quad & y_\mathrm{l} &= y_c - y_t \cos\theta, \end{aligned} \tag{1.12}$$

Copyright © 2025 Xiaowei He

where $\theta = \arctan \dfrac{\mathrm{d}y_c}{\mathrm{d}x}$, and $\dfrac{\mathrm{d}y_c}{\mathrm{d}x}$ is the gradient of the camber line.

Forces in equilibrium. Lift, drag, thrust, and weight are the four primary forces acting on an aircraft in flight. Figure 1.15 shows these forces on an aircraft in *equilibrium*, which is the simplest regime of flight—steady and level flight. Steady means not accelerating, and level means that there is no variation in altitude. This does not mean that the wings are level; the aircraft may still be turning in a steady turn.

Lift and drag are *aerodynamic* forces arising because of the relative motion between the aircraft and the surrounding air. Thrust is the *propulsive* force provided by the propulsive system, and the force due to *gravity* (inertial force) is called weight. Ultimately, we want to adequately predict an aircraft's motion. An understanding of lift, drag, and thrust is essential to this end.

- Lift $\boldsymbol{L}$: the aerodynamic force normal to the incident flow velocity, acting in a "lifting" sense.
- Drag $\boldsymbol{D}$: the aerodynamic force parallel to the incident flow velocity, opposing motion.
- Thrust $\boldsymbol{T}$: the propulsive force parallel to the aircraft longitudinal axis, providing motion.
- Weight $\boldsymbol{W}$: the inertial force acting downward along the direction of the gravitational acceleration; $\boldsymbol{W} = m\boldsymbol{g}$.

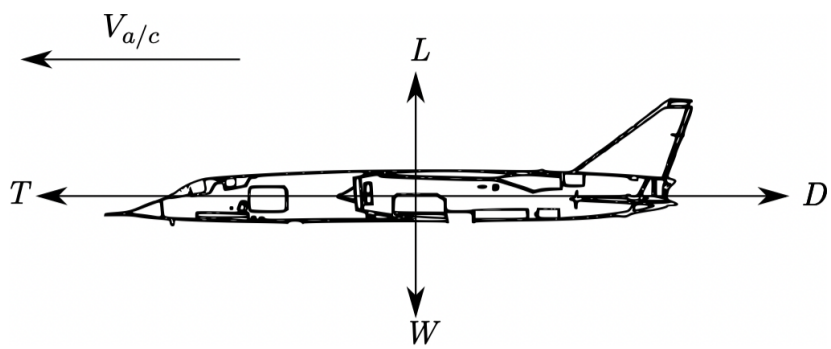

Figure 1.15: Four major forces acting on an aircraft [3].

Lift. Fundamentally, an airfoil provides a *pressure difference* by accelerating the flow over the upper surface and retarding the flow over the lower surface. Note that the misinterpretation of Bernoulli's equation where the air flows on the upper and lower surfaces have to "catch up" at the trailing edge, seen from many explanations, is *incorrect*. The exact physics of lift generation is not fully revealed, even in modern aerodynamics. Some classical lift theories suggest that the airfoil tends to "circulate" the air that provides lift. Hence, a symmetric airfoil at an angle of attack produces lift, and a cambered airfoil produces some lift at zero angle of attack. The flow is indeed accelerated over the upper surface and retarded over the lower surface, however, the contribution from the pressure difference described in Bernoulli's equation is far from generating enough lift. The surface pressure distribution, when integrated, gives rise to lift (and some drag). The lift coefficient is linearly proportional to the angle of attack before stall.

One important parameter that determines lift is the angle of attack α. We define the angle of attack as the angle between the incident velocity $\boldsymbol{V}_\infty$ chord line of the airfoil, as figure 1.16 shows. The net effect of the pressure and shear stress distributions integrated over the complete body surface is a resultant aerodynamic force $\boldsymbol{R}$ and moment $\boldsymbol{M}$ on the body. The resultant $\boldsymbol{R}$ can be split into two sets of components: lift $\boldsymbol{L}$ and drag $\boldsymbol{D}$ (relative to the freestream velocity $\boldsymbol{V}_\infty$), normal $\boldsymbol{N}$ and axial $\boldsymbol{A}$ forces (relative to the chord c). Note that the geometric relation is always about the *freestream* velocity when

Copyright © 2025 Xiaowei He

we talk about lift and drag. Hence, by definition, the two sets of force components are connected by

$$\begin{aligned} L &= N\cos\alpha - A\sin\alpha, \\ D &= N\sin\alpha + A\cos\alpha. \end{aligned} \tag{1.13}$$

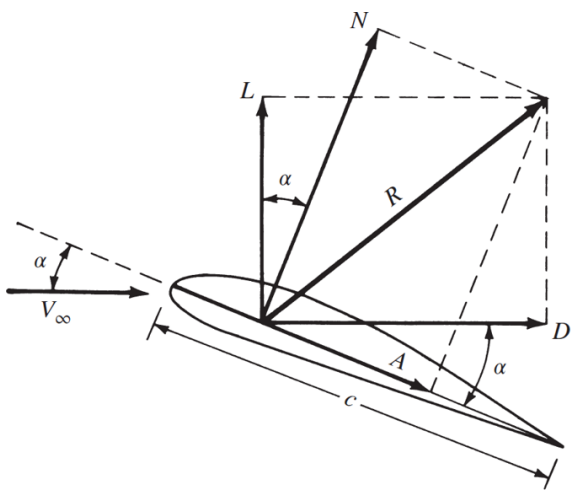

Figure 1.16: Angle of attack, resultant aerodynamic force, and the force components [4].

If plotted against the angle of attack, the lift coefficients of the airfoils look like figure 1.17. Observing the lift coefficient curve of a symmetric airfoil in figure 1.17a, the curve intersects the coordinates at $C_{L_0} = 0$ (where C_{L_0} is called zero angle of attack lift) because of flow symmetry. The lower angle of attack regime of the curve is linear, and it has the slope of $a = \dfrac{\mathrm{d}C_L}{\mathrm{d}\alpha} = 2\pi$. Beyond a certain angle of attack, the curve stops being linear as it approaches its maximum; this marks the onset of nonlinearity. At angles of attack beyond α_{stall}, the flow over the airfoil is separated, and the airfoil is fully stalled.

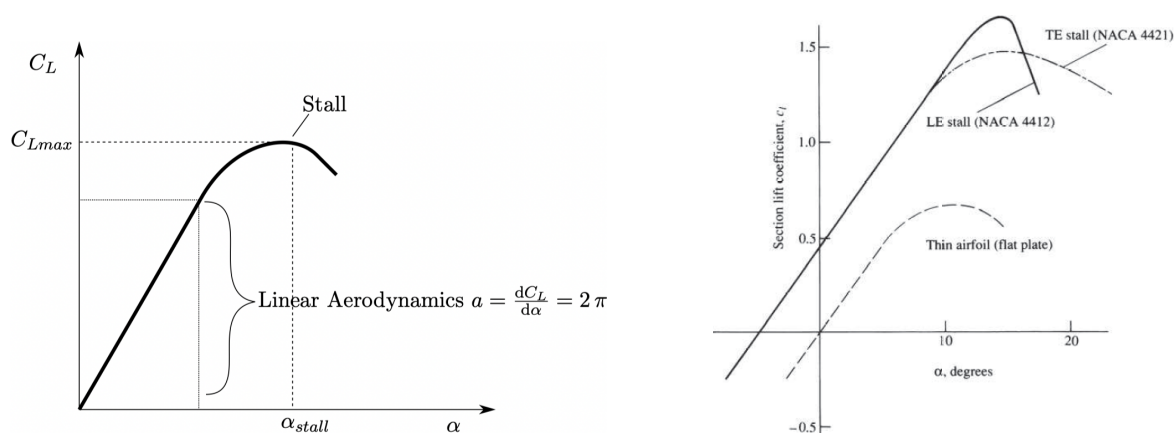

(a) Symmetric airfoil [3] (b) Cambered airfoil [4]

Figure 1.17: Lift coefficient curves.

When camber is introduced to the airfoil, the $C_L - \alpha$ curve is shifted to the left, and the airfoil produces nonzero C_{L_0} at $\alpha = 0°$, as shown in figure 1.17b. The two cambered airfoils, NACA 4412 and

Copyright © 2025 Xiaowei He

NACA 4421, have the same shape of the camber line but different thicknesses. From the thin airfoil theory, the linear lift slope and the zero-lift angle of attack should be the same for both airfoils. The major effect of the thickness of the airfoil is its effect on the value of the maximum lift and stall behaviors.

Source of aerodynamic loads. The aerodynamic forces and moments on the body are due to only two basic sources [4]:

- *Pressure* distribution over the body surface.
- *Shear stress* distribution over the body surface.

Both pressure p and shear stress τ have dimensions of force per unit area. As sketched in figure 1.18, p acts normal to the surface, and τ acts tangential to the surface. Shear stress is due to the "tugging action" on the surface, which is caused by friction between the body and the air.

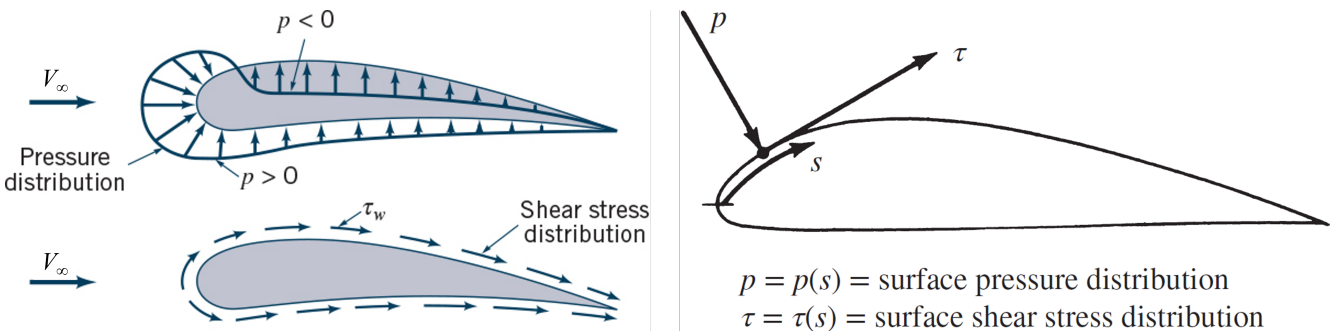

Figure 1.18: Pressure and shear stress distributions over an airfoil [4, 5].

The net effect of the p and τ distributions integrated over the complete body surface is a resultant aerodynamic force, R, and moment M, on the body, as sketched in figure 1.19.

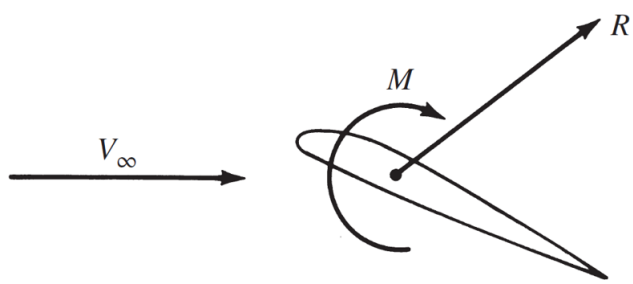

Figure 1.19: Resultant aerodynamic force and moment on the body [4].

Drag. As a component of aerodynamic force that opposes aircraft motion, there are two main sources of drag: *skin friction drag* and *pressure drag*.

Skin friction drag is a direct result of viscosity, which relates to the concept of a boundary layer (figure 1.20). Fundamentally, the fluid velocity closest to the surface is considered zero, and it increases with the distance from the surface until it reaches the freestream velocity. For the flow to be retarded, work needs to be done on it, and this is transferred through shear forces in the fluid and frictional forces between the fluid and the solid body. This force is applied to the body in the same direction as fluid motion and is called skin friction drag. Note that for more complex geometries such as airfoils, the local surface direction may not be the same as the freestream direction, so the component of the force parallel to the inclement freestream must be calculated. For a given Reynolds number, regardless of the

Copyright © 2025 Xiaowei He

aerodynamic shape, a laminar boundary layer will cause less skin friction drag than a turbulent boundary layer.

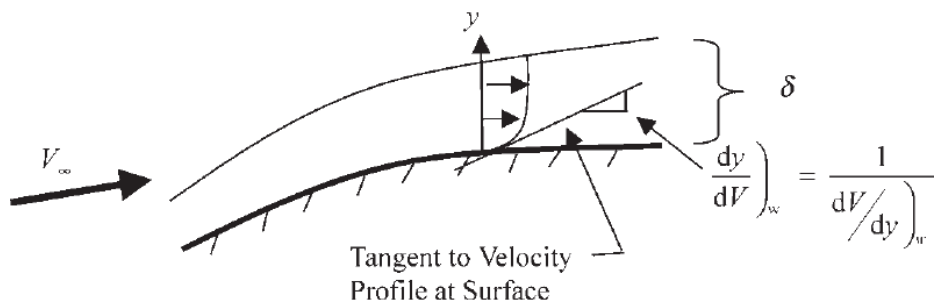

Figure 1.20: Boundary layer velocity profile [6].

Similar to that lift is caused by a pressure difference on an airfoil being resolved into the direction normal to the freestream velocity. If the pressure force is resolved in a direction parallel to the freestream, we arrive at pressure drag. It can be further subdivided into:

- **Form drag**—associated with the growth of a boundary layer. The boundary layer and a trailed wake will change the effective size of a body that a fluid must move around. Hence, a large boundary layer will cause more drag. In an ideal cylinder in 2-D flow, for example, the drag is zero (no wake, no pressure drag, and no friction). As we introduce viscosity, we also introduce the Reynolds number of the flow, which changes the attachment and separation points, resulting in form drag. Physically, the same thing happens for an airfoil. On an airfoil shown in figure 1.21, the pressure is highest at the stagnation point. Over the upper surface, the velocity increases to a maximum, and a minimum pressure is reached. Aft of this point, the pressure increases. When pressure increases in the streamwise direction, the pressure gradient is referred to as adverse. In contrast, if the pressure gradient decreases in the streamwise direction, the gradient is favorable. When the flow field has insufficient momentum (or energy) to overcome the adverse pressure gradient, it separates from the upper surface, and the airfoil stalls; as a result, drag increases and lift decreases.
- **Induced drag**—a 3-D effect associated with a trailing vortex system. A wing that produces lift will produce a tip vortex, causing the air to rotate behind the aircraft. The energy associated with imparting this rotational motion to the air is induced drag. In other words, induced drag is the penalty paid for generating lift on a finite wing.
- **Wave drag**—associated with shocks in transonic and supersonic flights. We will not cover it in this course.

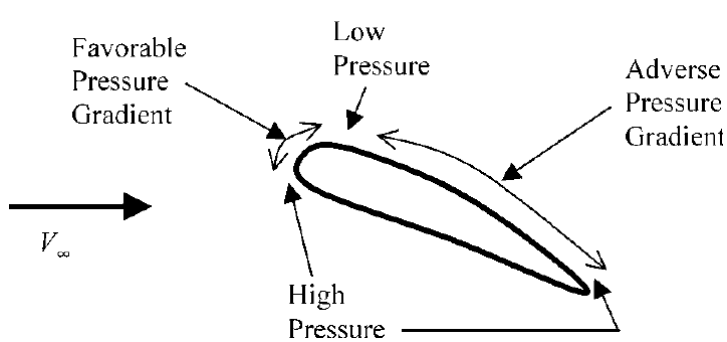

Figure 1.21: Pressure regions on an airfoil [6].

Copyright © 2025 Xiaowei He

Of the components of drag above, both skin friction and pressure drag are due to viscosity, and hence cannot be modeled in the potential flow theory. These two together are called *profile drag*, which is the combined drag due to *viscous effects*.

Aerodynamic coefficients. The *dimensional* lift and drag are denoted by L and D, respectively. In general, it is useful to remove units from expressions in engineering, for example, to work between unit systems (i.e., between metric and imperial unit systems) without conversion, to compare aircraft of differing sizes in terms of performance, and to perform scale model work of aircraft and extend the results to full-size.

Using dimensional analysis (Buckingham Π theorem), the aerodynamic load can be nondimensionalized and described as a function of some dimensionless parameters. For instance, lift, L, depends on flight conditions, air properties, and the airframe (geometry) such that

$$L = f(V_\infty, \alpha, a_\infty, \rho_\infty, \mu_\infty, c, b), \tag{1.14}$$

where v_∞ is the freestream speed, α is the angle of attack, a_∞ is the speed of sound of the freestream, ρ_∞ is the freestream air density, μ_∞ is the freestream viscosity, c is the chord, and b is the span. After applying Buckingham Π theorem, equation (1.14) can be expressed in the dimensionless form

$$\begin{aligned} \frac{L}{\frac{1}{2}\rho_\infty V_\infty^2 S} &= \phi\left(\frac{\rho_\infty V_\infty c}{\mu_\infty}, \frac{V_\infty}{a_\infty}, \alpha\right) \\ C_L &= \phi(Re, Ma, \alpha), \end{aligned} \tag{1.15}$$

where $S = bc$ is the platform area. We use C_L to denote the dimensionless lift which is the *lift coefficient*. Equation (1.15) indicates that the lift coefficient is determined by the Reynolds number, Re, Mach number, Ma, and the angle of attack. In most cases, the Reynolds number and Mach number are relatively constant while the airframe is also fixed. Therefore, the lift coefficient is determined by the angle of attack in the specific flow condition (e.g., the C_L curves shown in figure 1.17), which is the assumption that we will use throughout the course.

Conventionally, the aerodynamic forces and moments are nondimensionalized (or normalized) by the dynamic pressure of the freestream q_∞ and the planform area S due to the proportional relationships between the forces and these parameters. The freestream dynamic pressure

$$q_\infty = \frac{1}{2}\rho V_\infty^2 \tag{1.16}$$

is usually measured by Pitot tubes on the aircraft. Therefore, we have the *aerodynamic coefficients* regarding the forces and moments on aircraft as follows

- lift coefficient:

$$C_L = \frac{L}{q_\infty S}; \tag{1.17}$$

- drag coefficient:

$$C_D = \frac{D}{q_\infty S}; \tag{1.18}$$

- roll moment coefficient:

$$C_l = \frac{M_L}{q_\infty S b}; \tag{1.19}$$

Copyright © 2025 Xiaowei He

- pitch moment coefficient:

$$C_m = \frac{M_M}{q_\infty S\bar{\bar{c}}}; \tag{1.20}$$

- yaw moment coefficient:

$$C_n = \frac{M_N}{q_\infty Sb}. \tag{1.21}$$

Note that the characteristic length used to normalize the longitudinal moment (pitch moment) is the mean aerodynamic chord $\bar{\bar{c}}$, whereas the wing span b is used for the lateral moment (roll moment) and directional moment (yaw moment).

1.3.4 Classical control systems

We will discuss the stability and control of aircraft based on a *linear* system approach. Specifically, this course only involves linear time-invariant (LTI) systems which have two basic attributes [7]:

(1) A linear system response obeys the principle of superposition.

(2) The response of an LTI system can be expressed as the convolution of the input with the unit impulse response of the system.

The second property suggests that the response of an LTI system to an exponential input is also exponential. This result is the principal reason for the usefulness of the Fourier and Laplace transforms in the study of LTI systems.

Laplace transforms. Laplace transform is an integral transform that converts a function of a real variable (usually in the time domain) to a function of a complex variable (in the complex-valued frequency domain, also known as s-domain). In general, the transform converts differentiation and integration in the time domain into much easier multiplication and division in the Laplace domain. It simplifies linear ordinary differential equations and integral equations into algebraic polynomial equations. After solving the ODE in the Laplace domain, the inverse Laplace transform reverts to the original domain. Laplace transforms can be used to study the complete response characteristics of feedback systems, including the transient response.

For a suitable function in the time domain $f(t)$, we use $F(s) = \mathcal{L}\{f(t)\}$ to denote its Laplace transform, which is defined as

$$F(s) = \mathcal{L}\{f(t)\} = \int_0^\infty f(t)e^{-st}\mathrm{d}t, \tag{1.22}$$

where $s = \sigma + i\omega$ is a complex variable in the frequency complex domain, with real numbers σ and ω. The Laplace transforms of some commonly used time functions in this course are listed in table 1.1.

Table 1.1: Commonly used Laplace transforms.

Function	Time domain $f(t)$, $t \geqslant 0$	Laplace domain $F(s)$
unit impulse	$\delta(t)$	1
unit step	$u(t)$ or $1(t)$	$\frac{1}{s}$
ramp	t	$\frac{1}{s^2}$
quadratic	t^2	$\frac{2}{s^3}$

Copyright © 2025 Xiaowei He

Table 1.1: Commonly used Laplace transforms.

Function	Time domain $f(t)$, $t \geqslant 0$	Laplace domain $F(s)$
nth-power (integer n)	t^n	$\dfrac{n!}{s^{n+1}}$
exponential decay	e^{-at}	$\dfrac{1}{s+a}$
exponential approach	$1-e^{-at}$	$\dfrac{a}{s(s+a)}$
sine	$\sin \omega t$	$\dfrac{\omega}{s^2+\omega^2}$
cosine	$\cos \omega t$	$\dfrac{s}{s^2+\omega^2}$
sine with phase delay	$\sin(\omega t+\phi)$	$\dfrac{s\sin\phi+\omega\cos\phi}{s^2+\omega^2}$
exponentially decaying sine wave	$e^{-at}\sin \omega t$	$\dfrac{\omega}{(s+a)^2+\omega^2}$
exponentially decaying cosine wave	$e^{-at}\cos \omega t$	$\dfrac{s+a}{(s+a)^2+\omega^2}$
–	$\dfrac{t^{n-1}}{(n-1)!}$	$\dfrac{1}{s^n}$

Example 1.1

Find the Laplace transform of a function

$$f(t) = t^2 - e^{-2t}\sin 3t.$$

Solution: Using the table, we find that the Laplace transform is

$$F(s) = \frac{2}{s^3} + \frac{3}{(s+2)^2+9}.$$

One of the more important properties of the Laplace transform is that it is linear

$$\mathcal{L}\{af_1(t) + bf_2(t)\} = aF_1(s) + bF_2(s), \tag{1.23}$$

and scaling property is a special case of linearity

$$\mathcal{L}\{af(t)\} = aF(s). \tag{1.24}$$

The frequently used properties of the Laplace transform are listed in table 1.2.

Table 1.2: Commonly used properties of Laplace transform.

Property	Time domain $f(t)$, $t \geqslant 0$	Laplace domain $F(s)$
linearity (superposition)	$af_1(t) + bf_2(t)$	$aF_1(s) + bF_2(s)$

Copyright © 2025 Xiaowei He

Table 1.2: Commonly used properties of Laplace transform.

Property	Time domain $f(t)$, $t \geqslant 0$	Laplace domain $F(s)$
time shifting	$f(t-\tau)$, $\tau \geqslant 0$	$F(s)e^{-\tau s}$
time scaling	$f(at)$	$\frac{1}{a}F(\frac{s}{a})$
frequency shifting	$e^{-at}f(t)$	$F(s+a)$
derivative	$f'(t)$	$sF(s) - f(0^-)$
second derivative	$f''(t)$	$s^2F(s) - sf(0^-) - f'(0^-)$
general derivative	$f^{(n)}(t)$	$s^nF(s) - \sum_{k=1}^{n} s^{n-k}f^{(k-1)}(0^-)$
integration	$\int_0^t f(\tau)\mathrm{d}\tau$	$\frac{1}{s}F(s)$
multiplication	$f_1(t)f_2(t)$	$\frac{1}{2\pi i}\lim_{T\to\infty}\int_{\mathrm{Re}(\sigma)-iT}^{\mathrm{Re}(\sigma)+iT} F_1(\sigma)F_2(s-\sigma)\mathrm{d}\sigma$
multiplication by time	$tf(t)$	$-\frac{\mathrm{d}}{\mathrm{d}s}F(s)$
convolution	$(f_1 * f_2)(t) = \int_0^t f_1(\tau)f_2(t-\tau)\mathrm{d}\tau$	$F_1(s)F_2(s)$
final value theorem	$\lim_{t\to\infty} f(t)$	$\lim_{s\to 0} sF(s)$

Example 1.2

Use the Laplace transform to solve an ODE

$$0 = \ddot{y}(t) - 2\dot{y}(t) + 4y(t)$$

with boundary and initial conditions

$$y(0) = 1,\ \dot{y}(0) = 2.$$

Solution: We can obtain its Laplace transform using the derivative properties and solve an algebraic equation in the s-domain

$$0 = s^2Y(s) - sy(0) - \dot{y}(0) - 2sY(S) + 2y(0) + 4Y(s)$$
$$Y(s) = \frac{s}{s^2 - 2s + 4}.$$

Rearrange $Y(s)$

$$Y(s) = \frac{s}{(s-1)^2+3} = \frac{s-1}{(s-1)^2+(\sqrt{3})^2} + \frac{1}{\sqrt{3}}\frac{\sqrt{3}}{(s-1)^2+(\sqrt{3})^2}.$$

Then convert the equation from the s-domain to the time domain by the inverse Laplace transform $\mathcal{L}^{-1}$ using table 1.1 again

$$y(t) = \mathcal{L}^{-1}\{Y(s)\} = e^t\cos\sqrt{3}t + \frac{1}{\sqrt{3}}e^t\sin\sqrt{3}t.$$

Copyright © 2025 Xiaowei He

Another useful property of the Laplace transform in control known as the *final value theorem* allows for computing the constant steady-state value of a time function given its Laplace transform. If all poles (i.e., denominator roots) of $F(s)$ are in the left half of the s-plane, except for one at $s = 0$, then all terms of $f(t)$ will decay to zero except the term corresponding to the pole at $s = 0$, and that term corresponds to a constant in time. Thus, the final value is given by the coefficient associated with the pole at $s = 0$. Therefore, if all poles of $sF(s)$ are in the left half of the s-plane, then

$$\lim_{t\to\infty} f(t) = \lim_{s\to 0} sF(s). \tag{1.25}$$

Example 1.3

Find the final value of the system corresponding to

$$Y(s) = \frac{3(s+2)}{s(s^2+2s+10)}.$$

Solution: Applying the final value theorem, we have

$$y(t\to\infty) = sY(s)|_{s=0} = \frac{3\times 2}{10} = 0.6.$$

While one could use equation (1.25) on any $Y(s)$, care must be taken to apply the final value theorem only to *stable* systems.

Open-loop systems and transfer functions. In an open-loop system, the system input is *independent* of the process output. Figure 1.22 shows such a system which includes input, output, and a mathematical representation of itself— the plant. The plant models the relationship between the output and input. In control theory, we use *transfer functions* to describe such input-output relations.

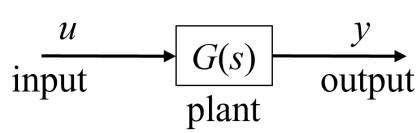

Figure 1.22: Block diagram of an open-loop system.

For continuous-time input $u(t)$ and output $y(t)$, the Laplace transforms gives

$$G(s) = \frac{Y(s)}{U(s)} = \frac{\mathcal{L}\{y(t)\}}{\mathcal{L}\{u(t)\}}, \tag{1.26}$$

where $G(s)$ is the transfer function of the plant. Rearranging the equation, we have

$$Y(s) = G(s)U(s), \tag{1.27}$$

which indicates that the output of the system is the *convolution* of the input and the plant.

Closed-loop systems. If we extract the output signal and feed it back to the input of the system, like figure 1.23 shows, we obtain a closed-loop system. In closed-loop systems, the input is *dependent* on the process output. The feedback loop measures the output through sensors, processes this measurement using a feedback transfer function (usually a constant gain), and then provides the feedback signal to a

Copyright © 2025 Xiaowei He

comparator that subtracts it from the input. Thus, we obtain an error signal that describes the difference between the target and the actual control result to be sent to the plant for the next control iteration. The open-loop part is also referred to as the feedforward loop.

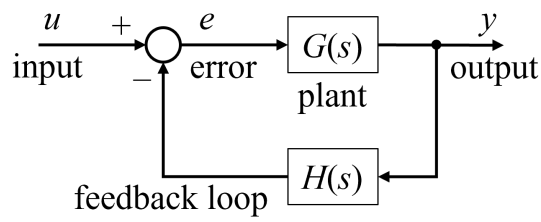

Figure 1.23: Block diagram of a closed-loop system.

The closed-loop transfer function is measured at the output. The output signal can be calculated from the closed-loop transfer function and the input signal. From the block diagram, we have the output and error signals, respectively,

$$\begin{aligned} Y(s) &= G(s)E(s), \\ E(s) &= U(s) - H(s)Y(s). \end{aligned} \tag{1.28}$$

Substitute the error signal into the output equation

$$Y(s) = G(s)[U(s) - H(s)Y(s)]. \tag{1.29}$$

Rearrange to separate the input and output

$$[1 + G(s)H(s)]Y(s) = G(s)U(s). \tag{1.30}$$

Thus, the closed-loop transfer function is

$$\frac{Y(s)}{U(s)} = \frac{G(s)}{1 + G(s)H(s)}. \tag{1.31}$$

Second-order systems and basics of stability The EOM of a second-order system has the second derivative terms as the highest order of differentiation. A classical example of a linear, second-order system is a mass-spring-damper system, as shown in figure 1.24.

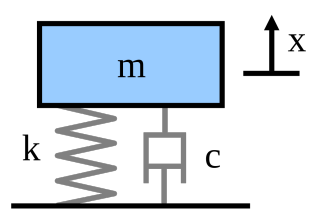

Figure 1.24: A mass-spring-damper system.

The state variable we are interested in is the position x of the object which has a mass m and is attached to a spring with a stiffness k and a damper with a damping constant c. If the external force (e.g., gravity, periodic forcing, etc.) is denoted by f, the EOM of the system is written as

$$m\ddot{x} + c\dot{x} + kx = f. \tag{1.32}$$

Copyright © 2025 Xiaowei He

Rearrange the EOM into the standard form

$$\ddot{x} + 2\zeta\omega_{\mathrm{n}}\dot{x} + \omega_{\mathrm{n}}^2 x = u, \tag{1.33}$$

where $\omega_{\mathrm{n}} = \sqrt{\dfrac{k}{m}}$ is the undamped natural frequency, $\zeta = \dfrac{c}{2m\omega_{\mathrm{n}}}$ is the damping ratio, and $u = \dfrac{f}{m}$ is the acceleration applied to the system.

The Laplace transform of the EOM, assuming zero initial condition, gives

$$s^2 X(s) + 2\zeta\omega_{\mathrm{n}} s X(s) + \omega_{\mathrm{n}}^2 X(s) = U(s). \tag{1.34}$$

Therefore, we have the second-order transfer function from the acceleration input to the displacement output

$$\frac{X(s)}{U(s)} = \frac{1}{s^2 + 2\zeta\omega_{\mathrm{n}} s + \omega_{\mathrm{n}}}. \tag{1.35}$$

The *characteristic equation* of a transfer function is obtained by setting the polynomial in the denominator of the transfer function equal to zero. The roots of the characteristic function will define the overall system dynamic characteristics and are called the *poles* of the system. The poles are locations in the s-plane where the magnitude of the transfer function becomes infinite. For example, the poles of the second-order system in equation (1.35) are

$$p_{1,2} = -\zeta\omega_{\mathrm{n}} \pm i\omega_{\mathrm{n}}\sqrt{1-\zeta^2} = -\zeta\omega_{\mathrm{n}} \pm i\omega_{\mathrm{d}}, \tag{1.36}$$

where $\omega_{\mathrm{d}} = \omega_{\mathrm{n}}\sqrt{1-\zeta^2}$.

The stability of a system can be determined by the position of the poles on the s-plane. If the real part of the pole is negative (i.e., the pole is on the left-half plane), the response is stable. Otherwise, it is not stable. If the real pole is on the imaginary axis ($\mathrm{Re}(p) = 0$), the system is called critically stable or neutrally stable (undamped). Time response characteristics for an impulse input are illustrated in figure 1.25. For $p_{1,2} = -\zeta\omega_{\mathrm{n}} \pm i\omega_{\mathrm{d}}$, if $\zeta > 0$, the system is stable. If $\mathrm{Re}(p_{1,2}) > 0$, the system is unstable, which occurs when $\zeta < 0$. If $\zeta = 0$, it is an undamped system that will oscillate at its natural frequency without periodic forcing. Figure 1.25 also shows the influence of the pole's position on the system damping and frequency characteristics. The further the pole is on the left-half plane from the imaginary axis, the higher the damping ratio is for the system; thus, the signal decays faster. The value of the imaginary part of the pole decides the pole's distance from the real axis. The system's natural frequency increases with the distance between the pole and the real axis (larger $\mathrm{Im}(p)$).

State-space representation. The idea of state-space comes from the state-variable method of describing differential equations. In this method, the differential equations describing a dynamic system are organized as a set of first-order differential equations in the vector-valued state of the system, and the solution is visualized as a trajectory of this state vector in space. The advantages of state-space design are particularly evident when the system to be controlled has more than one control input or multiple sensed outputs.

For a continuous linear time-invariant system with p inputs, q outputs, and n state variables, the standard state-space representation is

$$\dot{\boldsymbol{x}}(t) = \boldsymbol{A}\boldsymbol{x}(t) + \boldsymbol{B}\boldsymbol{u}(t) \tag{1.37}$$

$$\boldsymbol{y}(t) = \boldsymbol{C}\boldsymbol{x}(t) + \boldsymbol{D}\boldsymbol{u}(t), \tag{1.38}$$

Copyright © 2025 Xiaowei He

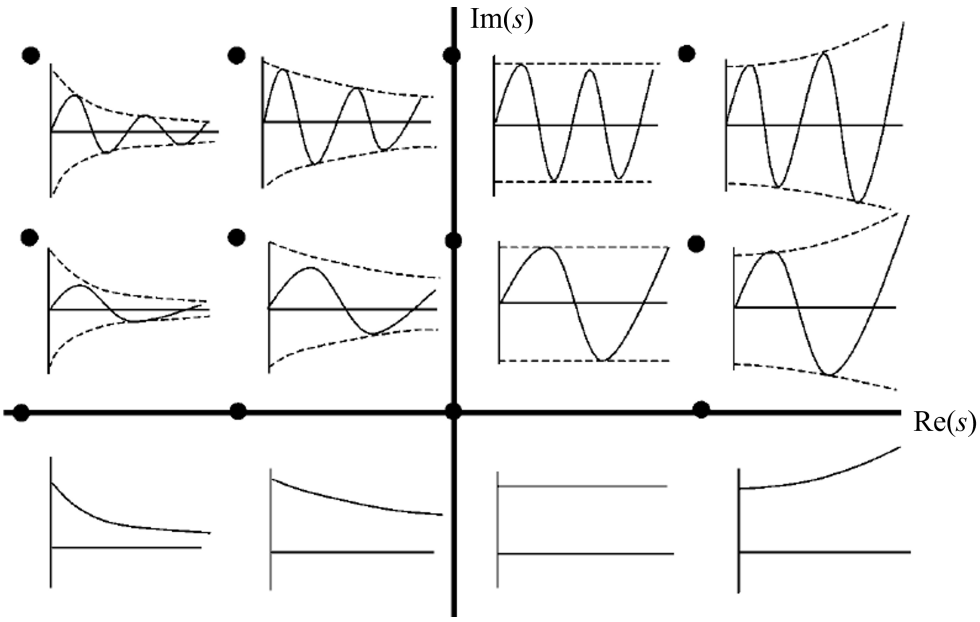

Figure 1.25: Time functions associated with poles in the s-plane [6].

where $\boldsymbol{x}$ is the vector of state variables $(n \times 1)$, $\dot{\boldsymbol{x}}$ is the time derivative of the state vector $(n \times 1)$, $\boldsymbol{u}$ is the input or control vector $(p \times 1)$, $\boldsymbol{y}$ is the output vector $(q \times 1)$, $\boldsymbol{A}$ is the system matrix $(n \times n)$, $\boldsymbol{B}$ is the input matrix $(n \times p)$, $\boldsymbol{C}$ is the output matrix $(q \times n)$, and $\boldsymbol{D}$ is the feedforward matrix $(q \times p)$. The block diagram of the state-space equations is shown in figure 1.26.

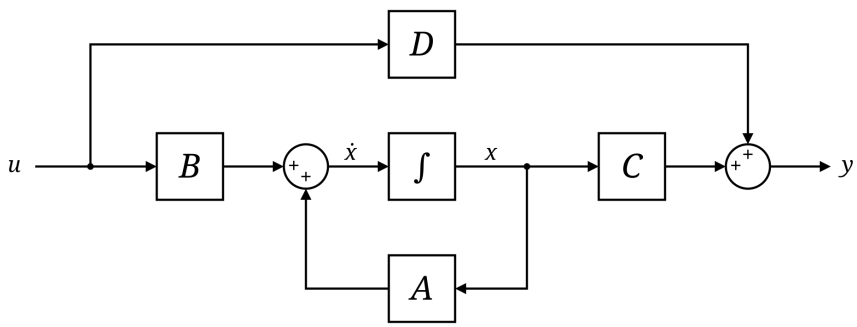

Figure 1.26: Block diagram of the linear state-space equations.

Equation (1.37) is the equation of motion or *state equation*, and equation (1.38) is called the *output equation*. For most aircraft problems, the output variables are chosen to be the state variables. Thus

$$\boldsymbol{y}(t) = \boldsymbol{x}(t) \quad \text{and} \quad q = n, \tag{1.39}$$

consequently, $\boldsymbol{C} = \boldsymbol{I}$ ($n \times n$ identity matrix) and $\boldsymbol{D} = \boldsymbol{0}$ ($n \times p$ zero matrix). Then the output equation is simplified to

$$\boldsymbol{y}(t) = \boldsymbol{I}\boldsymbol{x}(t) = \boldsymbol{x}(t). \tag{1.40}$$

By taking Laplace transform of equations (1.37) and (1.38) (assuming zero initial conditions) and

Copyright © 2025 Xiaowei He

rearranging, we obtain the transfer function matrix

$$\boldsymbol{G}(s) = \frac{\boldsymbol{Y}(s)}{\boldsymbol{U}(s)} = \boldsymbol{C}(s\boldsymbol{I} - \boldsymbol{A})^{-1}\boldsymbol{B} + \boldsymbol{D}. \tag{1.41}$$

In the case of EOM, $\boldsymbol{C} = \boldsymbol{I}$ and $\boldsymbol{D} = \boldsymbol{0}$, then

$$\boldsymbol{G}(s) = (s\boldsymbol{I} - \boldsymbol{A})^{-1}\boldsymbol{B}. \tag{1.42}$$

We now write the EOM of the mass-spring-damper system (equation (1.32)) in the state-space form. We first reduce the second-order EOM to a set of two first-order differential equations. The position x and velocity $\dot{x}$ are the state variables

$$\boldsymbol{x} = \begin{bmatrix} x \\ \dot{x} \end{bmatrix}. \tag{1.43}$$

Taking the time derivative gives

$$\frac{\mathrm{d}}{\mathrm{d}t}\boldsymbol{x} = \begin{bmatrix} \dot{x} \\ \ddot{x} \end{bmatrix}. \tag{1.44}$$

The system input is

$$\boldsymbol{u} = f(t). \tag{1.45}$$

Decompose equation (1.32) into two first-order equations

$$\begin{aligned} \frac{\mathrm{d}}{\mathrm{d}t}x &= \dot{x} \\ \frac{\mathrm{d}}{\mathrm{d}t}\dot{x} &= -\frac{k}{m}x - \frac{c}{m}\dot{x} + \frac{f(t)}{m}, \end{aligned} \tag{1.46}$$

and write in matrix form, we obtain the state equation

$$\dot{\boldsymbol{x}} = \begin{bmatrix} \dot{x} \\ \ddot{x} \end{bmatrix} = \begin{bmatrix} 0 & 1 \\ -\frac{k}{m} & -\frac{c}{m} \end{bmatrix} \begin{bmatrix} x \\ \dot{x} \end{bmatrix} + \begin{bmatrix} 0 \\ \frac{1}{m} \end{bmatrix} f(t). \tag{1.47}$$

The output variables are chosen to be the state variables $\boldsymbol{y}(t) = \boldsymbol{x}(t)$. If we further choose only to control the position of the mass, then the output equation can be reduced to

$$\boldsymbol{y} = \begin{bmatrix} 1 & 0 \end{bmatrix} \begin{bmatrix} x \\ \dot{x} \end{bmatrix}. \tag{1.48}$$

Copyright © 2025 Xiaowei He

2 Definitions

2.1 Aircraft axis systems

Since aircraft have six degrees of freedom, the description of their motion can be relatively complex. Therefore, motion is usually described by a number of variables that are related to a suitably chosen system of axes. We define different axis systems depending on what helps to simplify the mathematics we need to use. It is easier to define forces in an axis system where those forces are aligned with the reference system.

2.1.1 Earth axes

Newton's laws are only valid in an *inertial reference frame*—one that is not moving (or, more generally, does not experience an acceleration). We use the Earth as our inertial reference frame. Note that the Earth is obviously moving in terms of the solar system, but for flight mechanics purposes, the rotation of the Earth is considered slow compared to aircraft motions.

The accepted convention for defining earth axes determines that a reference point o_0 on the surface of the earth is the origin of a right-handed orthogonal system of axes ($o_0x_0y_0z_0$), where x_0 axis points to the north, y_0 axis points to the east, and z_0 axis points vertically "down" along the gravity vector, as illustrated in figure 2.1a.

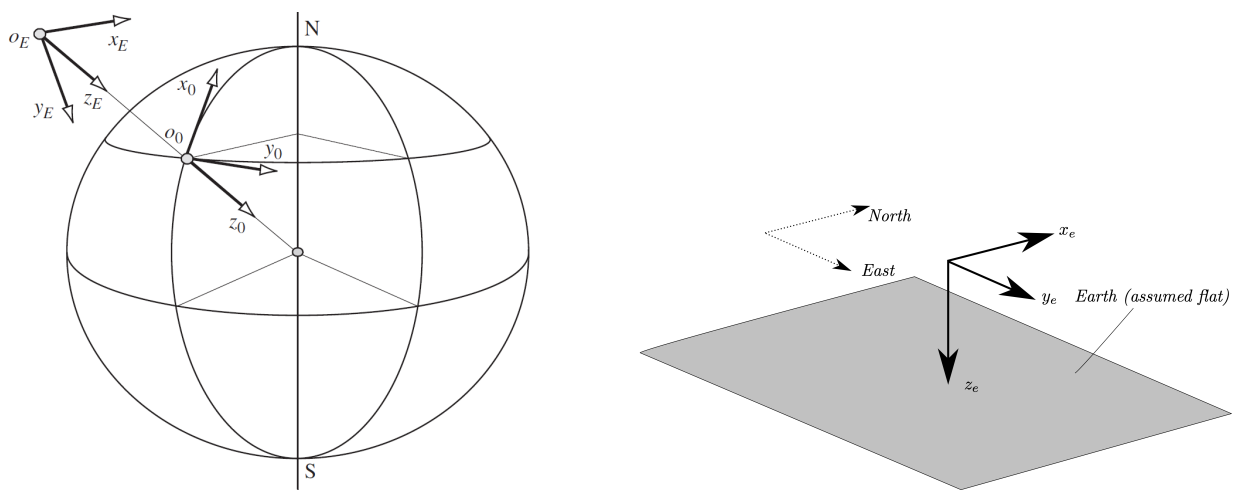

(a) Conventional earth axes [1]

(b) Earth axes horizontal plane [3]

Figure 2.1: Earth axes.

The x_0y_0 plane defines the local horizontal plane, which is tangential to the surface of the Earth. The flight path of an aircraft flying in the atmosphere in the vicinity of the reference point o_0 may thus be completely described by its coordinates in the axis system. This assumes a flat Earth where the vertical is "tied" to the gravity vector. For localized flight, this model is adequate, although it is best suited to navigation and performance applications where flight path trajectories are of primary interest. For investigations involving trans-global navigation, the axis system described is inappropriate; a spherical coordinate system is preferred. Similarly, for trans-atmospheric flight involving the launch and reentry of space vehicles, a spherical coordinate system is more appropriate. However, for flight dynamics applications, a simpler definition of Earth axes is preferred. Since only short-term motion is of interest, it is adequate to assume flight above a flat earth (figure 2.1b). The most common consideration is that

Copyright © 2025 Xiaowei He

of motion about straight and level flight. Straight and level flight assumes flight in a horizontal plane at a constant altitude; regardless of the subsequent motion of the aircraft, the attitude is determined with respect to the horizontal plane. Referring to figure 2.1a, the horizontal plane is defined by $(o_{\mathrm{E}}x_{\mathrm{E}}y_{\mathrm{E}})$ and is parallel to the x_0y_0 plane at the surface of the earth. It is only necessary to place the origin o_{E} in the atmosphere at the most convenient point, which is frequently coincident with the origin of the aircraft body-fixed axes. Earth axes $(o_{\mathrm{E}}x_{\mathrm{E}}y_{\mathrm{E}}z_{\mathrm{E}})$ defined in this way are called datum-path earth axes; they are "tied" to the earth by means of the gravity vector and provide the inertial reference frame for short-term aircraft motion.

2.1.2 Aircraft body-fixed axes

A number of aircraft body-fixed axis systems are in common use. However, for small perturbation analysis, only the generalized body axes and wind (or stability) axes need to be considered.

Generalized body axes. The most general axis system is known as a body axis system $(ox_{\mathrm{b}}y_{\mathrm{b}}z_{\mathrm{b}})$, which is fixed in the aircraft as shown in figure 2.2. It is a right-handed orthogonal axis system fixed in the aircraft and is constrained to move with it. Thus, when the aircraft is disturbed from its initial flight condition, the axes move with the airframe, and the motion is quantified in terms of perturbation variables referenced to the moving axes. The $x_{\mathrm{b}}z_{\mathrm{b}}$ plane defines the plane of symmetry of the aircraft, and the x_{b} axis is out of the nose along some reference line such as the geometrical horizontal fuselage datum. Thus, in normal flight attitudes, the y_{b} axis is directed to the starboard (right wing), and the z_{b} axis is directed "downward". The origin o of the axes is fixed at a convenient reference point in the airframe, which is usually, but not necessarily, coincident with the center of gravity (cg). The pilot sits in the body axis system, making it a very useful reference frame. Additionally, it is relatively easy to determine the moments and products of inertia in the body axis system because it is fixed to the aircraft.

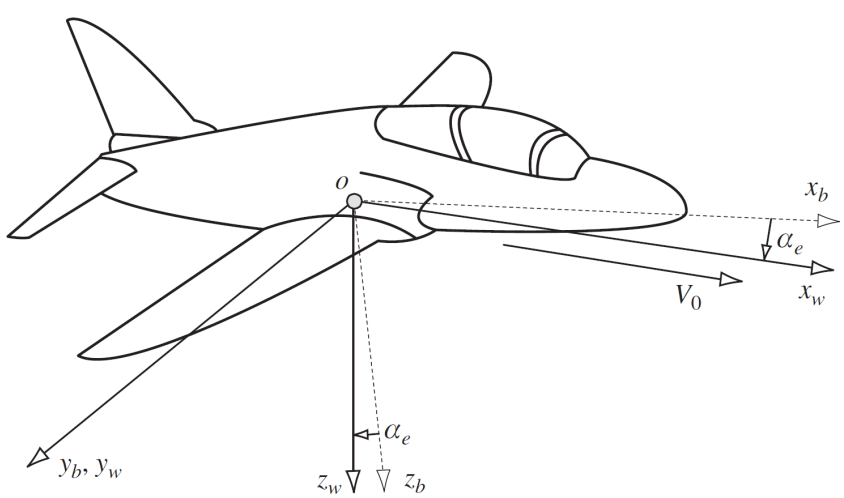

Figure 2.2: Body axis systems [1].

Aerodynamic, wind, or stability axes. It is often convenient to define a set of aircraft fixed axes such that the x axis is parallel to the total velocity vector $\boldsymbol{V}_0$ (i.e., $-\boldsymbol{V}_\infty$), as the $(ox_{\mathrm{w}}y_{\mathrm{w}}z_{\mathrm{w}})$ axes shown in figure 2.2. Such axes are referred to as aerodynamic, wind, or stability axes. In steady symmetric flight, wind axes $(ox_{\mathrm{w}}y_{\mathrm{w}}z_{\mathrm{w}})$ are a particular version of body axes that are rotated about the y_{b} axis through the steady body incidence angle α_{e} (i.e., angle of attack α) until the x_{w} axis aligns with the velocity vector $\boldsymbol{V}_0$. Thus, the $x_{\mathrm{w}}z_{\mathrm{w}}$ plane remains the plane of symmetry of the aircraft, and the y_{w} and the yb axes

Copyright © 2025 Xiaowei He

are coincident. There is a unique value of body incidence angle for every flight condition; therefore, for every flight condition, the wind axes orientation in the airframe is different. However, for any given flight condition, this orientation is defined and fixed in the aircraft at the outset and is constrained to move with it in subsequent disturbed flight. Typically, the body incidence might vary in the range $-10° \leqslant \alpha_e \leqslant 20°$ over a normal flight envelope. The wind axis system is particularly useful in defining the aerodynamic forces of lift and drag.

Perturbation variables. The motion of the aircraft is described in terms of force, moment, linear and angular velocities, and attitude resolved into components with respect to the chosen aircraft-fixed axis system. For convenience, it is preferable to assume a generalized body axis system initially. Thus the aircraft is initially assumed to be in steady rectilinear, but not necessarily level, flight when the body incidence is α_e and the steady velocity $\boldsymbol{V_0}$ resolves into components U_e, V_e, and W_e as indicated in figure 2.3. Here, we use subscript e to refer to *equilibrium, steady, or initial condition.* In steady nonaccelerating flight, the aircraft is in equilibrium, and the forces and moments acting on the airframe are in balance and sum to zero. This initial condition is usually referred to as *trimmed equilibrium.*

Whenever the aircraft is disturbed from equilibrium, the force and moment balance is upset, and the resulting transient motion is quantified in terms of the *perturbation variables.* The perturbation variables are shown in figure 2.3 and summarized in table 2.1.

Table 2.1: Motion variables.

	Trimmed equilibrium			Perturbed		
aircraft axis	x	y	z	x	y	z
force	0	0	0	X	Y	Z
moment	0	0	0	L	M	N
linear velocity	U_e	V_e	W_e	U	V	W
angular velocity	0	0	0	p	q	r
attitude	ϕ_e	θ_e	ψ_e	ϕ	θ	ψ

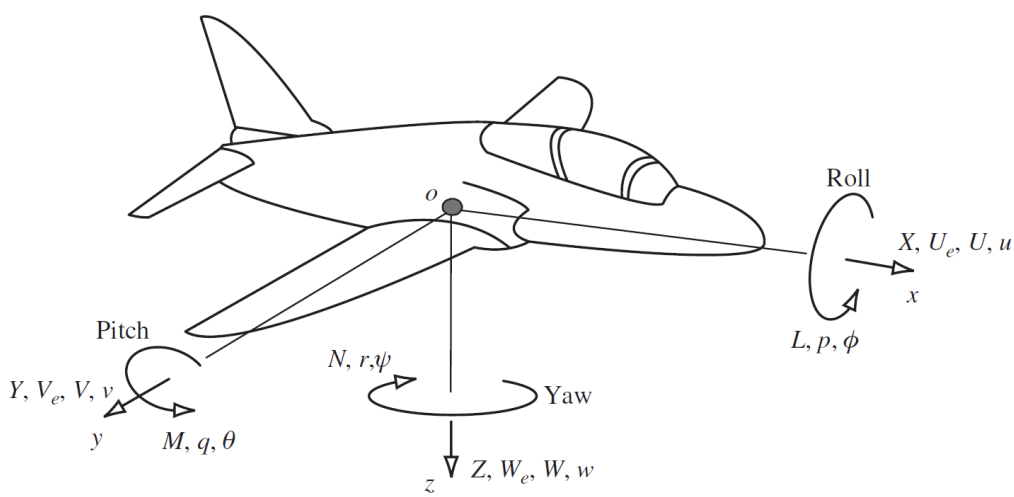

Figure 2.3: Motion variables notation [1].

The positive sense of the variables is determined by a right-handed axis system. Components of

Copyright © 2025 Xiaowei He

linear quantities, such as force, velocity, and so forth, are positive when their direction of action is the same as the direction of the axis to which they relate. The positive sense of the components of rotary quantities, moment, velocity, attitude, and so forth, is a right-handed rotation and may be determined as follows. Positive roll about the x axis is such that the y axis moves toward the z axis (right wing down); positive pitch about the y axis is such that the z axis moves toward the x axis (nose up); and positive yaw about the z axis is such that the x axis moves toward the y axis (nose to the right as seen by the pilot).

Table 2.2: Perturbation variables.

forces	X	axial force, drag
	Y	side force
	Z	normal force, lift
moments	L	roll moment
	M	pitch moment
	N	yaw moment
angular velocity	p	roll rate
	q	pitch rate
	r	yaw rate
linear velocity (of cg)	U	axial velocity
	V	lateral velocity
	W	normal velocity

A simple description of the perturbation variables is given in table 2.2. The intention is to provide some insight into the physical meaning of the many variables used in the model. Note that the components of the total linear velocity perturbations (U, V, W) are given by the sum of the steady equilibrium components and the transient perturbation components (u, v, w); thus

$$\begin{aligned} U &= U_{\mathrm{e}} + u, \\ V &= V_{\mathrm{e}} + v, \\ W &= W_{\mathrm{e}} + w. \end{aligned} \tag{2.1}$$

2.1.3 Quantities in different axes

It is easier to define certain quantities in one axis system over another.

Gravitational force—weight. The weight vector of the aircraft is conveniently represented in the Earth axis system, where there is only a component in the positive z_{E} direction because the vector acts toward the center of the Earth, that is,

$$\boldsymbol{F}_{\boldsymbol{g}_{\mathrm{E}}} = \boldsymbol{W}_{\mathrm{E}} = \begin{bmatrix} 0 \\ 0 \\ Z_g \end{bmatrix}_{\mathrm{E}} = \begin{bmatrix} 0 \\ 0 \\ mg \end{bmatrix}_{\mathrm{E}}. \tag{2.2}$$

Displacement. For positioning purposes, the aircraft location must be defined in Earth axes and is often of the center of gravity, thus,

$$\boldsymbol{X}_{cg_{\mathrm{E}}} = \begin{bmatrix} x_{cg} \\ y_{cg} \\ z_{cg} \end{bmatrix}_{\mathrm{E}}. \tag{2.3}$$

Copyright © 2025 Xiaowei He

Thrust. The thrust vector can be expressed in the body axis as

$$\boldsymbol{F}_{\boldsymbol{T}_\mathrm{b}} = \boldsymbol{T}_\mathrm{b} = \begin{bmatrix} X_T \\ Y_T \\ Z_T \end{bmatrix}_\mathrm{b} . \tag{2.4}$$

For laterally symmetric thrust, it simplifies to

$$\boldsymbol{T}_\mathrm{b} = \begin{bmatrix} T\cos\phi_T \\ 0 \\ -T\sin\phi_T \end{bmatrix}_\mathrm{b} , \tag{2.5}$$

where ϕ_T is the angle between the x_b axis and the thrust vector $\boldsymbol{T}$. Note that the positive direction of the x_b axis points at the nose of the aircraft, whereas the thrust vector is usually toward the aft. Thus ϕ_T is an obtuse angle. If we assume no thrust vectoring, which is the case in this course, the thrust vector can be further reduced to

$$\boldsymbol{T}_\mathrm{b} = \begin{bmatrix} T \\ 0 \\ 0 \end{bmatrix}_\mathrm{b} . \tag{2.6}$$

Aerodynamic force. The aerodynamic forces are conveniently displayed in the wind (stability) axes, where drag acts in the negative x direction and lift acts in the negative z direction,

$$\boldsymbol{F}_{\mathbf{a}_\mathrm{w}} = \begin{bmatrix} -D \\ Y_\mathrm{a} \\ -L \end{bmatrix}_\mathrm{w} , \tag{2.7}$$

where Y_a is the side component of aerodynamic force due to sideslip.

2.1.4 Euler angles and aircraft attitude

The angles defined by the right-handed rotation about the three axes of a right-handed system of axes are called *Euler angles*. The sense of the rotations and the order in which they are considered about the three axes are, in turn, very important because angles do not obey the commutative law. (Recall rigid body rotation reviewed in section 1.3.1.) The attitude of an aircraft is defined as the angular orientation of the airframe-fixed axes with respect to Earth axes. Attitude angles are, therefore, a particular application of Euler angles. With reference to figure 2.4, $(ox_0y_0z_0)$ are datum or reference axes, and $(ox_3y_3z_3)$ are aircraft-fixed axes, either generalized body axes or wind axes. The attitude of the aircraft, with respect to the datum axes, may be established by considering the rotation about each axis in turn required to bring $(ox_3y_3z_3)$ into coincidence with $(ox_0y_0z_0)$. Thus, first rotate about x_3 through the roll angle ϕ to $(ox_2y_2z_2)$. Second, rotate about y_2 through the pitch angle θ to $(ox_1y_1z_1)$. Third, rotate about z_1 through the yaw angle ψ to $(ox_0y_0z_0)$. When the attitude of the aircraft is considered with respect to earth axes, $(ox_0y_0z_0)$ and $(ox_\mathrm{E}y_\mathrm{E}z_\mathrm{E})$ are coincident.

The importance of the sequence of the Euler angle rotations cannot be overemphasized. When converting quantities from the Earth axes to the body axis, the order of rotation is reversed—yaw $\rightarrow$ pitch $\rightarrow$ roll. If the sequence is performed in a different order than ψ, θ, and ϕ, the final result will be incorrect. In the meantime, the physical senses of the Euler angles of an aircraft are

- **yaw** ψ—the angle between the projection of x_b axis onto the horizontal $x_\mathrm{E}y_\mathrm{E}$ plane of the Earth and the x_E axis, measures the lateral heading of the aircraft;

Copyright © 2025 Xiaowei He

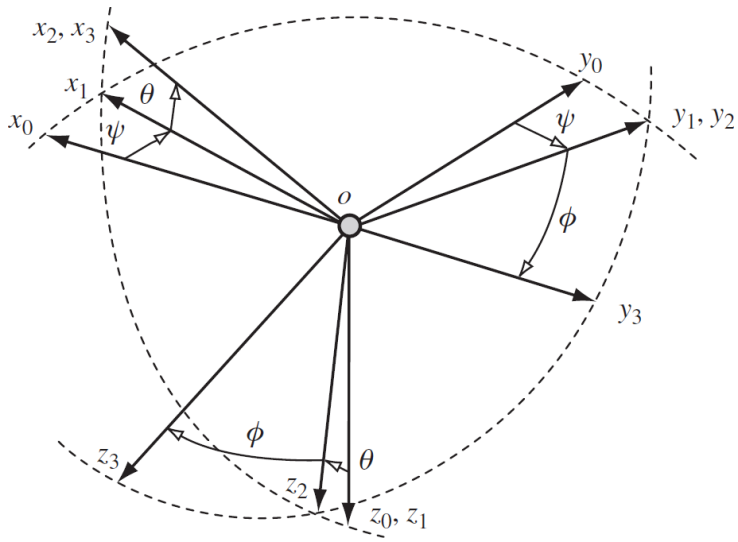

Figure 2.4: Motion variables notation [1].

- **pitch** θ—the angle between the x_b and the horizontal $x_\mathrm{E}y_\mathrm{E}$ plane on a vertical plane, measures the nose pointing in the longitudinal direction;
- **roll** ϕ—the angle between the y_b axis and the horizontal $x_\mathrm{E}y_\mathrm{E}$ plane measured in the $y_\mathrm{b}z_\mathrm{b}$ plane of the aircraft body axis system, is the same as the bank angle for a given yaw and pitch, and is a measure of the rotation about the x_b axis to put the aircraft in the desired position from a wing's horizontal condition.

The accepted limits on the Euler angles are

$$\begin{aligned} 0^\circ \leqslant \psi \leqslant 360^\circ \\ -90^\circ \leqslant \theta \leqslant 90^\circ \\ -180^\circ \leqslant \phi \leqslant 180^\circ. \end{aligned} \tag{2.8}$$

2.1.5 Axis transformation

It is frequently necessary to transform motion variables and other parameters from one system of axes to another. The angular relationships used to describe attitude may be generalized to describe the angular orientation of one set of axes with respect to another. A transformation matrix is desired to enable the definition of what a set of coordinates in one axis system is in the other. At this stage, we are not concerned with axial translation and only look at the effect of angular translation (yaw, pitch, and roll). That is, the two axes systems have co-located origins.

For a vector in the Earth axis system

$$\boldsymbol{X}_\mathrm{E} = \begin{bmatrix} x_\mathrm{E} \\ y_\mathrm{E} \\ z_\mathrm{E} \end{bmatrix}, \tag{2.9}$$

we want to find its coordinates expressed in the body axis system, for example, such that

$$\boldsymbol{X}_\mathrm{b} = \begin{bmatrix} x_\mathrm{b} \\ y_\mathrm{b} \\ z_\mathrm{b} \end{bmatrix} = \boldsymbol{R}(\phi, \theta, \psi)\boldsymbol{X}_\mathrm{E}, \tag{2.10}$$

Copyright © 2025 Xiaowei He

where $\boldsymbol{R}(\phi, \theta, \psi)$ is the *coordinate transformation matrix* (rotation matrix) defined by performing three individual rotations involving two intermediate axes systems.

Earth axes to intermediate axes $(ox_1y_1z_1)$ through yaw ψ. We perform an *Euler transform* to define $\boldsymbol{X}_\mathrm{E}$ in the intermediate axes $(ox_1y_1z_1)$, noting that $z_1 = z_\mathrm{E}$.

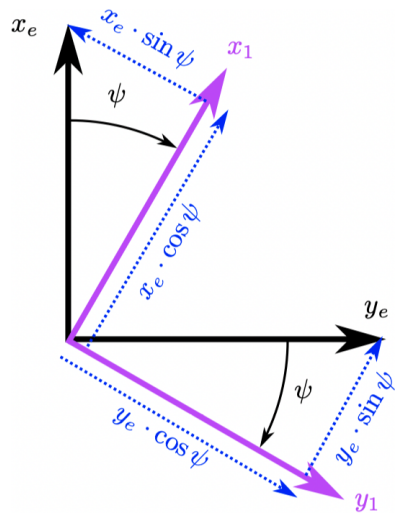

Figure 2.5: Euler rotation through yaw ψ [3].

Referring to figure 2.5, trigonometry gives

$$\begin{aligned} x_1 &= x_\mathrm{E}\cos\psi + y_\mathrm{E}\sin\psi \\ y_1 &= -x_\mathrm{E}\sin\psi + y_\mathrm{E}\cos\psi \\ z_1 &= z_\mathrm{E}. \end{aligned} \tag{2.11}$$

That is, in matrix form,

$$\begin{bmatrix} x_1 \\ y_1 \\ z_1 \end{bmatrix} = \begin{bmatrix} \cos\psi & \sin\psi & 0 \\ -\sin\psi & \cos\psi & 0 \\ 0 & 0 & 1 \end{bmatrix} \begin{bmatrix} x_\mathrm{E} \\ y_\mathrm{E} \\ z_\mathrm{E} \end{bmatrix} \tag{2.12}$$

so

$$\boldsymbol{X}_1 = \boldsymbol{R}_{\mathbf{yaw}}(\psi)\boldsymbol{X}_\mathrm{E}. \tag{2.13}$$

Intermediate axes $(ox_1y_1z_1)$ to intermediate axes $(ox_2y_2z_2)$ through pitch θ. Next rotated about y_1 axis through the pitch angle to obtain $\boldsymbol{X}_\mathrm{E}$ intermediate axes $(ox_2y_2z_2)$, noting $y_2 = y_1$.

According to figure 2.6, the vector in the $(ox_2y_2z_2)$ axes is

$$\begin{bmatrix} x_2 \\ y_2 \\ z_2 \end{bmatrix} = \begin{bmatrix} \cos\theta & 0 & -\sin\theta \\ 0 & 1 & 0 \\ \sin\theta & 0 & \cos\theta \end{bmatrix} \begin{bmatrix} x_1 \\ y_1 \\ z_1 \end{bmatrix}. \tag{2.14}$$

Plug in the result from the yaw rotation, and we have

$$\boldsymbol{X}_2 = \boldsymbol{R}_{\mathbf{pitch}}(\theta)\boldsymbol{X}_1 = \boldsymbol{R}_{\mathbf{pitch}}(\theta)\boldsymbol{R}_{\mathbf{yaw}}(\psi)\boldsymbol{X}_\mathrm{E}. \tag{2.15}$$

Intermediate axes $(ox_2y_2z_2)$ to body axes $(ox_\mathrm{b}y_\mathrm{b}z_\mathrm{b})$ through roll ϕ. The final rotation through the roll angle will give the coordinates of the vector in the body axes, of which the rotational axis is $x_\mathrm{b} = x_2$.

Copyright © 2025 Xiaowei He

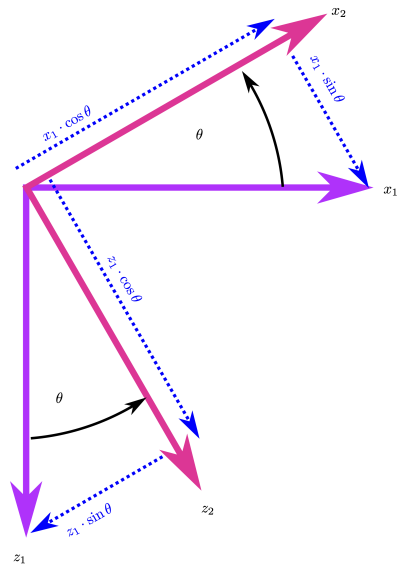

Figure 2.6: Euler rotation through pitch θ [3].

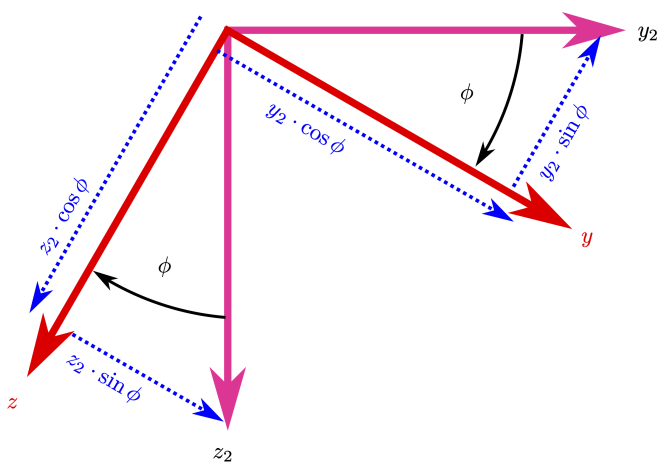

Figure 2.7: Euler rotation through roll ϕ [3].

The Euler transform in figure 2.7 shows that

$$\begin{bmatrix} x_\mathrm{b} \\ y_\mathrm{b} \\ z_\mathrm{b} \end{bmatrix} = \begin{bmatrix} 1 & 0 & 0 \\ 0 & \cos\phi & \sin\phi \\ 0 & -\sin\phi & \cos\phi \end{bmatrix} \begin{bmatrix} x_2 \\ y_2 \\ z_2 \end{bmatrix}, \tag{2.16}$$

which is

$$\boldsymbol{X}_\mathrm{b} = \boldsymbol{R}_\mathbf{roll}(\phi)\boldsymbol{X}_2. \tag{2.17}$$

By combining all three rotations, we obtain the Euler transformation from the Earth axes to the body axes

$$\begin{aligned} \boldsymbol{X}_\mathrm{b} &= \boldsymbol{R}_\mathbf{roll}(\phi)\boldsymbol{R}_\mathbf{pitch}(\theta)\boldsymbol{R}_\mathbf{yaw}(\psi)\boldsymbol{X}_\mathrm{E} \\ \boldsymbol{X}_\mathrm{b} &= \boldsymbol{R}(\phi,\theta,\psi)\boldsymbol{X}_\mathrm{E}, \end{aligned} \tag{2.18}$$

Copyright © 2025 Xiaowei He

where $\boldsymbol{R}(\phi,\theta,\psi)$ is the total transformation matrix

$$\begin{aligned}\boldsymbol{R}(\phi,\theta,\psi) &= \underbrace{\begin{bmatrix}1 & 0 & 0\\ 0 & \cos\phi & \sin\phi\\ 0 & -\sin\phi & \cos\phi\end{bmatrix}}_{\text{roll}}\underbrace{\begin{bmatrix}\cos\theta & 0 & -\sin\theta\\ 0 & 1 & 0\\ \sin\theta & 0 & \cos\theta\end{bmatrix}}_{\text{pitch}}\underbrace{\begin{bmatrix}\cos\psi & \sin\psi & 0\\ -\sin\psi & \cos\psi & 0\\ 0 & 0 & 1\end{bmatrix}}_{\text{yaw}}\\ &= \begin{bmatrix}\cos\theta\cos\psi & \cos\theta\sin\psi & -\sin\theta\\ \sin\phi\sin\theta\cos\psi-\cos\phi\sin\psi & \sin\phi\sin\theta\sin\psi+\cos\phi\cos\psi & \sin\phi\cos\theta\\ \cos\phi\sin\theta\cos\psi+\sin\phi\sin\psi & \cos\phi\sin\theta\sin\psi-\sin\phi\cos\psi & \cos\phi\cos\theta\end{bmatrix}.\end{aligned} \tag{2.19}$$

Inverse transformation. If transforming from the body axis system to the Earth axis system, we use the inverse of the transformation matrices, where the transformation becomes

$$\boldsymbol{X}_{\mathrm{E}} = \boldsymbol{R}^{-1}_{\mathbf{yaw}}(\psi)\boldsymbol{R}^{-1}_{\mathbf{pitch}}(\theta)\boldsymbol{R}^{-1}_{\mathbf{roll}}(\phi)\boldsymbol{X}_{\mathrm{b}} = \boldsymbol{R}^{-1}(\phi,\theta,\psi)\boldsymbol{X}_{\mathrm{b}}. \tag{2.20}$$

Note that the order of rotation is reversed from "yaw → pitch → roll" to "roll → pitch → yaw". Handily, $\boldsymbol{R}$ is orthogonal, meaning $\boldsymbol{R}\boldsymbol{R}^{\mathrm{T}} = \boldsymbol{I}$, thus $\boldsymbol{R}^{-1} = \boldsymbol{R}^{\mathrm{T}}$, where the superscript T indicates the transpose of the matrix. Hence

$$\boldsymbol{X}_{\mathrm{E}} = \boldsymbol{R}^{\mathrm{T}}_{\mathbf{yaw}}(\psi)\boldsymbol{R}^{\mathrm{T}}_{\mathbf{pitch}}(\theta)\boldsymbol{R}^{\mathrm{T}}_{\mathbf{roll}}(\phi)\boldsymbol{X}_{\mathrm{b}} = \boldsymbol{R}^{\mathrm{T}}(\phi,\theta,\psi)\boldsymbol{X}_{\mathrm{b}}. \tag{2.21}$$

Example 2.1

Express the aircraft's weight vector in the body axis system.

Solution: From equation (2.2) we have the weight vector in the Earth axis system

$$\boldsymbol{F}_{\boldsymbol{g}_{\mathrm{E}}} = \boldsymbol{W}_{\mathrm{E}} = \begin{bmatrix}0\\0\\Z_g\end{bmatrix}_{\mathrm{E}} = \begin{bmatrix}0\\0\\mg\end{bmatrix}_{\mathrm{E}}.$$

Apply the Euler rotation expressed in equation (2.18)

$$\begin{aligned}\boldsymbol{F}_{\boldsymbol{g}_{\mathrm{b}}} &= \boldsymbol{R}(\phi,\theta,\psi)\boldsymbol{F}_{\boldsymbol{g}_{\mathrm{E}}}\\ &= \begin{bmatrix}\cos\theta\cos\psi & \cos\theta\sin\psi & -\sin\theta\\ \sin\phi\sin\theta\cos\psi-\cos\phi\sin\psi & \sin\phi\sin\theta\sin\psi+\cos\phi\cos\psi & \sin\phi\cos\theta\\ \cos\phi\sin\theta\cos\psi+\sin\phi\sin\psi & \cos\phi\sin\theta\sin\psi-\sin\phi\cos\psi & \cos\phi\cos\theta\end{bmatrix}\begin{bmatrix}0\\0\\mg\end{bmatrix}_{\mathrm{E}}\\ &= \begin{bmatrix}-mg\sin\theta\\ mg\sin\phi\cos\theta\\ mg\cos\phi\cos\theta\end{bmatrix}_{\mathrm{b}}\end{aligned}$$

Example 2.2

Express the aerodynamic force vector in the body axis system, assuming no sideslip.

Solution: The aerodynamic force vector is defined in the stability/wind axes. Recall equation (2.7)

$$\boldsymbol{F}_{\mathbf{a}_{\mathrm{w}}} = \begin{bmatrix}-D\\ Y_{\mathrm{a}}\\ -L\end{bmatrix}_{\mathrm{w}}.$$

Copyright © 2025 Xiaowei He

Since there is no sideslip, the Euler angles are

$$\phi = 0, \qquad \theta = \alpha, \qquad \psi = 0,$$

where α is the angle of attack. This allows for reducing the Euler transform to $\boldsymbol{R}_{\mathbf{pitch}}(\theta)$ only, that is,

$$\begin{aligned} \boldsymbol{F}_{\mathbf{a}_\mathrm{b}} &= \boldsymbol{R}_{\mathbf{pitch}}(\theta)\boldsymbol{F}_{\mathbf{a}_\mathrm{w}} \\ \begin{bmatrix} X_\mathrm{a} \\ Y_\mathrm{a} \\ Z_\mathrm{a} \end{bmatrix}_\mathrm{b} &= \begin{bmatrix} \cos\theta & 0 & -\sin\theta \\ 0 & 1 & 0 \\ \sin\theta & 0 & \cos\theta \end{bmatrix} \begin{bmatrix} -D \\ Y_\mathrm{a} \\ -L \end{bmatrix}_\mathrm{w} = \begin{bmatrix} -D\cos\alpha + L\sin\alpha \\ Y_\mathrm{a} \\ -D\sin\alpha - L\cos\alpha \end{bmatrix}_\mathrm{b}. \end{aligned}$$

Note that no sideslip velocity does not mean no side force. Therefore, Y_a remains in the result vector.

2.1.6 Angular body rates

It is important to understand that the Euler angles are not defined in the same axis set, as yaw is defined in the Earth axes ($ox_\mathrm{E}y_\mathrm{E}z_\mathrm{E}$), pitch is defined in intermediate axes ($ox_1y_1z_1$), and roll is defined in intermediate exes ($ox_2y_2z_2$). Consequently,

$$\begin{bmatrix} p \\ q \\ r \end{bmatrix} \neq \boldsymbol{R}(\phi,\theta,\psi) \begin{bmatrix} \dot\phi \\ \dot\theta \\ \dot\psi \end{bmatrix}, \tag{2.22}$$

where p, q, and r are the *angular body rates* measured in the aircraft-fixed axes ($ox_\mathrm{b}y_\mathrm{b}z_\mathrm{b}$)

We construct a transformation matrix to express the body rates by the attitude rates $\dot\phi$, $\dot\theta$, $\dot\psi$ based on the axis systems in which each Euler angle is defined and the sequence of rotations, whereby each Euler angular rate has components in the body axes.

First: transform the attitude rate about Earth axis z_E, $\dot\psi$

$$\begin{bmatrix} \dot\psi_x \\ \dot\psi_y \\ \dot\psi_z \end{bmatrix}_\mathrm{b} = \boldsymbol{R}_{\mathbf{roll}}(\phi)\boldsymbol{R}_{\mathbf{pitch}}(\theta)\boldsymbol{R}_{\mathbf{yaw}}(\psi) \begin{bmatrix} 0 \\ 0 \\ \dot\psi \end{bmatrix}_\mathrm{E} = \begin{bmatrix} -\dot\psi\sin\theta \\ \dot\psi\sin\phi\cos\theta \\ \dot\psi\cos\phi\cos\theta \end{bmatrix}_\mathrm{b}. \tag{2.23}$$

Second: transform the attitude rate about intermediate axis y_1, $\dot\theta$

$$\begin{bmatrix} \dot\theta_x \\ \dot\theta_y \\ \dot\theta_z \end{bmatrix}_\mathrm{b} = \boldsymbol{R}_{\mathbf{roll}}(\phi)\boldsymbol{R}_{\mathbf{pitch}}(\theta) \begin{bmatrix} 0 \\ \theta \\ 0 \end{bmatrix}_1 = \begin{bmatrix} 0 \\ \dot\theta\cos\phi \\ -\dot\theta\sin\phi \end{bmatrix}_\mathrm{b}. \tag{2.24}$$

Third: transform the attitude rate about intermediate axis x_2, $\dot\phi$

$$\begin{bmatrix} \dot\phi_x \\ \dot\phi_y \\ \dot\phi_z \end{bmatrix}_\mathrm{b} = \boldsymbol{R}_{\mathbf{roll}}(\phi) \begin{bmatrix} \phi \\ 0 \\ 0 \end{bmatrix}_2 = \begin{bmatrix} \dot\phi \\ 0 \\ 0 \end{bmatrix}_\mathrm{b}. \tag{2.25}$$

The body angular rate vector ω_b is equal to the sum of the attitude rate vectors expressed in the

Copyright © 2025 Xiaowei He

body axes, that is,

$$\begin{aligned}
\boldsymbol{\omega}_\mathrm{b} &= \dot{\boldsymbol{\phi}}_\mathrm{b} + \dot{\boldsymbol{\theta}}_\mathrm{b} + \dot{\boldsymbol{\psi}}_\mathrm{b} \\
\begin{bmatrix} p \\ q \\ r \end{bmatrix}_\mathrm{b} &= \begin{bmatrix} \dot{\phi} \\ 0 \\ 0 \end{bmatrix}_\mathrm{b} + \begin{bmatrix} 0 \\ \dot{\theta}\cos\phi \\ -\dot{\theta}\sin\phi \end{bmatrix}_\mathrm{b} + \begin{bmatrix} -\dot{\psi}\sin\theta \\ \dot{\psi}\sin\phi\cos\theta \\ \dot{\psi}\cos\phi\cos\theta \end{bmatrix}_\mathrm{b} \\
&= \begin{bmatrix} 1 & 0 & -\sin\theta \\ 0 & \cos\phi & \sin\phi\cos\theta \\ 0 & -\sin\phi & \cos\phi\cos\theta \end{bmatrix} \begin{bmatrix} \dot{\phi} \\ \dot{\theta} \\ \dot{\psi} \end{bmatrix}
\end{aligned} \tag{2.26}$$

When the aircraft perturbations are small, such that ϕ, θ, and ψ may be treated as small angles, equation (2.26) may be approximated by

$$p = \dot{\phi}, \qquad q = \dot{\theta}, \qquad r = \dot{\psi}. \tag{2.27}$$

2.1.7 Velocity in Earth and body axes

The aircraft velocity vector $\boldsymbol{V}_0$ is defined in wind axes, hence we need to relate the incident flow to Earth and body axes through the trajectory and aerodynamic angles, respectively.

Trajectory angles. The trajectory angles define the orientation of the velocity vector in Earth axes, which are the track angle τ and flight path angle γ. We then resolve the aircraft velocity into Earth axis components

$$\boldsymbol{V}_\mathrm{E} = \begin{bmatrix} U_\mathrm{E} \\ V_\mathrm{E} \\ W_\mathrm{E} \end{bmatrix} = \begin{bmatrix} V_0\cos\gamma\cos\tau \\ V_0\cos\gamma\sin\tau \\ V_0\sin\gamma \end{bmatrix}. \tag{2.28}$$

The flight path angle is the angle between the velocity vector and its projection in the $x_\mathrm{E}y_\mathrm{E}$ plane. The track angle is the angle between that projection and due north, x_E.

The relationships of the Euler angles, aerodynamic angles, and trajectory angles are shown in figure 2.8. From there, we can relate them by

$$\gamma_\mathrm{e} = \theta_\mathrm{e} - \alpha_\mathrm{e} \qquad \tau_\mathrm{e} = \psi_\mathrm{e} + \beta_\mathrm{e}. \tag{2.29}$$

Note that this is in equilibrium conditions, as indicated by the subscript e.

Example 2.3

Aircraft accident investigators wish to calculate the descent rate of an aircraft at the moment of impact into the ocean. The flight data recorder outputs are in terms of the following aircraft variables:

Sideslip, yaw, pitch angles = 0°

Roll angle = 60°

Angle of Attack = 30°

Airspeed = 120 kn

Solution: Knowing the airspeed in measured in the body axes, $V_0 = 120\,\mathrm{kn} = 61.7\,\mathrm{m/s}$, first calculate the body axes components

$$\boldsymbol{V_0}_\mathrm{b} = \begin{bmatrix} U \\ V \\ W \end{bmatrix}_\mathrm{b} = \begin{bmatrix} V_0\cos\alpha\cos\beta \\ V_0\cos\alpha\sin\beta \\ V_0\sin\alpha \end{bmatrix}_\mathrm{b} = \begin{bmatrix} V_0\cos 30^\circ \\ 0 \\ V_0\sin 30^\circ \end{bmatrix}_\mathrm{b},$$

Copyright © 2025 Xiaowei He

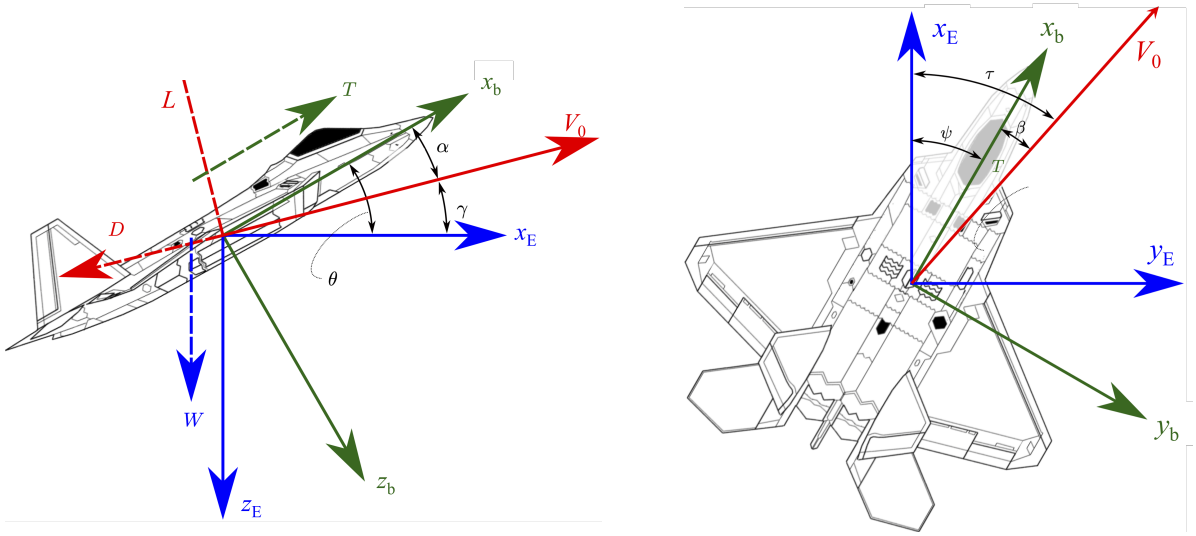

(a) Reference angles on xz plane

(b) Reference angles on xy plane

Figure 2.8: Velocity reference angles [3].

given $\alpha = 30°$ and $\beta = 0°$.

Then convert to Earth axes through the inverse Euler transformation matrix

$$\boldsymbol{V}_{\mathbf{0}_\mathrm{E}} = \begin{bmatrix} U \\ V \\ W \end{bmatrix}_\mathrm{E} = \boldsymbol{R}^{-1}\boldsymbol{V}_{\mathbf{0}_\mathrm{b}}.$$

The descent rate is the vertical component of $\boldsymbol{V}_{\mathbf{0}_\mathrm{E}}$

$$W_\mathrm{E} = U_\mathrm{b}(-\sin\theta) + V_\mathrm{b}\sin\phi\cos\theta + W_\mathrm{b}\cos\phi\cos\theta$$

With $\phi = 60°$ and $\theta = 0°$,

$$\begin{aligned} W_\mathrm{E} &= 0 + 0 + V_0 \sin 30° \cos 60° \\ &= 61.7\,\mathrm{m/s} \cdot \sin 30° \cos 60° \\ &= 15.4\,\mathrm{m/s}. \end{aligned}$$

2.2 Controls notation

2.2.1 Aerodynamic controls

Notation for aerodynamic controls can be application-dependent, especially when unconventional control surfaces are used. However, for conventional aircraft, there is a universally accepted notation, which accords with Hopkin [8], and it is simple to apply. Generally, a positive control action by the pilot results in a positive aircraft response, whereas a positive control surface displacement yields a negative aircraft response. Thus, aligned with what was reviewed in section 1.3.2,

- **in roll:** positive right push force on the stick ⇒ positive stick displacement ⇒ right aileron up and left aileron down (negative mean) ⇒ right wing down roll response (positive);
- **in pitch:** positive pull force on the stick ⇒ positive aft stick displacement ⇒ elevator trailing edge

Copyright © 2025 Xiaowei He

up (negative) ⇒ nose-up pitch response (positive);

- **in yaw:** positive push force on the right rudder pedal ⇒ positive rudder bar displacement ⇒ rudder trailing edge displaced to the right (negative) ⇒ nose to the right yaw response (positive).

Roll and pitch control stick displacements are denoted δ_ξ and δ_η, respectively, and rudder pedal displacement is denoted δ_ζ. Aileron, elevator, and rudder surface displacements are denoted ξ, η, and ζ, respectively, as indicated in figure 2.9. It should be noted that since ailerons act differentially, the displacement ξ is usually taken as the mean value of the separate displacements of each aileron.

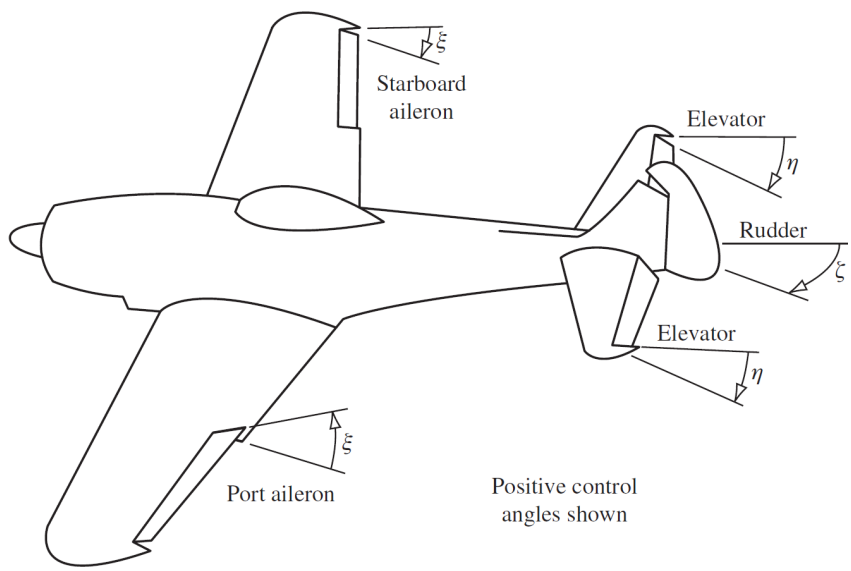

Figure 2.9: Aerodynamic controls notation [1].

2.2.2 Engine control

Engine thrust T is controlled by throttle lever displacement ϵ. Positive throttle lever displacement is usually in the forward push sense and results in a positive increase in thrust. For a turbojet engine, the relationship between thrust and throttle lever angle is approximated by a simple first-order lag transfer function,

$$\frac{T(s)}{\epsilon(s)} = \frac{k_T}{1 + s\tau_T}, \tag{2.30}$$

where k_T is a suitable gain constant and τ_T is the lag time constant, which is typically of the order of two or three seconds.

2.3 Attitude indicator

The attitude indicator (AI), also known as the gyro horizon or artificial horizon, is a flight instrument that informs the pilot of the aircraft's orientation relative to Earth's horizon and gives an immediate indication of the smallest orientation change. The miniature aircraft and horizon bar mimic the relationship of the aircraft relative to the actual horizon. The AI displays the precise bank (roll) and pitch angles of the aircraft in degrees. A typical AI display is shown in figure 2.10.

The top half of the instrument is blue, representing the sky, while the bottom half is brown, representing the ground. The white line separating them is the horizon. The bank index (roll scale) at the

Copyright © 2025 Xiaowei He

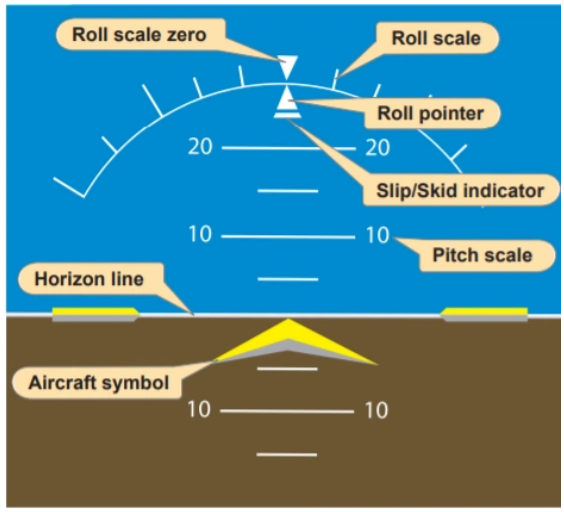

Figure 2.10: Attitude indicator display.

top shows the aircraft's angle of bank. The triangle on the top of the scale is the zero index. The hash marks on the scale represent the degree of bank. The bank scale always remains in the same position relative to the horizon line. The roll pointer indicates the direction and degree of bank and is always aligned with the aircraft symbol. Reference lines in the middle, parallel to the horizon, represent the pitch scale, indicating the degree of pitch, up or down, relative to the horizon. This scale is marked in 5-degree increments and labeled every 10 degrees. The pitch scale always remains parallel to the horizon. The interpretation of the bank and pitch scales is illustrated in figure 2.11.

Most modern AIs are integrated with a flight director system (FDS) to include flight direction on a 360-degree scale. Such a system is called an attitude direction indicator (ADI), which provides the pilot with a 3-D flight trajectory cue to maintain a desired path.

Copyright © 2025 Xiaowei He

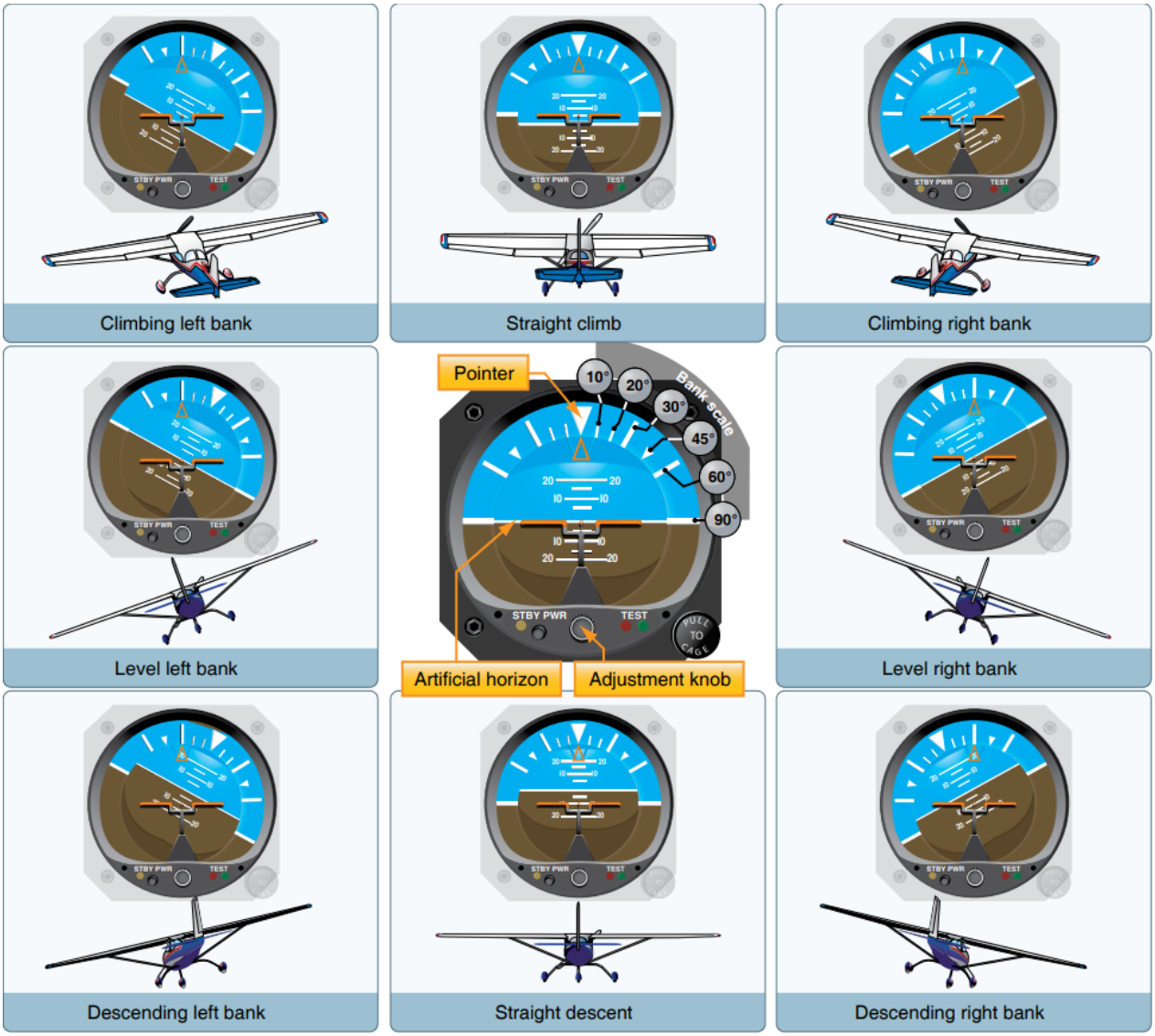

Figure 2.11: Attitude indicator relationship to aircraft orientation.

Copyright © 2025 Xiaowei He

3 Aircraft Performance

Aircraft performance is the branch of aerospace engineering that allows us to utilize relationships between thrust, drag, lift, and weight to determine allowable aircraft masses, fuel requirements, range limitations, and steady maneuver calculations.

We will start with building coordinates and basic concepts of aircraft and flights. Then analyze the kinematics and force conditions for different flight missions or phases, including level flight, takeoff, landing, climbs, gliding, and turns; and understand how the aircraft's performance is determined in these missions. These calculations are dependent on the aircraft upon which we are working, and since 1903, aircraft have changed a tremendous amount, as the comparison between the Wright Flyer and a Boeing 787-9 commercial jet, shown in table 3.1. However, the basic concepts and relationships are applicable to all aircraft and will be explored in this course.

Table 3.1: Aircraft parameters comparison.

Parameters	Wright Flyer	Boeing 787-9
length	6.43 m	62.81 m
wingspan	12.29 m	60.12 m
max. speed	48 km/h (26 kt)	956 km/h (516 kt)
max. range	0.26 km	14 010 km
max. takeoff weight	338 kg	254 700 kg
power plant	1 × piston engine	2 × turbofan engine
available thrust	0.53 kN	320 kN
passengers	1	296

3.1 Airspeed

An understanding of airspeed is critical to interpreting and discussing aircraft performance. An aircraft is moving with respect to an inertially fixed reference frame, but it is not connected to it; thus, it is difficult to make measurements between the two. To this point, we have only dealt with true airspeed. This section addresses indicated, calibrated, equivalent, and ground speed.

First, we will introduce some terminology:

- **static pressure** p—the pressure because of random molecular motion and is devoid of any contribution from the flow velocity;
- **total pressure** p_0—the pressure that exists at a stagnation point, or would exist at any point in the flow, if it were isentropically slowed to zero velocity;
- **indicated airspeed** V_i—the airspeed displayed in the cockpit and is obtained from pitot-static instrumentation and "fed" into the airspeed indicator;
- **calibrated airspeed** V_c—the indicated airspeed corrected for position error;
- **equivalent airspeed** V_e—the calibrated airspeed corrected for nonstandard sea-level pressure;
- **true airspeed (TAS)** V—airspeed relative to the air mass, which is equivalent airspeed corrected for non-standard, sea-level density;
- **ground speed** V_g—speed relative to the ground, which is true airspeed corrected for wind;

Copyright © 2025 Xiaowei He

- **position error** ΔV_{p}—obtained from flight test and is a correction between indicated and calibrated airspeed, used to account for errors in static port placement and known instrument errors;
- f **factor** f—a nonstandard sea-level pressure correction factor, and is the ratio between equivalent and calibrated airspeeds.

Aerodynamic performance (how much lift and drag is being produced) is a function of the aircraft's orientation and translation with respect to the incident wind, and not to the Earth. Similarly, the powerplant performance will be a function of the incident wind, not the ground speed. This gives us our first set of speeds and the relationship between them

$$V_{\mathrm{g}} = V + V_{\mathrm{wind}}, \tag{3.1}$$

where V_{wind} is the wind speed. The ground speed is the vector addition of the other two speeds. This is why ORD-BOS typically takes 2 hours and 20 minutes, but BOS-ORD takes 2 hours and 50 minutes; yet, in each case, the aircraft is flying at a typical cruise velocity, requiring the same amount of total thrust.

Airspeed measurement. A pitot-static tube (or a pitot tube with a separate static source) is used to measure an aircraft's airspeed. The static source senses the static pressure of the freestream air p_∞, and the pitot tube senses the air's total pressure p_0. These pressures are fed to either a mechanical or digital airspeed measurement system. In a mechanical system, static and total pressures are fed to opposite sides of a thin, metallic, airspeed diaphragm. The diaphragm is in a sealed case as shown in figure 3.1.

The mechanical expansion and contraction of the diaphragm (which is coupled to a system of gears and levers) translates the pressure difference ($p_0 - p_\infty$ or Δp) into a reading on the aircraft's airspeed indicator. The airspeed the pilot sees on the face of this instrument is called the indicated airspeed V_{i}. From the dynamic pressure equation, we know that

$$q_\infty = p_0 - p_\infty = \Delta p = \frac{1}{2}\rho V_{\mathrm{i}}^2, \tag{3.2}$$

thus,

$$V_{\mathrm{i}} = \sqrt{2\frac{\Delta p}{\rho}} \tag{3.3}$$

True airspeed. The following equation defines true airspeed as a function of density and pressure, and is valid for incompressible and compressible subsonic flow.

$$V = \sqrt{7\frac{p_\infty}{\rho}\left[\left(\frac{\Delta p}{p_\infty}+1\right)^{\frac{\gamma-1}{\gamma}} - 1\right]}, \tag{3.4}$$

where γ is the specific heat ratio, which is 1.4 for diatomic gases.

Calibrated airspeed. In the factory, airspeed indicators are machined with gears calibrated to use *sea-level standard atmospheric* values of p and ρ. So, in effect, an airspeed indicator is calibrated to solve the expression

$$V_{\mathrm{c}} = \sqrt{7\frac{p_{\mathrm{SL}}}{\rho_{\mathrm{SL}}}\left[\left(\frac{\Delta p}{p_{\mathrm{SL}}}+1\right)^{\frac{\gamma-1}{\gamma}} - 1\right]}, \tag{3.5}$$

Copyright © 2025 Xiaowei He

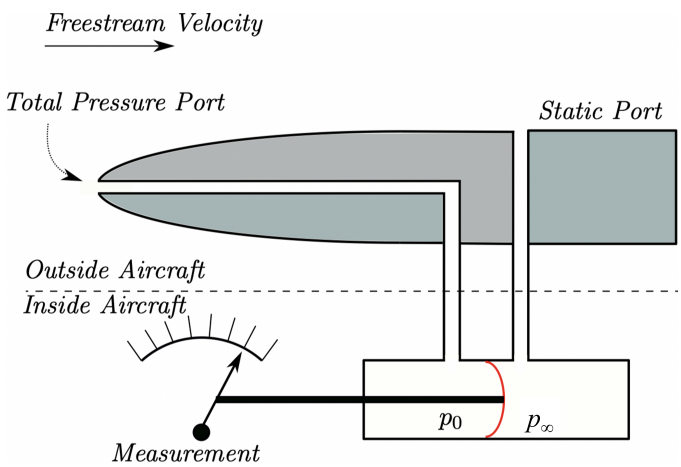

Figure 3.1: Aircraft pitot–static airspeed system [3].

where V_c is the calibrated airspeed. However, this is still not what is indicated on the airspeed indicator. The static ports on the aircraft may be located such that they do not accurately measure the freestream static pressure under all flight conditions. This is referred to as the position or installation error. Additionally, there may be small inaccuracies in the machining of the instrument. To account for these discrepancies, errors are quantified during flight testing and equated to a velocity change (ΔV_p) called position error. Therefore, the relationship between what is displayed on the airspeed indicator (indicated airspeed V_i) and the calibrated airspeed is given as

$$V_c = V_i + \Delta V_p. \tag{3.6}$$

To obtain true airspeed V from calibrated airspeed V_c, two corrections must be made—one for the actual existing pressure, and the other for the actual density. We adopt a two-step approach.

Equivalent airspeed. The first correction is for the actual pressure at a given altitude. This gives the equivalent airspeed

$$V_e = \sqrt{7\frac{p_\infty}{\rho_{SL}}\left[\left(\frac{\Delta p}{p_\infty}+1\right)^{\frac{\gamma-1}{\gamma}}-1\right]}. \tag{3.7}$$

Note that the values of actual pressure are used here, as opposed to the sea-level values in the calibrated airspeed. To relate V_c to V_e, a pressure correction factor f is used

$$V_e = fV_c. \tag{3.8}$$

Note that f depends only on Δp and p_∞. All other variables are constant.

The second step is to tackle the density correction. True airspeed may be calculated from equivalent airspeed by accounting for the actual density at the correct altitude

$$V = V_e\sqrt{\frac{\rho_{SL}}{\rho}} \tag{3.9}$$

Because the density ratio ρ_{SL}/ρ is usually $\geqslant 1$, V is usually $\geqslant V_e$. Notice, if we are flying at sea level on a standard day, $\rho_{SL}/\rho = 1$, and from the equation above, $V = V_e$. In other words, V_e is the same as true airspeed V at sea level on a standard day.

The following summarizes the discussion on airspeed:

Copyright © 2025 Xiaowei He

(1) indicated to calibrated: apply position error ΔV_p

$$V_\mathrm{c} = V_\mathrm{i} + \Delta V_\mathrm{p}; \tag{3.10}$$

(2) calibrated to equivalent: adjust for actual pressure at altitude

$$V_\mathrm{e} = f V_\mathrm{c}; \tag{3.11}$$

(3) equivalent to true: adjust for actual density at altitude

$$V = V_\mathrm{e}\sqrt{\frac{\rho_\mathrm{SL}}{\rho}}; \tag{3.12}$$

(4) true to ground speed: vector addition of wind to true airspeed

$$V_\mathrm{g} = V + V_\mathrm{wind}. \tag{3.13}$$

A handy aid used by pilots is the acronym ICE-T (Indicated, Calibrated, Equivalent, and True Airspeed). When used with the radical sign as shown in figure 3.2, it relates the magnitudes of all the different velocities to each other. Notice that indicated and calibrated airspeeds are nearly the same. Equivalent is usually less than calibrated, and true airspeed is usually greater than the others.

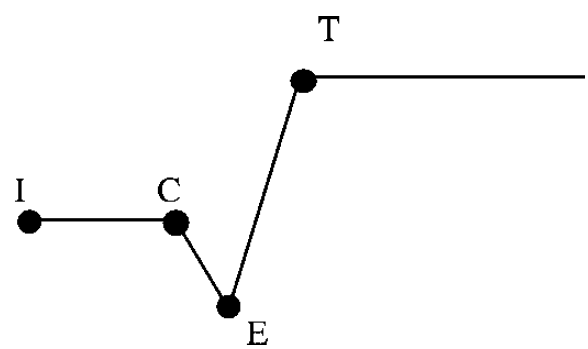

Figure 3.2: ICE-T convention [6].

3.2 Steady and level flight

Consider an aircraft flying a curvilinear path as shown in figure 3.3. To fly a curved path, a net force (F_net), composed of force components parallel and perpendicular to the flight path, must exist. In applying Newton's second law, acceleration parallel (linear or tangential) to the flight path is $\mathrm{d}V/\mathrm{d}t$, and acceleration perpendicular to the flight path (centripetal) is V^2/r, where r is the radius of curvature of the curvilinear path.

Copyright © 2025 Xiaowei He

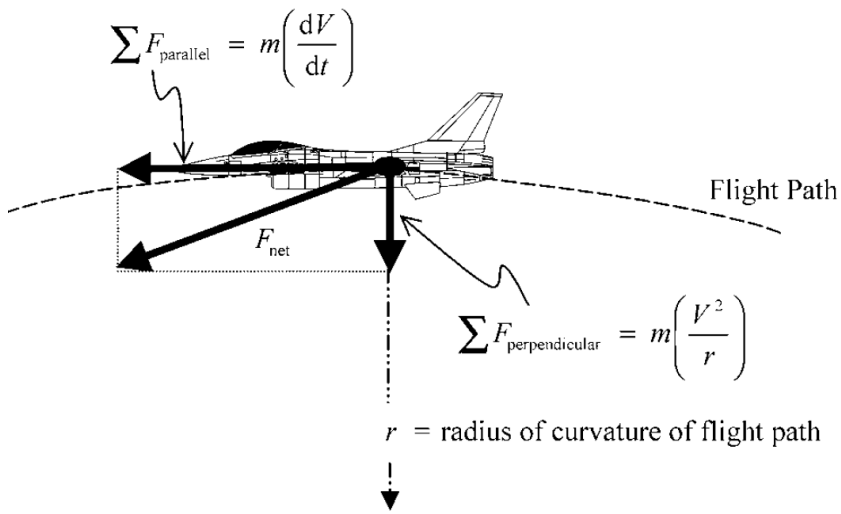

Figure 3.3: Aircraft flying a curvilinear path [6].

Figure 3.4 shows the lift, drag, thrust, and weight acting on an aircraft in steady and level flight.

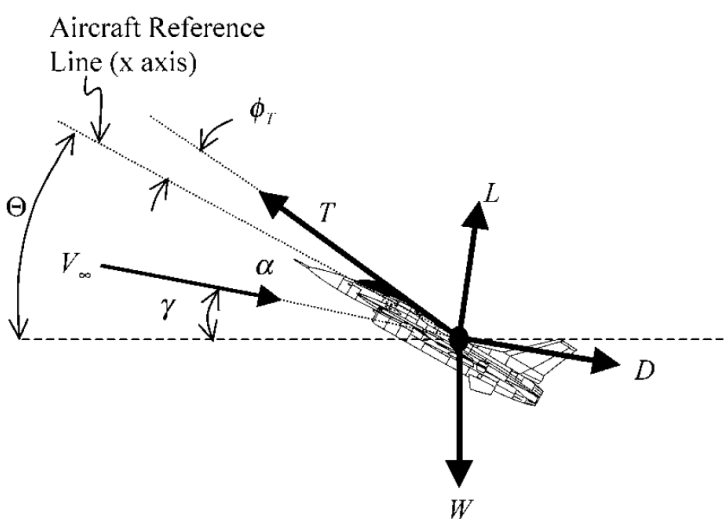

Figure 3.4: Forces and angles acting on an aircraft in flight [6].

A few points to remember about the figure:

(1) lift and drag, as discussed in section 1.3.3, are the components of the aerodynamic force perpendicular and parallel to the relative wind V_∞, i.e., defined in the wind (stability) axes;

(2) the x axis is a body-fixed axis, aligned with the "reference line" of the aircraft;

(3) the aircraft's angle of attack α is between the x axis and the relative wind V_∞;

(4) in general, the thrust vector is not aligned with the aircraft's reference line but is displaced through the thrust angle ϕ_T (recall equation (2.5));

(5) the flight path angle γ is the angle between the horizon ($x_\mathrm{E}y_\mathrm{E}$ plane) and the relative wind V_∞ (refer to figure 2.8a);

(6) the pitch angle θ is the angle between the aircraft's reference line x_b and the horizon ($x_\mathrm{E}y_\mathrm{E}$ plane),

Copyright © 2025 Xiaowei He

which is sometimes referred to as pitch attitude or the deck angle (on transports, the cargo deck is usually taken as the aircraft's reference line).

3.2.1 Equations of motion

Recall the brief review on dynamics from section 1.3.1, figure 3.4 is the free-body diagram of the equilibrium steady flight. Summing the external forces, parallel and perpendicular to the flight path, to apply Newton's second law

$$\begin{aligned} \Sigma F_{x_\mathrm{b}} = \Sigma F_{\parallel} &= m\frac{\mathrm{d}V}{\mathrm{d}t} = T\cos(\alpha+\phi_T) - D - W\sin\gamma, \\ \Sigma F_{x_\mathrm{b}} = \Sigma F_{\perp} &= m\frac{V^2}{r} = W\cos\gamma - L - T\sin(\alpha+\phi_T), \end{aligned} \tag{3.14}$$

Consider the special case of straight, level, and unaccelerated flight (SLUF). We will apply these assumptions to the general EOM from equation (3.14):

(1) we assume that the aircraft is a point mass, whereby we assume that the aircraft dimensions are negligible when compared to the dimensions of motion.

(2) "steady" means no acceleration, so we can infer from Newton's first law that the sum of forces acting on the aircraft is zero, which is the *equilibrium* steady flight condition.

(3) "straight" implies that the aircraft's radius of curvature approaches infinity; therefore, the centripetal acceleration term V^2/r goes to zero;

(4) the flight path angle γ is zero for "level" flight, then $\cos\gamma = 1$ and $\sin\gamma = 0$;

(5) linear acceleration $\mathrm{d}V/\mathrm{d}t$ is zero for "unaccelerated" flight.

If we assume the thrust angle and angle of attack are small, then $\cos(\alpha+\phi_T) \approx 1$ and $\sin(\alpha+\phi_T) \approx 0$. The EOM reduced to

$$L = W, \text{ (load factor } n = 1) \tag{3.15}$$

$$T = D. \tag{3.16}$$

A simple, yet useful, result for level unaccelerated flight is that an aircraft's lift balances its weight and the engines must produce sufficient thrust to overcome aerodynamic drag, as shown in figure 3.5.

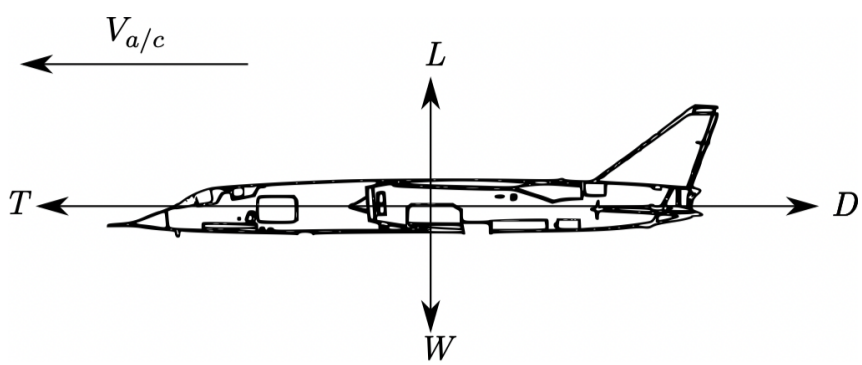

Figure 3.5: Force balance in steady, level, and unaccelerated flight [3].

Copyright © 2025 Xiaowei He

3.2.2 Vertical force

For equation (3.15), recall that lift coefficient is defined as

$$C_L = \frac{L}{\frac{1}{2}\rho V^2 S}. \tag{3.17}$$

Substituting L with W, we have

$$C_L = \frac{W}{\frac{1}{2}\rho V^2 S}. \tag{3.18}$$

Thus

$$V = \sqrt{\frac{2W}{\rho S C_L}}. \tag{3.19}$$

Equation (3.19) is called the aircraft speed equation for steady-level flight, and some basic aerodynamic behavior may be inferred from it.

- Slower flight is possible by reducing wing loading—reducing aircraft mass, or increasing wing area. Or by increasing C_L—increasing α.
- The minimum possible flight speed occurs at $C_{L_{\max}}$—just before stall. The *stall speed* may be determined if $C_{L_{\max}}$ is known.
- Flight speed may be increased by reducing ρ—by flying at increased altitude.

3.2.3 Longitudinal force

Similarly, for the longitudinal EOM equation (3.16), drag coefficient can be written as

$$C_D = \frac{D}{\frac{1}{2}\rho V^2 S} = \frac{T}{\frac{1}{2}\rho V^2 S}. \tag{3.20}$$

In flight performance, we assume that the aircraft is operating in the region of linear aerodynamics, and utilize a drag model

$$C_D = C_{D_0} + K C_L^2, \tag{3.21}$$

where C_D is the total drag, C_{D_0} is the zero-incidence drag, and KC_L^2 is the induced drag plus α-dependent form drag, in which

$$K = \frac{k}{\pi AR}. \tag{3.22}$$

The parameter k is between 1.1 and 1.4 for most aircraft, and $AR = b^2/S$ (equation (1.7)) is the wing aspect ratio. K and C_{D_0} are usually constants, but can depend on

- configuration changes (flap deployment);
- Reynolds number (speed and height); The *stall speed* may be determined if $C_{L_{\max}}$ is known.
- compressibility (shock waves).

Equation (3.21) assumes that the minimum drag occurs at zero lift. This is the case for a symmetric airfoil, but not for a cambered one. Since most aircraft have a cambered wing, equation (3.21) is modified to

$$C_D = C_{D_{\min}} + K(C_L - C_{L_0})^2. \tag{3.23}$$

The second equation is more realistic for real aircraft but adds complexity to the algebra, and the difference between C_{D_0} and $C_{D_{\min}}$ is very small even for wings of moderate camber [9].

Equations (3.19) and (3.21) underpin the basics of aircraft performance.

Copyright © 2025 Xiaowei He

3.3 Thrust and power curves

3.3.1 Thrust required

Frequently, the term thrust required T_{R} is used—it is the amount of thrust necessary to overcome drag, regardless of the maneuver. For SLUF, thrust required is simply equal to the total aircraft drag, as equation (3.16) suggested. Combining with the total drag equation (3.21), we have

$$T_{\mathrm{R}} = D = (C_{D_0} + KC_L^2)\frac{1}{2}\rho V^2 S. \tag{3.24}$$

Plug in equation (3.18)

$$T_{\mathrm{R}} = C_{D_0}\frac{1}{2}\rho V^2 S + \frac{K(nW)^2}{\frac{1}{2}\rho V^2 S}, \tag{3.25}$$

where $n = L/W$ is the load factor, which is 1 in the SLUF condition since $L = W$.

We can rearrange equation (3.25) into

$$T_{\mathrm{R}} = AV^2 + BV^{-2}, \tag{3.26}$$

where A represents the profile drag and B represents the induced drag, which are functions of density (therefore of altitude).

3.3.2 Minimum drag speed

The minimum thrust/drag speed can be shown by taking derivatives of the above equations

$$\frac{\mathrm{d}T_{\mathrm{R}}}{\mathrm{d}V} = 2AV - 2BV^{-3} = 0. \tag{3.27}$$

Solve for V

$$V_{\mathrm{md}} = \left[\frac{B}{A}\right]^{\frac{1}{4}} = \left[\frac{2W}{\rho S}\right]^{\frac{1}{2}}\left[\frac{K}{C_{D_0}}\right]^{\frac{1}{4}}. \tag{3.28}$$

3.3.3 Thrust curve

Thrust available T_{A}, on the other hand, is the amount of thrust available to the pilot and is strictly engine(s) dependent. T_{A} is a function of altitude, airspeed, and throttle setting. Figure 3.6 is a generic thrust curve, where T_{R} and T_{A} are plotted as a function of velocity (or Mach number).

A lot of information is captured in an aircraft's thrust curve. Remember that drag (therefore, T_{R}) changes with altitude, weight/load factor, and/or configuration. Change any of these, and the thrust required curve changes.

(1) Assume the pilot's maximum thrust available is represented by the $T_{\mathrm{A})_1}$ curve. Note the following:
   (a) At all airspeeds below V_5, thrust available exceeds thrust required. Therefore, by adjusting the throttle, SLUF can be achieved at any point on the T_{R} curve.
   (b) At low airspeeds, the aircraft is "stall limited". Even though there is sufficient thrust available to overcome drag (i.e., T_{R}), the aircraft stalls below V_1 (recall that equation (3.19) does not involve drag).
   (c) V_5 is the maximum velocity achievable in SLUF conditions.

(2) Assume the pilot adjusts the throttle to the thrust available represented by the $T_{\mathrm{A})_2}$ curve. Note the following:

Copyright © 2025 Xiaowei He

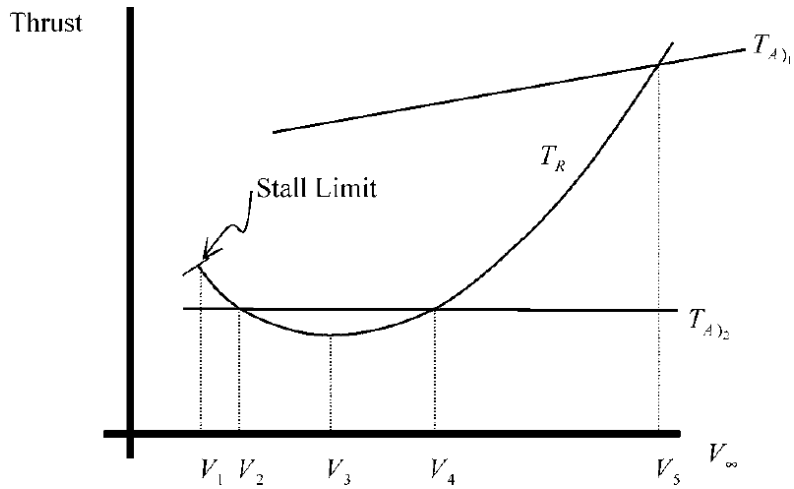

Figure 3.6: Generic thrust curves [6].

(a) SLUF can only be achieved at V_2 and V_4.

(b) Below V_2 and beyond V_4, the thrust required exceeds the thrust available. The aircraft will slow down to either the stall limit or to V_4.

(c) Between V_2 and V_4, thrust available exceeds thrust required, and the aircraft will accelerate to V_4. To stabilize the aircraft in SLUF at V_2, the pilot must generally reduce power, increase angle of attack, and then increase power back to $T_{\mathrm{A})_2}$ to achieve this slow flight condition.

(3) V_3 is an extremely significant airspeed at which total aircraft drag (or T_{R}) is a minimum (i.e., minimum drag speed defined in equation (3.28)). The ratio of lift to drag (L/D) is maximized. Also, parasite and induced drag are equal.

3.4 Thrust-to-weight ratio and wing loading

The thrust-to-weight ratio, T/W, and the wing loading, W/S, are the two most important parameters affecting aircraft performance. It is essential to recognize that wing loading and thrust-to-weight ratio are closely interrelated for most performance calculations. One example is the takeoff distance. A requirement for a short takeoff can be met by using a large wing (low W/S) with a relatively small engine (low T/W). Whereas the small engine will cause the aircraft to accelerate slowly, it only needs to reach a moderate speed to lift off the ground. On the other hand, the same takeoff distance can be met with a small wing (high W/S), provided that a large engine (high T/W) is also used. In this case, the aircraft must reach a high speed to lift off, the the large engine can rapidly accelerate the aircraft to that speed.

3.4.1 Thrust-to-weight ratio

An aircraft with a higher T/W can accelerate more quickly, climb more rapidly, reach a higher maximum speed, and sustain higher turn rates. On the other hand, the larger engines are heavier and will consume more fuel throughout the mission, which will drive up the aircraft's takeoff gross weight to perform the mission.

Table 3.2 provides typical values for T/W for jet aircraft. There is a wide variation for commercial transport. The higher values are for two-engine airplanes, while the lower values are for four-engine airplanes. At takeoff weights, a modern fighter plane approaches a T/W of 1.0, implying that the thrust

Copyright © 2025 Xiaowei He

is nearly equal to the weight. At combat conditions, when some fuel has been burned off, these aircraft have T/W values exceeding 1.0 and are capable of accelerating while going straight up.

Table 3.2: Thrust-to-weight ratio, T/W [10].

Aircraft type	Typical installed T/W
Jet trainer	0.4
Jet fighter (dogfighter)	0.9
Jet fighter (other)	0.6
Military cargo/bomber	0.25
Jet transport (higher value for fewer engines)	0.25–0.4

It is important to avoid confusing the takeoff T/W with the T/W at other conditions. During the flight, the weight drops as fuel is burned off. The thrust changes at different speeds, altitudes, and throttle settings. When a required T/W is calculated at a flight condition, it must be adjusted back to the original takeoff condition so that it can be compared to other required values of T/W.

Thrust matching. A simple calculation of the required T/W ratio during cruise can be performed using the "thrust matching" method. This compares the thrust available during cruise to the estimated aircraft drag. In SLUF, the weight must equal the lift (equation (3.15)), and the thrust must equal the drag (equation (3.16)). Combining these relationships indicates that the T/W must equal the inverse of L/D,

$$\left(\frac{T}{W}\right)_{\text{cruise}} = \frac{1}{(L/D)_{\text{cruise}}}. \tag{3.29}$$

Thrust-to-weight ratio is often determined by a climb requirement rather than by cruise conditions. T/W for a climb requirement can be found from a small adjustment to equation (3.29), such that

$$\left(\frac{T}{W}\right)_{\text{climb}} = \frac{1}{(L/D)_{\text{climb}}} + \frac{V_{\text{v}}}{V_\infty}, \tag{3.30}$$

where V_{v} is the vertical velocity of the aircraft, also known as the rate of climb (will be discussed in section 3.7.2). The T/W for climb is the T/W for level flight plus the extra thrust required for the climb gradient. Note that the L/D for climb might be lower than the L/D during cruising flight, especially during initial climb when the gear and flaps might still be down.

T/W to takeoff conditions. The required T/W for takeoff can be adjusted from cruise to takeoff conditions using equation (3.31),

$$\left(\frac{T}{W}\right)_{\text{takeoff}} = \left(\frac{T}{W}\right)_{\text{cruise}} \left(\frac{W_{\text{cruise}}}{W_{\text{takeoff}}}\right) \left(\frac{T_{\text{takeoff}}}{T_{\text{cruise}}}\right). \tag{3.31}$$

Note that the takeoff thrust value is in the numerator, not in the denominator, as was the case for the weight adjustment. Typically, a subsonic, high-bypass-ratio turbofan for a transport aircraft will have a cruise thrust of $20 - 25\%$ of the takeoff thrust, while a low-bypass afterburning turbofan or turbojet will have a cruise thrust of $40 - 70\%$ of the takeoff maximum value.

3.4.2 Wing loading

The wing loading, W/S is the weight of the aircraft divided by the area of the reference wing. Wing loading affects stall speed, climb rate, takeoff and landing distance, and turn performance. The wing

Copyright © 2025 Xiaowei He

loading determines the design lift coefficient and impacts drag through its effect upon wetted area and wing span—if the wing loading is reduced, the wing is larger. This usually improves performance, but the additional drag and empty weight due to the larger wing will increase the takeoff gross weight to perform the mission. Table 3.3 provides representative wing loadings.

Table 3.3: Wing loading, W/S [10].

Histroical trends	Typical takeoff W/S [kg/m^2]
Sailplane	30
Homebuilt	54
General aviation—single engine	83
General aviation—twin engine	127
Twin turboprop	195
Jet trainer	244
Jet fighter	342
Jet transport/bomber	586

For performance calculations, the weight term in W/S must be the actual weight of the aircraft at that time. When calculating performance for a known aircraft weight, the wing loading is reduced from the takeoff value to take into account the fuel that has been burned by that time.

Stall speed. The stall speed is the minimum airspeed at which an aircraft can fly to prevent a sudden loss of lift. The stall speed is directly determined by the wing loading and the maximum lift coefficient. Stall speed is a major contributor to flying safety, with a substantial number of fatal accidents each year due to "failure to maintain flying speed". Also, the liftoff speed during takeoff and the approaching speed during landing both depend on the stall speed.

The stall speed can be found from the fact that lift must equal weight when there is no vertical acceleration. At stall speed, the aircraft is utilizing its maximum lift coefficient such that

$$W = L = \frac{1}{2}\rho V_{\text{stall}}^2 S C_{L_{\max}} \ . \tag{3.32}$$

Therefore,

$$V_{\text{stall}} = \sqrt{\frac{2W}{\rho S C_{L_{\max}}}} = \sqrt{\frac{2}{\rho C_{L_{\max}}}\left(\frac{W}{S}\right)} \ . \tag{3.33}$$

As equation (3.33) shows, the stall speed is determined by the wing loading, maximum lift coefficient, and the local air density (which is altitude dependent).

3.5 Takeoff

Takeoff is one of the most demanding phases of flight. The aircraft's engines typically operate at maximum rating. Airspeeds are low, so control is minimal. Combine these considerations with low altitude, and there is little room for error. In this section, we will examine the forces during takeoff and apply Newton's second law to predict takeoff performance.

Copyright © 2025 Xiaowei He

3.5.1 Takeoff phases and ground roll distance

As shown in figure 3.7, takeoff performance includes a ground roll, aircraft rotation, transition, and climb-out phase. In our discussion, we will address only the ground-roll distance S_G. As shown, the velocity corresponding to S_G is V_G.

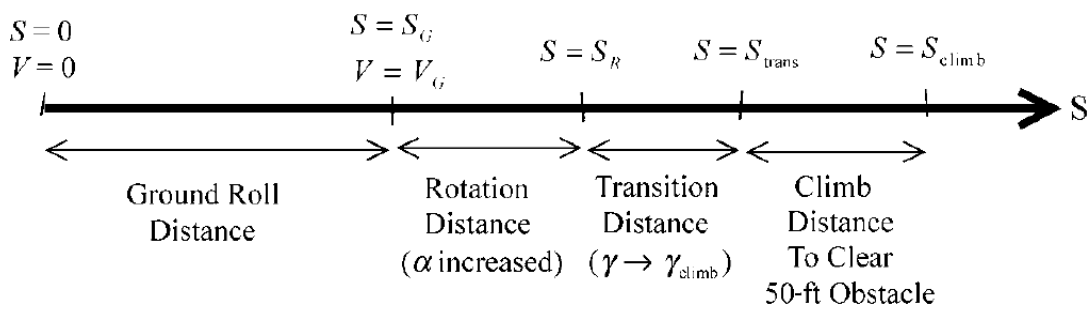

Figure 3.7: Takeoff phases [6].

V_G is the liftoff velocity V_LOF corrected for winds, such that $V_\mathrm{G} = V_\mathrm{LOF} + / - V_\mathrm{wind}$, in which we add for a tailwind or subtract for a headwind. The liftoff velocity is typically expressed as some factor above the aircraft's stall speed. We will use

$$V_\mathrm{LOF} = 1.1 V_\mathrm{stall}, \tag{3.34}$$

Referring to figure 3.7, we derive a general expression for the ground-roll distance assuming no wind and integrating between brake release (both S and V are equal to zero) and S_G (where V is V_G). By the chain rule,

$$\mathrm{d}S = \frac{\mathrm{d}S}{\mathrm{d}t}\frac{\mathrm{d}t}{\mathrm{d}V} = V\frac{1}{a}\mathrm{d}V, \tag{3.35}$$

where $a = \mathrm{d}V/\mathrm{d}t$ is the acceleration. Then integrate both sides from brake release to the ground roll distance S_G

$$\int_{S=0}^{S=S_\mathrm{G}} \mathrm{d}S = \int_{V=0}^{V=V_\mathrm{G}} \frac{1}{a} V \mathrm{d}V. \tag{3.36}$$

3.5.2 Forces during takeoff

To integrate the right-hand side of equation (3.36), we can (1) assume acceleration is a constant during the ground roll, or (2) account for acceleration change using a numerical approach. We will focus on the first approach in the following discussion. Nevertheless, the acceleration has to be evaluated in either case, which is obtained from Newton's second law.

We first identify the forces during the takeoff roll. Consider figure 3.8 in which the runway slope is greatly exaggerated. Lift, drag, thrust, and weight are shown. φ is the runway's slope—a positive slope is shown (worst case). Additionally, there is a retarding force R because of friction between the wheels and the runway. For small φ, the retarding force is approximated by

$$R \approx \mu_\mathrm{r}(W - L), \tag{3.37}$$

where μ_r is the rolling friction coefficient. Typical values of μ_r range between 0.02 for a dry concrete runway and 0.3 for very soft ground.

Copyright © 2025 Xiaowei He

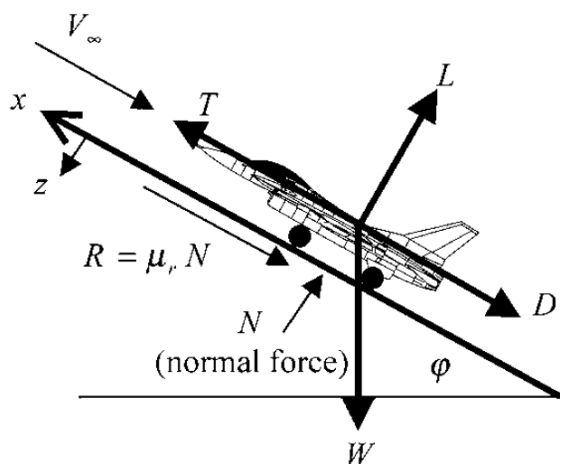

Figure 3.8: Forces during takeoff roll [6].

Apply Newton's second law in the x direction to obtain an expression for acceleration during the ground roll.

$$\Sigma F_x = ma_x = \frac{W}{g}a_x = T - D - W\sin\varphi - R. \tag{3.38}$$

If we, again, assume φ is small, hence $\sin\varphi \approx \varphi$, and

$$a_x \approx \frac{g}{W}[T - D - W\varphi - \mu_{\mathrm{r}}(W - L)] \tag{3.39}$$

If we further assume that the runway slope is zero. Additionally, ignore any thrust variation with velocity. Figure 3.9 shows how the forces change during the takeoff roll under these assumptions.

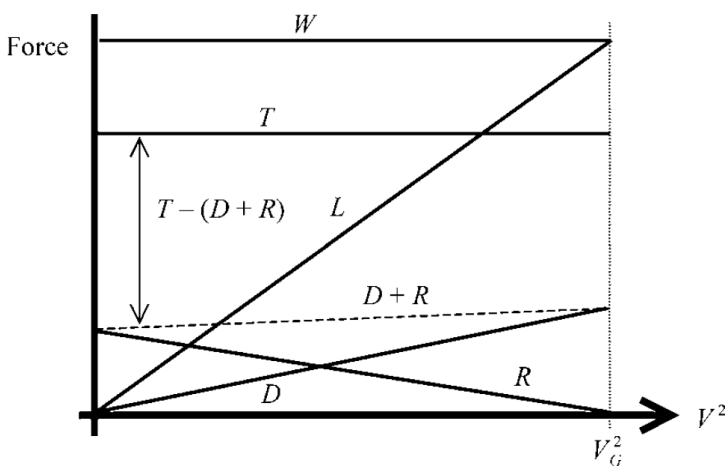

Figure 3.9: Variation of forces during takeoff roll [6].

Note the following:

- Lift and drag start at zero. They both increase through the takeoff roll; both forces are proportional to V_2.
- W is constant during the takeoff roll (ignoring fuel consumption).

Copyright © 2025 Xiaowei He

- R decreases during the takeoff roll because the normal force $N \approx W - L$ decreases as lift increases. R is zero at liftoff (weight is equal to lift).
- With the assumptions, the difference between thrust and $[D + \mu_\mathrm{r}(W - L)]$ is the net acceleration force (assuming $W\varphi$ is zero). This is a direct indicator of acceleration capability.

3.5.3 Average acceleration method

If we assume acceleration is constant (denoted by $\bar{a}$) during the takeoff roll, equation (3.36) can be integrated as

$$S_\mathrm{G} = \frac{1}{\bar{a}} \int_{V=0}^{V=V_\mathrm{G}} V \mathrm{d}V = \frac{1}{\bar{a}} \frac{V^2}{2}\bigg|_0^{V_\mathrm{G}} = \frac{V_\mathrm{G}^2}{2\bar{a}}. \tag{3.40}$$

A headwind will reduce V_G by the wind component parallel to the runway. Similarly, a tailwind will increase V_G. Thus, a headwind will decrease S_G and a tailwind will increase S_G. This is why the runway direction for takeoff (and landing) is generally selected based on having a headwind component. Equation (3.40) can be modified to account for a head or tailwind

$$S_\mathrm{G} = \frac{V_\mathrm{G}^2}{2\bar{a}} = \frac{(V_\mathrm{LOF} \pm V_\mathrm{wind})^2}{2\bar{a}}. \tag{3.41}$$

The minus sign is used for a headwind component and the plus sign is used for a tailwind component.

The averaged acceleration $\bar{a}$ can be represented by using average values of the variables in equation (3.39)

$$\bar{a} = \frac{g}{W}[T_\mathrm{avg} - D_\mathrm{avg} - W\varphi - \mu_\mathrm{r}(W - L_\mathrm{avg})], \tag{3.42}$$

for which, we assume thrust, aircraft weight, rolling friction coefficient, and runway slope are constant during the takeoff roll. To evaluate lift and drag, we will use an average velocity.

By definition,

$$D_\mathrm{avg} = \frac{D_{S=0} + D_{S=S_\mathrm{G}}}{2} = C_D \frac{1}{2}\rho V_\mathrm{avg}^2 S, \tag{3.43}$$

or

$$C_D \frac{1}{2}\rho V_\mathrm{avg}^2 S = \frac{C_D \frac{1}{2}\rho V_{S=0}^2 S + C_D \frac{1}{2}\rho V_{S=S_\mathrm{G}}^2 S}{2}. \tag{3.44}$$

For no wind conditions, $V_{S=0} = 0$, therefore

$$V_\mathrm{avg} = \frac{V_\mathrm{G}}{\sqrt{2}} = 0.707 V_\mathrm{LOF} \tag{3.45}$$

With a headwind or tailwind, V_avg could be adjusted slightly using this approach, but it is normally not, because the average velocity of equation (3.45) provides sufficient accuracy for the average acceleration method. If engine thrust data are available, thrust at V_avg should be used.

Additionally, recall that $D = (C_{D_0} + KC_L^2)\frac{1}{2}\rho V^2 S$, thus both L_avg and D_avg are functions of lift coefficient C_L, so is $\bar{a}$. Here $V = V_\mathrm{avg}$. If we maximize $\bar{a}$ with respect to C_L, we obtain an "optimal" lift coefficient $C_{L\mathrm{opt}}$. Taking partial derivatives for equation (3.42) we arrive at

$$\begin{aligned} 0 = \frac{\partial \bar{a}}{\partial C_L} &= \frac{\partial}{\partial C_L}\left(\frac{g}{W}[T_\mathrm{avg} - D_\mathrm{avg} - \mu_\mathrm{r}(W - L_\mathrm{avg}) - W\varphi]\right) \\ &= -2\frac{g}{W} K C_L \frac{1}{2}\rho V_\mathrm{avg}^2 S + \frac{g}{W}\mu_\mathrm{r}\frac{1}{2}\rho V_\mathrm{avg}^2 S. \end{aligned} \tag{3.46}$$

Copyright © 2025 Xiaowei He

Solving for C_L,

$$C_L = \frac{\mu_\mathrm{r}}{2K} = C_{L_\mathrm{opt}}. \tag{3.47}$$

At this point, L_avg and D_avg can be computed through C_{L_opt}, and $\bar{a}$ in equation (3.42) can be obtained.

Example 3.1

Using the average acceleration method, find the max power takeoff ground roll, with no wind and a zero runway slope, for a $5,443\,\mathrm{kg}$ ($12,000\,\mathrm{lbf}$) T-38 at sea level and $1,828\,\mathrm{m}$ ($6,000\,\mathrm{ft}$), respectively, given the following conditions:

$$S = 15.8\,\mathrm{m}^2\ (170\,\mathrm{ft}^2), \qquad C_{L_\mathrm{max}} = 0.88, \qquad \mu_\mathrm{r} = 0.025, \qquad C_{D_0} = 0.02, \qquad K = 0.2.$$

Additionally, the air density at sea level and $1,828\,\mathrm{m}$ are, respectively,

$$\rho_0 = 1.255\,\mathrm{kg/m^3}, \qquad \rho_1 = 1.049\,\mathrm{kg/m^3}.$$

Assume the average thrust of T-38 at these altitudes at certain demanded Mach numbers is

$$T_{\mathrm{avg}_0} \approx 26.69\,\mathrm{kN}\ (6,000\,\mathrm{lbf}), \qquad T_{\mathrm{avg}_1} \approx 22.69\,\mathrm{kN}\ (5,100\,\mathrm{lbf}).$$

Solution: First, work the problem for sea level. Using equation (3.33), we determine the stall speed

$$V_\mathrm{stall} = \sqrt{\frac{2mg}{\rho_0 S C_{L\mathrm{max}}}} = \sqrt{\frac{2 \cdot 5443\,\mathrm{kg} \cdot 9.81\,\mathrm{m/s^2}}{1.255\,\mathrm{kg/m^3} \cdot 15.8\,\mathrm{m^2} \cdot 0.88}} = 78.2\,\mathrm{m/s}.$$

Therefore, the liftoff speed is determined by equation (3.34)

$$V_\mathrm{LOF} = 1.1 V_\mathrm{stall} = 1.1 \cdot 78.2\,\mathrm{m/s} = 86.0\,\mathrm{m/s},$$

and the average velocity is determined by equation (3.45)

$$V_\mathrm{avg} = 0.707 V_\mathrm{LOF} = 0.707 \cdot 86.0\,\mathrm{m/s} = 60.8\,\mathrm{m/s}.$$

Thus, the average Mach number is

$$M_\mathrm{avg} = \frac{V_\mathrm{avg}}{a_\mathrm{SL}} = \frac{60.8\,\mathrm{m/s}}{343\,\mathrm{m/s}} = 0.18,$$

where a_SL is the speed of sound at sea level. The T-38 sea-level thrust and drag chart at max power and $0.18\,\mathrm{Ma}$ was given by

$$T_{\mathrm{avg}_0} \approx 26.69\,\mathrm{kN}.$$

To calculate L_avg and D_avg, first find C_{L_opt} by equation (1.38)

$$C_{L_\mathrm{opt}} = \frac{\mu_\mathrm{r}}{2K} = \frac{0.025}{2 \cdot 0.2} = 0.0625.$$

Then

$$C_{D_\mathrm{avg}} = C_{D_0} + K C_{L_\mathrm{opt}}^2 = 0.02 + 0.2 \cdot 0.0625^2 = 0.0208.$$

Copyright © 2025 Xiaowei He

Therefore, the average lift and drag are calculated

$$L_{\text{avg}} = C_{L_{\text{opt}}} \frac{1}{2}\rho_0 V_{\text{avg}}^2 S = 0.0625 \cdot \frac{1}{2} \cdot 1.255\,\text{kg/m}^3 \cdot (60.8\,\text{m/s})^2 \cdot 15.8\,\text{m}^2 = 2.29\,\text{kN},$$
$$D_{\text{avg}} = C_{D_{\text{avg}}} \frac{1}{2}\rho_0 V_{\text{avg}}^2 S = 0.0208 \cdot \frac{1}{2} \cdot 1.255\,\text{kg/m}^3 \cdot (60.8\,\text{m/s})^2 \cdot 15.8\,\text{m}^2 = 0.76\,\text{kN},$$

and the average acceleration is found as

$$\begin{aligned}\bar{a} &= \frac{g}{W}[T_{\text{avg}} - D_{\text{avg}} - \mu_{\text{r}}(W - L_{\text{avg}})] \\ &= \frac{9.81\,\text{m/s}^2}{5443\,\text{kg} \cdot 9.81\,\text{m/s}^2} \cdot [26.69\,\text{kN} - 0.76\,\text{kN} - 0.025 \cdot (5443\,\text{kg} \cdot 9.81\,\text{m/s}^2 - 2.29\,\text{kN})] \\ &= 4.53\,\text{m/s}^2.\end{aligned}$$

For no wind case, $V_{\text{G}} = V_{\text{LOF}}$ so the ground roll is

$$S_{\text{G}_{\text{SL}}} = \frac{V_{\text{G}}^2}{2\bar{a}} = \frac{(86.0\,\text{m/s})^2}{2 \cdot 4.53\,\text{m/s}^2} = 816.3\,\text{m}$$

The same steps can be used to calculate the ground roll at $1,828\,\text{m}$ with appropriate changes in air density, the speed of sound, and interpolation of the T-38 thrust curves (T_{avg_1}). This is left as one of the homework problems.

3.5.4 Numerical method

The average acceleration method discussed how to solve the takeoff distance problem, assuming that acceleration remains constant and can be defined at $V_{\text{avg}} = V_{\text{G}}/\sqrt{2}$. This may not be a good assumption for some airplanes if the acceleration varies significantly during the takeoff roll. For many airplanes, the takeoff acceleration drops off somewhat as V_{LOF} is approached. To obtain a more precise prediction of the takeoff roll, a numerical integration technique or a numerical method may be used.

Euler method. The Euler method for numerical integration may be used for the analysis of the acceleration during takeoff. Recall equation (3.39)

$$a_x \approx \frac{g}{W}[T - D - W\varphi - \mu_{\text{r}}(W - L)].$$

Rewrite equation (3.39) in terms of C_L and C_D

$$a = \frac{g}{W}\left[T - W\varphi - \mu_{\text{r}}W - (C_D - \mu C_L)\frac{1}{2}\rho V^2 S\right], \tag{3.48}$$

which gives the instantaneous acceleration at any point during the ground roll. Assuming the pitch attitude of the aircraft remains constant during the ground roll, the angle of attack of the aircraft will remain constant along with C_L and C_D. If we also assume that ρ, W, and μ_{r} remain constant, then the determination of the acceleration at any point during the ground roll becomes a function of the thrust T and the velocity V. Using the Euler method, the takeoff roll can be divided into several small time intervals. Assuming the acceleration is constant during each interval, obtain the velocity at the end of each interval. Figure 3.10 illustrates this approach.

The time interval, Δt, is usually a constant and made as small as practical (not larger than $0.1\,\text{s}$).

Copyright © 2025 Xiaowei He

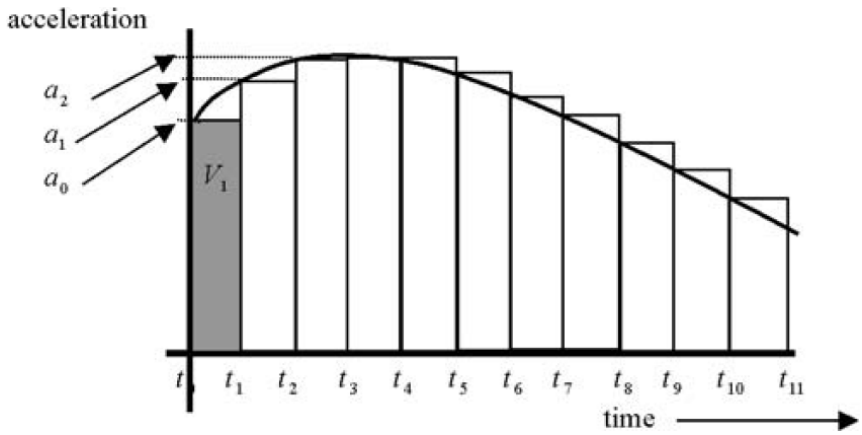

Figure 3.10: Euler integration to obtain velocity [6].

For the first interval, $V_0 = 0$ at $t_0 = 0$ (because this is at brake release), and the initial acceleration is

$$a_0 = \frac{g}{W}[T|_{V=0} - W\varphi - \mu_{\mathrm{r}} W]. \tag{3.49}$$

The velocity V_1 at time t_1 can be computed using the Euler method

$$V_1 = V_0 + a_0(t_1 - t_0) = a_0 \Delta t. \tag{3.50}$$

The velocity V_2 can be calculated in a similar way using the result for V_1 and equation (3.48) for acceleration

$$V_2 = V_1 + a_1(t_2 - t_1) = V_1 + a_1 \Delta t \tag{3.51}$$

with

$$a_1 = \frac{g}{W}\left[T - W\varphi - \mu_{\mathrm{r}} W - (C_D - \mu C_L)\frac{1}{2}\rho V_1^2 S\right]. \tag{3.52}$$

The general form of the Euler integration for velocity then becomes

$$V_{n+1} = V_n + a_n \Delta t. \tag{3.53}$$

Using this approach and a series of integrations, the ground roll velocity can be determined as a function of time.

The distance traveled during each time interval can be determined by applying the Euler method to the velocity versus time characteristics. Assuming that V is constant over each time interval, figure 3.11 illustrates this approach.

Remembering that S_0 and V_0 are zero, we have

$$S_1 = S_0 + V_0(t_1 - t_0) = 0, \tag{3.54}$$

and

$$S_2 = S_1 + V_1(t_2 - t_1) = S_1 + V_1 \Delta t, \tag{3.55}$$

or in general form,

$$S_{n+1} = S_n + V_n(t_{n+1} - t_n) = S_n + V_n \Delta t. \tag{3.56}$$

Copyright © 2025 Xiaowei He

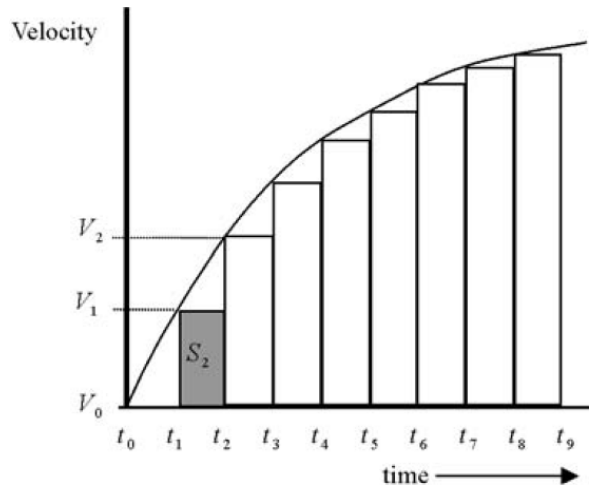

Figure 3.11: Euler integration to obtain distance [6].

Because the velocity curve is much steeper than the acceleration curve, the Euler method results in considerable error unless Δt is chosen to be very small. Greater accuracy can be achieved using Heun's predictor–corrector method (often referred to as the modified Euler method).

Heun's method. Heun's method uses an average of the dependent variable value for each time interval rather than the value at the beginning of the interval. For rapidly changing curves, such as takeoff velocity vs time, Heun's method improves the accuracy of the integration over that provided by the Euler method if the same Δt is used. This is illustrated in figure 3.12.

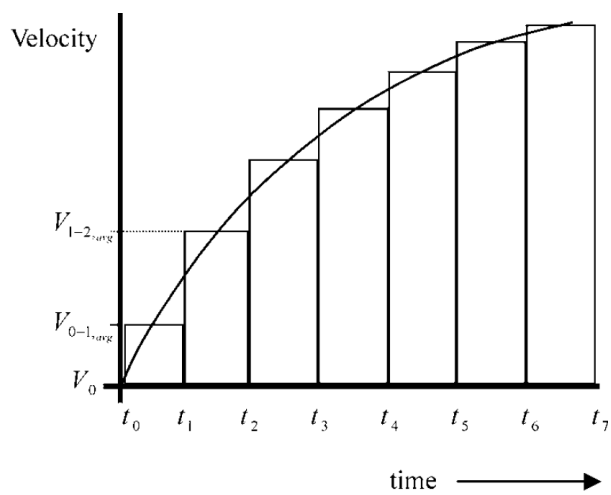

Figure 3.12: Euler integration to obtain distance [6].

For takeoff distance, the equations become

$$
\begin{aligned}
S_1 &= S_0 + \frac{V_0 + V_1}{2}\Delta t \\
S_2 &= S_1 + \frac{V_1 + V_2}{2}\Delta t,
\end{aligned}
\tag{3.57}
$$

Copyright © 2025 Xiaowei He

or in general form

$$S_{n+1} = S_n + \frac{V_n + V_{n+1}}{2}\Delta t. \tag{3.58}$$

Summary of the numerical approach. The Euler method works well for relatively flat curves, such as acceleration versus time during a takeoff roll. As discussed, Heun's method provides more accuracy when integrating the velocity vs time curve to obtain distance. Several other numerical integration methods may also be used; however, with the speed of modern computers, Δt can be made very small, and good accuracy can be obtained using the following approach to numerically determine takeoff distance:

(1) Choose a Δt as small as practical but not larger than 0.1 s.

(2) Compute a_0 using equation (3.48) and remembering that $V_0 = 0$ and $S_0 = 0$ at time $t_0 = 0$.

(3) Use the Euler method (equation (3.53)) to compute V_1.

(4) Use Heun's method (equation (3.58)) to compute S_1.

(5) Increment the time by $t_{n+1} = t_n + \Delta t$.

(6) Repeat Steps 2–5 for succeeding time intervals until $V_n = V_{\text{LOF}} \pm V_{\text{wind}}$. Remember that the acceleration term a_n in equation (3.53) is computed using equation (3.48) and V_n for each iteration.

If needed, even more accurate numerical methods such as a Runge–Kutta integration.

3.6 Landing

Landing is another very demanding phase of flight. As with takeoff, the aircraft is operating at airspeeds near the stall. In addition, precise control of the flight path is important to ensure touchdown at the desired point on the runway and with a minimum sink rate. Another challenge involved in landing is dissipating the energy of the aircraft once on the ground to bring it to a stop. Landing performance is very dependent on pilot technique.

3.6.1 Landing phases

Landing performance is generally divided into three phases:

(1) **Approach.** The approach is typically flown at approximately $1.3V_{\text{stall}}$ to allow a margin of safety above the stall for turbulence and control input perturbations.

(2) **Flare.** The flare is generally initiated within a wingspan of the ground and consists of a gradual power reduction to idle and an increase in the angle of attack to slow the aircraft to approximately $1.3V_{\text{stall}}$ for touchdown (V_{TD}) and to reduce the aircraft's sink rate.

(3) **Ground roll.** The ground-roll phase begins after touchdown with the objective of bringing the aircraft to a stop. To minimize the ground-roll distance, the total retarding force acting on the aircraft must be maximized. The retarding force may consist of brake application, drag from a drag chute and/or speed brakes, and reverse thrust, in addition to the normal drag of the aircraft. Pilot techniques are also important during the ground roll. For example, on some aircraft, holding full aft stick during the ground roll provides a favorable tradeoff between increased aircraft drag and reduced download on the main gear.

3.6.2 Forces and acceleration

The forces during landing ground roll include those discussed for takeoff in section 3.5. For landing, the rolling friction coefficient μ_{r} becomes much larger because of the application of brakes (≈ 0.5 for a dry concrete runway with the brakes fully applied), the drag D may become significantly larger because

Copyright © 2025 Xiaowei He

of speed brakes and/or a drag chute, and the aircraft thrust will be a small value or negative (if thrust reversing is used). Referring to equation (3.39) with the assumption of a level runway ($\varphi = 0$), we have

$$a_x \approx -\frac{g}{W}[-T + D + \mu_{\mathrm{r}}(W - L)]. \tag{3.59}$$

Note that the opposite signs in equation (3.59) emphasize deceleration, which gives $-a_x$ in the negative x direction.

The ground roll distance $S_{\mathrm{G_{LD}}}$ is estimated as

$$S_{\mathrm{G_{LD}}} = \int_{V_{\mathrm{TD}}}^{0} \frac{V}{a_x} \mathrm{d}V \tag{3.60}$$

Knowing

$$\begin{aligned} L &= C_L \frac{1}{2}\rho V^2 S \\ D &= C_D \frac{1}{2}\rho V^2 S = (C_{D_0} + K C_L^2)\frac{1}{2}\rho V^2 S, \end{aligned} \tag{3.61}$$

the integration gives

$$S_{\mathrm{G_{LD}}} = \frac{W}{g\rho S(C_D - \mu_{\mathrm{r}} C_L)} \ln\left[1 + \frac{(C_D - \mu_{\mathrm{r}} C_L)\rho S V_{\mathrm{TD}}^2}{2(-T + \mu_{\mathrm{r}} W)}\right]. \tag{3.62}$$

Equation (3.62) can be used to estimate the landing ground roll during the period of wheel braking. Remember that C_D must include the effects of speed brakes and/or a drag chute. Also note that this analysis assumes that the thrust (or reversed thrust) is acting parallel to the ground roll.

3.7 Gliding and climbs

3.7.1 Gliding flight

We first consider an unpowered glide shown in figure 3.13. The flight path angle γ is defined as the angle between the horizon and the relative wind. In this case, it is a negative angle (V_∞ is below the horizon). To avoid confusion, we will define $\bar{\gamma} = |\gamma|$ as the magnitude of the angle.

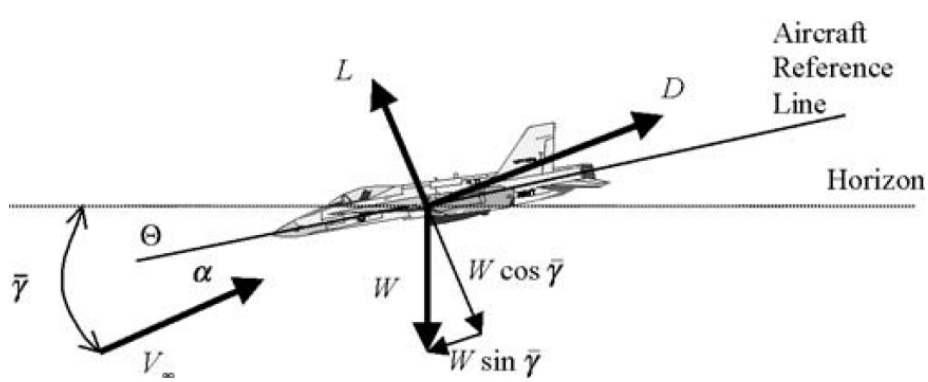

Figure 3.13: Unpowered gliding flight [6].

Assume a straight (but not level) and unaccelerated gliding flight. With no thrust, the aircraft has $T = 0$ but $D > 0$. In a steady glide, the x_{w} component of weight is equal to the drag. Summing forces

Copyright © 2025 Xiaowei He

parallel and perpendicular to the relative wind or flight path, the equations of motion for gliding flight are obtained. Note that both the linear and centripetal acceleration terms are zero.

$$\begin{aligned} \Sigma F_{\parallel} &= m\frac{\mathrm{d}V}{\mathrm{d}t} = W\sin\bar{\gamma} - D = 0, \\ \Sigma F_{\perp} &= m\frac{V^2}{r} = W\cos\bar{\gamma} - L = 0. \end{aligned} \tag{3.63}$$

Combining the results, we see that the gliding angle is determined by

$$\tan\bar{\gamma} = \frac{D}{L} = \frac{C_D}{C_L}. \tag{3.64}$$

So it can be seen that the best/shallowest glide (the smallest $\bar{\gamma}$) occurs at the minimum drag-to-lift ratio, i.e., at $C_{L_{\mathrm{md}}}$.

We can derive an expression for glide range using the geometry of a glide as shown in figure 3.14. From the geometry,

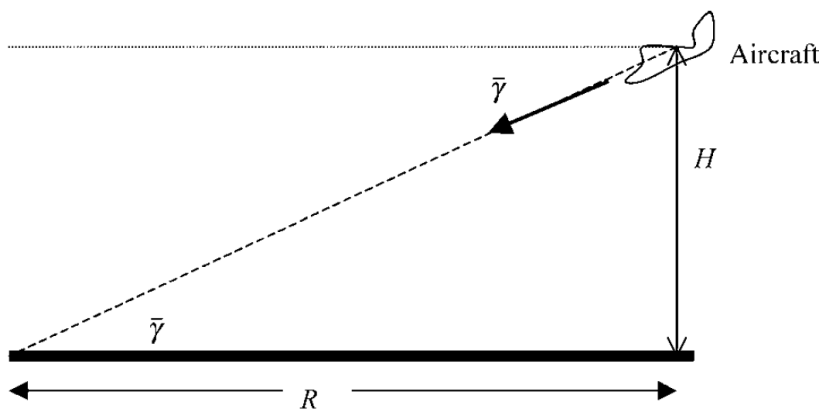

Figure 3.14: Geometry of a glide [6].

$$\tan\bar{\gamma} = \frac{H}{R}, \tag{3.65}$$

where H is the altitude at the start of the glide and R is the horizontal glide range. Combining with equation (3.64), we can see that the glide range is

$$R = H\left(\frac{L}{D}\right) = H\left(\frac{C_L}{C_D}\right). \tag{3.66}$$

The glide distance is a function of the initial altitude. By maximizing the lift-to-drag ratio, the glide range is maximized. Therefore, a pilot should fly at the airspeed (or, more correctly, the angle of attack) corresponding to $(C_L/C_D)_{\max}$.

3.7.2 Climbs

The same approach can be used to derive the equations of motion for climbs. An aircraft in a climb is shown in figure 3.15. The aircraft ascends with a climb angle γ, with the horizontal component of the aircraft's weight opposing the thrust.

Copyright © 2025 Xiaowei He

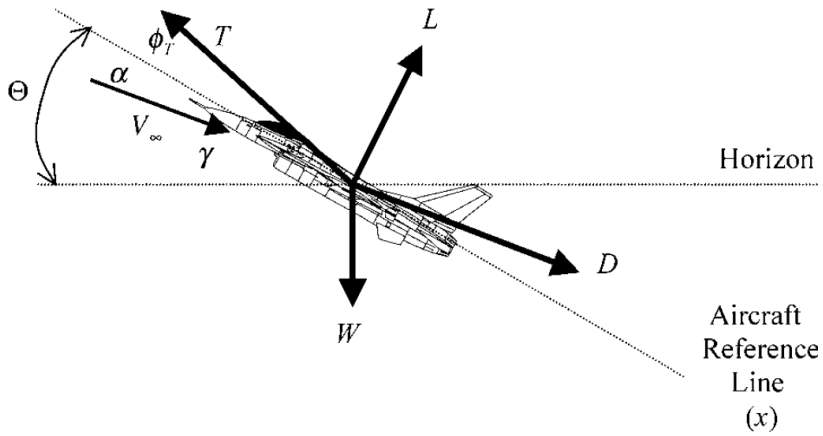

Figure 3.15: Geometry of a glide [6].

We again write the EOM in parallel and perpendicular directions of the flight path

$$\begin{aligned} \Sigma F_{\parallel} &= m\frac{\mathrm{d}V}{\mathrm{d}t} = T\cos(\alpha+\phi_T) - D - W\sin\gamma, \\ \Sigma F_{\perp} &= m\frac{V^2}{r} = W\cos\gamma - L - T\sin(\alpha+\phi_T). \end{aligned} \tag{3.67}$$

If assume a straight and unaccelerated climb, where $\alpha + \phi_T \approx 0$

$$\Sigma F_{\parallel} \Rightarrow \sin\gamma = \frac{T-D}{W}. \tag{3.68}$$

Referring to figure 3.16, the geometry gives the rate of climb (ROC)

$$ROC = V_{\mathrm{v}} = V_\infty \sin\gamma = V_\infty \frac{T-D}{W} = \frac{P_A - P_B}{W} = \frac{\text{excess power}}{\text{weight}}. \tag{3.69}$$

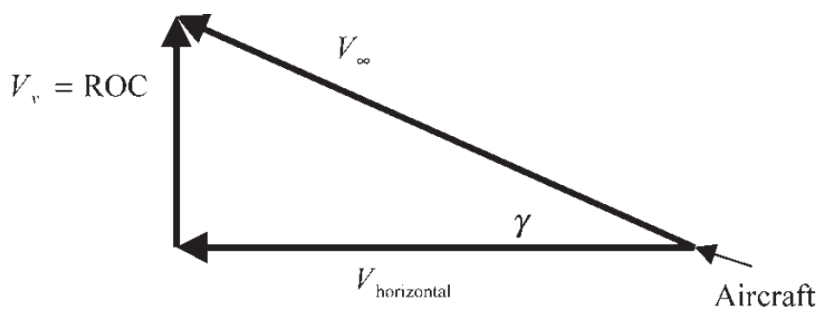

Figure 3.16: Geometry of a glide [6].

Climb performance. It should feel intuitively correct that

- the **maximum climb angle** requires the **maximum excess thrust**;
- the **maximum rate of climb** requires the **maximum excess power**.

These depend on the powerplant type and individual engine characteristics. For propeller and turbojet engines, some simplifications can be made about the propulsor that allow easy determination of one of the parameters—excess thrust for a turbojet, and excess power for a turboprop.

Copyright © 2025 Xiaowei He

- For **turbojet** aircraft and **low bypass ratio turbofan** aircraft, it is assumed that **thrust** remains constant with speed, and accordingly, power increases with speed.
- For **turboprop** aircraft and **high bypass ratio turbofan** aircraft, it is assumed that **power** remains constant with speed, and accordingly, thrust falls with speed.

3.8 Turns and V-n diagrams

Until this point, we have assumed straight flight in all discussions in which the aircraft's radius of curvature approached infinity. This is not the case when examining turning performance. In this section, we will develop equations to estimate turn radius and turn rate (deg/s) for three specific cases: level, pull-up, and pull-down. Additionally, we will introduce the concept of a "V-n diagram"; this diagram describes, in terms of velocity and load factor, an aircraft's operating envelope.

3.8.1 Acceleration and load factor

Accelerations of an airplane along its line of flight are comparatively straightforward. They are probably greatest during the take-off, or, in the negative sense, during the pull-up after landing. On the other hand, the accelerations due to a change in direction of flight are of tremendous importance and have a great impact on the turning performance.

When a body is compelled to move on a curved path, it is necessary to supply a force towards the center, this force being directly proportional to the acceleration required. Such a force is called the *centripetal force*. The body will cause a reaction, an outward force, on whatever makes it travel on a curved path. This reaction is sometimes referred to as the *centrifugal force*. If an airplane is traveling at a velocity of V [m/s] on the circumference of a circle of radius R [m], then the acceleration towards the center of the circle is V^2/R [m/s^2]. Therefore, the centripetal (or centrifugal) force is $m\times$acceleration, where m is the mass of the airplane in [kg],

$$F_{\text{ctr}} = \frac{mV^2}{R}\,[\text{N}]. \tag{3.70}$$

In practice, airplanes very rarely travel for any length of time on the arc of a circle; but that does not alter the principle, since any small arc of a curve is, for all practical purposes, an arc of some circle with some radius, so all it means is that the center and the radius of the circle keep changing as the airplane maneuvers.

The acceleration being V^2/R shows that the two factors that decide the acceleration, and therefore the necessary force, are velocity and radius, the velocity being squared having the greatest effect. Thus, curves at high speed or those with tight turns at small radii require large forces towards the center of the curve.

For instance, for an airplane traveling at 82 m/s on a radius of 200 m, the acceleration is 34 m/s^2, which is a little less than 4$\times$ the acceleration due to gravity. For convenience, this is often written as $4g$. However, before we proceed, we need to clarify some misunderstandings about the use of the symbol g. This letter is used to represent several different things. First, it represents the gravitational constant. By multiplying the mass by the gravitational constant g, we obtain the weight (written in mathematical terms, $W = mg$). The gravitational constant g has a value of 9.81 m/s^2 on the Earth's surface, and this makes it look like an acceleration. In this context, it is not an acceleration. For example, a book resting on a fixed table has no acceleration, but it does have a weight equal to $m \times g$ [N]. The trouble is that g is also used to represent the acceleration due to gravity. If the book falls off the table, it will accelerate at 9.81 m/s^2; the acceleration will then be equal to g (9.81 m/s^2). Although g is commonly used to represent

Copyright © 2025 Xiaowei He

two different things, it always has a value of $9.81\,\mathrm{m/s^2}$, so we can still use it for both purposes, as long as we make quite clear whether we are talking about an acceleration or a weight. On the other hand, pilots (and racing car drivers) often talk about pulling a certain number of gs. In this case, the gs count for the *load factor*. This quantity is not an acceleration; it is just a number. It has no units and simply represents a factor that, when multiplied by the weight, gives the total force that must be applied to a body to balance the combined effects of gravity and centripetal acceleration. In other words, the load factor is the ratio of the applied force to the weight, representing how loads and stresses in the airframe increase during a maneuver.

3.8.2 Level turns

The aircraft in figure 3.17 (rear view) is performing a level turn. To maintain a constant altitude, the velocity vector must act in the horizontal plane; thus, the vertical component of the lift vector must equal the weight.

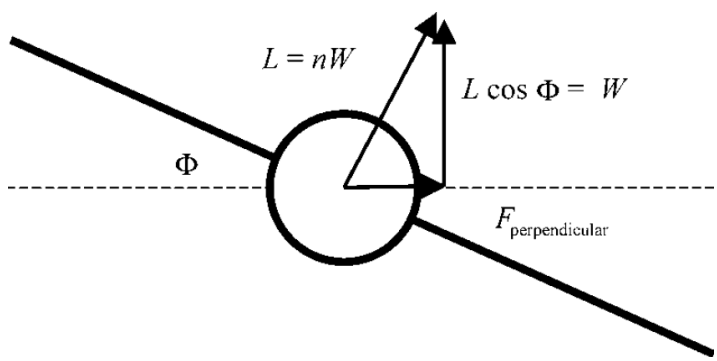

Figure 3.17: Aircraft in a level turn [6].

Summing forces in the vertical direction

$$\Sigma F_{\mathrm{v}} = L\cos\phi - W = 0, \tag{3.71}$$

which gives

$$\frac{L}{W} = \frac{1}{\cos\phi} = n, \tag{3.72}$$

where n is defined as the *load factor*. The load factor is generally referred to as the number of gs that the aircraft is pulling. Equation (3.72) defines the relationship between load factor and bank angle for a level turn. Note that the equation is independent of aircraft type. Therefore, any aircraft in a sustained level 60-degree banked turn will be pulling $2g$.

We then sum forces in the horizontal plane perpendicular to the velocity vector and set them equal to the centripetal force. From the geometry, we can derive expressions for the turn radius R and the turn rate ω. From the Pythagorean theorem, we have

$$\begin{aligned} \Sigma F_{\mathrm{h}} &= m\frac{V^2}{R} = \frac{WV^2}{gR} = L\sin\phi = \sqrt{L^2 - W^2} = W\sqrt{n^2-1} \\ \frac{V^2}{gR} &= \sqrt{n^2-1}. \end{aligned} \tag{3.73}$$

Solving for the turn radius R,

$$R = \frac{V^2}{g\sqrt{n^2-1}}. \tag{3.74}$$

Copyright © 2025 Xiaowei He

The velocity in equation (3.74) is the true airspeed of the aircraft or V_∞.

Because turn rate is equal to V_∞/R, it is obtained by plugging in equation (3.74)

$$\omega = \dot{\psi} = \frac{V_\infty}{R} = \frac{g\sqrt{n^2-1}}{V_\infty}. \tag{3.75}$$

Using consistent units in equation (3.75), the units of turn rate will fall out to be radians per second [rad/s]. In terms of a physical interpretation, turn rate is typically presented in degrees per second [deg/s]. The conversion between radian and degree is 1 [rad] = 57.3 [deg].

A physical interpretation of equations (3.74) and (3.75) is that a combination of low airspeed and high g loading will give the best level-turn performance. This is also true for the next two cases—pull-up and pull-down. However, what equations (3.74) and (3.75) do not show is the ability of the aircraft to sustain the turn. Sustained turns require that sufficient thrust be available to overcome the drag in the turn. Sustained turning capability can be evaluated by calculating the aircraft's drag for a given turning condition and comparing it to the thrust available. To sustain a turn, the following relationship must be satisfied

$$T_{\mathrm{R_{TF}}} = C_D q_\infty S = (C_{D_0} + KC_L^2) q_\infty S, \tag{3.76}$$

where $T_{\mathrm{R_{TF}}}$ is the thrust required to sustain a turning flight, $q_\infty = \frac{1}{2}\rho V^2$ is the dynamic pressure. Because the lift coefficient in a turn is directly proportional to the load factor

$$C_L = \frac{L}{q_\infty S} = \frac{nW}{q_\infty S}, \tag{3.77}$$

the induced drag significantly increases in a turn, and, consequently, the thrust available must be sufficient to match the total drag, or the turn will not be sustained.

Example 3.2

Determine the load factor, bank angle, and turn radius for an aircraft in a level turn at a true airspeed of 120 kn and a turn rate of 15 deg/s.

Solution: First, convert the airspeed and turn rate to consistent units.

$$V_\infty = 120\,\mathrm{kn} \cdot \frac{1.852\,\mathrm{km/h}}{\mathrm{kn}} \cdot \frac{0.278\,\mathrm{m/s}}{\mathrm{km/h}} = 61.8\,\mathrm{m/s},$$
$$\omega = 15\,\mathrm{deg/s} \cdot \frac{\mathrm{rad}}{57.3\,\mathrm{deg}} = 0.262\,\mathrm{rad/s}.$$

Use equation (3.75)

$$\omega = \frac{g\sqrt{n^2-1}}{V_\infty},$$

and solve for load factor n

$$n = \sqrt{\left(\frac{\omega V_\infty}{g}\right)^2 + 1} = \sqrt{\left(\frac{0.262\,\mathrm{rad/s} \cdot 61.8\,\mathrm{m/s}}{9.81\,\mathrm{m/s^2}}\right)^2 + 1} = 1.93$$

Use equation (3.74) to find the turn radius

$$R = \frac{V^2}{g\sqrt{n^2-1}} = R = \frac{(61.8\,\mathrm{m/s})^2}{9.81\,\mathrm{m/s^2}\sqrt{1.93^2-1}} = 235.8\,\mathrm{m}.$$

Copyright © 2025 Xiaowei He

Or, by recognizing that $V_\infty = R\omega$,

$$R = \frac{V_\infty}{\omega} = \frac{61.8\,\mathrm{m/s}}{0.262\,\mathrm{rad/s}} = 235.9\,\mathrm{m}.$$

The bank angle is found from equation (3.72)

$$\phi = \arccos\frac{1}{n} = \arccos\frac{1}{1.93} = 1.026\,\mathrm{rad} = 58.8\,\mathrm{deg}.$$

Correct bank angles. From equations (3.72) and (3.73), we can obtain a relation among the bank (roll) angle, the velocity, and the turn radius

$$\tan\phi = \frac{V^2}{gR}. \tag{3.78}$$

This simple formula shows that there is a correct bank angle, ϕ, for any turn of radius, R, at a velocity, V, and that this bank angle is quite independent of the weight of the aircraft.

Thus, we see that an increase in velocity needs an increase in the bank angle, whereas if the radius of the turn is increased, the bank angle may be reduced. Figure 3.18 shows the correct bank angle for a fixed radius (varying speeds) and a fixed speed (varying radii); notice again how the speed has more effect on the angle than does the radius of turn. Meanwhile, from equation (3.72), the correct bank angle can also be found through the load factor that is determined by the speed and turn radius by solving for n in equation (3.73).

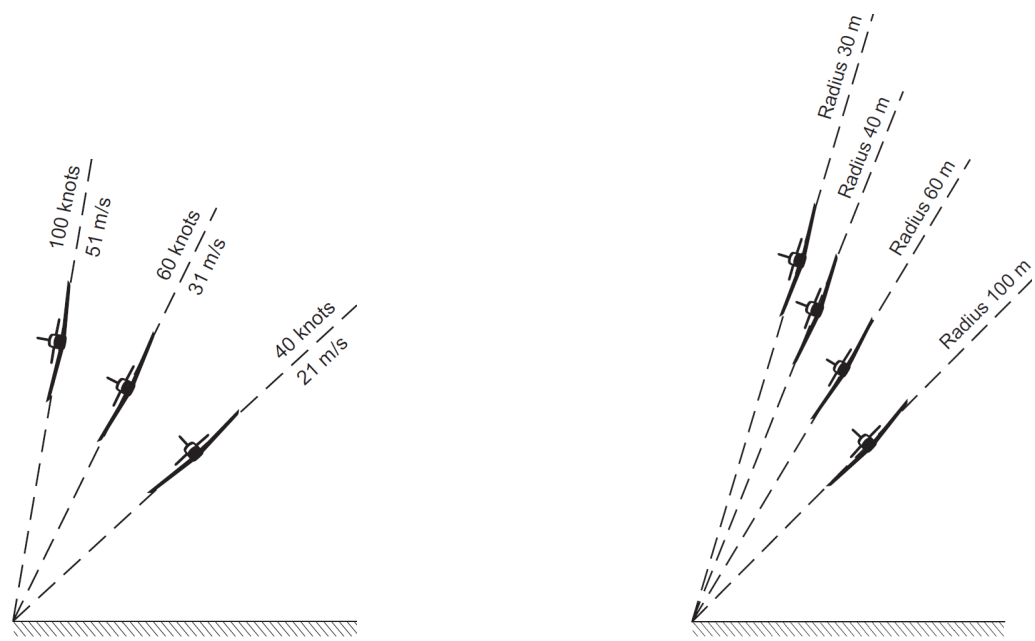

(a) Correct bank angles at fixed turn radius of 50 m

(b) Correct bank angles at fixed speed of 60 kt.

Figure 3.18: Correct bank angles in turns [11].

Flat turns. It should be noted that the banked turn discussed above is not the only way to change the lateral direction of an airplane in flight. An airplane can also be turned without a bank angle, which

Copyright © 2025 Xiaowei He

is called a flat turn. In a flat turn, the rudder is utilized to create the side force with wings held level. However, this is typically not preferred, because:

- Very inefficient; small side force, and therefore large turn radius.
- Drag increases due to fuselage sideslip; increased fuel burn.
- Dynamic pressure imbalance on wings requires aileron adjustment.
- Perceived centrifugal force by occupants.

3.8.3 Pull-ups

Assume an aircraft is in level flight at the bottom of a loop as shown in figure 3.19 At the start of the loop, the pilot pulls back on the stick, initiating the loop.

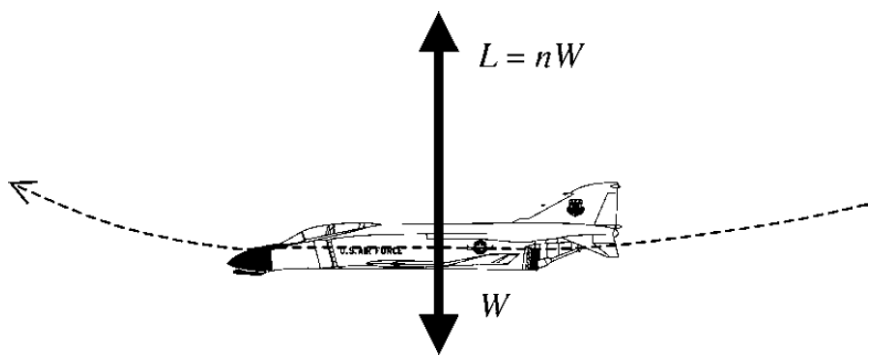

Figure 3.19: Aircraft in a pull-up [6].

Newton's second law in the centripetal force direction gives

$$\Sigma F_\perp = m\frac{V_\infty^2}{R} = \frac{WV_\infty^2}{gR} = L - W = nW - W = W(n-1). \tag{3.79}$$

Solving for turn radius R,

$$R = \frac{V_\infty^2}{g(n-1)}, \tag{3.80}$$

and the turn rate ω is obtained

$$\omega = \dot{\theta} = \frac{V_\infty}{R} = \frac{g(n-1)}{V_\infty}. \tag{3.81}$$

Example 3.3

An F-22 is performing a 5-g pull-up at 500 kn true airspeed. What is the turn rate and turn radius?

Solution: Convert the airspeed to consistent units

$$V_\infty = 500\,\text{kn} \cdot \frac{1.852\,\text{km/h}}{\text{kn}} \cdot \frac{0.278\,\text{m/s}}{\text{km/h}} = 257.4\,\text{m/s}$$

The turn rate can be determined by equation (3.81)

$$\omega = \frac{g(n-1)}{V_\infty} = \frac{9.81\,\text{m/s}^2 \cdot (5-1)}{257.4\,\text{m/s}} = 0.152\,\text{rad/s} = 0.152\,\text{rad/s} \cdot \frac{57.3\,\text{deg}}{\text{rad}} = 8.7\,\text{deg/s}.$$

Copyright © 2025 Xiaowei He

Then, the turn radius can be determined by equation (3.80)

$$R = \frac{V_\infty^2}{g(n-1)} = \frac{(257.4\,\mathrm{m/s})^2}{9.81\,\mathrm{m/s^2}\cdot(5-1)} = 1688.4\,\mathrm{m}.$$

Acceleration and load factor in pull-up. Consider an aircraft with a mass of 1 000 kg, which therefore has a weight of $1\,000g$ [N] since $W = mg$. In the case of this aircraft pulling out of a dive, where it is subjected to a centripetal acceleration of $3g$ at the bottom of the maneuver. The centripetal force required to provide this acceleration will be $1\,000 \times 3g$ [N] since $F = ma$. Now, $1\,000 \times 3g$ [N] is a force equal to 3 times the weight. This centripetal force will be provided by the lift from the wings. However, the wing has to support the weight of the aircraft, $1\,000g$ [N], as well as providing the centripetal acceleration, $1\,000 \times 3g$ [N], so the total lift force must be $1\,000 \times (1g + 3g)$ [N], which is $4\times$ the weight. The pilot, therefore, refers to this as a $4g$ maneuver. Not only will the lift and the stresses on the airframe be four times their normal level flight value, but the pilot will also feel as though one weighs four times as much as usual. From the above, a $4g$ pullout involves a $3g$ centripetal acceleration.

Pulling out of a dive. Some of the effects of the pull-out maneuver are important for aircraft structure design and pilots' safety. First, we have seen that the wings will have to generate more lift in order to provide the necessary centripetal acceleration. This means that the bending stresses in the wing will increase. In fact, in a $3g$, they will be three times as high as for normal level flight. Design and safety requirements and regulations specify the maximum load factor that the aircraft must be able to withstand, and all stresses in the aircraft must be determined for this condition. The required load factor will depend on the usage. Fully aerobatic types have a high specified maximum load factor, whereas civil transports have a lower requirement. The pilot will be made aware of the maximum number of gs that the aircraft is permitted to be subjected to.

In order to provide the necessary increase in lift, the lift coefficient, C_L, must be increased by increasing the angle of attack. This goes up as the square root of the g factor. There is a point where $C_{L_{\max}}$ is reached, and any attempt to further increase it will result in the aircraft stalling. The greater the centripetal acceleration required, the higher the stalling speed will be. Stalling whilst attempting to pull out too steeply is a condition that pilots must avoid at all times. The consequences can be disastrous, as many dive-bomber pilots have found to their cost. Figure 3.20 illustrates the case of an aircraft, having a level flight stall speed of 30 m/s, pulling out of a steep dive. The load factor or g level, the stall speed, and the centripetal accelerations are given for various cases.

Apart from the loads on the airframe, any maneuver involving large centripetal accelerations will have a physical effect on the pilot. The pilot's head will feel heavy, and one will experience difficulty in moving one's arms, which now feel several times heavier than normal. Even at $1.5g$, writing becomes difficult. Worse than this, however, are the effects that the centripetal acceleration can have on his blood circulation. At around 4 to $5g$, one's heart, which is a pressure pump, will start to have difficulty pumping blood to one's head, and if this is too severe, everything will appear to turn gray at first, and then one will be in danger of "blacking out" and losing consciousness.

3.8.4 Pull-downs

The aircraft is now inverted (avoiding negative gs) at the top of a loop as shown in figure 3.21. Similar to the pull-up (except that the lift is now in the same direction as the weight), the EOM in the perpendicular direction to the flight path is

$$\Sigma F_\perp = m\frac{V_\infty^2}{R} = \frac{WV_\infty^2}{gR} = L + W = nW + W = W(n+1). \tag{3.82}$$

Copyright © 2025 Xiaowei He

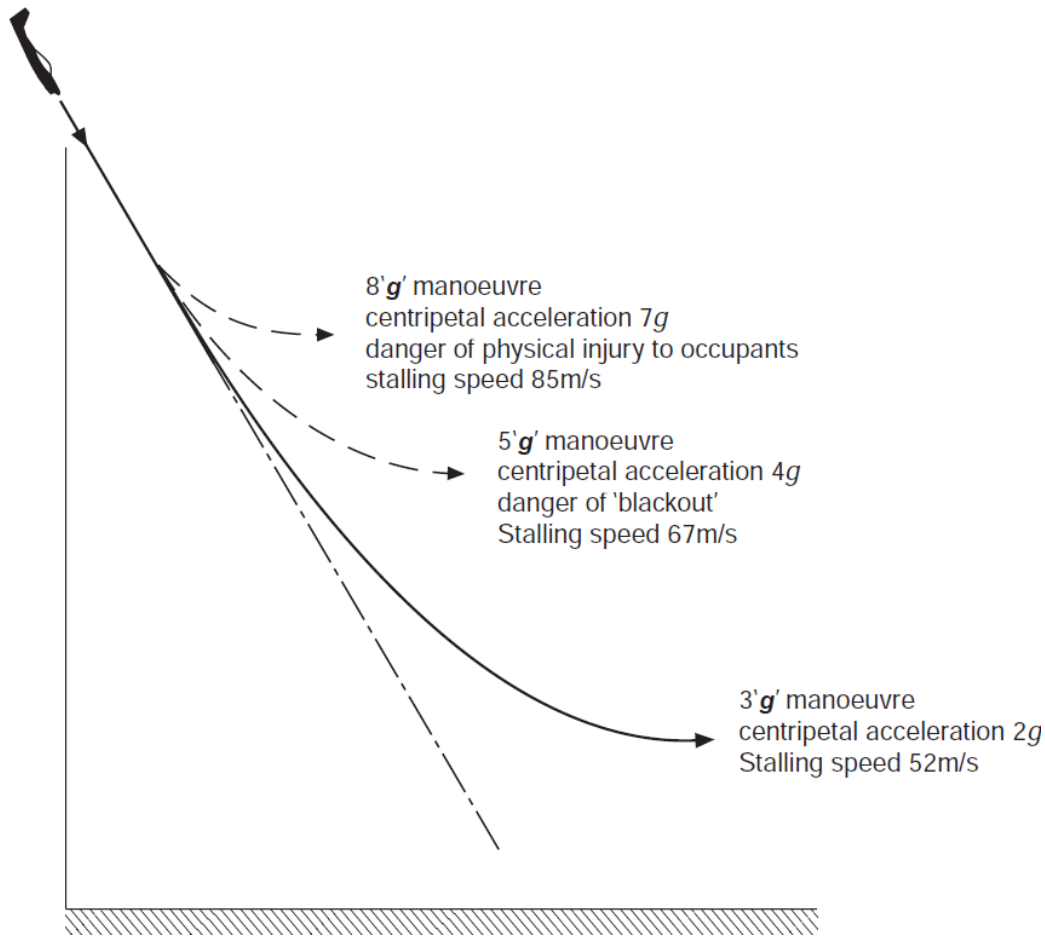

Figure 3.20: Pulling out of a dive [11].

Solving for turn radius and rate,

$$R = \frac{V_\infty^2}{g(n+1)}, \tag{3.83}$$

$$\omega = \dot{\theta} = \frac{g(n+1)}{V_\infty}. \tag{3.84}$$

The inverted pull-down gives the best turning performance because the weight of the aircraft helps perform the turn.

Example 3.4

The F-22 in example 3.3 is at the same conditions (500 kn, and pulling 5 g) but executes a pull-down. Compare the turn rate and turn radius to that achieved for the pull-up.

Solution: From example 3.3, the true airspeed in consistent units is $V_\infty = 257.4\,\mathrm{m/s}$. Use equation (3.84) to determine the turn rate

$$\omega = \frac{g(n+1)}{V_\infty} = \frac{9.81\,\mathrm{m/s^2} \cdot (5+1)}{257.4\,\mathrm{m/s}} = 0.229\,\mathrm{rad/s} = 13.1\,\mathrm{deg/s},$$

Copyright © 2025 Xiaowei He

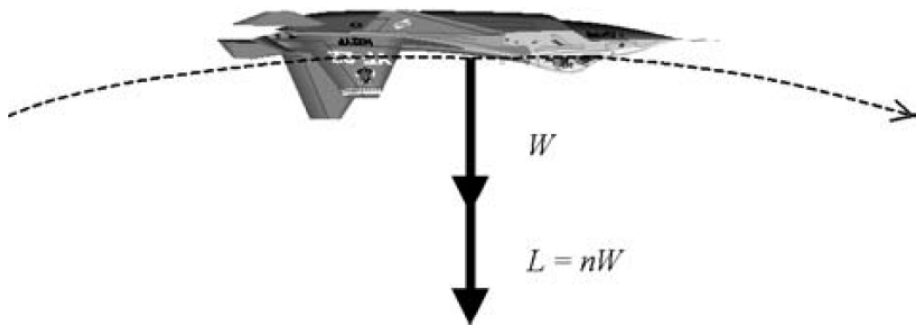

Figure 3.21: Aircraft in a pull-down [6].

and equation (3.83) to determine the turn rate

$$R = \frac{V_\infty^2}{g(n+1)} = \frac{(257.4\,\mathrm{m/s})^2}{9.81\,\mathrm{m/s^2}\cdot(5+1)} = 1125.6\,\mathrm{m}.$$

In comparing these values with those for the pull-up case, the turn rate is significantly higher, and the turn radius is significantly smaller. This leads to the conclusion that, with the same load factor and airspeed, a pull-down will result in a quicker, tighter turn than a pull-up.

Acceleration and load factor in pull-down. Consider the same aircraft of 1 000 kg in the pull-up example is at the top of a loop at the same speed, and with the same radius of curvature. At the top of the loop, the centripetal acceleration required will still be $3g$, and the total force required to produce this will still be $1\,000 \times 3g$ [N]. However, the weight of the aircraft, $1\,000 \times g$ [N], will provide part of the centripetal force required, leaving the wing lift (now pulling downward) to provide the extra $1\,000 \times 2g$ [N]. Notice that although the centripetal acceleration is $3g$, the wings only have to provide twice as much lift force as in level flight, that is $2\times$ the weight. Also, the pilot will not be squashed so firmly into his seat as at the bottom of the pull-out maneuver, as one's weight is trying to pull him out of the seat. Because the lift required is only $2\times$ the weight, the load factor is only 2, and the pilot would call this a $2g$ maneuver.

3.8.5 V-n diagrams

Most U.S. Air Force aircraft have a V-n diagram in the flight manual. The V-n diagram represents the relationship between the aircraft velocity (V) and the load factor (n), of which the pilots memorize the limits. In general, aircraft are limited in their performance capabilities by aerodynamics (e.g., stall), structure, and/or engine capabilities. A V-n diagram captures an aircraft's operating envelope.

Aircraft are limited aerodynamically by stall. In section 3.5, we developed equation (3.33) for stall airspeed, assuming a load factor of 1, or $L = W$). Now we write it in a more general form where L is replaced by nW

$$V_{\text{stall}} = \sqrt{\frac{2nW}{\rho_\infty S C_{L_{\max}}}}. \tag{3.85}$$

When pulling gs, an aircraft stalls at a higher airspeed—a V-n diagram will show this trend. Additionally, an aircraft can withstand only a finite amount of g loading until it structurally fails. This g loading is typically denoted by $n_{\max}$. At one airspeed, called the **corner velocity**, an aircraft is operating

Copyright © 2025 Xiaowei He

at the brink of stall, and pulling max g (or maximum load factor),

$$\text{corner velocity} = V^* = \sqrt{\frac{2n_{\max}W}{\rho_\infty S C_{L_{\max}}}}. \tag{3.86}$$

Recall that in the discussion of turns, maximum performance is obtained at a combination of low airspeed and high g loading—this is the corner velocity. This equation identifies both an aerodynamic (through the maximum lift coefficient) and a structural (through maximum load factor) limitation for performance.

Figure 3.22 is a typical V-n diagram with velocity (or sometimes Mach number) on the horizontal axis and load factor on the vertical axis.

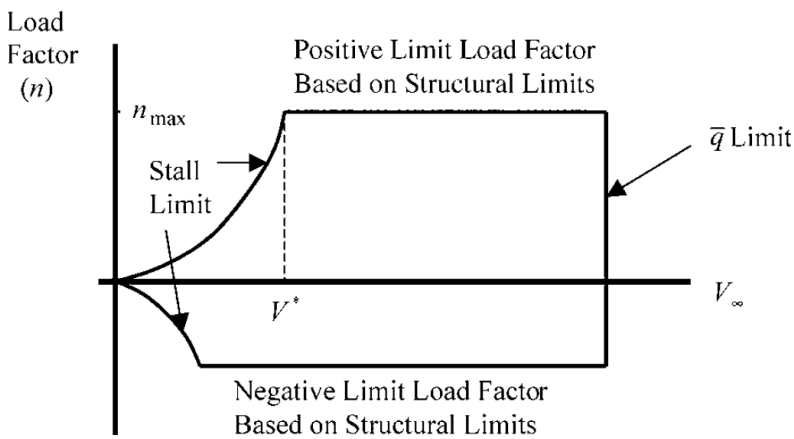

Figure 3.22: Typical V-n diagram [6].

The following are the key points about an aircraft's V-n diagram:

- A V-n diagram is good for one weight, altitude, and configuration.
- The area inside is called the operating envelope, in which the aircraft can be safely operated at combinations of airspeed and load factor.
- Refer to the positive and negative stall limits—again, the higher the load factor, the higher the stall airspeed. At a load factor of 1 (lift equal to weight), the 1-g stall limit is identified.
- The corner velocity V^* is at the corner of the aircraft's stall limit and structural limit.
- Positive and negative limit load factors are identified—the aircraft will sustain damage if these are exceeded. Structurally, an aircraft is typically designed to handle more positive than negative gs (as is the pilot).
- At the high airspeeds, the aircraft reaches a "q limit" or "redline". This could be an aeroelastic limit or a temperature limit. Undesirable structure and handling qualities occur if this limit is exceeded.
- If equivalent velocity V_e is used on the horizontal axis of the V-n diagram, then the V_e-n diagram will not be affected by altitude changes.

The effects of changes in weight and altitude are shown in figures 3.23a and 3.23b, respectively.

Copyright © 2025 Xiaowei He

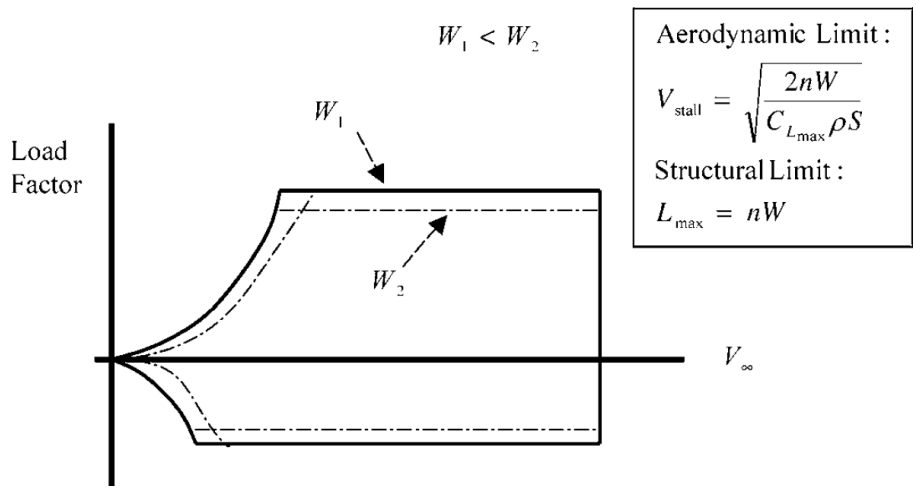

(a) Effect of weight on V-n diagram

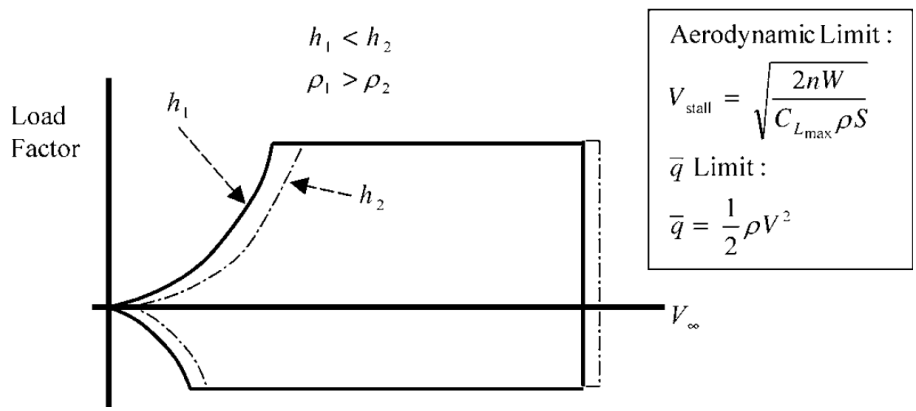

(b) Effect of altitude on V-n diagram

Figure 3.23: Variations in V-n diagrams [6].

3.9 Energy maneuverability

Energy is a primary factor in controlling and maneuvering an aircraft. If an attacker has too much energy, it may be easy to get in range but difficult to prevent an overshoot. Too little energy and the attacker may not be able to get in range at all. If the defender has more energy than the attacker, an escape may be possible; however, if the defender has too little energy, they will lose maneuverability.

In aviation, the term "energy" does not refer to the fuel nor the thrust it produces. Instead, thrust is referred to as "power". Energy is the state of the fighter's mass at any given time and is the result of the power. Energy comes in two forms, which are kinetic and potential. Kinetic energy is a function of the fighter's mass and speed, while potential energy is a function of its mass, gravity, and altitude. The combined potential and kinetic energy is called the total energy. Because the energy package is the combination of mass, speed, and altitude, a fighter flying at low altitude but a high speed may have the same total energy as a fighter of equal mass, but flying at a low speed and high altitude.

Copyright © 2025 Xiaowei He

3.9.1 Energy height

The total energy (potential plus kinetic) of an aircraft is

$$E = mgh + \frac{1}{2}mV^2. \tag{3.87}$$

Consider a B-52 that weights 488 000 lb and an F-16 that weights 26 000 lb are both in flight at 20 000 ft and 400 kt. The B-52 clearly has more total energy because it has more mass. However, because we know intuitively the F-16 is superior in air combat, total energy does not appear to be a useful parameter for comparison.

If we normalize the total energy with respect to weight, that is, energy per unit weight, we obtain the specific energy as

$$E_{\mathrm{S}} = \frac{E}{W} = h + \frac{V^2}{2g} = H_E. \tag{3.88}$$

Because the specific energy has the dimensions of length, it is also called energy height, H_E. Since H_E is only a function of altitude and velocity, contours of constant H_E can be plotted on the altitude versus velocity (true airspeed) plane as shown in figure 3.24.

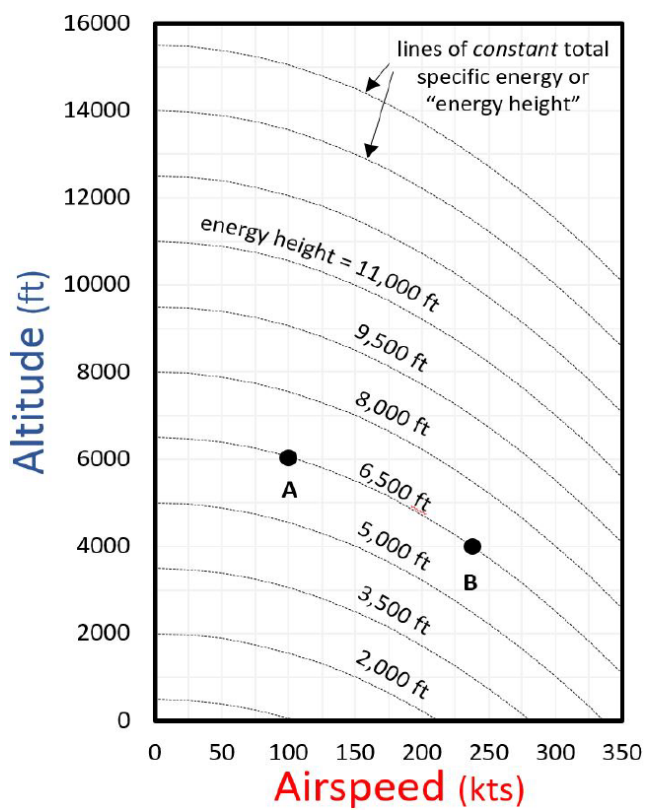

Figure 3.24: Energy height contours [12].

The position of an airplane in the altitude-airspeed map represents its total specific energy E_{S}, or energy height, H_E, in figure 3.24. The H_E contours indicate the maximum height that an airplane would reach from its current altitude if it were to trade all its speed for altitude. Different positions of an airplane along a given energy height line have the same total energy regardless of their location on the

Copyright © 2025 Xiaowei He

line (e.g., A and B). Thus, even though the airplane in point A is cruising at 100 kt and 6 000 ft, it has the same total specific energy expressed in height (6 500 ft) when cruising at 240 kt and 4 000 ft (B). This also means that the airplane in either position, A or B, would be able to "zoom" to the same maximum altitude of 6 500 ft by trading all its speed for altitude. The lines of constant energy height can be used as idealized trajectories to depict an airplane moving from one energy state to another solely through energy exchange (e.g., A to B). If the airplane rapidly exchanges altitude and airspeed, it would follow along the energy height line while, in the short term, maintaining constant total energy.

3.9.2 Weight specific excess power

In the B-52 vs F-16 example, the two aircraft have equivalent energy height, which still does not depict the F-16's maneuvering advantage over the B-52. The next iteration will be to form the time derivative of energy height, which represents the aircraft's ability to change (increase or decrease) its energy height, that is,

$$\frac{\mathrm{d}H_E}{\mathrm{d}t} = \frac{\mathrm{d}h}{\mathrm{d}t} + \frac{V}{g}\frac{\mathrm{d}V}{\mathrm{d}t}. \tag{3.89}$$

This equation contains two parameters that directly relate to a pilot flying an airplane: $\mathrm{d}h/\mathrm{d}t$, which is the rate of climb, and $\mathrm{d}V/\mathrm{d}t$, which is the rate of change of true airspeed, or acceleration.

It can be shown that

$$\frac{\mathrm{d}h}{\mathrm{d}t} + \frac{V}{g}\frac{\mathrm{d}V}{\mathrm{d}t} = \frac{(T-D)V}{W}, \tag{3.90}$$

of which the right-hand side is the excess power divided by weight. Therefore, we denote the new value as weight specific excess power by

$$P_\mathrm{S} = \frac{(T-D)V}{W} = \frac{\mathrm{d}h}{\mathrm{d}t} + \frac{V}{g}\frac{\mathrm{d}V}{\mathrm{d}t}. \tag{3.91}$$

The weight specific excess power, P_S, indicates the energy maneuverability of an aircraft. In simple terms, P_S is a measure of the aircraft's ability at a given flight condition (altitude and airspeed) to climb and/or accelerate.

P_S plots. For a given aircraft, contours of P_S can be plotted on the altitude vs velocity plane, with contours of constant H_E also displayed. Figure 3.25 demonstrates the P_S contours of a hypothetical airplane and its energy trajectories to move from one energy state to another. The airplane can move along energy height lines by simply exchanging energy (e.g., A to B). However, to move across energy height lines, the airplane needs to increase or decrease total energy while distributing the energy change between altitude and airspeed. Thus, the ability of an airplane to go from one energy height to another (e.g., from A to positions C, D, or E) is a function of P_S, measured in rate of change in distance or height (unit of velocity).

Examine the energy positions depicted in figure 3.25. The airplane in position A is flying at 4 000 ft and 150 kt with a total energy equivalent to 5 000 ft. Since positions C, D, and E are located at higher energy heights (11 000 ft, 9 500 ft, and 6 500 ft respectively), the only way for the airplane to reach them from position A is by increasing its total energy (i.e., increasing thrust above drag, or $P_\mathrm{S} > 0$). The reverse is also true. If the airplane is in position C, D, or E, the only way for it to get back to position A is by decreasing its total energy (i.e., decreasing thrust below drag, or $P_\mathrm{S} < 0$). In other words, the rate at which the airplane can move from one energy height to another—e.g., how swiftly it can climb/descend at a steady speed, or accelerate/ decelerate in level flight—is a function of specific excess power, which can be positive ($P_\mathrm{S} > 0$) or negative ($P_\mathrm{S} < 0$) depending on whether the airplane needs to move to an energy height that demands more or less total energy.

Copyright © 2025 Xiaowei He

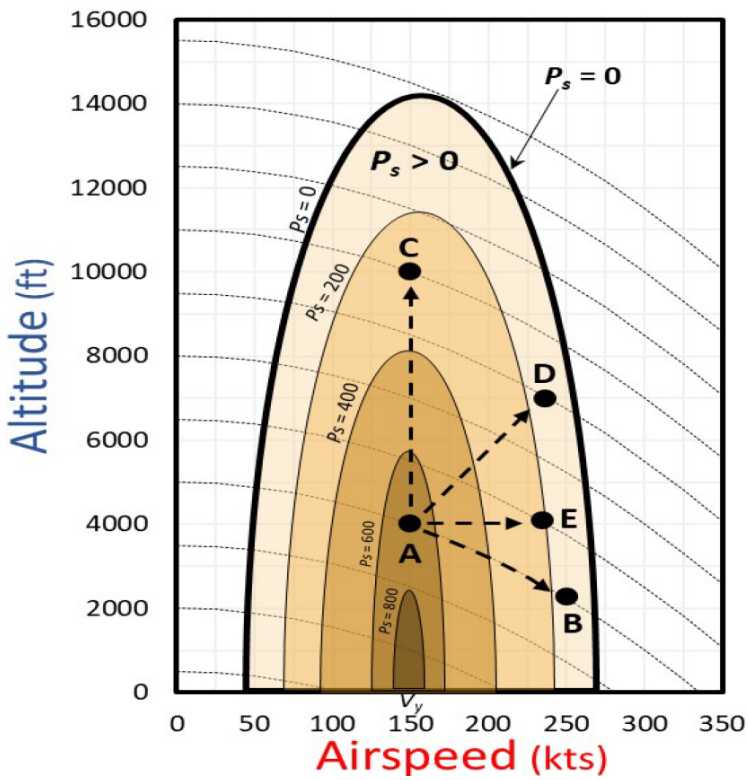

Figure 3.25: Specific excess power contours and energy trajectories [12].

At the edge of the energy envelope, where available $P_S = 0$ at full throttle, the airplane can no longer climb while maintaining airspeed or accelerate without descending. Inside this envelope, inner contours increase in value, reaching a "peak" where available P_S is maximized. Note that PS at full throttle is maximized at a specific airspeed (V_Y), decreasing in value at slower or faster airspeeds. At V_Y, the airplane can attain the maximum rate of climb while maintaining airspeed or the maximum acceleration without descending.

3.9.3 Energy control

An "energy-control" map can help visualize the basic energy control rules. Shown in figure 3.26, the energy-control map depicts not only the trajectories of an airplane transitioning from an arbitrary initial energy state (1) to other target states (2, 3, 4, 5, 6, and 7), but also the changes in energy caused by the throttle (blue/red arrows) and the elevator (green arrows). In other words, it allows pilots to visualize the basic control rules for moving an airplane from one state to another. The edge of the sustainable energy state envelope (where $P_S = 0$ at full throttle) is also illustrated.

Note that the line of constant total energy (dashed line) that divides the area in the map requiring more total energy (blue area) from that which requires less energy (red area) is depicted relative to the arbitrary initial energy state (1). The throttle adds (blue arrow) or subtracts (red arrow) the amount of total energy demanded by the new target energy state, while the elevator (green arrows) distributes the correct amount of total energy between potential and kinetic energies. By balancing the simultaneous actions of the controls, the airplane can follow the desired energy trajectory.

As illustrated in figure 3.26, moving the airplane from position 1 to the energy states in 2 and 3 calls

Copyright © 2025 Xiaowei He

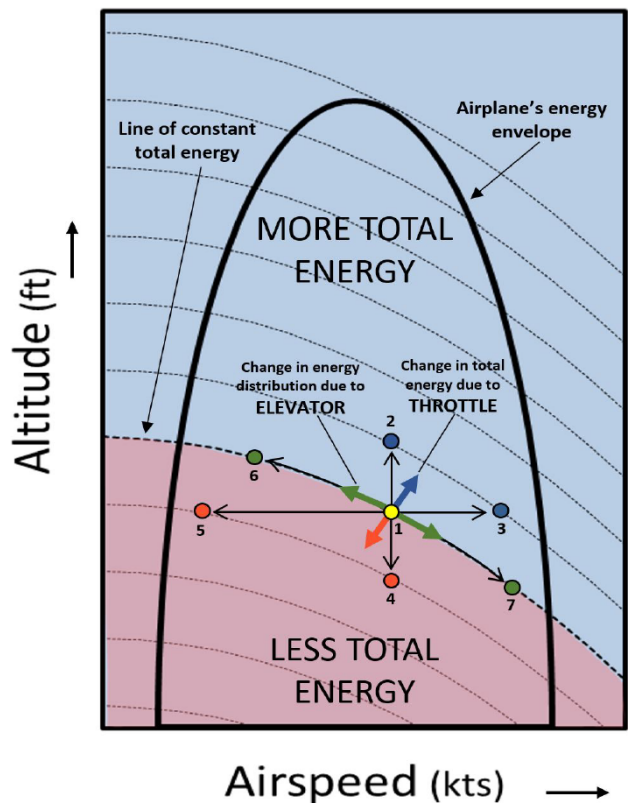

Figure 3.26: Energy-control map [12].

for a higher throttle setting to increase total energy by the same amount (in this example, positions 2 and 3 are located at the same higher-energy height). The difference between these two energy trajectories (1-to-2 and 1-to-3) lies in the way the total energy change is distributed by the elevator through changes in pitch attitude. Changes in total energy by adjusting throttle setting (blue/red arrows) extend across lines of constant total energy (dashed line), while changes in energy distribution by adjusting the elevator deflection (green arrows) extend along the lines of constant total energy (equal energy height). Appropriate changes in total energy via the throttle and/or changes in energy distribution via the elevator, depicted by their respective energy "arrows", determine the direction of a given energy trajectory between two energy states. To visualize this effect, compare the trajectory from 1-to-2 with that from 1-to-3 and notice the way the corresponding elevator energy arrows (left green arrow = up-elevator; right green arrow = down-elevator) are positioned in relation to the throttle energy arrow (blue arrow = increased throttle).

3.9.4 Minimum time-to-climb trajectory

A P_S plot for an aircraft can also be used to develop minimum time-to-climb flight trajectories. Consider the nominal P_S plot for a supersonic aircraft as shown in figure 3.27. The minimum time-to-climb trajectory is constructed by locating the points of tangency between P_S contours and H_E contours. This allows for locating the point of maximum P_S (maximum ability to increase energy height) for every value of H_E. Connecting these points gives a flight profile that minimizes the time to reach the maximum attainable altitude. Note that the "transfer" from the subsonic climb trajectory to the supersonic climb is a dive to accelerate quickly through the transonic region and minimize the effects of transonic drag.

Copyright © 2025 Xiaowei He

Also, when examining the subsonic trajectory, it shows that, for a high-thrust fighter, the minimum time-to-climb is obtained by staying low and accelerating to transonic speeds, then pitching up into a steep climb at approximately constant indicated airspeed (i.e., dynamic pressure). The key point is to realize that minimum time-to-climb is not accomplished by maximizing climb rate at all altitudes, but rather by maximizing P_S, or the aircraft's ability to increase H_E, at all energy heights.

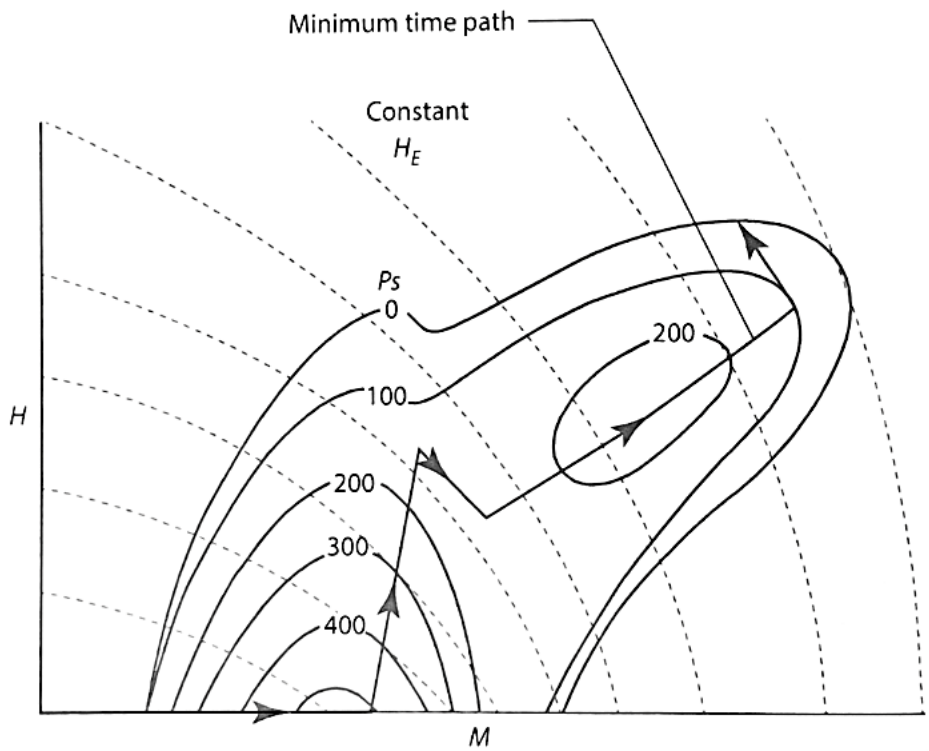

Figure 3.27: Minimum time-to-climb trajectory [6].

Copyright © 2025 Xiaowei He

4 Aircraft Static Stability

The static stability of an aircraft is generally the first type of stability that a designer evaluates in a new aircraft configuration. Static stability criteria for the three rotational modes of the aircraft (pitch, roll, and yaw, i.e., longitudinal, lateral, and directional) must be considered individually. Accepted design practice for most aircraft has been to achieve some degree of static stability for each of these rotational degrees of freedom. A trade-off typically exists between static stability and maneuverability. A high degree of static stability would normally result in an aircraft that is easy to fly but has low maneuverability (trainer aircraft, for example). Fighter aircraft designs would incorporate low levels of static stability so that enhanced maneuvering capabilities could be achieved. However, with the advent of high authority fly-by-wire control systems in aircraft such as the F-16, the Space Shuttle, and the X-29, acceptable levels of both static stability and maneuverability can be achieved. Some degree of static instability in the basic airframe design is intentionally incorporated in these aircraft to achieve enhanced maneuvering capabilities, while the fly-by-wire system provides automatic control inputs to achieve the appearance of static stability from the pilot's perspective. Static stability concepts provide a first step in achieving a design with acceptable flying qualities.

4.1 Static stability overview

4.1.1 Trim equilibrium

In normal flight, it is usual for the pilot to adjust the controls of an aircraft such that, on release of the controls, it continues to fly steadily at the chosen flight condition. This means the pilot is relieved of the tedium of constantly adjusting control inputs to maintain equilibrium and of holding the associated control forces. The aircraft is then said to be *trimmed*, and the trim state defines the initial equilibrium condition about which the dynamics of interest may be studied. All aircraft are equipped with a means for presetting, or adjusting, the *datum*, *equilibrium*, or *trim* setting of the primary control surfaces. The ailerons, elevator, and rudder are all fitted with trim tabs for this purpose, which in all but the simplest aircraft may be adjusted from the cockpit in flight. However, all aircraft are fitted with a continuously adjustable elevator trim tab for the maintenance of longitudinal trim, which is continuously variable with flight conditions.

The object of trimming is to bring the forces and moments acting on the aircraft into a state of balance, or equilibrium. That is the condition when the net axial, normal, and side forces, and the net roll, pitch, and yaw moments are all zero. The force balance is often expressed approximately as the requirement that the lift equal the weight and the thrust equal the drag, since, by definition, the net side force must be zero in trimmed symmetric flight. Provided the aircraft is stable, it will then remain in equilibrium until it is disturbed by pilot control inputs or by external influences such as turbulence. The transient motion following such a disturbance is characterized by dynamic stability characteristics, and the stable aircraft will eventually settle into its equilibrium state once more.

4.1.2 Static stability

Static stability is generally defined as the initial tendency of an airplane, following a perturbation from a trimmed flight condition, to develop aerodynamic forces or moments that are in a direction to return the aircraft to the trimmed flight condition.

There are three categories of static stability that we can describe qualitatively: *statically stable*, *statically neutral*, and *statically unstable*. These are also called positive static stability, neutral static stability, and negative static stability (static instability). A simplified set of stability examples is shown

Copyright © 2025 Xiaowei He

in figure 4.1, where a ball begins in trim or steady-state equilibrium (dotted ball) on three different surfaces. Then the direction of the resulting force that develops after the ball is perturbed from the trim condition determines the type of static stability the system has. In the case shown in figure 4.1a, the ball is perturbed from the bottom of the bowl, and the resulting force tends to return it to the trim condition; thus, the system is statically stable. In the figure 4.1b case, when the ball is perturbed on a flat surface, no restoring force develops, and the ball would find a new equilibrium condition after a disturbance; the system is statically neutral. In the last case shown in figure 4.1c, when the ball is perturbed, the resulting force tends to make the ball further diverge from the trimmed position; thus, the system is statically unstable.

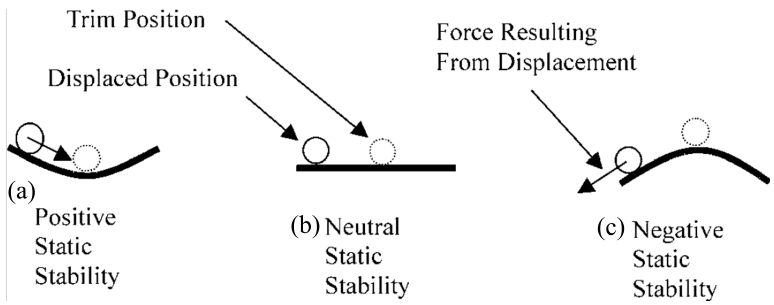

Figure 4.1: Examples of static stabilities [6].

For an aircraft, static stability is generally evaluated relative to a steady-state trimmed flight condition. If the aircraft is perturbed or displaced from the trimmed flight condition with a gust, for example, then the initial aerodynamic moment that results will determine the type of static stability that the aircraft has. As illustrated in figure 4.2, an aircraft initially flies in trim condition (figure 4.2a). If a gust produces a perturbation from the trimmed angle of attack, and an aerodynamic moment results that would rotate the aircraft back toward the trimmed condition, like in figure 4.2b, then we have positive static stability. If no aerodynamic moment results (figure 4.2c), we have neutral static stability. Finally, if an aerodynamic moment results that tends to increase the perturbation (figure 4.2d), we have negative static stability or static instability. Because pitching or longitudinal motion is depicted figure 4.2, we refer to the aircraft as having longitudinal static stability, neutral longitudinal static stability, or negative longitudinal static stability.

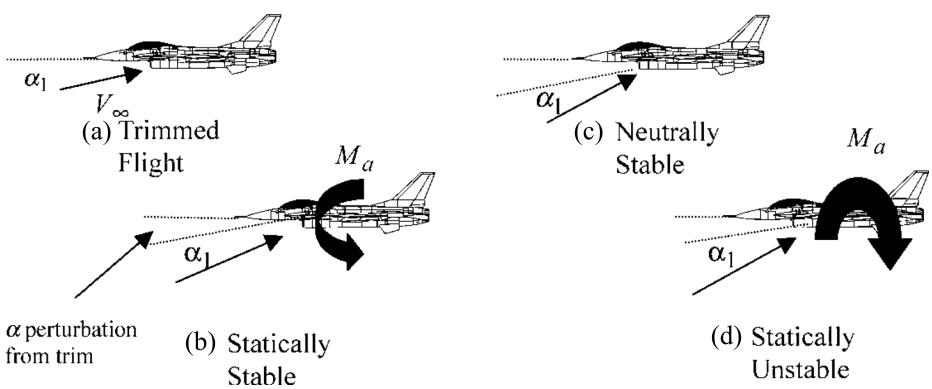

Figure 4.2: Examples of an aircraft in perturbed flight [6].

In establishing trim equilibrium, the pilot adjusts the elevator angle and thrust to obtain a lift force sufficient to support the weight and thrust sufficient to balance the drag at the desired speed and flight

Copyright © 2025 Xiaowei He

path angle. Since the airframe is symmetric, the equilibrium side force is zero. Provided that the speed is above the minimum drag speed, the force balance will remain stable with speed. Therefore, the static stability of the aircraft reduces to a consideration of the effects of angular disturbances about the three axes. Following such a disturbance, the aerodynamic forces and moments will no longer be in equilibrium, and in a statically stable aircraft, the resultant moments will cause the aircraft to converge on its initial condition.

4.2 Longitudinal static stability

4.2.1 Conditions of stability

Consider a positive incidence disturbance from equilibrium. This is in the nose-up sense and results in an increase in incidence α and hence in lift coefficient C_L. On a stable aircraft, the resulting pitching moment must be restored, that is, in the negative or nose-down sense. And the converse must be true following a nose-down disturbance. Thus the condition for longitudinal static stability may be determined by plotting the total aircraft pitching moment M or, equivalently, pitching moment coefficient C_m for variation in incidence α about the trim value α_e, as shown in figure 4.3. The nose-up disturbance increases α and takes the aircraft to the out-of-trim point p where the pitching moment coefficient becomes negative and is therefore restored. This property describes the *pitch stiffness* of an aircraft. A nose-down disturbance leads to a similar conclusion. As indicated, the aircraft is stable when the slope of this plot is negative. Thus, the condition for stable longitudinal trim at incidence α_e may be expressed as

$$C_m = 0$$

and

$$\frac{\mathrm{d}C_m}{\mathrm{d}\alpha} < 0. \tag{4.1}$$

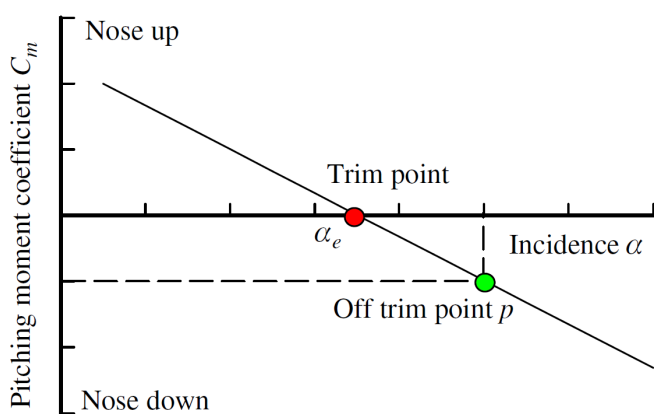

Figure 4.3: Examples of an aircraft in perturbed flight [1].

This observation is strictly valid only when it is assumed that the aerodynamic force and moment coefficients are functions of incidence only. This is usually an acceptable approximation for subsonic aircraft and, indeed, the plot of total aircraft pitching moment coefficient against incidence may well be very nearly linear as shown in figure 4.3. However, this argument becomes increasingly inappropriate with increasing Mach number. As compressibility effects become significant, the aerodynamic force

Copyright © 2025 Xiaowei He

and moment coefficients become functions of both incidence and Mach number. When this occurs, equation (4.1) may not always guarantee that stable trim can be achieved.

The more complex analysis by Gates and Lyon [13] takes speed effects into account and defines a general requirement for longitudinal static stability as

$$\frac{\mathrm{d}C_m}{\mathrm{d}C_L} < 0. \tag{4.2}$$

For subsonic aircraft equations (4.1) and (4.2) are completely interchangeable since α and C_L are linearly, or very nearly linearly, related by the lift curve slope a.

Inspection of figure 4.3 indicates that it is not possible to achieve trim unless the zero-incidence ($\alpha = 0$) pitch moment coefficient for the aircraft is positive, which determines the additional constraint for a stable trimmable aircraft:

$$C_m|_{\alpha=0} > 0. \tag{4.3}$$

More generally, it is a requirement that the zero-lift ($C_L = 0$)) pitch moment coefficient be positive as well for a trimmable aircraft:

$$C_m|_{C_L=0} > 0. \tag{4.4}$$

It is important to recognize that the pitch moment referred to in equations (4.3) and (4.4) is the *whole-aircraft* pitch moment, not to be confused with the *wing-body* zero-lift pitch moment coefficient C_{m_0}.

4.2.2 Degree of longitudinal stability

The condition for an aircraft to possess longitudinal static stability at a given trim condition is that the gradient of the $C_m - \alpha$ plot is negative. A large range of values of the gradient is possible, and the magnitude of the gradient determines the degree of stability possessed by the aircraft. Variation in the degree of longitudinal static stability is illustrated in figure 4.4. The degree of stability is described in terms of stability margin, which quantifies how much stability the aircraft has over and above zero or neutral stability. Thus, for example, the longitudinal static stability margin is directly related to the gradient of the $C_m - \alpha$ plot.

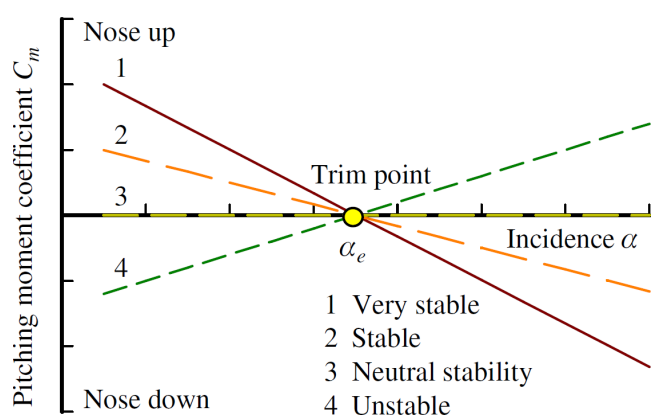

Figure 4.4: Degree of longitudinal static stability [1].

With reference to figure 4.4, and for a given disturbance in α, the corresponding restoring pitch moment C_m is greatest for a very stable aircraft. The magnitude of the restoring moment decreases as the

Copyright © 2025 Xiaowei He

degree of stability, or stability margin, is reduced and becomes zero at neutral stability. When the aircraft is unstable, the moment is of the opposite sign and is therefore divergent. Thus, the higher the degree of stability, the greater the restoring moment following a disturbance. This means that a very stable aircraft has significant pitch stiffness and will be very resistant to upset, which in turn means that greater control actions will be needed to encourage the aircraft to change its trim state or to maneuver. The stability margins determine the magnitude of the control actions, quantified in terms of displacement and force, required to trim the aircraft. A consequence of this is that too much stability can be as hazardous as too little stability, since the available control power is limited.

4.2.3 Power effects

The most significant variation in longitudinal static stability arises from the effects of power. Direct effects result from the point of application and line of action of the thrust forces with respect to the *cg*. As illustrated in figure 4.5, a high thrust line results in a nose-down pitching moment and vice versa. In normal trimmed flight, the thrust moment is additive to the aerodynamic moment, and the total pitching moment is trimmed to zero by adjustment of the elevator. However, any aerodynamic perturbation about trim that results in a thrust perturbation is potentially capable of giving rise to a nonlinear stability characteristic. The precise nature of the variation in stability is dependent on the operating characteristics of the installed power unit, which may not be easy to identify.

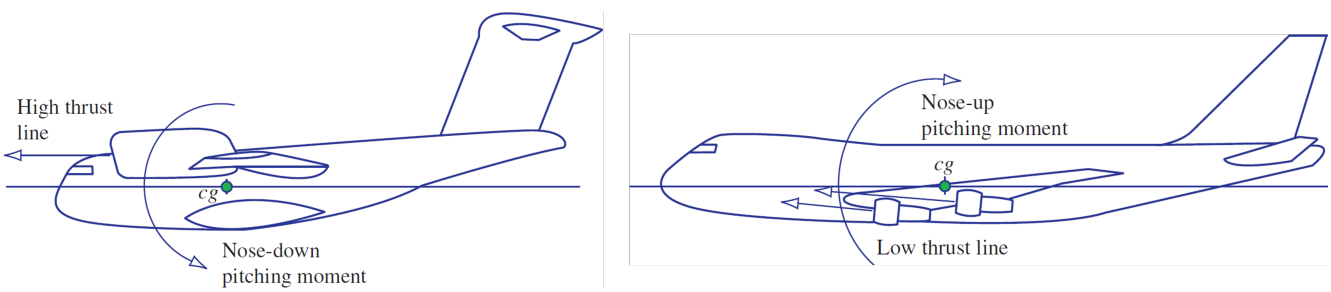

Figure 4.5: Typical thrust line effects on pitch moment [1].

Indirect power effects are caused by the induced flow associated with a propeller and its wake or the intake and exhaust of a gas turbine engine. Some of the more obvious induced-flow effects are illustrated in figure 4.6. The process of turning the incident flow through the body incidence angle into the propeller disc or the engine intake creates a normal force at the propeller or engine intake, as shown. In general, this effect gives rise to a nose-up pitching moment. The magnitude of the normal force is dependent on the body incidence angle and on the increase in flow energy at the propeller disc or engine intake. The force, therefore, varies considerably with trim condition.

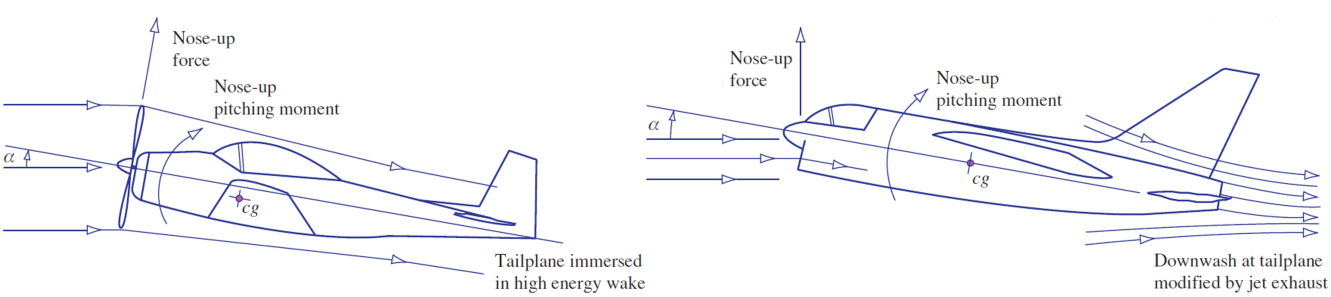

Figure 4.6: Typical induced-flow effects on pitch moment [1].

Copyright © 2025 Xiaowei He

The wake behind a propeller is a region of high-energy flow, which modifies the aerodynamic operating conditions over parts of the wing and tailplane. The greatest effect on pitch moment arises from the tailplane. The effectiveness of the tailplane is enhanced simply because of increased flow velocity and reduced downwash angle. These two effects together increase the nose-down pitch moment available and hence increase the degree of stability of the aircraft. The induced-flow effects associated with propeller-driven aircraft can have a significant influence on longitudinal static stability. These effects also change with aerodynamic conditions, especially at high angles of attack. It is therefore quite common to see some nonlinearity in the pitching moment trim plot for such an aircraft at high values of lift coefficient. It should also be noted that the propeller wake rotates about the longitudinal axis. Although less significant, the rotating flow has some influence on the aircraft's lateral-directional static stability.

The exhaust from a jet engine, being a region of very high velocity and reduced pressure, creates an inflow field, as indicated in figure 4.6. The influence on pitch moment depends on the relative location of the aerodynamic surfaces of the aircraft and the engine exhaust. When the tailplane is immersed in this induced-flow field, there is a change in the downwash angle. Thus, the effect is to increase static stability when the downwash angle is reduced and vice versa. In general, this effect is not very significant, except for aircraft with engines mounted in pods on the rear fuselage, where the tailplane is very close to the exhaust wake.

4.2.4 The pitch moment equation

A fully representative general pitch moment equation is difficult to develop since it is very dependent on the geometry of the aircraft. However, it is possible to develop a simple approximation that is sufficiently representative for most preliminary studies and provides considerable insight into the basic requirements for static stability and trim.

For the development of the simplest possible pitch moment equation, it is usual to define a model showing only the normal forces and pitching moments acting on the aircraft. It is assumed that in steady-level flight, the thrust and drag are in equilibrium and act through the *cg*; it is further assumed that, for small disturbances in incidence, changes in this equilibrium are insignificant. These assumptions, therefore, imply that small disturbances in incidence cause significant changes in lift forces and pitch moments only. The model defined in these terms is shown in figure 4.7.

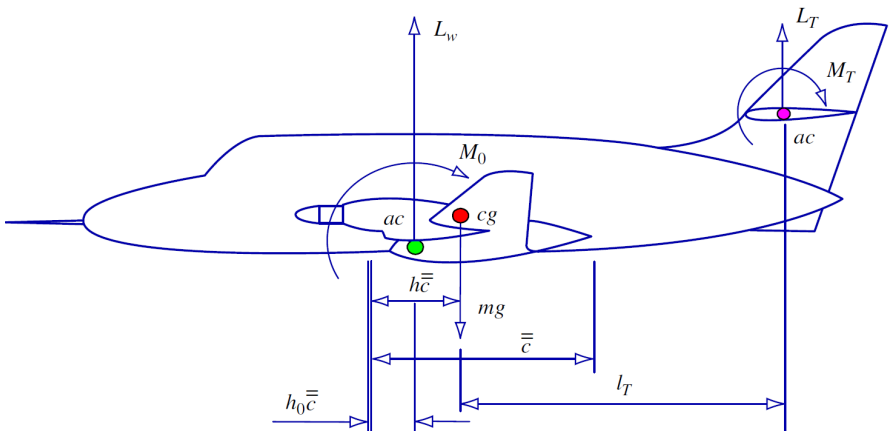

Figure 4.7: Simple pitching moment model [1].

For the purposes of modeling pitch behavior, the model comprises two parts: the wing-fuselage combination and the tailplane. It is thus assumed that the wing-fuselage combination behaves aerody-

Copyright © 2025 Xiaowei He

namically like a wing alone. However, this is not strictly true since the fuselage may make significant aerodynamic contributions and, in any event, its presence interferes with the aerodynamic properties of the wing to a greater or lesser extent. However, for conventional subsonic aircraft with a wing of reasonably high aspect ratio, this is a very satisfactory approximation. The tailplane is treated as a separate component since it provides the principal aerodynamic mechanism for controlling longitudinal static stability and trim. The following analysis establishes the fundamental importance of the tailplane parameters to longitudinal static stability.

The wing-fuselage lift L_w and residual pitch moment M_0 act at the aerodynamic center *ac* of the combination, which is assumed to be coincident with the aerodynamic center of the wing alone. Similarly, the lift L_T and pitch moment M_T of the tailplane are assumed to act at its aerodynamic center. The longitudinal geometry of the model is entirely related to the mean aerodynamic chord *mac* as shown in figure 4.7. An expression for the total pitching moment M about the *cg* may therefore be written as

$$M = M_0 + L_\mathrm{w}(h - h_0)\bar{\bar{c}} - L_\mathrm{T} l_\mathrm{T} + M_\mathrm{T}.$$

If it is assumed that the tailplane airfoil section is symmetric, then M_T becomes zero. We can write the coefficient form of the moment equation as

$$C_m = C_{m_0} + C_{L_\mathrm{w}}(h - h_0) - C_{L_\mathrm{T}}\overline{V}_\mathrm{T}, \tag{4.5}$$

where

$$\overline{V}_\mathrm{T} = \frac{S_\mathrm{T} l_\mathrm{T}}{S\bar{\bar{c}}}$$

is the tail volume ratio, which is a measure of the aerodynamic effectiveness of the tailplane as a stabilizing device with a typical range of $0.5 \leqslant \overline{V}_T \leqslant 1.3$.

To facilitate further analysis of pitch moment, it is necessary to express the tailplane lift coefficient C_{L_T} in terms of more accessible tailplane parameters. The tailplane lift coefficient may be expressed as

$$C_{L_\mathrm{T}} = a_0 + a_1\alpha_T + a_2\eta + a_3\beta_\eta, \tag{4.6}$$

where a_0, a_1, a_2, and a_3 are constant aerodynamic coefficients, α_T is the local incidence, η is the elevator angle, and β_η is the elevator trim tab angle. Note that, since a symmetric tailplane airfoil section is assumed, a_0 is zero. The local tailplane incidence is influenced by the *tailplane setting angle* η_T and the local flow distortion due to the effect of the downwash field behind the wing. The flow geometry is shown in figure 4.8.

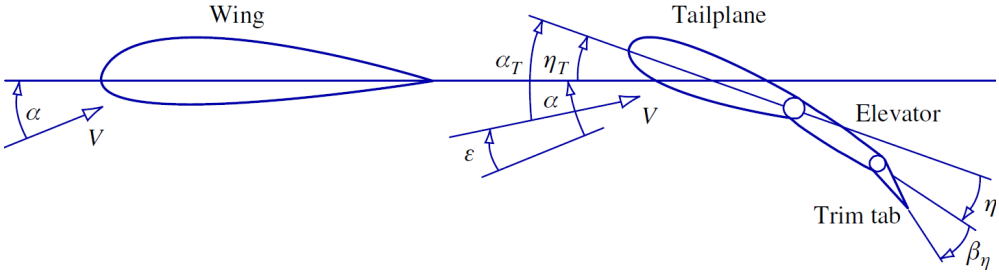

Figure 4.8: Wing-tailplane flow geometry [1].

The angle of attack of the tailplane is given by

$$\alpha_\mathrm{T} = \alpha - \varepsilon + \eta_\mathrm{T},$$

Copyright © 2025 Xiaowei He

where ε is the downwash angle at the tailplane. Since, to a good approximation, for small disturbances, the downwash angle is a function of wing-body incidence α only,

$$\alpha - \varepsilon = \alpha\left(1 - \frac{\mathrm{d}\varepsilon}{\mathrm{d}\alpha}\right) = \frac{C_{L_\mathrm{w}}}{a}\left(1 - \frac{\mathrm{d}\varepsilon}{\mathrm{d}\alpha}\right),$$

hence

$$\alpha_\mathrm{T} = \frac{C_{L_\mathrm{w}}}{a}\left(1 - \frac{\mathrm{d}\varepsilon}{\mathrm{d}\alpha}\right) + \eta_\mathrm{T}. \tag{4.7}$$

Note that a in equation (4.7) is the slope of the lift curve as reviewed in section 1.3.3.

Substituting the expression for α_T given by equation (4.7) into equation (4.6), substituting the resulting expression for C_{L_T} into equation equation (4.5), and noting that a_0 is zero, the pitch moment equation in its simplest and most general form is obtained:

$$C_m = C_{m_0} + C_{L_\mathrm{w}}(h - h_0) - \overline{V}_\mathrm{T}\left[C_{L_\mathrm{w}}\frac{a_1}{a}\left(1 - \frac{\mathrm{d}\varepsilon}{\mathrm{d}\alpha}\right) + a_2\eta + a_3\beta_\eta + a_1\eta_\mathrm{T}\right]. \tag{4.8}$$

Elevator angle to trim. As discussed in section 4.2.1, the condition for trim is that the total pitch moment be adjustable to zero (i.e., $C_m = 0$). Applying this condition to equation (4.8), the elevator angle required to trim the aircraft is given by

$$\eta = \frac{1}{\overline{V}_\mathrm{T} a_2}[C_{m_0} + C_{L_\mathrm{w}}(h - h_0)] - \frac{C_{L_\mathrm{w}}}{a}\left(\frac{a_1}{a_2}\right)\left(1 - \frac{\mathrm{d}\varepsilon}{\mathrm{d}\alpha}\right) - \frac{a_3}{a_2}\beta_\eta - \frac{a_1}{a_2}\eta_\mathrm{T}.$$

When the elevator tab is set at its neutral position ($\beta_\eta = 0$) and for a given *cg* position h, the elevator angle to trim varies only with lift coefficient. For any other tab setting, a different elevator angle is required to trim. Therefore, the elevator and elevator tab, to an extent, provide interchangeable means for achieving longitudinal trim.

Condition for longitudinal static stability. The basic requirement for an aircraft to be statically stable at a given trim condition is stated in equations (4.1) and (4.2). By differentiating equation (4.8) with respect to C_L or, equivalently, C_{L_w}, and noting that η_T and C_{m_0} are constants, the condition for the aircraft to be stable is given by

$$\frac{\partial C_m}{\partial C_{L_\mathrm{w}}} < 0,$$

where

$$\frac{\partial C_m}{\partial C_{L_\mathrm{w}}} = (h - h_0) - \overline{V}_\mathrm{T}\left[\frac{a_1}{a}\left(1 - \frac{\mathrm{d}\varepsilon}{\mathrm{d}\alpha}\right) + a_2\frac{\partial\eta}{\partial C_{L_\mathrm{w}}} + a_3\frac{\partial\beta_\eta}{\partial C_{L_\mathrm{w}}}\right]. \tag{4.9}$$

Thus, at a given *cg* position h, the longitudinal static stability of the aircraft and the aerodynamic control characteristics, that is, *elevator angle to trim* $\frac{\partial\eta}{\partial C_{L_\mathrm{w}}}$ and *elevator tab angle to trim* $\frac{\partial\beta_\eta}{\partial C_{L_\mathrm{w}}}$, are interdependent. Further analysis is usually carried out by separating the effects of elevator angle and tab angle in equation (4.9). *Controls-fixed stability* is concerned with the interdependence of elevator angle to trim and stability, whereas *controls-free stability* is concerned with the interdependence of elevator tab angle to trim and stability.

However, if we only look at the wing aerodynamic effect (ignoring the controls of the tailplane) for a moment, we have a most simplified form of the longitudinal stability condition

$$\frac{\partial C_m}{\partial C_{L_\mathrm{w}}} = (h - h_0),$$

Copyright © 2025 Xiaowei He

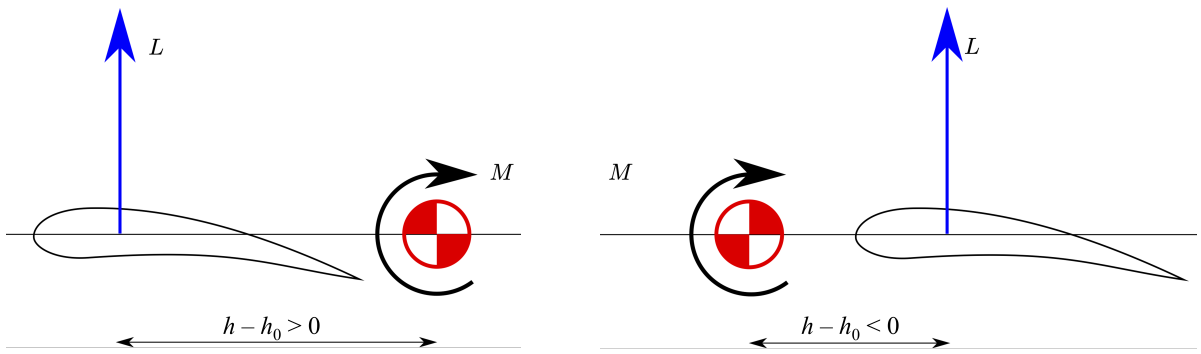

(a) *ac* ahead of *cg* (b) *ac* aft of *cg*

Figure 4.9: Effects of positions of *ac* and *cg* on longitudinal static stability [3].

which emphasizes the importance of the relative position between the aerodynamic center *ac* and the center of gravity *cg*. The two possibilities of the *ac* position relative to *cg* are illustrated in figure 4.9.

Consider the case with the *ac* ahead of the *cg* shown in figure 4.9a. The lift is directly proportional to the angle of attack α, and the nose-up moment M is directly proportional to the lift. The positions of *cg* and *ac* from the longitudinal reference h and h_0 gives

$$h - h_0 = \frac{\partial C_m}{\partial C_{L_\mathrm{w}}} > 0.$$

Therefore, with the *ac* ahead of the *cg*, the aircraft is statically unstable in pitch. In contrast, figure 4.9b shows a *ac* aft of *cg* configuration in which

$$h - h_0 = \frac{\partial C_m}{\partial C_{L_\mathrm{w}}} < 0,$$

and the aircraft is statically stable in pitch.

4.2.5 Controls-fixed stability

The condition described as *controls-fixed* is taken to mean the condition when the elevator and elevator tab are held at constant settings corresponding to the prevailing trim condition. In practice, this means that the pilot is flying the aircraft with one's hands on the controls and is holding the controls at the *fixed* setting required to trim. This assumes that the aircraft is stable and remains in trim.

Since the controls are fixed,

$$\frac{\mathrm{d}\eta}{\mathrm{d}C_{L_\mathrm{w}}} = \frac{\mathrm{d}\beta_\eta}{\mathrm{d}C_{L_\mathrm{w}}} = 0, \tag{4.10}$$

and equation (4.9) may be written as

$$\frac{\partial C_m}{\partial C_{L_\mathrm{w}}} = (h - h_0) - \overline{V}_\mathrm{T}\frac{a_1}{a}\left(1 - \frac{\mathrm{d}\varepsilon}{\mathrm{d}\alpha}\right), \tag{4.11}$$

or as

$$K_n = -\frac{\mathrm{d}C_m}{ddC_{L_\mathrm{w}}} = h_n - h, \tag{4.12}$$

Copyright © 2025 Xiaowei He

where K_n is the *controls-fixed stability margin*, the slope of the $C_m - C_L$ plot. The location of the controls-fixed neutral point h_n on the mean aerodynamic chord, $\bar{\bar{c}}$, is therefore given by

$$h_n = h_0 + \overline{V}_{\mathrm{T}} \frac{a_1}{a} \left(1 - \frac{\mathrm{d}\varepsilon}{\mathrm{d}\alpha}\right). \tag{4.13}$$

For a statically stable aircraft, the stability margin K_n is positive, and the greater its value, the greater the degree of stability. With reference to equation (4.12), it is clear that the aircraft is stable when the cg position h is ahead of the controls-fixed neutral point h_n. The acceptable margins of stability, therefore, determine the permitted range of *cg* position in a given aircraft. The aft limit often corresponds with the controls-fixed neutral point, whereas the forward limit is determined by the maximum permissible stability margin. Recall from section 4.2.2 that too much stability can be as hazardous as too little.

The meaning of controls-fixed stability is easily interpreted by considering the pilot actions required to trim an aircraft in a controls-fixed sense. It is assumed at the outset that the aircraft is in fact stable and hence can be trimmed to an equilibrium flight condition. When the aircraft is in a trimmed initial equilibrium state, the pitching moment is zero, and equation (4.8) may be written as

$$0 = C_{m_0} + C_{L_{\mathrm{w}}}(h - h_0) - \overline{V}_{\mathrm{T}} \left[C_{L_{\mathrm{w}}} \frac{a_1}{a} \left(1 - \frac{\mathrm{d}\varepsilon}{\mathrm{d}\alpha}\right) + a_2\eta + a_3\beta_\eta + a_1\eta_{\mathrm{T}} \right]. \tag{4.14}$$

It is assumed that the pilot is holding the controls at the required elevator angle, the power is set to give steady level flight, and the elevator tab is set at its datum, $\beta_\eta = 0$. To retrim the aircraft at a new flight condition in a controls-fixed sense, the pilot must move the controls to the new elevator setting and then hold the controls at that setting. For example, to retrim at a higher speed in a more nose-down attitude, the pilot moves the control column forward until one's new condition is established and then holds the column at that position. This leaves the aircraft in a descending condition unless the power is increased sufficiently to maintain level flight at the higher speed. However, power variations are not allowed for in the simple model reviewed here.

Thus, trimming a stable aircraft at any condition in its speed envelope simply requires the selection of the correct elevator angle, all other parameters remaining constant. The variable in the controls-fixed stability analysis is therefore the elevator angle to trim. Differentiating equation (4.14) with respect to $C_{L_{\mathrm{w}}}$ and making the same assumptions as before, but allowing elevator angle, η, to vary with trim, it may be shown, after some rearrangement, that

$$\frac{\mathrm{d}\eta}{\mathrm{d}C_{L_{\mathrm{w}}}} = -\frac{1}{\overline{V}_{\mathrm{T}} a_2}(h_n - h) = -\frac{K_n}{\overline{V}_{\mathrm{T}} a_2}. \tag{4.15}$$

Since $\overline{V}_{\mathrm{T}}$ and a_2 are constants, the elevator angle to trim characteristic $\mathrm{d}\eta/\mathrm{d}C_{L_{\mathrm{w}}}$ is thus proportional to the controls-fixed stability margin K_n. Measurements of elevator angle to trim for a range of flight conditions, subject to the assumptions described, provide a practical means for determining controls-fixed stability characteristics from flight experiments. However, in such experiments, it is not generally possible to completely eliminate the effects of power on the results.

Example 4.1

The practical evaluation of controls-fixed static stability centers on the application of section 4.2.4 and equations (4.14) and (4.15) to a stable aircraft. It is relatively straightforward to obtain measurements of the elevator angle, η, required to trim an aircraft at a chosen value of lift coefficient, C_L. Provided that the power and elevator trim tab angle, β_η, are maintained at constant settings through-

Copyright © 2025 Xiaowei He

out the measurement process, the equations apply directly. A flight test exercise conducted in a Handley Page Jetstream under these conditions provided the trim data plotted in figure 4.10 for three different cg positions. At any given value of lift coefficient, C_L, the corresponding value of elevator angle to trim, η, is given by the solution of section 4.2.4 or, alternatively, equation (4.14). The plots are clearly nonlinear, and the nonlinearity in this aircraft is almost entirely due to the effects of power.

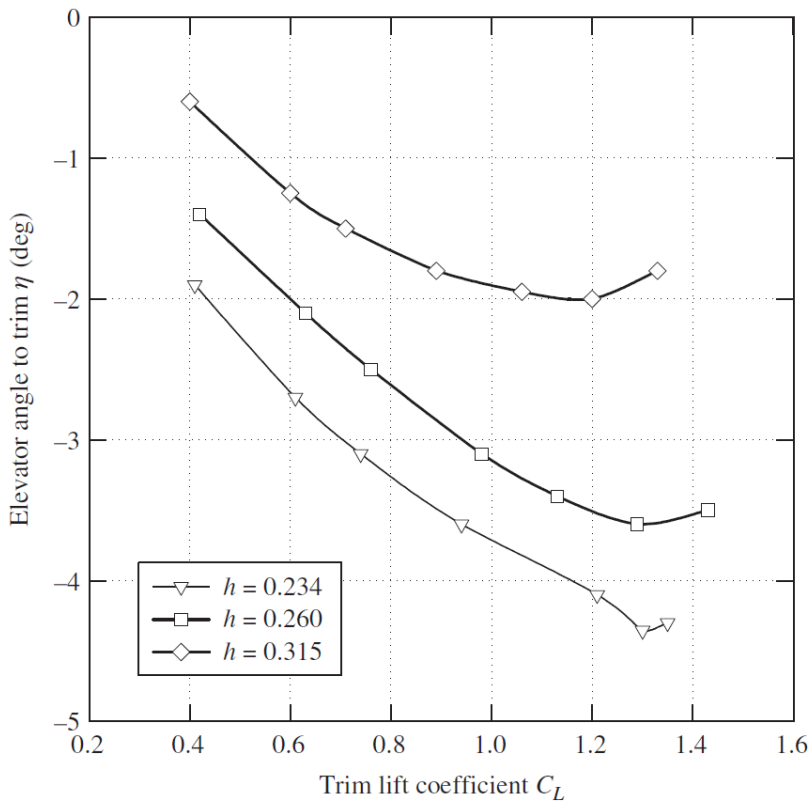

Figure 4.10: Plot of elevator angle to trim [1].

Since the gradients of the plots shown in figure 4.10 are all negative, the aircraft is statically stable in accordance with equation (4.15). However, for any given cg position, the gradient varies with lift coefficient, indicating a small variation in stability margin. In a detailed analysis, the stability margin would be evaluated at each value of trimmed lift coefficient in order to quantify the variation in stability. In the present example, the quality of the data was not good enough to allow such a complete analysis. To establish the location of the controls-fixed neutral point h_n, equation (4.15) must be solved at each value of trim lift coefficient. This is most easily done graphically, as shown in figure 4.11.

Copyright © 2025 Xiaowei He

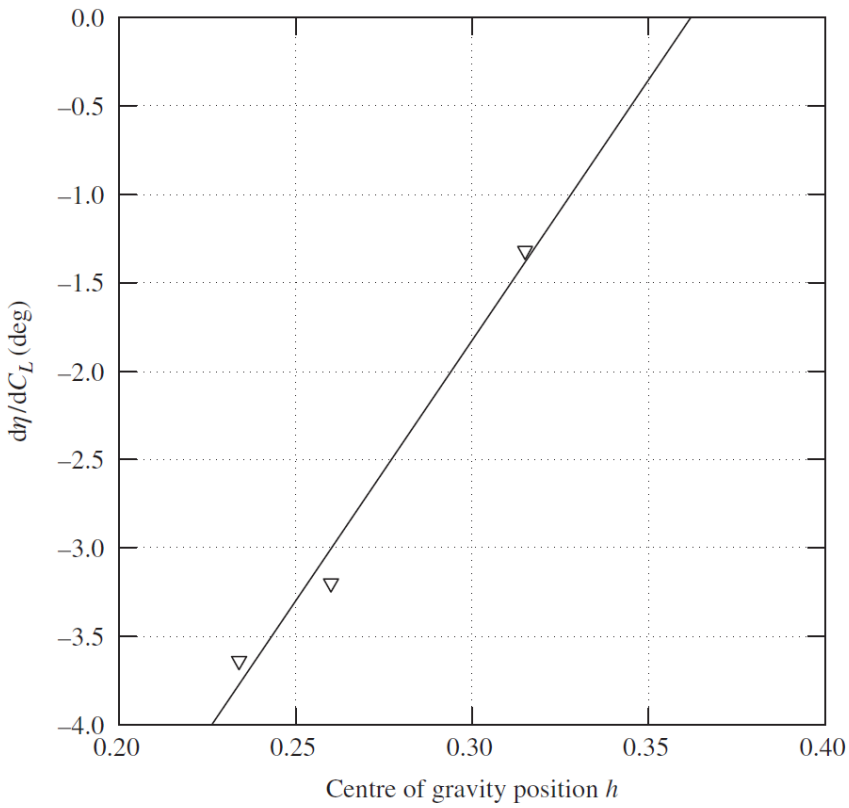

Figure 4.11: Determination of controls-fixed neutral point [1].

Equation (4.15) is solved by plotting $\mathrm{d}\eta/\mathrm{d}C_L$ against *cg* position h as shown. In this example, the mean gradient for each *cg* position, rather than the value at each trim point, is plotted. Since equation (4.15) represents a linear plot, a straight line may be fitted to the three data points as shown. Extrapolation to the neutral stability point at which $\mathrm{d}\eta/\mathrm{d}C_L = 0$ corresponds with a *cg* position of approximately $h = 0.37$. Clearly, three data points through which to draw a line are barely adequate for this kind of evaluation. A controls-fixed neutral point h_n at 37% of *mac* correlates well with the known properties of the aircraft. The most aft cg position permitted is in fact at 37% of *mac*. With the location of the controls-fixed neutral point established, the controls-fixed stability margin Kn for each cg position follows from the application of equation (4.15).

In a more thorough stability evaluation, a greater number of data points would be required, and data of higher quality would be essential. Although limited, the present example does illustrate the typical controls-fixed longitudinal static stability characteristics of a well-behaved classical aircraft.

4.3 Lateral-directional static stability

Lateral-directional static stability is concerned with the ability of the aircraft to recover equilibrium following a sideslip disturbance; it is the lateral-directional equivalent to longitudinal static stability in its interpretation. The lateral-directional equilibrium trim state is determined by the condition when the net side force and the net roll and yaw moments are all zero. Since conventional aircraft are geometrically symmetric, the side force is zero in trimmed rectilinear flight; whenever the aircraft experiences a sideslip disturbance, the resulting out-of-trim side force always acts in a sense to oppose the disturbance. Such a condition is always stable, so the lateral-directional stability properties of the aircraft reduce to a

Copyright © 2025 Xiaowei He

consideration of roll and yaw moment response to a sideslip disturbance. As for longitudinal stability, the transient motion following such a disturbance is characterized by dynamic stability properties, and the stable aircraft will eventually settle to its equilibrium state once more.

A positive sideslip disturbance is shown in figure 4.12, in which the aircraft slips to the right with velocity v. Thus, the disturbed aircraft velocity vector $\boldsymbol{V}$ is displaced to the right through the sideslip angle β, and it can be determined that

$$\tan\beta = \frac{v}{U},$$

where U is the axial component of velocity in the disturbance. Since the disturbance is assumed to be small, and in reality a sideslip angle greater than 10° would be considered excessive, it is usual to write

$$\beta \cong \frac{v}{U} \cong \frac{v}{V_0},$$

where V_0 is the undisturbed equilibrium velocity of the aircraft. As shown in figure 4.12, in the disturbance the nose of the aircraft is displaced to the left of the velocity vector, and the sideslip angle β is equivalent to the yaw angle $-\psi$ since the disturbance is assumed small.

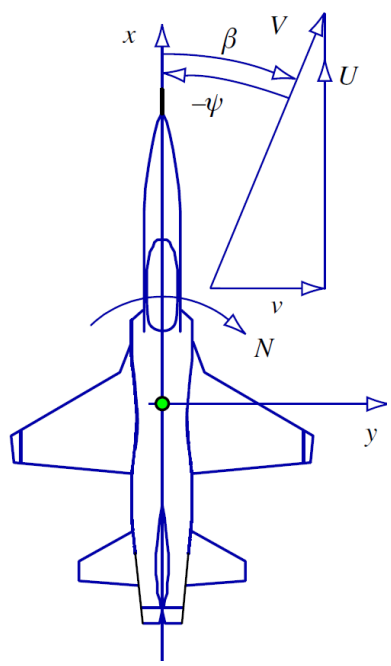

Figure 4.12: Sideslip disturbance [1].

Because the lateral-directional static stability of the aircraft is usually fixed by design, it usually remains more or less constant throughout the flight envelope. The lateral-directional stability margins, therefore, remain nominally constant for all flight conditions. This situation may well break down when large-amplitude maneuvering is considered. Under such circumstances, normally linear aerodynamic behavior may become very nonlinear and cause dramatic changes to observed lateral-directional stability and control characteristics. Although of considerable interest to the flight dynamicist, nonlinear behavior is beyond the scope of this course. Nominally constant lateral-directional static stability is assumed throughout.

Copyright © 2025 Xiaowei He

4.3.1 Lateral static stability

Lateral static stability is concerned with the ability of the aircraft to maintain wings-level equilibrium in the roll sense. Wing dihedral is the most visible parameter that confers lateral static stability on an aircraft, although there are many other contributions, some of which are destabilizing. Since all aircraft are required to fly with their wings level in the steady trim state, lateral static stability is designed in from the outset. Dihedral is the easiest parameter to adjust in the design process in order to "tune" the degree of stability to an acceptable level. Remember that too much lateral static stability results in an aircraft that is reluctant to maneuver in roll, so it is important to obtain the correct degree of stability in order not to compromise aileron control power.

The effect of dihedral as a means for providing lateral static stability is easily appreciated by considering the situation depicted in figure 4.13. Following a small positive disturbance in sideslip β, the right wing tends to drop, and the aircraft slides "downhill" to the right with a sideslip velocity v. Consider the resulting change in the aerodynamic conditions on the leading right wing, which has a dihedral angle Γ. Since the wing has dihedral, the sideslip velocity has a small component v' resolved perpendicular to the plane of the wing panel, of which

$$v' = v \sin \Gamma.$$

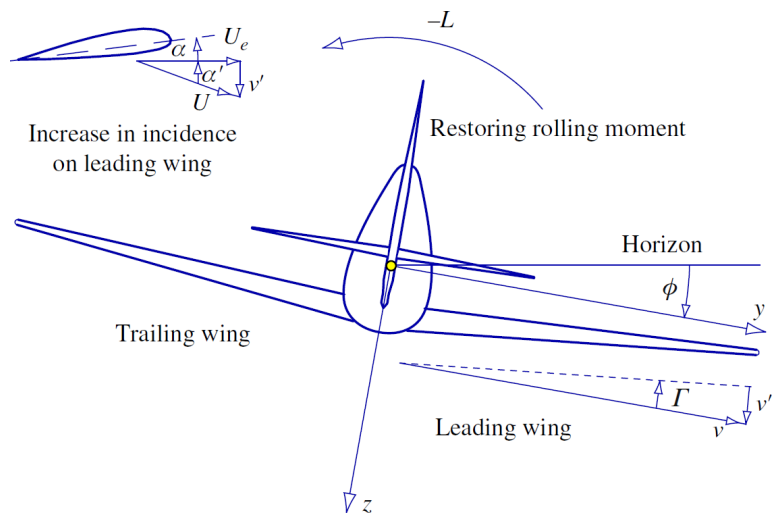

Figure 4.13: Dihedral effect [1].

The velocity component v' combines with the axial velocity component U_e to increase the angle of attack of the leading wing by α'. Since $v' \ll U_\mathrm{e}$, the change in the angle of attack α' is small, and the total disturbed axial velocity component $U \cong U_\mathrm{e}$. The increase in the angle of attack on the leading wing gives rise to an increase in lift, which in turn gives rise to a restoring roll moment $-L$. The corresponding aerodynamic change on the left wing trailing edge into the sideslip results in a small decrease in lift, which also produces a restoring roll moment. The net effect is therefore to create a negative roll moment, which causes the aircraft to recover its zero sideslip wings-level equilibrium. Thus, the condition for an aircraft to be laterally stable is that the roll moment resulting from a positive disturbance in sideslip be negative, or, in mathematical terms,

$$\frac{\mathrm{d}C_l}{\mathrm{d}\beta} < 0, \tag{4.16}$$

Copyright © 2025 Xiaowei He

where C_l is the roll moment coefficient. This is shown graphically in figure 4.14 and may be interpreted in a similar way to the pitch moment plot shown in figure 4.3.

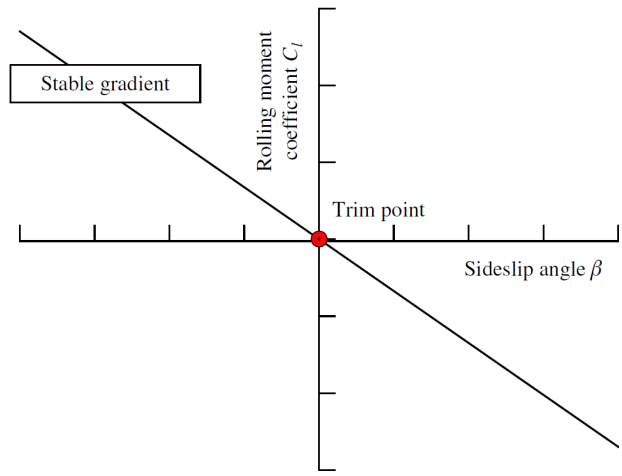

Figure 4.14: $C_l - \beta$ plot for a stable aircraft [1].

Note that the trim point for all flight conditions corresponds with zero sideslip angle, and that the gradient of the roll moment against sideslip plot must be negative for stability. As in the case of longitudinal static stability, the magnitude of the gradient determines the degree of lateral static stability; the correct value provides a satisfactory balance between stability and roll control of the aircraft.

The sequences of events following a sideslip disturbance are shown for a laterally stable, neutrally stable, and unstable aircraft in figure 4.15. However, it must be remembered that, once disturbed, the subsequent motion will be determined by the lateral dynamic stability characteristics as well.

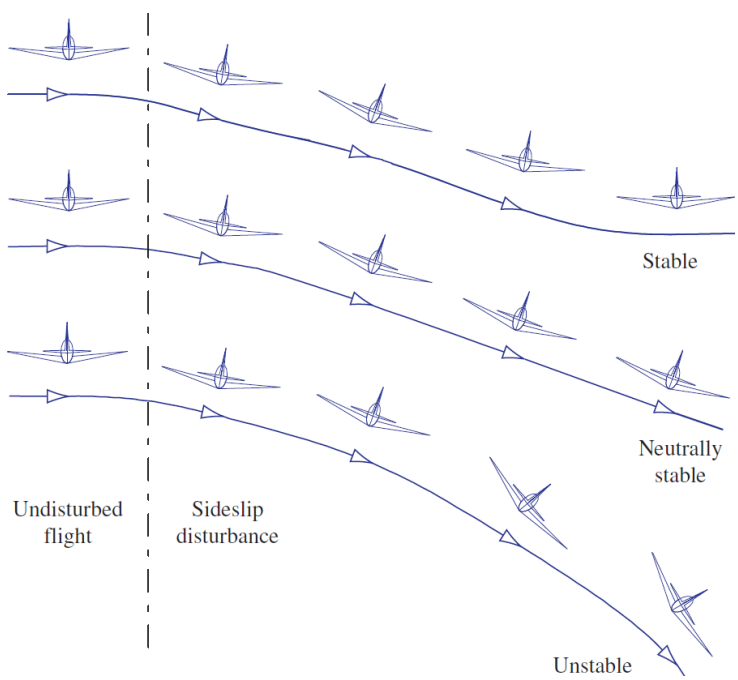

Figure 4.15: Effect of dihedral on lateral stability [1].

Copyright © 2025 Xiaowei He

Wing sweep can also make a significant positive contribution to lateral static stability. For this reason, dihedral is not commonly seen on swept-wing combat aircraft in order to avoid an excessive level of lateral stability, which would compromise roll maneuver performance. Instead, anhedral (negative dihedral), which is destabilizing, is used on some swept-wing combat aircraft as a means of "tuning" lateral static stability to an acceptable level.

With reference to figure 4.12, a wing in sideslip is effectively yawed through the sideslip angle such that $\psi = -\beta$. A swept wing in sideslip is therefore treated as a yawed wing, and it must be remembered that the disturbed aircraft tends to roll in the direction of sideslip. The lift on a yawed wing is determined by the component of velocity normal to the quarter-chord line in subsonic flight and normal to the leading edge in supersonic flight.

With reference to figure 4.16, consider a chordwise section c_h on the right wing panel, which is perpendicular to the quarter-chord line. Subsonic flow conditions are assumed, and the flow direction is parallel to the chord line. In the steady equilibrium flight condition, the chordwise component of velocity is given by

$$V_c = V_0 \cos \Lambda_{1/4}.$$

In the presence of a positive sideslip disturbance, this becomes

$$V_c' = \frac{V_0}{\cos \beta} \cos(\Lambda_{1/4} - \beta) \cong V_0 \cos(\Lambda_{1/4} - \beta),$$

where β is the sideslip angle, which is small by definition. Since $V_c' \geqslant V_c$, the lift on the right wing panel is increased in sideslip, which creates a negative roll moment to restore the aircraft to wings-level flight. On the left wing panel, there is a corresponding reduction in chordwise velocity in sideslip, which also creates a negative roll moment. It is therefore evident that wing sweep gives rise to a positive contribution to the lateral static stability of an aircraft.

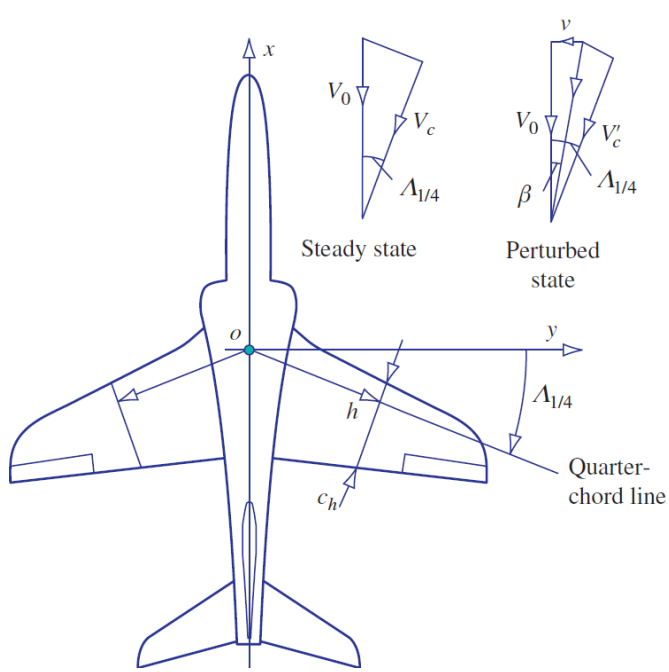

Figure 4.16: Swept wing in sideslip [1].

Copyright © 2025 Xiaowei He

The fin also contributes to lateral static stability, but its contribution can be stabilizing, destabilizing, or neutral depending on the steady trim condition when sideslip is experienced. With reference to figure 4.12, when in a sideslip, the fin is at incidence to the flow direction equal to the sideslip angle, which causes the fin to generate lift perpendicular to the flow direction.

4.3.2 Directional static stability

Directional static stability is concerned with the ability of the aircraft to yaw or weathercock into the wind in order to maintain directional equilibrium. Since all aircraft are required to fly with zero sideslip in the yaw sense, positive directional stability is designed in from the outset. The fin (vertical stabilizer/tail) is the most visible contributor to directional static stability, although, as in the case of lateral stability, there are many other contributions, some of which are destabilizing. Again, it is useful to remember that too much directional static stability results in an aircraft that is reluctant to maneuver directionally, so obtaining the correct degree of stability is important.

Consider an aircraft subject to a positive sideslip disturbance as shown in figure 4.17. The combination of sideslip velocity v and axial velocity component U results in a positive sideslip angle β. Note that a positive sideslip angle equates to a negative yaw angle since the nose of the aircraft has swung to the left of the resultant total velocity vector $\boldsymbol{V}$. In the disturbance, the fin is at a nonzero angle of attack equivalent to the sideslip angle β. It therefore generates lift L_{F}, which acts in the sense shown, thereby creating a positive yaw moment N. The yaw moment is stabilizing since it causes the aircraft to yaw to the right until the sideslip angle is reduced to zero. The condition for an aircraft to be directionally stable is thus readily established:

$$\frac{\mathrm{d}C_n}{\mathrm{d}\beta} > 0 \text{ or, equivalently, } \frac{\mathrm{d}C_n}{\mathrm{d}\psi} < 0, \tag{4.17}$$

where C_n is the yaw moment coefficient.

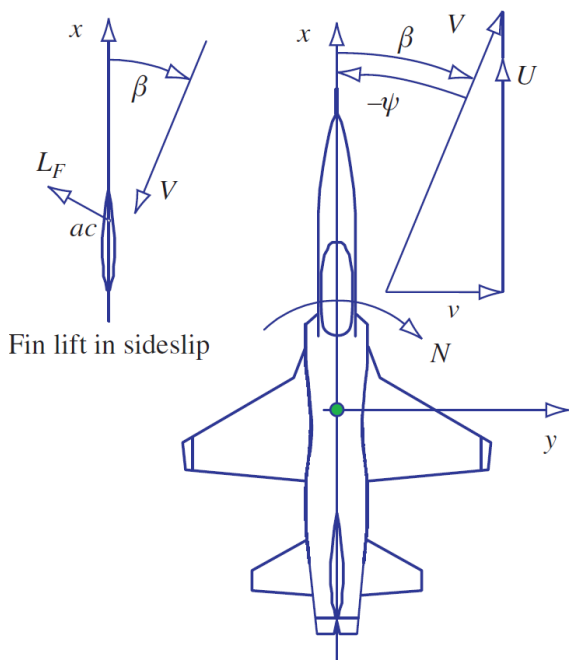

Figure 4.17: Directional weathercock effect [1].

Copyright © 2025 Xiaowei He

A typical plot of yaw moment against sideslip angle for a directionally stable aircraft is given in figure 4.18. It shows the results of a wind tunnel test on a simple conventional aircraft model. For small disturbances in yaw, the plot is reasonably linear since it is dominated by the lifting properties of the fin. However, as the fin approaches the stall, its lifting properties deteriorate and other influences begin to dominate, resulting ultimately in a loss of directional stability. The main destabilizing contribution comes from the fuselage, which at small yaw angles is masked by the powerful fin effect. The addition of a dorsal fin significantly delays the onset of fin stall, thereby enabling directional static stability to be maintained at higher yaw disturbance angles.

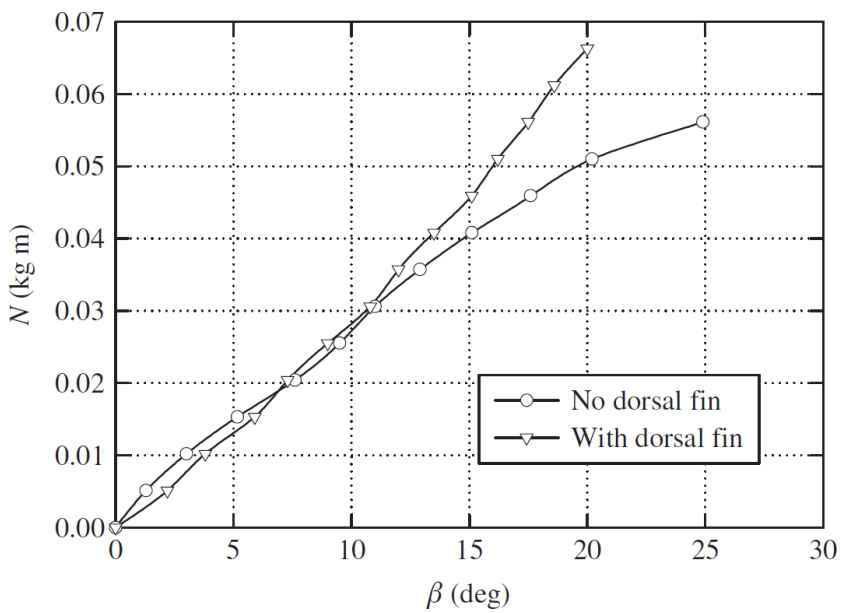

Figure 4.18: Plot of yaw moment against sideslip for a stable aircraft [1].

Fin effectiveness also deteriorates with increasing body incidence angle since the base of the fin becomes increasingly immersed in the fuselage wake, which reduces its effectiveness. This problem has become particularly evident in modern combat aircraft. Such aircraft typically have two engines mounted side by side in the rear fuselage. This results in a broad flat fuselage ahead of the fin, creating a substantial wake that dramatically reduces fin effectiveness at moderate to high angles of incidence. For this reason, many aircraft of this type have noticeably large fins and, in some cases, have two fins attached to the outer edges of the upper rear fuselage.

Additional sources of yaw moment in sideslip that contribute to the overall directional static stability of the aircraft may be identified, although they may not be so easy to quantify. For example, as shown in figures 4.13 and 4.15, the dihedral effect gives rise to differential lift across the wing span when in a sideslip disturbance. The associated differential-induced drag generates a yaw moment, which usually gives rise to a contribution to directional static stability. The side area of the fuselage, especially in very large aircraft, also makes some contribution to directional static stability. The side area ahead of and aft of the *cg* generates yaw moment in sideslip, and the magnitude and sign depend on the distribution of side area about the *cg*. Typically, the yaw moment due to sideslip arising from the side area is often negative and hence destabilizing.

Copyright © 2025 Xiaowei He

5 Aircraft Equations of Motion

The derivation of aircraft equations of motion is based on the application of Newton's second law of motion, Generalization of Newton's second law to a rigid body, together with analytical consideration of momentum leads to the principles of linear and angular momentum, which are equation (1.4) reviewed in section 1.3.1:

$$\begin{aligned} \Sigma \boldsymbol{F} &= m\boldsymbol{a}, \\ \Sigma \boldsymbol{M} &= \boldsymbol{I}\boldsymbol{\alpha}, \end{aligned} \tag{5.1}$$

which states that

$$\begin{aligned} \text{force} &= \text{mass} \times \text{inertial acceleration}, \\ \text{moment} &= \text{moment of inertia} \times \text{angular acceleration}. \end{aligned} \tag{5.2}$$

Thus, the derivation of aircraft equations of motion requires that Newton's second law be developed and expressed in terms of the motion variables defined in section 2.1.2. The derivation is classical in the sense that the equations of motion are differential equations derived from first principles.

5.1 Aircraft force equations

The force equations consist of aircraft response (in terms of accelerations) on the left-hand side of the equations, and the applied forces on the right-hand side of the equations. Newton's second law states that the time rate of change of linear momentum is equal to the summation of the applied forces acting on the aircraft's center of gravity:

$$m\frac{\mathrm{d}\boldsymbol{V}}{\mathrm{d}t}\bigg|_{\text{inertial}} = \boldsymbol{F}. \tag{5.3}$$

It is extremely important to understand that Newton's second law is only valid in an inertial reference frame. An inertial reference frame is an axis system that is fixed in space with no relative motion. For the purposes of analyzing aircraft, it will be assumed that the Earth axis system is an inertial reference frame, even though it does have rotation. It is assumed that the rotation rate of the Earth is small compared to the rotation rates of the aircraft.

5.1.1 Aircraft response of force equations

In developing the response side of the aircraft force equations, several additional assumptions will be made. First, it is assumed that the aircraft is a rigid body. This assumes that the different parts of the aircraft are not moving with respect to each other. The mass of the aircraft is also assumed to be constant, which is reasonable over a relatively short duration of time. Then, in the Earth axes, Newton's second law is rewritten as

$$m\frac{\mathrm{d}\boldsymbol{V}}{\mathrm{d}t}\bigg|_{\mathrm{E}} = m\boldsymbol{a}_{\mathrm{E}} = \boldsymbol{F}. \tag{5.4}$$

While Newton's second law is only valid with respect to an inertial reference frame (Earth axes), the equations can be expressed in the vehicle body axis system. If the equations are expressed in the body axis system, the fact that the system is rotating with respect to an inertial reference frame must be taken into account. Recall the general motion of a rigid body reviewed in section 1.3.1, the acceleration can be written as

$$\boldsymbol{a}_{\mathrm{b}} = \frac{\mathrm{d}\boldsymbol{V}_{\mathrm{b}}}{\mathrm{d}t} + \boldsymbol{\omega}_{\mathrm{b}} \times \boldsymbol{V}_{\mathrm{b}}. \tag{5.5}$$

Copyright © 2025 Xiaowei He

The velocity vector in the body axis system $\boldsymbol{V}_\mathrm{b}$ is defined as

$$\boldsymbol{V}_\mathrm{b} = \begin{bmatrix} U \\ V \\ W \end{bmatrix}_\mathrm{b}, \tag{5.6}$$

where U, V, and W are the velocities in the x, y, and z body axes, respectively. The aircraft angular rate in the body axis system $\boldsymbol{\omega}_\mathrm{b}$ is defined as

$$\boldsymbol{\omega}_\mathrm{b} = \begin{bmatrix} p \\ q \\ r \end{bmatrix}_\mathrm{b}, \tag{5.7}$$

where p, q, and r are the roll, pitch, and yaw rates, respectively, expressed in the body axes. (Note that they are *not* equivalent to the attitude rates $\dot{\phi}$, $\dot{\theta}$, and $\dot{\psi}$, as explained in section 2.1.6.) Therefore, we have

$$\boldsymbol{a}_\mathrm{b} = \begin{bmatrix} \dot{U} \\ \dot{V} \\ \dot{W} \end{bmatrix}_\mathrm{b} + \begin{vmatrix} \boldsymbol{i} & \boldsymbol{j} & \boldsymbol{k} \\ p & q & r \\ U & V & W \end{vmatrix}_\mathrm{b} = \begin{bmatrix} \dot{U} + qW - rV \\ \dot{V} + rU - pW \\ \dot{W} + pV - qU \end{bmatrix}_\mathrm{b}. \tag{5.8}$$

Multiplying the inertial acceleration in the body axis system by the mass of the aircraft yields the three force equations

$$m\boldsymbol{a}_\mathrm{b} = m \begin{bmatrix} \dot{U} + qW - rV \\ \dot{V} + rU - pW \\ \dot{W} + pV - qU \end{bmatrix}_\mathrm{b} = \begin{bmatrix} X \\ Y \\ Z \end{bmatrix}_\mathrm{b} = \boldsymbol{F}_\mathrm{b}, \tag{5.9}$$

where X, Y, and Z are the force components in x, y, and z body axes, respectively.

5.1.2 Applied forces

The left-hand side of equation (5.9) is the response side of the force equations. The right-hand side of each equation consists of the applied forces that act on the aircraft. They consist of gravity forces, aerodynamic forces, and thrust forces. From section 2.1.3, we know that

$$\boldsymbol{F}_{\boldsymbol{g}_\mathrm{E}} = \begin{bmatrix} 0 \\ 0 \\ mg \end{bmatrix}_\mathrm{E}, \qquad \boldsymbol{F}_{\mathrm{a_w}} = \begin{bmatrix} -D \\ Y_\mathrm{a} \\ -L \end{bmatrix}_\mathrm{w}, \qquad \boldsymbol{F}_{\boldsymbol{T}\mathrm{b}} = \begin{bmatrix} T\cos\phi_T \\ Y_T \\ -T\sin\phi_T \end{bmatrix}_\mathrm{b}. \tag{5.10}$$

Because the left-hand sides of equation (5.9) are developed in the body axis system, the right-hand side must also be in the body axis system. Therefore, each of the forces must be represented in the body axis system for the equations to be valid. Using axis transformation and the results of examples 2.1 and 2.2,

$$\begin{aligned} \boldsymbol{F}_{\boldsymbol{g}_\mathrm{b}} &= \boldsymbol{R}(\phi,\theta,\psi)\boldsymbol{F}_{\boldsymbol{g}_\mathrm{E}} = \begin{bmatrix} -mg\sin\theta \\ mg\sin\phi\cos\theta \\ mg\cos\phi\cos\theta \end{bmatrix}_\mathrm{b}, \\ \boldsymbol{F}_{\mathrm{a_b}} &= \boldsymbol{R}(\theta=\alpha)\boldsymbol{F}_{\mathrm{a_w}} = \begin{bmatrix} -D\cos\alpha + L\sin\alpha \\ Y_\mathrm{a} \\ -D\sin\alpha - L\cos\alpha \end{bmatrix}_\mathrm{b}. \end{aligned} \tag{5.11}$$

Then we can add these force vectors in the same reference frame

$$\boldsymbol{F}_\mathrm{b} = \boldsymbol{F}_{\boldsymbol{g}_\mathrm{b}} + \boldsymbol{F}_{\mathrm{a_b}} + \boldsymbol{F}_{\boldsymbol{T}_\mathrm{b}} = \begin{bmatrix} -mg\sin\theta + (-D\cos\alpha + L\sin\alpha) + T\cos\phi_T \\ mg\sin\phi\cos\theta + Y_\mathrm{a} + Y_T \\ mg\cos\phi\cos\theta + (-D\sin\alpha - L\cos\alpha) - T\sin\phi_T \end{bmatrix}_\mathrm{b}. \tag{5.12}$$

Copyright © 2025 Xiaowei He

Now combining equations (5.9) and (5.12) we have derived the three force equations of a rigid body aircraft, of which the body axis system is co-located with its *cg*

$$\begin{aligned} m(\dot{U} + qW - rV) &= -mg\sin\theta + (-D\cos\alpha + L\sin\alpha) + T\cos\phi_T, \\ m(\dot{V} + rU - pW) &= mg\sin\phi\cos\theta + Y_{\mathrm{a}} + Y_T, \\ m(\dot{W} + pV - qU) &= mg\cos\phi\cos\theta + (-D\sin\alpha - L\cos\alpha) - T\sin\phi_T. \end{aligned} \tag{5.13}$$

5.2 Aircraft moment equations

Newton's second law for rotational motion states that the time rate of change in the angular momentum of the aircraft is equal to the applied moments acting on the aircraft, that is,

$$\left.\frac{\mathrm{d}\boldsymbol{H}}{\mathrm{d}t}\right|_{\text{inertial}} = \boldsymbol{M}. \tag{5.14}$$

$\boldsymbol{H}$ is the angular momentum of the aircraft and is defined as

$$\boldsymbol{H} = \boldsymbol{I}\boldsymbol{\omega}, \tag{5.15}$$

where $\boldsymbol{I}$ is the inertia tensor of the aircraft and $\boldsymbol{\omega}$ is the angular body rate of the aircraft. The inertia tensor of an aircraft is

$$\boldsymbol{I}_{\mathrm{b}} = \begin{bmatrix} I_{xx} & -I_{xy} & -I_{xz} \\ -I_{xy} & I_{yy} & -I_{yz} \\ -I_{xz} & -I_{yz} & I_{zz} \end{bmatrix}_{\mathrm{b}}. \tag{5.16}$$

Aircraft inertia tensor. Newton's second law relates mass to acceleration, and mass may be considered as a body's tendency to resist a change in velocity. The analog for rotation is *moments of inertia*, which are on the diagonal of the inertia tensor $\boldsymbol{I}$. For example, I_{xx} indicates the resistance to rotation about the x-axis of the aircraft. The off-diagonal terms of the inertia tensor are the *products of inertia*, which indicate the symmetry of the aircraft. In general, the inertia tensor describes the mass distribution of an aircraft as shown in figure 5.1.

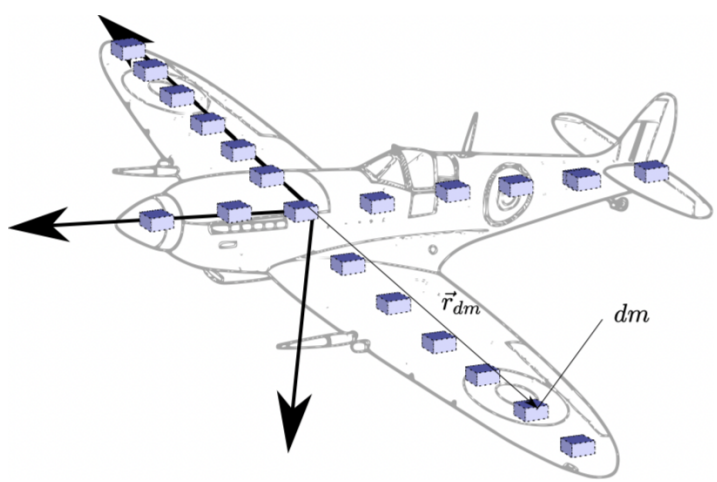

Figure 5.1: Aircraft inertia tensor as mass distributions [3].

From basic dynamics, the moments of inertia are defined as

$$I_{xx} = \int (y^2 + z^2)\mathrm{d}m, \qquad I_{yy} = \int (x^2 + z^2)\mathrm{d}m, \qquad I_{zz} = \int (x^2 + y^2)\mathrm{d}m, \tag{5.17}$$

Copyright © 2025 Xiaowei He

and the products of inertia are defined as

$$I_{xy} = \int xy\mathrm{d}m, \qquad I_{xz} = \int xz\mathrm{d}m, \qquad I_{yz} = \int yz\mathrm{d}m. \tag{5.18}$$

Simplification of the inertia tensor via symmetry. In general, most aircraft are symmetric about a longitudinal/vertical plane (xz plane slice it down the middle), and will also tend to have the principal yaw tensor axis aligned with z_b, as illustrated in figure 5.2. Therefore, we have $I_{xy} = 0$ and $I_{yz} = 0$. However, the I_{xz} is not necessarily zero because the aircraft is not symmetrical from top to bottom about the xy plane and not symmetrical from front to rear about the yz plane.

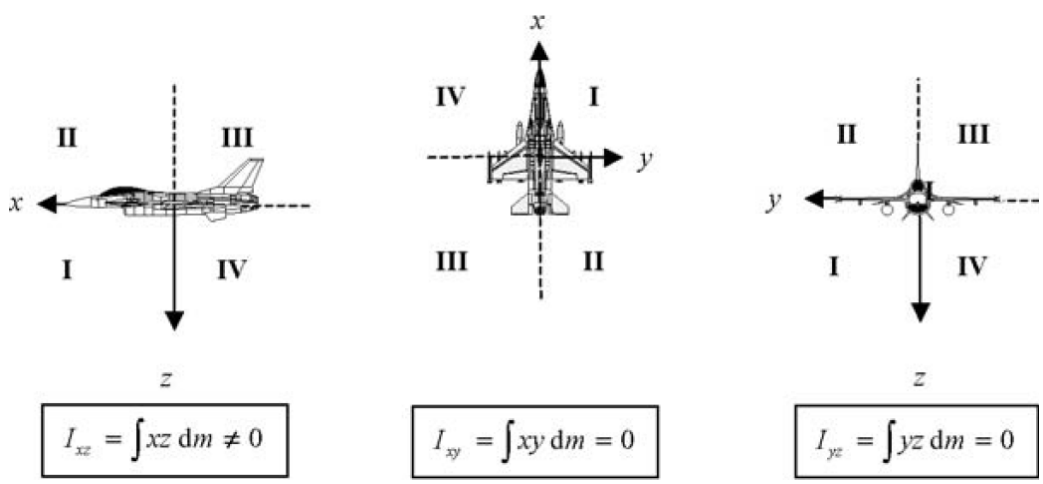

Figure 5.2: Aircraft products of inertia [6].

Consequently, the inertia tensor of an aircraft can be simplified to

$$\boldsymbol{I}_\mathrm{b} = \begin{bmatrix} I_{xx} & 0 & -I_{xz} \\ 0 & I_{yy} & 0 \\ -I_{xz} & 0 & I_{zz} \end{bmatrix}_\mathrm{b}. \tag{5.19}$$

Thus, the angular momentum of an aircraft is

$$\boldsymbol{H}_\mathrm{b} = \boldsymbol{I}_\mathrm{b}\boldsymbol{\omega}_\mathrm{b} = \begin{bmatrix} I_{xx} & 0 & -I_{xz} \\ 0 & I_{yy} & 0 \\ -I_{xz} & 0 & I_{zz} \end{bmatrix}_\mathrm{b} \begin{bmatrix} p \\ q \\ r \end{bmatrix}_\mathrm{b} = \begin{bmatrix} pI_{xx} - rI_{xz} \\ qI_{yy} \\ rI_{zz} - pI_{xz} \end{bmatrix}_\mathrm{b} \tag{5.20}$$

5.2.1 Aircraft response of moment equations

Again, Newton's second law must be used in an inertial reference frame, which is the Earth reference frame in our case. Since the inertia tensor and the angular body rates are defined in the body reference frame, we transform all quantities into the body axes for convenience and to be consistent with the force equations. Similar to the acceleration, the time rate of change of the angular momentum in the Earth axes can be expressed in the body-fixed axes as

$$\frac{\mathrm{d}\boldsymbol{H}}{\mathrm{d}t} = \frac{\mathrm{d}\boldsymbol{H}_\mathrm{b}}{\mathrm{d}t} + \boldsymbol{\omega}_\mathrm{b} \times \boldsymbol{H}_\mathrm{b} \tag{5.21}$$

Copyright © 2025 Xiaowei He

Plugging in equation (5.16) and $\boldsymbol{\omega}_\mathrm{b}$ we have

$$\frac{\mathrm{d}\boldsymbol{H}}{\mathrm{d}t} = \frac{\mathrm{d}}{\mathrm{d}t}\begin{bmatrix} pI_{xx} - rI_{xz} \\ qI_{yy} \\ rI_{zz} - pI_{xz} \end{bmatrix}_\mathrm{b} + \begin{vmatrix} \boldsymbol{i} & \boldsymbol{j} & \boldsymbol{k} \\ p & q & r \\ pI_{xx} - rI_{xz} & qI_{yy} & rI_{zz} - pI_{xz} \end{vmatrix} \tag{5.22}$$

Assuming that the mass distribution of the aircraft is constant, such as neglecting fuel slosh, the moments and products of inertia do not change with time; that is, the time derivatives of elements of the inertia tensor are all zero. Therefore,

$$\frac{\mathrm{d}\boldsymbol{H}}{\mathrm{d}t} = \begin{bmatrix} \dot{p}I_{xx} - \dot{r}I_{xz} \\ \dot{q}I_{yy} \\ \dot{r}I_{zz} - \dot{p}I_{xz} \end{bmatrix}_\mathrm{b} + \begin{bmatrix} q(rI_{zz} - pI_{xz}) - rqI_{yy} \\ r(pI_{xx} - rI_{xz}) - p(rI_{zz} - pI_{xz}) \\ pqI_{yy} - q(pI_{xx} - rI_{xz}) \end{bmatrix}_\mathrm{b} \tag{5.23}$$

$$\frac{\mathrm{d}\boldsymbol{H}}{\mathrm{d}t} = \begin{bmatrix} \dot{p}I_{xx} + qr(I_{zz} - I_{yy}) - (\dot{r} + pq)I_{xz} \\ \dot{q}I_{yy} - pr(I_{zz} - I_{xx}) + (p^2 + r^2)I_{xz} \\ \dot{r}I_{zz} + pq(I_{yy} - I_{xx}) + (qr - \dot{p})I_{xz} \end{bmatrix}_\mathrm{b} = \begin{bmatrix} L \\ M \\ N \end{bmatrix}_\mathrm{b} = \boldsymbol{M}_\mathrm{b}, \tag{5.24}$$

where L, M, and N are the components of the moment vector on x, y, and z axes, i.e., roll, pitch, and yaw moments. Note not to confuse roll moment with lift or pitch moment with the resultant moment vector.

The aircraft response side of equation (5.24) has three types of terms:

- Angular acceleration terms. Represent a change to angular momentum due to a change in angular rate about that axis. For example, if we take the roll moment EOM and assume the gyro precession and coupling terms are negligible, we have

$$\dot{p}I_{xx} = L. \tag{5.25}$$

  If a roll moment L is applied to the aircraft (such as with an aileron deflection), this equation predicts that an angular acceleration in roll $\dot{p}$ will result. For a given applied roll moment, the larger the moment of inertia I_{xx}, the smaller the roll angular acceleration $\dot{p}$. The angular acceleration.

- Gyro precession terms. Describe the precession of the aircraft because of the combination of angular momentum about an axis and an applied moment, and the respective differences in their moments of inertia. For example, consider the roll moment EOM for the case of a roll pull-up. Assume the angular acceleration and coupling terms are negligible along with I_{zz}

$$-qrI_{yy} = L. \tag{5.26}$$

  Noticing that qI_{yy} is the angular momentum in pitch,

$$-r(qI_{yy}) = L. \tag{5.27}$$

  If the pilot applies a positive roll moment to the aircraft by deflecting the ailerons, this equation predicts that a negative yaw rate r must result.

- Coupling terms. Describe the inertial coupling tendency of the aircraft, which can be identified by the I_{xz} product of inertia. A nonzero value of I_{xz} indicates inertial asymmetry of the aircraft. Consider the pitch moment EOM with the gyro precession and applied pitching moment terms assumed negligible and zero yaw rate r.

$$p^2 I_{xz} = -\dot{q}I_{yy}. \tag{5.28}$$

Copyright © 2025 Xiaowei He

We assume the aircraft is doing a high-speed fly-by and has a negative I_{xz}. If the pilot does a snap roll in either direction, this equation predicts that a positive angular acceleration $\dot{q}$ will result. This will cause the aircraft to pitch up and could lead to serious effects if the pilot does not anticipate the pitch up. It can be counteracted with a nose-down stick input.

5.2.2 Applied moments

The applied moments consist of the aerodynamic roll L_a, pitch M_a, and yaw N_a moments, and the roll, pitch, and yaw moments because of thrust, L_T, M_T, and N_T, respectively. There are no moments because of gravity because the weight vector acts through the center of gravity, and the moment arms are zero. Also, any moments because of rotating masses (such as jet engines) on or within the aircraft have been neglected. Therefore,

$$\begin{aligned}
\dot{p}I_{xx} + qr(I_{zz} - I_{yy}) - (\dot{r} + pq)I_{xz} &= L_\mathrm{a} + L_T, \\
\dot{q}I_{yy} - pr(I_{zz} - I_{xx}) + (p^2 + r^2)I_{xz} &= M_\mathrm{a} + N_T, \\
\dot{r}I_{zz} + pq(I_{yy} - I_{xx}) + (qr - \dot{p})I_{xz} &= N_\mathrm{a} + N_T.
\end{aligned} \tag{5.29}$$

5.3 Decoupled equations of motion

The six aircraft equations of motion (equations (5.13) and (5.29)) can be decoupled into two sets of three equations. These are the three longitudinal EOM and the three lateral-directional EOM. This is convenient in that it requires only three equations to be solved simultaneously for many flight conditions. For example, an aircraft in wings-level flight with no sideslip and a pitching motion can be analyzed using only the longitudinal EOM because the aircraft does not have any lateral-directional motion.

5.3.1 Longitudinal equations of motion

The three longitudinal EOM consist of the x-force, y-moment, and z-force equations,

$$\begin{aligned}
m(\dot{U} + qW - rV) &= -mg\sin\theta + (-D\cos\alpha + L\sin\alpha) + T\cos\phi_T, \\
\dot{q}I_{yy} - pr(I_{zz} - I_{xx}) + (p^2 + r^2)I_{xz} &= M_\mathrm{a} + N_T, \\
m(\dot{W} + pV - qU) &= mg\cos\phi\cos\theta + (-D\sin\alpha - L\cos\alpha) - T\sin\phi_T.
\end{aligned} \tag{5.30}$$

The L in equation (5.30) refers to lift and not roll moment. The longitudinal EOM pictures an aircraft with its xz plane coincident with an xz plane fixed in space. Longitudinal motion consists of those movements where the aircraft would only move within that xz plane, that is, translation in the x direction, translation in the z direction, and rotation about the y axis. In each of these cases, the xz plane of the aircraft would be moving within an xz plane fixed in space.

5.3.2 Lateral-directional equations of motion

The lateral-directional EOM consist of the x-moment, y-force, and z-moment equations,

$$\begin{aligned}
\dot{p}I_{xx} + qr(I_{zz} - I_{yy}) - (\dot{r} + pq)I_{xz} &= L_\mathrm{a} + L_T, \\
m(\dot{V} + rU - pW) &= mg\sin\phi\cos\theta + Y_\mathrm{a} + Y_T, \\
\dot{r}I_{zz} + pq(I_{yy} - I_{xx}) + (qr - \dot{p})I_{xz} &= N_\mathrm{a} + N_T.
\end{aligned} \tag{5.31}$$

For any lateral-directional motion, the xz plane would move out of some xz plane fixed in space. Translation in the y direction, roll about the x axis, and yaw about the z axis would all cause the xz plane of the aircraft to move out of that arbitrarily fixed xz plane in space.

Copyright © 2025 Xiaowei He

5.3.3 Kinematic equations

Taking a closer look at equations (5.30) and (5.31), we find that there are six EOM but nine unknowns, which are,

$$\underbrace{U, \quad V, \quad W}_{\text{translational velocities}} \quad , \qquad \underbrace{p, \quad q, \quad r}_{\text{rotational velocities}} \quad , \qquad \underbrace{\phi, \quad \theta, \quad \psi}_{\substack{\text{Euler angles} \\ \text{(aircraft attitudes)}}} \quad , \tag{5.32}$$

In order to completely solve the aircraft problem, three more equations are required. These additional equations are obtained by relating the body rates (p, q, and r) to the attitude rates ($\dot{\phi}$, $\dot{\theta}$, and $\dot{\psi}$), where the following equality must be satisfied because the magnitude of the body rates must equal the magnitude of attitude rates (recall equation (2.26)). Note that these are vector equations.

$$\boldsymbol{\omega}_{\mathrm{b}} = p\boldsymbol{i} + q\boldsymbol{j} + r\boldsymbol{k} = \dot{\boldsymbol{\phi}}_{\mathrm{b}} + \dot{\boldsymbol{\theta}}_{\mathrm{b}} + \dot{\boldsymbol{\psi}}_{\mathrm{b}} \tag{5.33}$$

In other words,

$$\sqrt{p^2 + q^2 + r^2} = \sqrt{\dot{\boldsymbol{\phi}}^2 + \dot{\boldsymbol{\theta}}^2 + \dot{\boldsymbol{\psi}}^2}. \tag{5.34}$$

Example 5.1

An aircraft has the following Euler angles and Euler rates:

$$\begin{aligned} \phi &= 90\,\mathrm{deg}, & \dot{\phi} &= 0\,\mathrm{deg/s}, \\ \theta &= 0\,\mathrm{deg}, & \dot{\theta} &= 0\,\mathrm{deg/s}, \\ \psi &= 0\,\mathrm{deg}, & \dot{\psi} &= 10\,\mathrm{deg/s}. \end{aligned}$$

Solution: Applying equation (2.26) yields:

$$\begin{aligned} p &= \dot{\phi} - \dot{\psi}\sin\theta = 0\,\mathrm{deg/s}, \\ q &= \dot{\theta} + \dot{\psi}\sin\phi\cos\theta = 10\,\mathrm{deg/s} \cdot \sin 90^\circ \cos 0^\circ = 10\,\mathrm{deg/s}, \\ r &= -\dot{\phi}\sin\phi + \dot{\psi}\cos\phi \cdot \cos\theta = 0\,\mathrm{deg/s}. \end{aligned}$$

Note that for this flight condition, a 10 deg/s Euler yaw rate ψ is felt by the pilot as a 10 deg/s pitch rate q.

Copyright © 2025 Xiaowei He

6 Linearized Equations of Motion

The six aircraft equations of motion are nonlinear differential equations. They can be solved with a variety of numerical integration techniques to obtain time histories of motion variables, but it is nearly impossible to obtain closed solutions (equations for each variable). Because valuable insight can be obtained from closed solutions regarding the dynamic response of the aircraft, we will use the small perturbation approach to linearize the equations of motion and facilitate the definition of closed solutions. In addition, the dynamic derivatives associated with the definition of applied forces and moments on the aircraft will be discussed.

6.1 Linearization theory

6.1.1 Small perturbations

Linearization of the aircraft equations of motion begins with consideration of perturbed flight. Perturbed flight is defined relative to a steady-state (trimmed) flight condition using a combination of steady-state and perturbed variables for aircraft motion parameters and for forces and moments. The basic assumption is that aircraft motion comprises small disturbances from a trim/equilibrium state. This is a valid assumption for most flight conditions; however, care must be taken when exploring high-maneuver flight, as such analyses require solutions to the full nonlinear equations of motion via numerical methods. Each motion variable, Euler angle, force, and moment in the equations of motion are redefined as the summation of a steady-state/equilibrium value (designated with the subscript e) and a perturbed value (designated with lowercase symbols or with $'$) as summarized below.

- Rates:

$$\begin{aligned} U &= U_\mathrm{e} + u, & V &= V_\mathrm{e} + v, & W &= W_\mathrm{e} + w; \\ p &= p_\mathrm{e} + p', & q &= q_\mathrm{e} + q', & r &= r_\mathrm{e} + r'. \end{aligned} \tag{6.1}$$

- Attitudes:

$$\phi = \phi_\mathrm{e} + \phi', \qquad \theta = \theta_\mathrm{e} + \theta', \qquad \psi = \psi_\mathrm{e} + \psi'. \tag{6.2}$$

- Forces and moments

$$\begin{aligned} X &= X_\mathrm{e} + X', & Y &= Y_\mathrm{e} + Y', & Z &= Z_\mathrm{e} + Z'; \\ L &= L_\mathrm{e} + l, & M &= M_\mathrm{e} + m, & N &= N_\mathrm{e} + n. \end{aligned} \tag{6.3}$$

- Controls:

$$\xi = \xi_\mathrm{e} + \xi', \qquad \eta = \eta_\mathrm{e} + \eta', \qquad \zeta = \zeta_\mathrm{e} + \zeta'. \tag{6.4}$$

6.1.2 Fundamentals of linearization

Linearization makes it possible to use tools for studying linear systems to analyze the behavior of a nonlinear function near a given point. The linearization of a function is the first-order term of its Taylor expansion around the point of interest, which is the equilibrium state in our case. For a system defined by the equation

$$\dot{x} = f(x, t), \tag{6.5}$$

the linearized system can be written as

$$\dot{x} \approx f(x_\mathrm{e}, t) + \left.\frac{\partial f}{\partial x}\right|_{x_\mathrm{e}, t} (x - x_\mathrm{e}) = f(x_\mathrm{e}, t) + \left.\frac{\partial f}{\partial x}\right|_{x_\mathrm{e}, t} x', \tag{6.6}$$

Copyright © 2025 Xiaowei He

where x_e is the equilibrium point, and $x' = x - x_e$ represents the small perturbation (*not* the first derivative of x).

Example 6.1

Find the first-order approximation of $\sin\theta$ and $\cos\theta$ assuming small θ values.

Solution: Since θ is small, the point of interest is $\theta_0 = 0$. Use Taylor series to expand $\sin\theta$ round θ_0 and keep the first-order term

$$\sin\theta \approx \sin\theta_0 + \cos\theta_0 \cdot (\theta - \theta_0) = \theta \text{ (in radians)}.$$

Similarly,

$$\cos\theta \approx \cos\theta_0 - \sin\theta_0 \cdot (\theta - \theta_0) = 1.$$

Linearization procedure. The following steps will be taken to linearize the equations of motion:

(1) Recast each variable in terms of a steady-state value and a perturbed value ($A = A_e + a$). Multiply out and use trig identities.

(2) Apply the small-angle assumption to trig functions of perturbed angles ($\cos\theta \approx 1$; $\sin\theta \approx \theta$).

(3) Assume powers and products of small perturbations are negligible ($ab \approx 0$; $a^2 \approx 0$).

(4) Remove the steady-state equation from the perturbed equation. The remaining perturbed equation is a linearized differential equation with the perturbed variables as the unknowns.

Example 6.2

Linearize the following nonlinear differential equation.

$$\dot{C} = AB\sin\Omega.$$

Solution: Rewrite the state variables in the small perturbation form

$$A = A_e + a, \qquad B = B_e + b, \qquad C = C_e + c, \qquad \Omega = \Omega_e + \omega,$$

and substitute into the differential equation

$$\begin{aligned}\dot{C}_e + \dot{c} &= (A_e + a)(B_e + b)\sin(\Omega_e + \omega)\\ \dot{C}_e + \dot{c} &= (A_eB_e + A_eb + aB_e + ab)(\sin\Omega_e\cos\omega + \cos\Omega_e\sin\omega).\end{aligned}$$

Under small-angle assumptions, $\cos\omega \approx 1$ and $\sin\omega \approx \omega$, thus

$$\dot{C}_e + \dot{c} = (A_eB_e + A_eb + aB_e + ab)(\sin\Omega_e + \omega\cos\Omega_e).$$

Assuming powers and products of small perturbations are negligible

$$ab \approx 0, \qquad a\omega \approx 0, \qquad b\omega \approx 0,$$

$$\dot{C}_e + \dot{c} = A_eB_e\sin\Omega_e + A_eb\sin\Omega_e + aB_e\sin\Omega_e + A_eB_e\omega\cos\Omega_e.$$

The steady-state equation can be identified by substituting the equilibrium terms into the original differential equation

$$\dot{C}_e = A_eB_e\sin\Omega_e.$$

Subtracting the steady-state equation from the previous step on both sides, we have the linearized differential equation in terms of the perturbation variables a, b, c, and ω

$$\dot{c} = A_eb\sin\Omega_e + aB_e\sin\Omega_e + A_eB_e\omega\cos\Omega_e.$$

Copyright © 2025 Xiaowei He

6.2 Linearized aircraft equations of motion

Together, equations (5.13) and (5.29) comprise the six degrees of freedom equations of motion of a rigid symmetric airframe having a uniform mass distribution in undisturbed and uncontrolled conditions. Further development of the equations of motion requires that the terms on the right-hand side of the equations adequately describe the perturbation or disturbing forces and moments. The traditional approach, after Bryan [14], is to assume that the disturbing forces and moments are due to aerodynamic effects ($_\mathrm{a}$), gravitational effects (g), movement of aerodynamic controls ($_\mathrm{c}$), power effects ($_\mathrm{p}$), and the effects of atmospheric disturbances ($_\mathrm{d}$). Here we rewrite them in a generalized form that includes these terms.

$$\begin{aligned}
m(\dot{U} + qW - rV) &= X_\mathrm{a} + X_g + X_\mathrm{c} + X_\mathrm{p} + X_\mathrm{d}, \\
m(\dot{V} + rU - pW) &= Y_\mathrm{a} + Y_g + Y_\mathrm{c} + Y_\mathrm{p} + Y_\mathrm{d}, \\
m(\dot{W} + pV - qU) &= Z_\mathrm{a} + Z_g + Z_\mathrm{c} + Z_\mathrm{p} + Z_\mathrm{d}, \\
\dot{p}I_{xx} + qr(I_{zz} - I_{yy}) - (\dot{r} + pq)I_{xz} &= L_\mathrm{a} + L_g + L_\mathrm{c} + L_\mathrm{p} + L_\mathrm{d}, \\
\dot{q}I_{yy} - pr(I_{zz} - I_{xx}) + (p^2 + r^2)I_{xz} &= M_\mathrm{a} + M_g + M_\mathrm{c} + M_\mathrm{p} + M_\mathrm{d}, \\
\dot{r}I_{zz} + pq(I_{yy} - I_{xx}) + (qr - \dot{p})I_{xz} &= N_\mathrm{a} + N_g + N_\mathrm{c} + N_\mathrm{p} + N_\mathrm{d}.
\end{aligned} \tag{6.7}$$

6.2.1 Trim state assumptions

Equation (6.7) may be simplified with a few reasonable assumptions on the trim (or steady-state) flight condition.

- Initially, the aircraft is assumed to be flying in steady, trimmed, rectilinear flight with zero roll, sideslip, and yaw angles.

  $$\phi_\mathrm{e} = \beta_\mathrm{e} = \psi_\mathrm{e} = 0.$$

  Thus,

  $$\phi = \phi', \qquad \psi = \psi'.$$

- At this flight condition, the velocity of the aircraft is V_0. Since there is no sideslip,

  $$V_\mathrm{e} = 0.$$

  Thus,

  $$V = v.$$

- The angular velocity components are all zero for wings-level, straight flight.

  $$p_\mathrm{e} = q_\mathrm{e} = r_\mathrm{e} = 0.$$

  Thus,

  $$p = p'. \qquad q = q', \qquad r = r'.$$

- Initially, there are no resultant accelerations on the aircraft (equilibrium state).

  $$\dot{U}_\mathrm{e} = \dot{V}_\mathrm{e} = \dot{W}_\mathrm{e} = \dot{p}_\mathrm{e} = \dot{q}_\mathrm{e} = \dot{r}_\mathrm{e} = 0.$$

  Thus,

  $$\dot{U} = \dot{u}, \qquad \dot{V} = \dot{v}, \qquad \dot{W} = \dot{w}, \qquad \dot{p} = \dot{p}, \qquad \dot{q} = \dot{q}, \qquad \dot{r} = \dot{r},$$

Copyright © 2025 Xiaowei He

- A stable, undisturbed atmosphere is also assumed, such that

$$X_\mathrm{d} = Y_\mathrm{d} = Z_\mathrm{d} = L_\mathrm{d} = M_\mathrm{d} = N_\mathrm{d} = 0.$$

Applying the assumptions stated above and using the linearization procedure from section 6.1, we linearize the response side of the aircraft equations of motion and reduce the forcing side

$$\begin{aligned} m(\dot{u} + qW_\mathrm{e}) &= X_\mathrm{a} + X_g + X_\mathrm{c} + X_\mathrm{p}, \\ m(\dot{v} + rU_\mathrm{e} - pW_\mathrm{e}) &= Y_\mathrm{a} + Y_g + Y_\mathrm{c} + Y_\mathrm{p}, \\ m(\dot{w} - qU_\mathrm{e}) &= Z_\mathrm{a} + Z_g + Z_\mathrm{c} + Z_\mathrm{p}, \\ \dot{p}I_{xx} + \dot{r}I_{xz} &= L_\mathrm{a} + L_g + L_\mathrm{c} + L_\mathrm{p}, \\ \dot{q}I_{yy} &= M_\mathrm{a} + M_g + M_\mathrm{c} + M_\mathrm{p}, \\ \dot{r}I_{zz} - \dot{p}I_{xz} &= N_\mathrm{a} + N_g + N_\mathrm{c} + N_\mathrm{p}. \end{aligned} \tag{6.8}$$

6.2.2 Gravitational terms

We now linearized the right-hand (forcing) side of equation (6.8) by starting with the easier terms — gravitational terms. The weight force mg acting on the aircraft may be resolved into components acting in each of the three aircraft axes. When the aircraft is disturbed, these components vary according to the perturbations in attitude, thereby contributing to the disturbed motion.

From section 5.1.2 we know that

$$\boldsymbol{F_g} = \begin{bmatrix} -mg\sin\theta \\ mg\sin\phi\cos\theta \\ mg\cos\phi\cos\theta \end{bmatrix}$$

Since the aircraft is flying wings-level in the initial symmetric flight condition, the components of weight appear only in the plane of symmetry, as shown in figure 6.1. Thus, in the steady state, the components of weight resolved into aircraft axes are

$$\begin{bmatrix} X_{g_\mathrm{e}} \\ Y_{g_\mathrm{e}} \\ Z_{g_\mathrm{e}} \end{bmatrix} = \begin{bmatrix} -mg\sin\theta_\mathrm{e} \\ 0 \\ mg\cos\theta_\mathrm{e} \end{bmatrix}.$$

From section 5.2.2, the origin of the aircraft body axes is coincident with the *cg*, and there is no weight moment about any axis. Therefore,

$$L_g = M_g = N_g = 0. \tag{6.9}$$

During the disturbance, the aircraft attitude perturbation is (ϕ, θ', ψ), and the components of weight in the disturbed aircraft axes may be derived with the aid of the transformation equation (2.18) from section 2.1.5. By definition, the angular perturbations are small, thus, small-angle approximations may be used in the direction cosine matrix to give the following relationship

$$\begin{bmatrix} X_g \\ Y_g \\ Z_g \end{bmatrix} = \begin{bmatrix} 1 & \psi & -\theta' \\ -\psi & 1 & \phi \\ \theta' & -\phi & 1 \end{bmatrix} \begin{bmatrix} X_{g_\mathrm{e}} \\ Y_{g_\mathrm{e}} \\ Z_{g_\mathrm{e}} \end{bmatrix} = \begin{bmatrix} 1 & \psi & -\theta' \\ -\psi & 1 & \phi \\ \theta' & -\phi & 1 \end{bmatrix} \begin{bmatrix} -mg\sin\theta_\mathrm{e} \\ 0 \\ mg\cos\theta_\mathrm{e} \end{bmatrix}. \tag{6.10}$$

Copyright © 2025 Xiaowei He

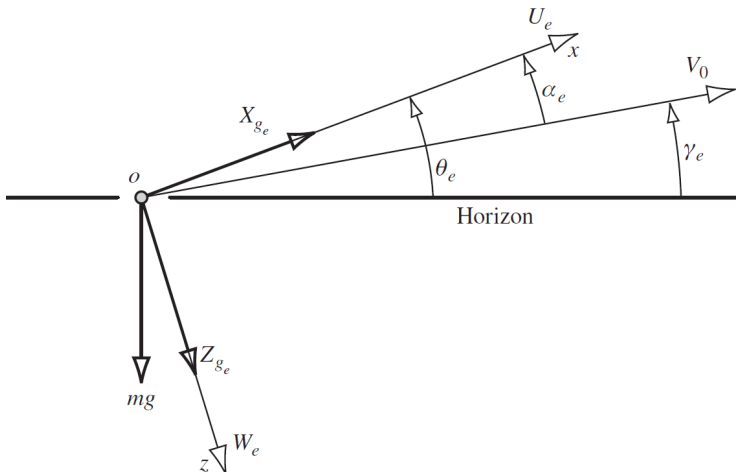

Figure 6.1: Steady state weight components in the plane of symmetry [1].

Again, the products of small quantities have been neglected. Thus, the gravitational force components in the small perturbation equations of motion are given by

$$\begin{aligned} X_g &= -mg\sin\theta_\mathrm{e} - mg\theta'\cos\theta_\mathrm{e}, \\ Y_g &= mg\psi\sin\theta_\mathrm{e} + mg\phi\cos\theta_\mathrm{e}, \\ Z_g &= mg\cos\theta_\mathrm{e} - mg\theta'\sin\theta_\mathrm{e}. \end{aligned} \tag{6.11}$$

6.2.3 Aerodynamic terms

Whenever the aircraft is disturbed from its equilibrium, the aerodynamic balance is obviously upset. To describe the aerodynamic changes that occur during a disturbance explicitly is a considerable challenge, given the subtle interactions present in the motion. However, although limited in scope, the method first described by Bryan [14] works extremely well for classical aircraft when the motion of interest is limited to (relatively) small perturbations. Although the approach is unchanged, the rather more modern notation of Hopkin [8] is adopted.

The usual procedure is to assume that the aerodynamic force and moment terms in equation (6.8) are dependent only on the disturbed motion variables and their derivatives. Mathematically, this can be expressed as a function comprising the sum of several Taylor series, each series involving one motion variable or one derivative of a motion variable. Since the motion variables are (u, v, w) and (p, q, r), the aerodynamic term X_a in the axial force equation, for example, may be expressed as

$$\begin{aligned} X_\mathrm{a} = X_{\mathrm{a_e}} &+ \left(\frac{\partial X}{\partial U}u + \mathcal{O}(u^2)\right) + \left(\frac{\partial X}{\partial V}v + \mathcal{O}(v^2)\right) + \left(\frac{\partial X}{\partial W}w + \mathcal{O}(w^2)\right) \\ &+ \left(\frac{\partial X}{\partial p}p + \mathcal{O}(p^2)\right) + \left(\frac{\partial X}{\partial q}q + \mathcal{O}(q^2)\right) + \left(\frac{\partial X}{\partial r}r + \mathcal{O}(r^2)\right) \\ &+ \left(\frac{\partial X}{\partial \dot{U}}\dot{u} + \mathcal{O}(\dot{u}^2)\right) + \left(\frac{\partial X}{\partial \dot{V}}\dot{v} + \mathcal{O}(\dot{v}^2)\right) + \left(\frac{\partial X}{\partial \dot{W}}\dot{w} + \mathcal{O}(\dot{w}^2)\right) \\ &+ \left(\frac{\partial X}{\partial \dot{p}}\dot{p} + \mathcal{O}(\dot{p}^2)\right) + \left(\frac{\partial X}{\partial \dot{q}}\dot{q} + \mathcal{O}(\dot{q}^2)\right) + \left(\frac{\partial X}{\partial \dot{r}}\dot{r} + \mathcal{O}(\dot{r}^2)\right) \\ &+ \text{series terms in higher-order derivatives,} \end{aligned} \tag{6.12}$$

Copyright © 2025 Xiaowei He

where $X_{\mathrm{a_e}}$ is a constant term. Since the motion variables are small, for all practical aircraft, only the first-order term in each of the series functions is significant. Further, the only significantly higher-order derivative terms commonly encountered are those involving $\dot{w}$. Thus equation (6.12) is simplified to

$$X_{\mathrm{a}} = X_{\mathrm{a_e}} + \frac{\partial X}{\partial U}u + \frac{\partial X}{\partial V}v + \frac{\partial X}{\partial W}w + \frac{\partial X}{\partial p}p + \frac{\partial X}{\partial q}q + \frac{\partial X}{\partial r}r + \frac{\partial X}{\partial \dot{W}}\dot{w}. \tag{6.13}$$

Since taking partial derivatives regarding U, V, W, and $\dot{w}$ is equivalent to u, v, w, and $\dot{w}$, the equation above can be written as

$$X_{\mathrm{a}} = X_{\mathrm{a_e}} + \frac{\partial X}{\partial u}u + \frac{\partial X}{\partial v}v + \frac{\partial X}{\partial w}w + \frac{\partial X}{\partial p}p + \frac{\partial X}{\partial q}q + \frac{\partial X}{\partial r}r + \frac{\partial X}{\partial \dot{w}}\dot{w}. \tag{6.14}$$

Using an alternative shorthand notation for the derivatives,

$$X_{\mathrm{a}} = X_{\mathrm{a_e}} + \mathring{X}_u u + \mathring{X}_v v + \mathring{X}_w w + \mathring{X}_p p + \mathring{X}_q q + \mathring{X}_r r + \mathring{X}_{\dot{w}}\dot{w}. \tag{6.15}$$

The coefficients $\mathring{X}_u$, $\mathring{X}_v$, $\mathring{X}_w$, and so on, are called *aerodynamic stability derivatives*, and the dressing $\circ$ denotes them to be *dimensional*. In a similar way, the force and moment terms in the remaining equation (6.8) are determined. For example, the aerodynamic term in the roll moment equation is given by

$$L_{\mathrm{a}} = L_{\mathrm{a_e}} + \mathring{L}_u u + \mathring{L}_v v + \mathring{L}_w w + \mathring{L}_p p + \mathring{L}_q q + \mathring{L}_r r + \mathring{L}_{\dot{w}}\dot{w}. \tag{6.16}$$

Physical significance of stability derivatives. The derivatives above are significant in a way that they represent the aircraft's response to small perturbations around a trim state. That is, the derivatives are numbers for an aircraft, collected either through numerical simulation or wind tunnel experiments, whereby the aircraft is moved through a range of angles and rates, and the changes to the forces and moments are measured. As a consequence, the derivatives are only valid for the point at which they have been evaluated. That is, each derivative will change with the given trim state and be a function of variables like forward speed, Mach number, angle of attack, aircraft configuration, etc. For example, if the linearized equations of motion are being used to assess the stability of an aircraft at a flight speed of 200 kn, then it is the values of (u, v, w) and (p, q, r) at a trimmed speed of 200 kn which are used to calculate the derivatives, yielding values of the derivatives in the equations above that are specific to that speed and/or attitude.

6.2.4 Aerodynamic control terms

The primary aerodynamic controls are the ailerons (ξ), elevator (η), and rudder (ζ). Since the forces and moments created by control deflections arise from changes in aerodynamic conditions, it is usual to quantify their effect in terms of *aerodynamic control derivatives*. The assumptions applied to the aerodynamic terms are also applied to the control terms; thus, for example, the pitch moment due to aerodynamic controls may be expressed as

$$M_{\mathrm{c}} = \frac{\partial M}{\partial \xi}\xi' + \frac{\partial M}{\partial \eta}\eta' + \frac{\partial M}{\partial \zeta}\zeta', \tag{6.17}$$

where ξ, η, and ζ are the aileron angle, elevator angle, and rudder angle, respectively. Since the equation describes the effect of the aerodynamic controls with respect to the prevailing trim condition, it is important to realize that the control angles (ξ', η', ζ') are measured relative to the trim settings $(\xi_{\mathrm{e}}, \eta_{\mathrm{e}}, \zeta_{\mathrm{e}})$, respectively. Again, the shorthand notation may be used

$$M_{\mathrm{c}} = \mathring{M}_\xi \xi' + \mathring{M}_\eta \eta' + \mathring{M}_\zeta \zeta'. \tag{6.18}$$

Copyright © 2025 Xiaowei He

The aerodynamic control terms in the remaining equations of motion are assembled in a similar way. If it is required to study the response of an aircraft to other aerodynamic controls, such as flaps, spoilers, leading-edge devices, etc., additional terms may be appended to the control effect equation and the remaining equations of motion as required.

6.2.5 Power terms

Power, and hence thrust T, is usually controlled by throttle lever angle ϵ, and the relationship between the two variables for a simple turbojet engine is given by equation (2.30) in section 2.2.2

$$\frac{T(s)}{\epsilon(s)} = \frac{k_T}{1 + s\tau_T}.$$

Movement of the throttle lever causes a change in thrust, which in turn gives rise to a change in the components of force and moment acting on the aircraft. It is mathematically convenient to describe these effects in terms of engine thrust derivatives. For example, the normal force due to thrust may be expressed in the usual shorthand notation

$$Z_{\mathrm{p}} = \mathring{Z}_T T'. \tag{6.19}$$

The contributions to the remaining equations of motion are expressed similarly. As for the aerodynamic controls, power changes are measured with respect to the prevailing trim setting. Therefore, T' quantifies the thrust perturbation relative to the trim setting T_{e}.

6.2.6 Equations of motion for small perturbations

Substitute the appropriate expressions for the aerodynamic, gravitational, aerodynamic control, and thrust terms into equation (6.8), and the following equations are obtained

$$\begin{aligned}
m(\dot{u} + qW) =& \overbrace{X_{\mathrm{a_e}} + \mathring{X}_u u + \mathring{X}_v v + \mathring{X}_w w + \mathring{X}_p p + \mathring{X}_q q + \mathring{X}_r r + \mathring{X}_{\dot{w}} \dot{w}}^{\text{aerodynamic terms}} \\
& \underbrace{-mg\sin\theta_{\mathrm{e}} - mg\theta'\cos\theta_{\mathrm{e}}}_{\text{gravitational terms}} \underbrace{+\mathring{X}_\xi \xi' + \mathring{X}_\eta \eta' + \mathring{X}_\zeta \zeta'}_{\text{aerodynamic control terms}} \underbrace{+\mathring{X}_T T'}_{\text{power term}}, \\
m(\dot{v} + rU_{\mathrm{e}} - pW_{\mathrm{e}}) =& Y_{\mathrm{a_e}} + \mathring{Y}_u u + \mathring{Y}_v v + \mathring{Y}_w w + \mathring{Y}_p p + \mathring{Y}_q q + \mathring{Y}_r r + \mathring{Y}_{\dot{w}} \dot{w} \\
& + mg\psi\sin\theta_{\mathrm{e}} + mg\phi\cos\theta_{\mathrm{e}} + \mathring{Y}_\xi \xi' + \mathring{Y}_\eta \eta' + \mathring{Y}_\zeta \zeta' + \mathring{Y}_T T', \\
m(\dot{w} - qU_{\mathrm{e}}) =& Z_{\mathrm{a_e}} + \mathring{Z}_u u + \mathring{Z}_v v + \mathring{Z}_w w + \mathring{Z}_p p + \mathring{Z}_q q + \mathring{Z}_r r + \mathring{Z}_{\dot{w}} \dot{w} \\
& + mg\cos\theta_{\mathrm{e}} - mg\theta'\sin\theta_{\mathrm{e}} + \mathring{Z}_\xi \xi' + \mathring{Z}_\eta \eta' + \mathring{Z}_\zeta \zeta' + \mathring{Z}_T T', \\
\dot{p}I_{xx} + \dot{r}I_{xz} =& L_{\mathrm{a_e}} + \mathring{L}_u u + \mathring{L}_v v + \mathring{L}_w w + \mathring{L}_p p + \mathring{L}_q q + \mathring{L}_r r + \mathring{L}_{\dot{w}} \dot{w} \\
& + \mathring{L}_\xi \xi' + \mathring{L}_\eta \eta' + \mathring{L}_\zeta \zeta' + \mathring{L}_T T', \\
\dot{q}I_{yy} =& M_{\mathrm{a_e}} + \mathring{M}_u u + \mathring{M}_v v + \mathring{M}_w w + \mathring{M}_p p + \mathring{M}_q q + \mathring{M}_r r + \mathring{M}_{\dot{w}} \dot{w} \\
& + \mathring{M}_\xi \xi' + \mathring{M}_\eta \eta' + \mathring{M}_\zeta \zeta' + \mathring{M}_T T', \\
\dot{r}I_{zz} - \dot{p}I_{xz} =& N_{\mathrm{a_e}} + \mathring{N}_u u + \mathring{N}_v v + \mathring{N}_w w + \mathring{N}_p p + \mathring{N}_q q + \mathring{N}_r r + \mathring{N}_{\dot{w}} \dot{w} \\
& + \mathring{N}_\xi \xi' + \mathring{N}_\eta \eta' + \mathring{N}_\zeta \zeta' + \mathring{N}_T T'.
\end{aligned} \tag{6.20}$$

Copyright © 2025 Xiaowei He

In the steady trimmed flight condition, all of the perturbation variables and their derivatives are, by definition, zero. Thus, the perturbed equation (6.20) reduces to the steady-state equations

$$X_{\mathrm{a_e}} = mg\sin\theta_{\mathrm{e}}, \qquad Y_{\mathrm{a_e}} = 0, \qquad Z_{\mathrm{a_e}} = -mg\cos\theta_{\mathrm{e}}, \qquad L_{\mathrm{a_e}} = 0, \qquad M_{\mathrm{a_e}} = 0, \qquad N_{\mathrm{a_e}} = 0. \tag{6.21}$$

Equation (6.21) therefore identify the constant trim terms which may be substituted into equation (6.20) and, following rearrangement, they may be written as

$$\begin{aligned}
m\dot{u} - \mathring{X}_u u - \mathring{X}_v v - \mathring{X}_{\dot{w}}\dot{w} - \mathring{X}_w w \\
-\mathring{X}_p p - (\mathring{X}_q - mW_{\mathrm{e}})q - \mathring{X}_r r + mg\theta'\cos\theta_{\mathrm{e}} &= \mathring{X}_\xi \xi' + \mathring{X}_\eta \eta' + \mathring{X}_\zeta \zeta' + \mathring{X}_T T', \\
-\mathring{Y}_u u + m\dot{v} - \mathring{Y}_v v - \mathring{Y}_{\dot{w}}\dot{w} - \mathring{Y}_w w \\
-(\mathring{Y}_p + mW_{\mathrm{e}})p - \mathring{Y}_q q - (\mathring{Y}_r - mU_{\mathrm{e}})r \\
-mg\phi\cos\theta_{\mathrm{e}} - mg\psi\sin\theta_{\mathrm{e}} &= \mathring{Y}_\xi \xi' + \mathring{Y}_\eta \eta' + \mathring{Y}_\zeta \zeta' + \mathring{Y}_T T', \\
-\mathring{Z}_u u - \mathring{Z}_v v - (\mathring{Z}_{\dot{w}} - m)\dot{w} - \mathring{Z}_w w \\
-\mathring{Z}_p p - (\mathring{Z}_q + mU_{\mathrm{e}})q - \mathring{Z}_r r + mg\theta'\sin\theta_{\mathrm{e}} &= \mathring{Z}_\xi \xi' + \mathring{Z}_\eta \eta' + \mathring{Z}_\zeta \zeta' + \mathring{Z}_T T', \\
-\mathring{L}_u u - \mathring{L}_v v - \mathring{L}_{\dot{w}}\dot{w} - \mathring{L}_w w \\
+I_{xx}\dot{p} - \mathring{L}_p p - \mathring{L}_q q - I_{xz}\dot{r} - \mathring{L}_r r &= \mathring{L}_\xi \xi' + \mathring{L}_\eta \eta' + \mathring{L}_\zeta \zeta' + \mathring{L}_T T', \\
-\mathring{M}_u u - \mathring{M}_v v - \mathring{M}_{\dot{w}}\dot{w} - \mathring{M}_w w \\
-\mathring{M}_p p + I_{yy}\dot{q} - \mathring{M}_q q - \mathring{M}_r r &= \mathring{M}_\xi \xi' + \mathring{M}_\eta \eta' + \mathring{M}_\zeta \zeta' + \mathring{M}_T T', \\
-\mathring{N}_u u - \mathring{N}_v v - \mathring{N}_{\dot{w}}\dot{w} - \mathring{N}_w w \\
-I_{xz}\dot{p} - \mathring{N}_p p - \mathring{N}_q q + I_{zz}\dot{r} - \mathring{N}_r r &= \mathring{N}_\xi \xi' + \mathring{N}_\eta \eta' + \mathring{N}_\zeta \zeta' + \mathring{N}_T T'.
\end{aligned} \tag{6.22}$$

Equation (6.22) is the *small perturbation equations of motion*, referenced to aircraft body axes, which describe the transient response of an aircraft about the trimmed flight condition following a small input disturbance. They comprise six simultaneous *linear* differential equations written traditionally with the forcing (input) terms on the right-hand side. As written, and subject to the assumptions made in their derivation, the equations of motion are perfectly general and describe motion in which longitudinal and lateral dynamics may be fully coupled. However, for the vast majority of aircraft, when only small-perturbation transient motion is considered, as is the case here, the longitudinal-lateral coupling is usually negligible. Consequently, it is convenient to simplify the equations by assuming that longitudinal and lateral motion is fully decoupled, as discussed in section 5.3.

6.3 Linearized longitudinal equations of motion

Similar to what was discussed in section 5.3, we decouple the linearized equations of motion into longitudinal and lateral-directional parts. Decoupled longitudinal motion is motion in response to a disturbance constrained to the longitudinal plane of symmetry, the xz plane, only. The motion is therefore described by the axial force X, the normal force Z, and the pitch moment M equations only. Since no lateral-directional motion is involved, the motion variables V, p, and r and their derivatives are all zero. Also, decoupled longitudinal-lateral motion means that the aerodynamic coupling derivatives are negligibly small and may be taken as zero, whence

$$\mathring{X}_v = \mathring{X}_p = \mathring{X}_r = \mathring{Z}_v = \mathring{Z}_r = \mathring{M}_v = \mathring{M}_p = \mathring{M}_r = 0. \tag{6.23}$$

Copyright © 2025 Xiaowei He

Similarly, since aileron or rudder deflections do not usually cause motion in the longitudinal plane of symmetry, the coupling aerodynamic control derivatives may also be taken as zero, thus

$$\mathring{X}_\xi = \mathring{X}_\zeta = \mathring{Z}_\xi = \mathring{Z}_\zeta = \mathring{M}_\xi = \mathring{M}_\zeta = 0. \tag{6.24}$$

The equations of longitudinal symmetric motion are therefore obtained by extracting the axial force, normal force, and pitch moment equations from equation (6.22) and the assumptions above as appropriate. Whence

$$\begin{aligned} m\dot{u} - \mathring{X}_u u - \mathring{X}_{\dot{w}}\dot{w} - \mathring{X}_w w - (\mathring{X}_q - mW_\mathrm{e})q + mg\theta' \cos\theta_\mathrm{e} &= \mathring{X}_\eta \eta' + \mathring{X}_T T', \\ -\mathring{Z}_u u - (\mathring{Z}_{\dot{w}} - m)\dot{w} - \mathring{Z}_w w - (\mathring{Z}_q + mU_\mathrm{e})q + mg\theta' \sin\theta_\mathrm{e} &= \mathring{Z}_\eta \eta' + \mathring{Z}_T T', \\ -\mathring{M}_u u - \mathring{M}_{\dot{w}}\dot{w} - \mathring{M}_w w + I_{yy}\dot{q} - \mathring{M}_q q &= \mathring{M}_\eta \eta' + \mathring{M}_T T'. \end{aligned} \tag{6.25}$$

Equation (6.25) is the most general form of the dimensional decoupled equations of longitudinal symmetric motion referenced to aircraft body axes. If it is assumed that the aircraft is in level flight and that the reference axes are wind or stability axes, then

$$\theta_\mathrm{e} = W_\mathrm{e} = 0, \tag{6.26}$$

and equation (6.7) further simplifies to

$$\begin{aligned} m\dot{u} - \mathring{X}_u u - \mathring{X}_{\dot{w}}\dot{w} - \mathring{X}_w w - \mathring{X}_q q + mg\theta' &= \mathring{X}_\eta \eta' + \mathring{X}_T T', \\ -\mathring{Z}_u u - (\mathring{Z}_{\dot{w}} - m)\dot{w} - \mathring{Z}_w w - (\mathring{Z}_q + mU_\mathrm{e})q &= \mathring{Z}_\eta \eta' + \mathring{Z}_T T', \\ -\mathring{M}_u u - \mathring{M}_{\dot{w}}\dot{w} - \mathring{M}_w w + I_{yy}\dot{q} - \mathring{M}_q q &= \mathring{M}_\eta \eta' + \mathring{M}_T T'. \end{aligned} \tag{6.27}$$

Equation (6.27) represents the simplest possible form of the decoupled longitudinal equations of motion. Further simplification is only generally possible when the numerical values of the coefficients in the equations are known since some coefficients are often negligibly small.

6.4 Linearized lateral-directional equations of motion

Decoupled lateral-directional motion involves roll, yaw, and sideslip only. It is therefore described by the equations for side force Y, roll moment L, and yaw moment N. Since no longitudinal motion is involved, the longitudinal motion variables U, W, and q and their derivatives are all zero. Also, decoupled longitudinal-lateral motion means that the aerodynamic coupling derivatives are negligibly small and may be taken as zero, whence

$$\mathring{Y}_u = \mathring{Y}_{\dot{w}} = \mathring{Y}_w = \mathring{Y}_q = \mathring{L}_u = \mathring{L}_{\dot{w}} = \mathring{L}_w = \mathring{L}_q = \mathring{N}_u = \mathring{N}_{\dot{w}} = \mathring{N}_w = \mathring{N}_q = 0. \tag{6.28}$$

Similarly, since the airframe is symmetric, elevator deflection and thrust variation do not usually cause lateral-directional motion, and the coupling aerodynamic control derivatives may also be taken as zero, thus

$$\mathring{Y}_\eta = \mathring{Y}_T = \mathring{L}_\eta = \mathring{L}_T = \mathring{N}_\eta = \mathring{N}_T = 0. \tag{6.29}$$

The equations of lateral asymmetric motion are therefore obtained by extracting the side force, roll moment, and yaw moment equations from equation (6.22) and these assumptions as appropriate

$$\begin{aligned} m\dot{v} - \mathring{Y}_v v - (\mathring{Y}_p + mW_\mathrm{e})p - (\mathring{Y}_r - mU_\mathrm{e})r - mg\phi\cos\theta_\mathrm{e} - mg\psi\sin\theta_\mathrm{e} &= \mathring{Y}_\xi \xi' + \mathring{Y}_\zeta \zeta', \\ -\mathring{L}_v v + I_{xx}\dot{p} - \mathring{L}_p p - I_{xz}\dot{r} - \mathring{L}_r r &= \mathring{L}_\xi \xi' + \mathring{L}_\zeta \zeta', \\ -\mathring{N}_v v - I_{xz}\dot{p} - \mathring{N}_p p - I_{zz}\dot{r} - \mathring{N}_r r &= \mathring{N}_\xi \xi' + \mathring{N}_\zeta \zeta'. \end{aligned} \tag{6.30}$$

Copyright © 2025 Xiaowei He

Equation (6.30) is the most general form of the dimensional decoupled equations of lateral-directional asymmetric motion referenced to the aircraft body axes. If it is assumed that the aircraft is in level flight and that the reference axes are wind or stability axes, as before,

$$\theta_{\mathrm{e}} = W_{\mathrm{e}} = 0, \tag{6.31}$$

then, equation (6.30) simplifies to

$$\begin{aligned} m\dot{v} - \mathring{Y}_v v - \mathring{Y}_p p - (\mathring{Y}_r - mU_{\mathrm{e}})r - mg\phi &= \mathring{Y}_\xi \xi' + \mathring{Y}_\zeta \zeta', \\ -\mathring{L}_v v + I_{xx}\dot{p} - \mathring{L}_p p - I_{xz}\dot{r} - \mathring{L}_r r &= \mathring{L}_\xi \xi' + \mathring{L}_\zeta \zeta', \\ -\mathring{N}_v v - I_{xz}\dot{p} - \mathring{N}_p p - I_{zz}\dot{r} - \mathring{N}_r r &= \mathring{N}_\xi \xi' + \mathring{N}_\zeta \zeta'. \end{aligned} \tag{6.32}$$

Equation (6.32) represents the simplest possible form of the decoupled lateral-directional equations of motion.

6.5 The dimensionless equations of motion

Traditionally, the development of the equations of motion and investigations of stability and control involving their use have been securely resident in the domain of the aerodynamicist. Many aerodynamic phenomena are most conveniently explained in terms of dimensionless *aerodynamic coefficients*, such as lift coefficient, Mach number, Reynolds number, etc., and often this mechanism provides the only practical means for making progress. The advantage of this approach is that the aerodynamic properties of an aircraft can be completely described in terms of dimensionless parameters that are independent of airframe geometry and flight conditions. The small perturbation equations of motion of an aircraft can be treated in the same way. This, in turn, leads to the concept of the dimensionless derivative, which is just another aerodynamic coefficient and may be interpreted in much the same way. However, the dimensionless equations of motion are of little use to the modern flight dynamicist other than as a means for explaining the origin of the dimensionless derivatives. The development of the dimensionless decoupled small perturbation equations of motion is outlined below solely for this purpose.

As formally described by Hopkin [8], the equations of motion are rendered dimensionless by dividing each one by a generalized force or moment parameter as appropriate. Sometimes the dimensionless equations of motion are referred to as aero-normalised, and the corresponding derivative coefficients are referred to as aero-normalised derivatives. To illustrate the procedure, consider the axial force equation taken from the decoupled longitudinal equations of motion, equation (6.27):

$$m\dot{u} - \mathring{X}_u u - \mathring{X}_{\dot{w}}\dot{w} - \mathring{X}_w w - \mathring{X}_q q + mg\theta' = \mathring{X}_\eta \eta' + \mathring{X}_T T'. \tag{6.33}$$

Since Equation (6.33) has the units of force, it may be rendered dimensionless by dividing, or normalizing, each term by the aerodynamic force parameter $\frac{1}{2}\rho V_0^2 S$, where S is the reference wing area. The following parameters are defined:

- *Dimensionless time*:

$$t^+ = \frac{t}{t_{\mathrm{c}}}, \tag{6.34}$$

where

$$t_{\mathrm{c}} = \frac{\bar{\bar{c}}}{V_0} \tag{6.35}$$

is the *convective time*.

Copyright © 2025 Xiaowei He

- *Dimensionless velocities*:

$$\begin{aligned}\hat{u} &= \frac{u}{V_0},\\ \hat{w} &= \frac{w}{V_0},\\ \hat{q} &= qt_c = q\frac{\bar{\bar{c}}}{V_0}.\end{aligned} \tag{6.36}$$

Since level flight is assumed, the lift and weight are equal, thus

$$mg = \frac{1}{2}\rho V_0^2 S C_L, \tag{6.37}$$

and the dimensionless weight can be substituted by the lift coefficient, C_L.

Thus, dividing equation (6.33) by the aerodynamic force parameter and making use of the parameters defined through equations (6.34) to (6.37), the following is obtained:

$$\begin{aligned}&\left(\frac{m}{\frac{1}{2}\rho S\bar{\bar{c}}}\right)\frac{\dot{u}t_c}{V_0} - \left(\frac{\mathring{X}_u}{\frac{1}{2}\rho V_0 S}\right)\frac{u}{V_0} - \left(\frac{\mathring{X}_{\dot{w}}}{\frac{1}{2}\rho S\bar{\bar{c}}}\right)\frac{\dot{w}t_c}{V_0}\\ &- \left(\frac{\mathring{X}_w}{\frac{1}{2}\rho V_0 S}\right)\frac{w}{V_0} - \left(\frac{\mathring{X}_q}{\frac{1}{2}\rho V_0 S\bar{\bar{c}}}\right)qt_c + \left(\frac{mg}{\frac{1}{2}\rho V_0^2 S}\right)\theta' = \left(\frac{\mathring{X}_\eta}{\frac{1}{2}\rho V_0^2 S}\right)\eta' + \frac{\mathring{X}_T T'}{\frac{1}{2}\rho V_0^2 S},\end{aligned} \tag{6.38}$$

which is more conveniently written as

$$\hat{\dot{u}} - X_u\hat{u} - X_{\dot{w}}\hat{\dot{w}} - X_w\hat{w} - X_q\hat{q} + C_L\theta' = X_\eta\eta' + X_T T', \tag{6.39}$$

in which the derivatives denoted X_u, $X_{\dot{w}}$, X_w, X_q, X_η, and X_T are the dimensionless or aero-normalized derivatives.

In a similar way, the remaining longitudinal equations of motion may be rendered dimensionless. Note that the aerodynamic moment parameter used to divide the pitch moment equation is $\frac{1}{2}\rho V_0^2 S\bar{\bar{c}}$. Whence

$$\begin{aligned}-Z_u\hat{u} + \hat{\dot{w}} - Z_{\dot{w}}\hat{\dot{w}} - Z_w\hat{w} - Z_q\hat{q} - \hat{q} &= Z_\eta\eta' + Z_T T'\\ -M_u\hat{u} - M_{\dot{w}}\hat{\dot{w}} - M_w\hat{w} + i_{yy}\hat{\dot{q}} - M_q\hat{q} &= M_\eta\eta' + M_T T',\end{aligned} \tag{6.40}$$

where

$$i_{yy} = \frac{I_{yy}}{m\bar{\bar{c}}^2}, \tag{6.41}$$

is the dimensionless pitch inertia.

Similarly, the lateral-directional equations of motion, equation (6.32), may be rendered dimensionless by dividing the side force equation by the aerodynamic force parameter $\frac{1}{2}\rho V_0^2 S$ and the roll and yaw moment equations by the aerodynamic moment parameter $\frac{1}{2}\rho V_0^2 Sb$, where for lateral-directional motion the reference length is the wing span b. The inertias are normalized by mb^2 accordingly. Thus, the dimensionless lateral-directional equations of motion are given by

$$\begin{aligned}\hat{\dot{v}} - Y_v\hat{v} - Y_p\hat{p} - Y_r\hat{r} - \hat{r} - C_L\phi &= Y_\xi\xi' + Y_\zeta\zeta'\\ -L_v\hat{v} + i_{xx}\hat{\dot{p}} - L_p\hat{p} - i_{xz}\hat{\dot{r}} - L_r\hat{r} &= L_\xi\xi' + L_\zeta\zeta'\\ -N_v\hat{v} - i_{xz}\hat{\dot{p}} - N_p\hat{p} + i_{zz}\hat{\dot{r}} - N_r\hat{r} &= N_\xi\xi' + N_\zeta\zeta'.\end{aligned} \tag{6.42}$$

Copyright © 2025 Xiaowei He

6.6 Equations of motion in state space form

The solution of the equations of motion poses few problems today since very powerful computational tools are readily available. Because computers excel at handling numerical matrix calculations, the use of matrix methods for solving linear dynamic system problems has become an important topic in modern applied mathematics. In particular, matrix methods, combined with digital computers, have led to the development of a relatively new field in modern control systems theory. For small perturbations, the aircraft is a classical example of a linear dynamic system, and the solution to the aircraft's equations of motion is frequently a prelude to flight control system design and analysis. It is therefore convenient and straightforward to use multivariable system theory tools in the solution of the equations of motion, but it is first necessary to arrange them in a suitable format.

As reviewed in section 1.3.4, the idea of state-space comes from the state-variable method of describing differential equations. The motion, or *state*, of any linear dynamic system may be described by a minimum set of variables called the *state variables*. The number of state variables required to completely describe the motion of the system is dependent on the number of degrees of freedom the system has. Thus, the motion of the system is described in a multidimensional vector space called the *state space*, the number of state variables being equal to the number of dimensions. Recalling equations (1.37) and (1.38), the equation of motion, or *state equation*, together with the *output equation*, provides a complete description of a linear time-invariant (LTI) multivariable system

$$\begin{aligned} \dot{\boldsymbol{x}}(t) &= \boldsymbol{A}\boldsymbol{x}(t) + \boldsymbol{B}\boldsymbol{u}(t), \\ \boldsymbol{y}(t) &= \boldsymbol{C}\boldsymbol{x}(t) + \boldsymbol{D}\boldsymbol{u}(t). \end{aligned} \tag{6.43}$$

As stated before, for most aircraft problems, the output variables are chosen to be the state variables. Thus

$$\boldsymbol{y}(t) = \boldsymbol{x}(t), \tag{6.44}$$

consequently, $\boldsymbol{C} = \boldsymbol{I}$ (identity matrix) and $\boldsymbol{D} = \boldsymbol{0}$ (zero matrix). Then the output equation simplifies to

$$\boldsymbol{y}(t) = \boldsymbol{I}\boldsymbol{x}(t) = \boldsymbol{x}(t). \tag{6.45}$$

and it is only necessary to derive the state equation from the aircraft equations of motion.

Consider, for example, the longitudinal equations of motion in equation (6.27) referenced to aircraft body axes. These may be rewritten with the acceleration terms on the left-hand side as follows

$$\begin{aligned} m\dot{u} - \mathring{X}_{\dot{w}}\dot{w} &= \mathring{X}_u u + \mathring{X}_w w + (\mathring{X}_q - mW_{\mathrm{e}})q - mg\theta' \cos\theta_{\mathrm{e}} + \mathring{X}_\eta \eta' + \mathring{X}_T T', \\ m\dot{w} - \mathring{Z}_{\dot{w}}\dot{w} &= \mathring{Z}_u u + \mathring{Z}_w w + (\mathring{Z}_q + mU_{\mathrm{e}})q - mg\theta' \sin\theta_{\mathrm{e}} + \mathring{Z}_\eta \eta' + \mathring{Z}_T T', \\ -\mathring{M}_{\dot{w}}\dot{w} + I_{yy}\dot{q} &= \mathring{M}_u u + \mathring{M}_w w + \mathring{M}_q q + \mathring{M}_\eta \eta' + \mathring{M}_T T'. \end{aligned} \tag{6.46}$$

Since the longitudinal motion of the aircraft is described by four state variables u, w, q, and θ', four differential equations are required. Thus, the additional equation is the auxiliary equation relating pitch rate to attitude rate, which for small perturbations is

$$\dot{\theta}' = q. \tag{6.47}$$

Equations (6.46) and (6.47) may be combined and written in matrix form

$$\boldsymbol{M}\dot{\boldsymbol{x}}(t) = \tilde{\boldsymbol{A}}\boldsymbol{x}(t) + \tilde{\boldsymbol{B}}\boldsymbol{u}(t), \tag{6.48}$$

Copyright © 2025 Xiaowei He

where

$$\boldsymbol{x}(t) = \begin{bmatrix} u \\ w \\ q \\ \theta' \end{bmatrix}, \qquad \boldsymbol{u}(t) = \begin{bmatrix} \eta' \\ T' \end{bmatrix}, \qquad \boldsymbol{M} = \begin{bmatrix} m & -\mathring{X}_{\dot{w}} & 0 & 0 \\ 0 & m - \mathring{Z}_{\dot{w}} & 0 & 0 \\ 0 & -\mathring{M}_{\dot{w}} & I_{yy} & 0 \\ 0 & 0 & 0 & 1 \end{bmatrix}, \tag{6.49}$$

$$\tilde{\boldsymbol{A}} = \begin{bmatrix} \mathring{X}_u & \mathring{X}_w & \mathring{X}_q - mW_\mathrm{e} & -mg\cos\theta_\mathrm{e} \\ \mathring{Z}_u & \mathring{Z}_w & \mathring{Z}_q + mU_\mathrm{e} & -mg\sin\theta_\mathrm{e} \\ \mathring{M}_u & \mathring{M}_w & \mathring{M}_q & 0 \\ 0 & 0 & 1 & 0 \end{bmatrix}, \qquad \tilde{\boldsymbol{B}} = \begin{bmatrix} \mathring{X}_\eta & \mathring{X}_T \\ \mathring{Z}_\eta & \mathring{Z}_T \\ \mathring{M}_\eta & \mathring{M}_T \\ 0 & 0 \end{bmatrix}. \tag{6.50}$$

The longitudinal state equation is derived by pre-multiplying equation (6.48) by the inverse of the *mass matrix* $\boldsymbol{M}$; whence

$$\dot{\boldsymbol{x}}(t) = \boldsymbol{A}\boldsymbol{x}(t) + \boldsymbol{B}\boldsymbol{u}(t), \tag{6.51}$$

where

$$\boldsymbol{A} = \boldsymbol{M}^{-1}\tilde{\boldsymbol{A}} = \begin{bmatrix} x_u & x_w & x_q & x_\theta \\ z_u & z_w & z_q & z_\theta \\ m_u & m_w & m_q & m_\theta \\ 0 & 0 & 1 & 0 \end{bmatrix}, \qquad \boldsymbol{B} = \boldsymbol{M}^{-1}\tilde{\boldsymbol{B}} = \begin{bmatrix} x_\eta & x_T \\ z_\eta & z_T \\ m_\eta & m_T \\ 0 & 0 \end{bmatrix}. \tag{6.52}$$

The elements of the state matrix $\boldsymbol{A}$ are the aerodynamic stability derivatives, referenced to aircraft body axes, in concise form; the elements of the input matrix $\boldsymbol{B}$ are the control derivatives, also in concise form. The definitions of the concise derivatives follow directly from the above relationships. Thus, the longitudinal state equation may be written out in full as

$$\begin{bmatrix} \dot{u} \\ \dot{w} \\ \dot{q} \\ \dot{\theta}' \end{bmatrix} = \begin{bmatrix} x_u & x_w & x_q & x_\theta \\ z_u & z_w & z_q & z_\theta \\ m_u & m_w & m_q & m_\theta \\ 0 & 0 & 1 & 0 \end{bmatrix} \begin{bmatrix} u \\ w \\ q \\ \theta' \end{bmatrix} + \begin{bmatrix} x_\eta & x_T \\ z_\eta & z_T \\ m_\eta & m_T \\ 0 & 0 \end{bmatrix} \begin{bmatrix} \eta' \\ T' \end{bmatrix}, \tag{6.53}$$

and the output equation is

$$\boldsymbol{y}(t) = \boldsymbol{I}\boldsymbol{x}(t) = \begin{bmatrix} 1 & 0 & 0 & 0 \\ 0 & 1 & 0 & 0 \\ 0 & 0 & 1 & 0 \\ 0 & 0 & 0 & 1 \end{bmatrix} \begin{bmatrix} u \\ w \\ q \\ \theta' \end{bmatrix}. \tag{6.54}$$

The longitudinal small-perturbation motion of the aircraft is completely described by the four state variables u, w, q, and θ'. The output equation determines that, in this instance, the output variables are chosen to be the same as the four state variables.

The lateral-directional small perturbation equations in equation (6.30), referenced to aircraft body axes, may be treated in the same way to obtain the lateral state equation

$$\begin{bmatrix} \dot{v} \\ \dot{p} \\ \dot{r} \\ \dot{\phi} \\ \dot{\psi} \end{bmatrix} = \begin{bmatrix} y_v & y_p & y_r & y\phi & y_\psi \\ l_v & l_p & l_r & l\phi & l_\psi \\ n_v & n_p & n_r & n\phi & n_\psi \\ 0 & 1 & 0 & 0 & 0 \\ 0 & 0 & 1 & 0 & 0 \end{bmatrix} \begin{bmatrix} v \\ p \\ r \\ \phi \\ \psi \end{bmatrix} + \begin{bmatrix} y_\xi & y_\zeta \\ l_\xi & l_\zeta \\ n_\xi & n_\zeta \\ 0 & 0 \\ 0 & 0 \end{bmatrix} \begin{bmatrix} \xi' \\ \zeta' \end{bmatrix}. \tag{6.55}$$

Copyright © 2025 Xiaowei He

Note that when the lateral equations of motion are referenced to wind axes, equation (6.32), the lateral-directional state equation is reduced from fifth order to fourth order to become

$$\begin{bmatrix} \dot{v} \\ \dot{p} \\ \dot{r} \\ \dot{\phi} \end{bmatrix} = \begin{bmatrix} y_v & y_p & y_r & y\phi & y_\psi \\ l_v & l_p & l_r & l\phi & l_\psi \\ n_v & n_p & n_r & n\phi & n_\psi \\ 0 & 1 & 0 & 0 & 0 \end{bmatrix} \begin{bmatrix} v \\ p \\ r \\ \phi \end{bmatrix} + \begin{bmatrix} y_\xi & y_\zeta \\ l_\xi & l_\zeta \\ n_\xi & n_\zeta \\ 0 & 0 \end{bmatrix} \begin{bmatrix} \xi' \\ \zeta' \end{bmatrix}. \tag{6.56}$$

However, in this case, the derivatives are referenced to aircraft wind axes rather than body axes and generally have slightly different values.

Copyright © 2025 Xiaowei He

7 Aircraft Dynamics

Aircraft dynamics focuses on the time history of aircraft motion after the aircraft is disturbed from an equilibrium or trim condition. This motion may be first-order (exponential response) or second-order (oscillatory response) and will have either positive dynamic stability (aircraft returns to the trim condition as time goes to infinity), neutral dynamic stability (aircraft neither returns to trim nor diverges further from the disturbed condition), or dynamic instability (aircraft diverges from the trim condition and the disturbed condition as time goes to infinity). The study of dynamic stability is important to understanding aircraft handling qualities and the design features that make an airplane fly well or not as well while performing specific mission tasks. The differential equations that define the aircraft equations of motion form the starting point for the study of dynamic stability.

7.1 Cramer's rule

7.1.1 General case

Cramer's rule describes a mathematical process for solving sets of simultaneous linear algebraic equations. It may be used to solve the equations of motion algebraically. Since Cramer's rule involves the use of matrix algebra, it is easily implemented in a digital computer.

To solve the system of n simultaneous linear algebraic equations described in matrix form as

$$\boldsymbol{y} = \boldsymbol{A}\boldsymbol{x}, \tag{7.1}$$

where $\boldsymbol{x}$ and $\boldsymbol{y}$ are column vectors and $\boldsymbol{A}$ is matrix of constant coefficients. Cramer's rule states that

$$\boldsymbol{x} = \boldsymbol{A}^{-1}\boldsymbol{y} = \frac{\operatorname{adj}(\boldsymbol{A})}{\det(\boldsymbol{A})}\boldsymbol{y}, \tag{7.2}$$

where the solution for x_i, the ith row of equation (7.2), is given by

$$x_i = \frac{1}{|\boldsymbol{A}|}(A_{1i}y_1 + A_{2i}y_2 + \cdots + A_{ni}y_n). \tag{7.3}$$

The significant observation is that the numerator of equation (7.3) is equivalent to the determinant of $\boldsymbol{A}$, with the ith column replaced by the vector $\boldsymbol{y}$. Thus, the solution of equations equation (7.1) to find all the x_i reduces to the relatively simple problem of evaluating $n+1$ determinants.

7.1.2 Explicit formulas for small systems

Two-equation system. Consider the linear system

$$\begin{aligned} y_1 &= a_{11}x_1 + a_{12}x_2 \\ y_2 &= a_{21}x_1 + a_{22}x_2 \end{aligned}, \tag{7.4}$$

which in matrix form is

$$\begin{bmatrix} y_1 \\ y_2 \end{bmatrix} = \begin{bmatrix} a_{11} & a_{12} \\ a_{21} & a_{22} \end{bmatrix} \begin{bmatrix} x_1 \\ x_2 \end{bmatrix}. \tag{7.5}$$

Assuming $a_{11}a_{22} - a_{12}a_{21}$ is nonzero, x_1 and x_2 can be found with Cramer's rule as

$$x_1 = \frac{\begin{vmatrix} y_1 & a_{12} \\ y_2 & a_{22} \end{vmatrix}}{\begin{vmatrix} a_{11} & a_{12} \\ a_{21} & a_{22} \end{vmatrix}} = \frac{y_1a_{22} - a_{22}y_2}{a_{11}a_{22} - a_{12}a_{21}}, \qquad x_2 = \frac{\begin{vmatrix} a_{11} & y_1 \\ a_{21} & y_2 \end{vmatrix}}{\begin{vmatrix} a_{11} & a_{12} \\ a_{21} & a_{22} \end{vmatrix}} = \frac{a_{11}y_1 - y_2a_{21}}{a_{11}a_{22} - a_{12}a_{21}}. \tag{7.6}$$

Copyright © 2025 Xiaowei He

Three-equation system. The rules for 3×3 matrices are similar. Given

$$\begin{aligned} y_1 &= a_{11}x_1 + a_{12}x_2 + a_{13}x_3 \\ y_2 &= a_{21}x_1 + a_{22}x_2 + a_{23}x_3 \ , \\ y_3 &= a_{31}x_1 + a_{32}x_2 + a_{33}x_3 \end{aligned} \tag{7.7}$$

which in matrix form is

$$\begin{bmatrix} y_1 \\ y_2 \\ y_3 \end{bmatrix} = \begin{bmatrix} a_{11} & a_{12} & a_{13} \\ a_{21} & a_{22} & a_{23} \\ a_{31} & a_{32} & a_{33} \end{bmatrix} \begin{bmatrix} x_1 \\ x_2 \\ x_3 \end{bmatrix} . \tag{7.8}$$

Then the values of x_1, x_2, and x_3 can be found as follows

$$x_1 = \frac{\begin{vmatrix} y_1 & a_{12} & a_{13} \\ y_2 & a_{22} & a_{23} \\ y_3 & a_{32} & a_{33} \end{vmatrix}}{\begin{vmatrix} a_{11} & a_{12} & a_{13} \\ a_{21} & a_{22} & a_{23} \\ a_{31} & a_{32} & a_{33} \end{vmatrix}}, \qquad x_2 = \frac{\begin{vmatrix} a_{11} & y_1 & a_{13} \\ a_{21} & y_2 & a_{23} \\ a_{31} & y_3 & a_{33} \end{vmatrix}}{\begin{vmatrix} a_{11} & a_{12} & a_{13} \\ a_{21} & a_{22} & a_{23} \\ a_{31} & a_{32} & a_{33} \end{vmatrix}}, \qquad x_3 = \frac{\begin{vmatrix} a_{11} & a_{12} & y_1 \\ a_{21} & a_{22} & y_2 \\ a_{31} & a_{32} & y_3 \end{vmatrix}}{\begin{vmatrix} a_{11} & a_{12} & a_{13} \\ a_{21} & a_{22} & a_{23} \\ a_{31} & a_{32} & a_{33} \end{vmatrix}}. \tag{7.9}$$

Example 7.1

Consider a system in which it is required to solve the simultaneous linear algebraic equations

$$\begin{aligned} y_1 &= x_1 + 2x_2 + 3x_3 \\ y_2 &= 2x_1 + 4x_2 + 5x_3 \ , \\ y_3 &= 3x_1 + 5x_2 + 6x_3 \end{aligned}$$

or, in matrix form,

$$\begin{bmatrix} y_1 \\ y_2 \\ y_3 \end{bmatrix} = \begin{bmatrix} 1 & 2 & 3 \\ 2 & 4 & 5 \\ 3 & 5 & 6 \end{bmatrix} \begin{bmatrix} x_1 \\ x_2 \\ x_3 \end{bmatrix} .$$

Applying Cramer's rule to solve for x_i,

$$x_1 = \frac{\begin{vmatrix} y_1 & 2 & 3 \\ y_2 & 4 & 5 \\ y_3 & 5 & 6 \end{vmatrix}}{\begin{vmatrix} 1 & 2 & 3 \\ 2 & 4 & 5 \\ 3 & 5 & 6 \end{vmatrix}} = \frac{y_1 \cdot 4 \cdot 6 + 2 \cdot 5 \cdot y_3 + 3 \cdot y_2 \cdot 5 - 3 \cdot 4 \cdot y_3 - 2 \cdot y_2 \cdot 6 - y_1 \cdot 5 \cdot 5}{-1} = y_1 - 3y_2 + 2y_3,$$

$$x_2 = \frac{\begin{vmatrix} 1 & y_1 & 3 \\ 2 & y_2 & 5 \\ 3 & y_3 & 6 \end{vmatrix}}{\begin{vmatrix} 1 & 2 & 3 \\ 2 & 4 & 5 \\ 3 & 5 & 6 \end{vmatrix}} = \frac{1 \cdot y_2 \cdot 6 + y_1 \cdot 5 \cdot 3 + 3 \cdot 2 \cdot y_3 - 3 \cdot y_2 \cdot 3 - y_1 \cdot 2 \cdot 6 - 1 \cdot 5 \cdot y_3}{-1} = -3y_1 + 3y_2 - y_3,$$

Copyright © 2025 Xiaowei He

$$x_3 = \frac{\begin{vmatrix} 1 & 2 & y_1 \\ 2 & 4 & y_2 \\ 3 & 5 & y_3 \end{vmatrix}}{\begin{vmatrix} 1 & 2 & 3 \\ 2 & 4 & 5 \\ 3 & 5 & 6 \end{vmatrix}} = \frac{1 \cdot 4 \cdot y_3 + 5 \cdot y_2 \cdot 3 + y_1 \cdot 2 \cdot 5 - y_1 \cdot 4 \cdot 3 - 2 \cdot 2 \cdot y_3 - 1 \cdot y_2 \cdot 5}{-1} = -2y_1 - y_2.$$

7.2 Aircraft transfer functions

The *Laplace transformation* and *transfer functions* were briefly reviewed in section 1.3.4. The Laplace transform method has been, and continues to be, used extensively. By transforming the differential equations, they become algebraic equations expressed in terms of the Laplace operator s. Their manipulation to obtain a solution then becomes a relatively straightforward exercise in algebra. The problem is thus transformed into one of solving a set of simultaneous linear algebraic equations, a process that can be readily accomplished using computational methods. The input-output response relation or transfer characteristic is described by a simple algebraic transfer function in terms of the Laplace operator. The time response is then found by finding the inverse Laplace transform of the transfer function for the input of interest.

7.2.1 Aircraft input-output relations

Aircraft response transfer functions describe the dynamic relations between the input variables and the output variables. The relations are indicated diagrammatically in figure 7.1, and it is clear that a number of possible input-output relationships exist. When the mathematical model of the aircraft comprises the decoupled small-perturbation equations of motion, transfer functions relating longitudinal input variables to lateral-directional output variables do not exist, and vice versa. This may not necessarily be the case when the aircraft is described by a fully coupled set of small-perturbation equations of motion. For example, such a description is quite usual when modeling a helicopter.

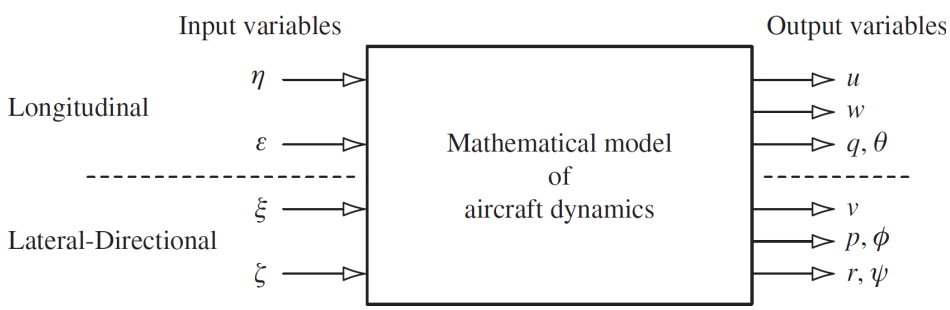

Figure 7.1: Steady state weight components in the plane of symmetry [1].

Transfer functions are written as a ratio of two polynomials in the Laplace operator s, where the numerator represents the output and the denominator represents the input. In simple terms,

$$\text{transfer function} = \mathcal{L}\left\{\frac{\text{output}}{\text{input}}\right\}. \tag{7.10}$$

For example, the transfer function of pitch attitude $\theta(s)$ response to elevator $\eta(s)$ is denoted as

$$\frac{\theta(s)}{\eta(s)} \equiv \frac{N_\eta^\theta(s)}{\Delta(s)} \tag{7.11}$$

Copyright © 2025 Xiaowei He

where $N_\eta^\theta(s)$ is the unique numerator polynomial in s that relates pitch attitude response to elevator input, and $\Delta(s)$ is the denominator polynomial in s which is common to all longitudinal response transfer functions. Similarly, roll rate $p(s)$ response to aileron $\xi(s)$ is denoted

$$\frac{p(s)}{\xi(s)} \equiv \frac{N_\xi^p(s)}{\Delta(s)}, \tag{7.12}$$

where in this instance, $\Delta(s)$ is the denominator polynomial which is common to all of the lateral-directional response transfer functions.

The denominator polynomial, $\Delta(s)$, is called the *characteristic polynomial* and, when equated to zero, defines the *characteristic equation*. Thus, $\Delta(s)$ completely describes the longitudinal or lateral-directional stability characteristics of the aircraft as appropriate, and the roots, or poles, describe its *stability modes*. Thus, the stability characteristics of an aircraft can be determined by inspection of the response transfer functions.

All proper transfer functions have a numerator polynomial that is at least one order less than the denominator polynomial, although occasionally improper transfer functions crop up in aircraft applications. For example, the transfer function describing acceleration response to an input variable is improper; the numerator and denominator polynomials are of the same order. Care is needed when working with improper transfer functions, as computational tools may sometimes be unable to handle them correctly.

7.2.2 The longitudinal response transfer functions

The Laplace transforms of the differential quantities $\dot{x}(t)$ and $\ddot{x}(t)$ are given by

$$\begin{aligned}\mathcal{L}\left\{\dot{x}(t)\right\} &= sx(s) - x(0)\\ \mathcal{L}\left\{\ddot{x}(t)\right\} &= s^2x(s) - sx(0) - \dot{x}(0),\end{aligned}$$

where $x(0)$ and $\dot{x}(0)$ are the initial conditions at $t = 0$. Taking the Laplace transform of the longitudinal equations of motion (equation (6.25)), referred to body axes, assuming zero initial conditions, and since only small-perturbation motion is considered, write

$$\dot{\theta}(t) = q(t), \tag{7.13}$$

then

$$\begin{aligned}\left(ms - \mathring{X}_u\right)u(s) - \left(\mathring{X}_{\dot{w}} + \mathring{X}_w\right)w(s) - \left(\left(\mathring{X}_q - mW_\mathrm{e}\right)s - mg\cos\theta_\mathrm{e}\right)\theta(s) &= \mathring{X}_\eta\eta(s) + \mathring{X}_T T(s),\\ -\mathring{Z}_u u(s) - \left(\left(\mathring{Z}_{\dot{w}} - m\right)s + \mathring{Z}_w\right)w(s) - \left(\left(\mathring{Z}_q + mU_\mathrm{e}\right)s - mg\sin\theta_\mathrm{e}\right)\theta(s) &= \mathring{Z}_\eta\eta(s) + \mathring{Z}_T T(s),\\ -\mathring{M}_u u(s) - \left(\mathring{M}_{\dot{w}} + \mathring{M}_w\right)w(s) + \left(I_{yy}s - \mathring{M}_q s\right)\theta(s) &= \mathring{M}_\eta\eta(s) + \mathring{M}_T T(s),\end{aligned} \tag{7.14}$$

or, in matrix format

$$\begin{bmatrix}\left(ms - \mathring{X}_u\right) & -\left(\mathring{X}_{\dot{w}} + \mathring{X}_w\right) & -\left(\left(\mathring{X}_q - mW_\mathrm{e}\right)s - mg\cos\theta_\mathrm{e}\right)\\ -\mathring{Z}_u & -\left(\left(\mathring{Z}_{\dot{w}} - m\right)s + \mathring{Z}_w\right) & -\left(\left(\mathring{Z}_q + mU_\mathrm{e}\right)s - mg\sin\theta_\mathrm{e}\right)\\ -\mathring{M}_u & -\left(\mathring{M}_{\dot{w}} + \mathring{M}_w\right) & \left(I_{yy}s - \mathring{M}_q s\right)\end{bmatrix}\begin{bmatrix}u(s)\\ w(s)\\ \theta(s)\end{bmatrix} = \begin{bmatrix}\mathring{X}_\eta & \mathring{X}_T\\ \mathring{Z}_\eta & \mathring{Z}_T\\ \mathring{M}_\eta & \mathring{M}_T\end{bmatrix}\begin{bmatrix}\eta(s)\\ T(s)\end{bmatrix}. \tag{7.15}$$

Cramer's rule can now be applied to obtain the longitudinal response transfer functions describing the response to elevators. Assume that the thrust remains constant, which means that the throttle is

Copyright © 2025 Xiaowei He

fixed at its trim setting T_e, and $T(s) = 0$. Therefore, after dividing through by $\eta(s)$, equation (7.15) may be simplified to

$$\begin{bmatrix} \left(ms - \mathring{X}_u\right) & -\left(\mathring{X}_{\dot{w}} + \mathring{X}_w\right) & -\left(\left(\mathring{X}_q - mW_\mathrm{e}\right)s - mg\cos\theta_\mathrm{e}\right) \\ -\mathring{Z}_u & -\left(\left(\mathring{Z}_{\dot{w}} - m\right)s + \mathring{Z}_w\right) & -\left(\left(\mathring{Z}_q + mU_\mathrm{e}\right)s - mg\sin\theta_\mathrm{e}\right) \\ -\mathring{M}_u & -\left(\mathring{M}_{\dot{w}} + \mathring{M}_w\right) & \left(I_{yy}s - \mathring{M}_q s\right) \end{bmatrix} \begin{bmatrix} \dfrac{u(s)}{\eta(s)} \\ \dfrac{w(s)}{\eta(s)} \\ \dfrac{\theta(s)}{\eta(s)} \end{bmatrix} = \begin{bmatrix} \mathring{X}_\eta \\ \mathring{Z}_\eta \\ \mathring{M}_\eta \end{bmatrix}, \tag{7.16}$$

which is of the same form as equation (7.1). Cramer's rule may be applied directly, and the elevator response transfer functions are given by

$$\frac{u(s)}{\eta(s)} \equiv \frac{N_\eta^u(s)}{\Delta(s)}, \qquad \frac{w(s)}{\eta(s)} \equiv \frac{N_\eta^w(s)}{\Delta(s)}, \qquad \frac{\theta(s)}{\eta(s)} \equiv \frac{N_\eta^\theta(s)}{\Delta(s)}. \tag{7.17}$$

Since the Laplace transform of equation (7.13) is $s\theta(s) = q(s)$, the pitch rate response transfer function follows as

$$\frac{q(s)}{\eta(s)} \equiv \frac{N_\eta^q(s)}{\Delta(s)} = \frac{sN_\eta^\theta(s)}{\Delta(s)}. \tag{7.18}$$

The numerator polynomials are given by the following determinants

$$N_\eta^u(s) = \begin{vmatrix} \mathring{X}_\eta & -\left(\mathring{X}_{\dot{w}} + \mathring{X}_w\right) & -\left(\left(\mathring{X}_q - mW_\mathrm{e}\right)s - mg\cos\theta_\mathrm{e}\right) \\ \mathring{Z}_\eta & -\left(\left(\mathring{Z}_{\dot{w}} - m\right)s + \mathring{Z}_w\right) & -\left(\left(\mathring{Z}_q + mU_\mathrm{e}\right)s - mg\sin\theta_\mathrm{e}\right) \\ \mathring{M}_\eta & -\left(\mathring{M}_{\dot{w}} + \mathring{M}_w\right) & \left(I_{yy}s - \mathring{M}_q s\right) \end{vmatrix},$$

$$N_\eta^w(s) = \begin{vmatrix} \left(ms - \mathring{X}_u\right) & \mathring{X}_\eta & -\left(\left(\mathring{X}_q - mW_\mathrm{e}\right)s - mg\cos\theta_\mathrm{e}\right) \\ -\mathring{Z}_u & \mathring{Z}_\eta & -\left(\left(\mathring{Z}_q + mU_\mathrm{e}\right)s - mg\sin\theta_\mathrm{e}\right) \\ -\mathring{M}_u & \mathring{M}_\eta & \left(I_{yy}s - \mathring{M}_q s\right) \end{vmatrix}, \qquad , \tag{7.19}$$

$$N_\eta^\theta(s) = \begin{vmatrix} \left(ms - \mathring{X}_u\right) & -\left(\mathring{X}_{\dot{w}} + \mathring{X}_w\right) & \mathring{X}_\eta \\ -\mathring{Z}_u & -\left(\left(\mathring{Z}_{\dot{w}} - m\right)s + \mathring{Z}_w\right) & \mathring{Z}_\eta \\ -\mathring{M}_u & -\left(\mathring{M}_{\dot{w}} + \mathring{M}_w\right) & \mathring{M}_\eta \end{vmatrix}$$

and the common denominator polynomial is given by the determinant

$$\Delta(s) = \begin{vmatrix} \left(ms - \mathring{X}_u\right) & -\left(\mathring{X}_{\dot{w}} + \mathring{X}_w\right) & -\left(\left(\mathring{X}_q - mW_\mathrm{e}\right)s - mg\cos\theta_\mathrm{e}\right) \\ -\mathring{Z}_u & -\left(\left(\mathring{Z}_{\dot{w}} - m\right)s + \mathring{Z}_w\right) & -\left(\left(\mathring{Z}_q + mU_\mathrm{e}\right)s - mg\sin\theta_\mathrm{e}\right) \\ -\mathring{M}_u & -\left(\mathring{M}_{\dot{w}} + \mathring{M}_w\right) & \left(I_{yy}s - \mathring{M}_q s\right) \end{vmatrix}. \tag{7.20}$$

The thrust response transfer functions may be derived by assuming the elevator to be fixed at its trim value; thus $\eta(s) = 0$, and $T(s)$ is written in place of $\eta(s)$. Then the derivatives $\mathring{X}_\eta$, $\mathring{Z}_\eta$, and $\mathring{M}_\eta$ in equation (7.19) are replaced by $\mathring{X}_T$, $\mathring{Z}_T$, and $\mathring{M}_T$, respectively. Meanwhile, note that the denominator polynomial $\Delta(s)$ remains the same, as it is still the longitudinal system response.

Copyright © 2025 Xiaowei He

7.2.3 The lateral-directional response transfer functions

The lateral-directional response transfer functions may be obtained by exactly the same means as the longitudinal transfer functions. The Laplace transform, assuming zero initial conditions, of the lateral–directional equations of motion referred to body axes (equation (6.30)) may be written in matrix form as follows

$$\begin{bmatrix} \left(ms - \mathring{Y}_v\right) & -\begin{pmatrix} \left(\mathring{Y}_p + mW_\mathrm{e}\right)s \\ + mg\cos\theta_\mathrm{e} \end{pmatrix} & -\begin{pmatrix} \left(\mathring{Y}_r - mU_\mathrm{e}\right)s \\ + mg\sin\theta_\mathrm{e} \end{pmatrix} \\ -\mathring{L}_v & \left(I_{xx}s^2 - \mathring{L}_p s\right) & -\left(I_{xz}s^2 + \mathring{L}_r s\right) \\ -\mathring{N}_v & -\left(I_{xz}s^2 + \mathring{N}_p s\right) & \left(I_{zz}s^2 - \mathring{N}_r s\right) \end{bmatrix} \begin{bmatrix} v(s) \\ \phi(s) \\ \psi(s) \end{bmatrix} = \begin{bmatrix} \mathring{Y}_\xi & \mathring{Y}_\zeta \\ \mathring{L}_\xi & \mathring{L}_\zeta \\ \mathring{N}_\xi & \mathring{N}_\zeta \end{bmatrix} \begin{bmatrix} \xi(s) \\ \zeta(s) \end{bmatrix}, \tag{7.21}$$

where $s\phi(s) = p(s)$ and $s\psi(s) = r(s)$. By holding the rudder at its trim setting, $\zeta(s) = 0$, the aileron response transfer functions may be obtained by applying Cramer's rule to equation (7.21). Similarly, by holding the ailerons at the trim setting, $\xi(s) = 0$, the rudder response transfer functions may be obtained. For example, the roll rate response to ailerons is given by

$$\frac{N_\xi^p(s)}{\Delta(s)} \equiv \frac{p(s)}{\xi(s)} = \frac{s\phi(s)}{\xi(s)} \equiv \frac{sN_\xi^\phi(s)}{\Delta(s)}, \tag{7.22}$$

where the numerator polynomial is given by

$$N_\xi^p(s) = s \begin{vmatrix} \left(ms - \mathring{Y}_v\right) & \mathring{Y}_\xi & -\begin{pmatrix} \left(\mathring{Y}_r - mU_\mathrm{e}\right)s \\ + mg\sin\theta_\mathrm{e} \end{pmatrix} \\ -\mathring{L}_v & \mathring{L}_\xi & -\left(I_{xz}s^2 + \mathring{L}_r s\right) \\ -\mathring{N}_v & \mathring{N}_\xi & \left(I_{zz}s^2 - \mathring{N}_r s\right) \end{vmatrix}, \tag{7.23}$$

and the denominator polynomial is given by

$$\Delta(s) = \begin{vmatrix} \left(ms - \mathring{Y}_v\right) & -\begin{pmatrix} \left(\mathring{Y}_p + mW_\mathrm{e}\right)s \\ + mg\cos\theta_\mathrm{e} \end{pmatrix} & -\begin{pmatrix} \left(\mathring{Y}_r - mU_\mathrm{e}\right)s \\ + mg\sin\theta_\mathrm{e} \end{pmatrix} \\ -\mathring{L}_v & \left(I_{xx}s^2 - \mathring{L}_p s\right) & -\left(I_{xz}s^2 + \mathring{L}_r s\right) \\ -\mathring{N}_v & -\left(I_{xz}s^2 + \mathring{N}_p s\right) & \left(I_{zz}s^2 - \mathring{N}_r s\right) \end{vmatrix}. \tag{7.24}$$

7.2.4 Units of transfer functions

It is important to remember that all transfer functions have units, which should always be indicated if confusion is to be avoided. For example, the units of the transfer function $\dfrac{\theta(s)}{\eta(s)} \equiv \dfrac{N_\eta^\theta(s)}{\Delta(s)}$ are rad/rad or equivalently, deg/deg. Angular measure is usually, and correctly, quantified in radians, and care must be applied when interpreting transfer functions since the radian is a very large angular quantity in the context of aircraft small-perturbation motion. This becomes especially important when dealing with transfer functions in which the input and output variables have different units. For instance, the transfer

Copyright © 2025 Xiaowei He

function describing speed response to elevator $\dfrac{u(s)}{\eta(s)} \equiv \dfrac{N_\eta^u(s)}{\Delta(s)}$ has units $\dfrac{\text{m/s}}{\text{rad}}$, and one radian of elevator input is impossibly large. It is therefore very important to remember that one radian is equivalent to 57.3 degrees.

7.2.5 Response to controls

Time histories for the aircraft response to controls are readily obtained by finding the inverse Laplace transform of the appropriate transfer function expression. For example, the roll rate response to aileron is given by (recall from section 1.3.4 that the output of the system is the convolution of the input and the plant)

$$p(s) = G(s)\xi(s) \equiv \frac{N_\xi^p(s)}{\Delta(s)}\xi(s), \tag{7.25}$$

assuming that the aircraft is initially in trimmed flight. The aileron input $\xi(s)$ is the Laplace transform of the required input function. For example, two commonly used inputs are the *impulse* and *step* functions, where impulse of magnitude k is given by

$$\xi(s) = k, \tag{7.26}$$

and step of magnitude k is given by

$$\xi(s) = \frac{k}{s}. \tag{7.27}$$

To continue with the example, the *time response* of roll rate to an aileron step input of magnitude k is given by

$$p(t) = \mathcal{L}^{-1}\left\{\frac{N_\xi^p(s)}{\Delta(s)}\frac{k}{s}\right\}. \tag{7.28}$$

Final value and initial value theorems. It is often not necessary to have a complete time response solution merely to obtain the characteristics of the dynamic modes. The principal mode characteristics, damping ratio, and natural frequency, are directly obtainable on inspection of the characteristic polynomial $\Delta(s)$ in any aircraft transfer function. Recalling from section 1.3.4, the *final value theorem*, the steady-state gain is readily established by

$$\lim_{t\to\infty} f(t) = \lim_{s\to 0} sF(s). \tag{7.29}$$

The corresponding *initial value theorem* states that

$$\lim_{t\to 0} f(t) = \lim_{s\to\infty} sF(s). \tag{7.30}$$

Example 7.2

The transfer function describing pitch attitude response to elevator for the Lockheed F-104 Starfighter is given by

$$\frac{N_\eta^\theta(s)}{\Delta(s)} = \frac{-4.664(s+0.135)(s+0.267)}{(s^2+0.033s+0.022)(s^2+0.0893+4.884)}\ [\text{rad/rad}].$$

Applying the initial value and final value theorems to find the initial and steady-state values for the pitch attitude response.

The Laplace transform of a unit step input is $1/s$ [deg], therefore, assuming the unit step input to

Copyright © 2025 Xiaowei He

be in degree units, the Laplace transform of the unit step response of the pitch attitude is given by

$$\theta(s) = \frac{N_\eta^\theta(s)}{\Delta(s)}\frac{1}{s} = \frac{-4.664(s+0.135)(s+0.267)}{s(s^2+0.033s+0.022)(s^2+0.0893+4.884)}\ [\text{deg}].$$

Applying the final value theorem, we obtain

$$\theta(t)_{t\to\infty} = \lim_{s\to 0}\left(s\frac{-4.664(s+0.135)(s+0.267)}{s(s^2+0.033s+0.022)(s^2+0.0893+4.884)}\right)\ [\text{deg}] = -1.565\,\text{deg},$$

and applying the initial value theorem, we obtain

$$\theta(t)_{t\to 0} = \lim_{s\to\infty}\left(s\frac{-4.664(s+0.135)(s+0.267)}{s(s^2+0.033s+0.022)(s^2+0.0893+4.884)}\right)\ [\text{deg}] = 0\,\text{deg}.$$

7.2.6 Acceleration response transfer functions

Acceleration response transfer functions are frequently required but are not given directly by the solution of the equations of motion described previously. Recalling the aircraft force equations (equation (5.13)) from section 5.1, expressions for the components of inertial acceleration of which the body axis system is co-located with its *cg* are given as

$$\begin{aligned}\dot{U} + qW - rV &= a_x\\ \dot{V} + rU - pW &= a_y,\\ \dot{W} + pV - qU &= a_z.\end{aligned} \tag{7.31}$$

Assuming small-perturbation motion such that the usual simplifications can be made, equation (7.31) may be restated as

$$\begin{aligned}a_x &= \dot{u} + qW_\text{e} - rV_\text{e},\\ a_y &= \dot{v} + rU_\text{e} - pW_\text{e},\\ a_z &= \dot{w} + pV_\text{e} - qU_\text{e}.\end{aligned} \tag{7.32}$$

If, for example, the normal acceleration response to elevator referred to the *cg* is required, the Laplace transform of the normal acceleration, assuming zero initial conditions, may be written as

$$a_z(s) = sw(s) + s\phi(s)V_\text{e} - s\theta(s)U_\text{e}. \tag{7.33}$$

Or, expressed in terms of elevator response transfer functions,

$$a_z(s) = s\frac{N_\eta^w(s)}{\Delta(s)}\eta(s) + sV_\text{e}\frac{N_\eta^\phi(s)}{\Delta(s)}\eta(s) - sU_\text{e}\frac{N_\eta^\theta(s)}{\Delta(s)}\eta(s) = \frac{s\left(N_\eta^w(s) + N_\eta^\phi(s) - N_\eta^\theta(s)\right)\eta(s)}{\Delta(s)}. \tag{7.34}$$

Thus, the required normal acceleration response transfer function may be written as

$$\frac{N_\eta^{a_z}(s)}{\Delta(s)} \equiv \frac{a_z(s)}{\eta(s)} = \frac{s\left(N_\eta^w(s) + N_\eta^\phi(s) - N_\eta^\theta(s)\right)}{\Delta(s)}. \tag{7.35}$$

Transfer functions for the remaining acceleration response components may be derived in a similar manner.

Copyright © 2025 Xiaowei He

7.3 The state-space method

7.3.1 The transfer function matrix

The general state equations describing a linear dynamic system may be written as

$$\begin{aligned} \dot{\boldsymbol{x}}(t) &= \boldsymbol{A}\boldsymbol{x}(t) + \boldsymbol{B}\boldsymbol{u}(t), \\ \boldsymbol{y}(t) &= \boldsymbol{C}\boldsymbol{x}(t) + \boldsymbol{D}\boldsymbol{u}(t). \end{aligned} \tag{7.36}$$

The assembly of the equations of motion in this form, for the particular application to aircraft, was explained in section 6.6. Since $\boldsymbol{A}$, $\boldsymbol{B}$, $\boldsymbol{C}$, and $\boldsymbol{D}$ are matrices of constant coefficients, the Laplace transform of dynamic system, assuming zero initial conditions, is

$$\begin{aligned} s\boldsymbol{x}(s) &= \boldsymbol{A}\boldsymbol{x}(s) + \boldsymbol{B}\boldsymbol{u}(s), \\ y(s) &= \boldsymbol{C}\boldsymbol{x}(s) + \boldsymbol{D}\boldsymbol{u}(s). \end{aligned} \tag{7.37}$$

The state equation may be rearranged and written as

$$\boldsymbol{x}(s) = (s\boldsymbol{I} - \boldsymbol{A})^{-1}\boldsymbol{B}\boldsymbol{u}(s), \tag{7.38}$$

where $\boldsymbol{I}$ is the identity matrix and is the same order as $\boldsymbol{A}$. Thus, elimination the state vector$\boldsymbol{x}(s)$, by combining the output equation and equation (7.38), the output vector $\boldsymbol{y}(s)$ is given by

$$\boldsymbol{y}(s) = \left[\boldsymbol{C}(s\boldsymbol{I} - \boldsymbol{A})^{-1}\boldsymbol{B} + \boldsymbol{D}\right]\boldsymbol{u}(s) = \boldsymbol{G}(s)\boldsymbol{u}(s), \tag{7.39}$$

where $\boldsymbol{G}(s)$ is called the transfer function matrix. In general, the transfer function matrix has the form

$$\boldsymbol{G}(s) = \frac{1}{\Delta(s)}\boldsymbol{N}(s), \tag{7.40}$$

and $\boldsymbol{N}(s)$ is a polynomial matrix whose elements are all of the response transfer function numerators. The denominator $\Delta(s)$ is the characteristic polynomial and is common to all transfer functions. Thus, the application of the state-space method to the solution of the equations of motion enables all response transfer functions to be obtained in a single computation.

When dealing with the solution of the equations of motion of aircraft, it is usually required that $\boldsymbol{y}(s) = \boldsymbol{x}(s)$, that is, the output vector and state vector are chosen to be the same. In this case, equation (7.39) may be simplified since $\boldsymbol{C} = \boldsymbol{I}$ and $\boldsymbol{D} = \boldsymbol{0}$; therefore,

$$\boldsymbol{G}(s) = (s\boldsymbol{I} - \boldsymbol{A})^{-1}\boldsymbol{B} = \frac{\operatorname{adj}(s\boldsymbol{I} - \boldsymbol{A})\boldsymbol{B}}{|s\boldsymbol{I} - \boldsymbol{A}|}. \tag{7.41}$$

It is evident that the polynomial numerator of the transfer function matrix is given by

$$\boldsymbol{N}(s) = \operatorname{adj}(s\boldsymbol{I} - \boldsymbol{A})\boldsymbol{B}, \tag{7.42}$$

and the characteristic polynomial is given by

$$\Delta(s) = |s\boldsymbol{I} - \boldsymbol{A}|. \tag{7.43}$$

Copyright © 2025 Xiaowei He

7.3.2 The longitudinal transfer function matrix

The concise state equations are given by

$$\begin{bmatrix} \dot{u} \\ \dot{w} \\ \dot{q} \\ \dot{\theta} \end{bmatrix} = \begin{bmatrix} x_u & x_w & x_q & x_\theta \\ z_u & z_w & z_q & z_\theta \\ m_u & m_w & m_q & m_\theta \\ 0 & 0 & 1 & 0 \end{bmatrix} \begin{bmatrix} u \\ w \\ q \\ \theta \end{bmatrix} + \begin{bmatrix} x_\eta & x_T \\ z_\eta & z_T \\ m_\eta & m_T \\ 0 & 0 \end{bmatrix} \begin{bmatrix} \eta \\ T \end{bmatrix}, \tag{7.44}$$

and

$$\boldsymbol{y}(t) = \boldsymbol{I}\boldsymbol{x}(t) = \begin{bmatrix} 1 & 0 & 0 & 0 \\ 0 & 1 & 0 & 0 \\ 0 & 0 & 1 & 0 \\ 0 & 0 & 0 & 1 \end{bmatrix} \begin{bmatrix} u \\ w \\ q \\ \theta \end{bmatrix}. \tag{7.45}$$

Substituting for $\boldsymbol{A}$, $\boldsymbol{B}$, and $\boldsymbol{I}$ in equation (7.41), the longitudinal transfer function matrix is given by

$$\boldsymbol{G}(s) = \begin{bmatrix} s - x_u & -x_w & -x_q & -x_\theta \\ -z_u & s - z_w & -z_q & -z_\theta \\ -m_u & -m_w & s - m_q & -m_\theta \\ 0 & 0 & -1 & s \end{bmatrix}^{-1} \begin{bmatrix} x_\eta & x_T \\ z_\eta & z_T \\ m_\eta & m_T \\ 0 & 0 \end{bmatrix}. \tag{7.46}$$

An algebraic manipulation leads to

$$\boldsymbol{G}(s) = \frac{1}{\Delta(s)} \begin{bmatrix} N_\eta^u(s) & N_T^u(s) \\ N_\eta^w(s) & N_T^w(s) \\ N_\eta^q(s) & N_T^q(s) \\ N_\eta^\theta(s) & N_T^\theta(s) \end{bmatrix}. \tag{7.47}$$

In this case, the numerator and denominator polynomials are expressed in terms of the concise derivatives.

7.3.3 The lateral-directional transfer function matrix

The lateral-directional state equations are given in terms of concise derivatives by

$$\begin{bmatrix} \dot{v} \\ \dot{p} \\ \dot{r} \\ \dot{\phi} \\ \dot{\psi} \end{bmatrix} = \begin{bmatrix} y_v & y_p & y_r & y\phi & y_\psi \\ l_v & l_p & l_r & l\phi & l_\psi \\ n_v & n_p & n_r & n\phi & n_\psi \\ 0 & 1 & 0 & 0 & 0 \\ 0 & 0 & 1 & 0 & 0 \end{bmatrix} \begin{bmatrix} v \\ p \\ r \\ \phi \\ \psi \end{bmatrix} + \begin{bmatrix} y_\xi & y_\zeta \\ l_\xi & l_\zeta \\ n_\xi & n_\zeta \\ 0 & 0 \\ 0 & 0 \end{bmatrix} \begin{bmatrix} \xi \\ \zeta \end{bmatrix}. \tag{7.48}$$

Thus substituting for $\boldsymbol{A}$, $\boldsymbol{B}$, and $\boldsymbol{I}$ in equation (7.41), the lateral-directional transfer function matrix is given by

$$\boldsymbol{G}(s) = \begin{bmatrix} s - y_v & -y_p & -y_r & -y_\phi & -y_\psi \\ -l_v & s - l_p & -l_r & -l_\phi & -l_\phi \\ -n_v & -n_p & s - n_r & -n_\phi & -n_\psi \\ 0 & -1 & 0 & s & 0 \\ 0 & 0 & -1 & 0 & s \end{bmatrix}^{-1} \begin{bmatrix} y_\xi & y_\zeta \\ l_\xi & l_\zeta \\ n_\xi & n_\zeta \\ 0 & 0 \\ 0 & 0 \end{bmatrix}, \tag{7.49}$$

Copyright © 2025 Xiaowei He

and may be written as

$$\boldsymbol{G}(s) = \frac{1}{\Delta(s)} \begin{bmatrix} N_\xi^v(s) & N_\zeta^v(s) \\ N_\xi^p(s) & N_\zeta^p(s) \\ N_\xi^r(s) & N_\zeta^r(s) \\ N_\xi^\phi(s) & N_\zeta^\phi(s) \\ N_\xi^\psi(s) & N_\zeta^\psi(s) \end{bmatrix}. \tag{7.50}$$

7.4 Longitudinal dynamics

7.4.1 Longitudinal transfer functions and response to controls

It is convenient to review the longitudinal response to elevators about a trim state in which thrust is held constant. The longitudinal state equation (6.53) may then be written as

$$\begin{bmatrix} \dot{u} \\ \dot{w} \\ \dot{q} \\ \dot{\theta} \end{bmatrix} = \begin{bmatrix} x_u & x_w & x_q & x_\theta \\ z_u & z_w & z_q & z_\theta \\ m_u & m_w & m_q & m_\theta \\ 0 & 0 & 1 & 0 \end{bmatrix} \begin{bmatrix} u \\ w \\ q \\ \theta \end{bmatrix} + \begin{bmatrix} x_\eta \\ z_\eta \\ m_\eta \\ 0 \end{bmatrix} \eta, \tag{7.51}$$

of which the four response transfer functions are obtained as

$$\begin{aligned} \frac{u(s)}{\eta(s)} &\equiv \frac{N_\eta^u(s)}{\Delta(s)} = \frac{k_u(s+1/\tau_u)(s^2+2\zeta_u\omega_u s+\omega_u^2)}{(s^2+2\zeta_\mathrm{p}\omega_\mathrm{p} s+\omega_\mathrm{p}^2)(s^2+2\zeta_\mathrm{s}\omega_\mathrm{s} s+\omega_\mathrm{s}^2)}, \\ \frac{w(s)}{\eta(s)} &\equiv \frac{N_\eta^w(s)}{\Delta(s)} = \frac{k_w(s+1/\tau_\alpha)(s^2+2\zeta_\alpha\omega_\alpha s+\omega_\alpha^2)}{(s^2+2\zeta_\mathrm{p}\omega_\mathrm{p} s+\omega_\mathrm{p}^2)(s^2+2\zeta_\mathrm{s}\omega_\mathrm{s} s+\omega_\mathrm{s}^2)}, \\ \frac{q(s)}{\eta(s)} &\equiv \frac{N_\eta^q(s)}{\Delta(s)} = \frac{k_q(s+1/\tau_{\theta_1})(s+1/\tau_{\theta_2})}{(s^2+2\zeta_\mathrm{p}\omega_\mathrm{p} s+\omega_\mathrm{p}^2)(s^2+2\zeta_\mathrm{s}\omega_\mathrm{s} s+\omega_\mathrm{s}^2)}, \\ \frac{\theta(s)}{\eta(s)} &\equiv \frac{N_\eta^\theta(s)}{\Delta(s)} = \frac{k_\theta(s+1/\tau_{\theta_1})(s+1/\tau_{\theta_2})}{(s^2+2\zeta_\mathrm{p}\omega_\mathrm{p} s+\omega_\mathrm{p}^2)(s^2+2\zeta_\mathrm{s}\omega_\mathrm{s} s+\omega_\mathrm{s}^2)}, \end{aligned} \tag{7.52}$$

where $k_{u,w,q,\theta}$ are constant gains of the transfer functions (note that they are not DC gains), $\tau_{u,\alpha,\theta_{1,2}}$ are time constants, $\zeta_{\mathrm{p,s}}$ are damping ratios regarding phugoid and short-period modes which will be discussed later (not to confuse with the rudder angle ζ), and $\omega_{\mathrm{p,s}}$ are undamped natural frequency of the two modes mentioned (refer to the discussion on second-order systems in section 1.3.4).

The solution to the equations of motion yields polynomial descriptions of the transfer function numerators and a common denominator. The polynomials factorize into real and complex pairs of roots. Since the roots are interpreted as time constants, damping ratios, and natural frequencies, this formatting style makes the essential information instantly available. It should also be noted that the numerator and denominator factors are typical for a conventional aircraft. Sometimes complex pairs of roots may become two real roots and vice versa. However, this does not usually mean that the dynamic response characteristics of the aircraft become dramatically different. Differences in the interpretation of response may be evident, but will not necessarily be large.

The common denominator of the transfer functions describes the characteristic polynomial, which in turn describes the stability characteristics of the aircraft. Thus, the response of all variables to an

Copyright © 2025 Xiaowei He

elevator input is dominated by the denominator parameters: damping ratios and natural frequencies. The differences between the individual responses are entirely determined by their respective numerators. It is therefore important to fully appreciate the role of the numerator in determining response dynamics. The response shapes of the individual variables are determined by the common denominator and "colored" by their respective numerators. The numerator plays no part in determining stability in a linear system, which is how aircraft are modeled in this course.

The response of the Ling-Temco-Vought A-7A Corsair II aircraft based on aerodynamic data obtained from Teper [15] to a unit step (1°) elevator input is shown in figure 7.2, where the flight condition corresponds to level cruising flight at an altitude of $15,000\,\text{ft}$ ($4,572\,\text{m}$) at Mach 0.3. The responses show both dynamic stability modes, the short-period pitch oscillation and the phugoid. However, the magnitude of each stability mode differs in each response variable. For example, the short-period pitch oscillation is most visible as the initial transient in the variables w, q, and α, whereas the phugoid mode is visible in all variables, although the relative magnitudes vary considerably. The stability of the responses is the same, as determined by the common denominator of the transfer functions, but the differences between the response variables are determined by the unique numerator of each response transfer function.

Copyright © 2025 Xiaowei He

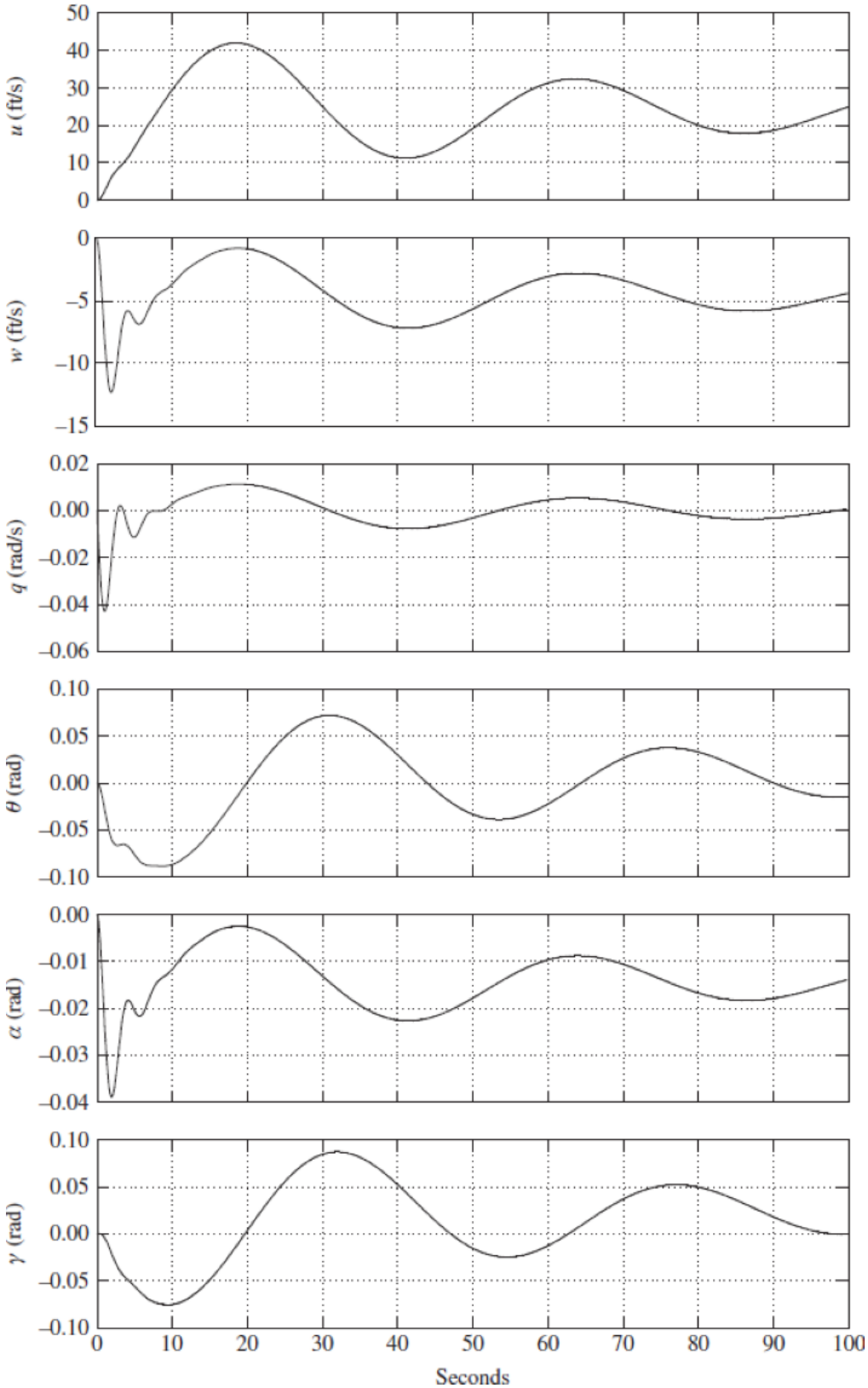

Figure 7.2: Aircraft response to a 1° elevator step input [1].

Copyright © 2025 Xiaowei He

7.4.2 Longitudinal characteristic equation

The longitudinal characteristic polynomial for a classical aircraft is fourth order; it determines the common denominator in the longitudinal response transfer functions and, when equated to zero, defines the characteristic equation, which may be written as

$$As^4 + Bs^3 + Cs^2 + Ds + E = 0, \tag{7.53}$$

which is most commonly factorized into two pairs of complex roots and is written as

$$\underbrace{(s^2 + 2\zeta_\mathrm{p}\omega_\mathrm{p}s + \omega_\mathrm{p}^2)}_{\text{phugoid mode}}\underbrace{(s^2 + 2\zeta_\mathrm{s}\omega_\mathrm{s}s + \omega_\mathrm{s}^2)}_{\text{short-period mode}} = 0. \tag{7.54}$$

As explained, the second-order characteristics in equation (7.54) describe the phugoid and short-period stability modes, respectively. The stability modes provide a complete description of the longitudinal stability properties of the aircraft subject to the constraint of small-perturbation motion. Interpretation of the characteristic equation written in this way is most readily accomplished if reference is first made to the properties of the classical mechanical mass-spring-damper system, which were reviewed in section 1.3.4.

Thus, the longitudinal dynamics of the aircraft may be likened to a pair of loosely coupled mass-spring-damper systems, and the interpretation of the motion of the aircraft following a disturbance from equilibrium may be made by direct comparison with the behavior of the mechanical mass-spring-damper. However, the damping and frequency characteristics of the aircraft are not mechanical in origin; they derive entirely from the aerodynamic properties of the airframe. The connection between the observed dynamics of the aircraft and its aerodynamic characteristics is made by referring to the definitions of the coefficients in terms of aerodynamic stability derivatives. The relationships between the damping ratios and the undamped frequencies of equation (7.54), and their aerodynamic drivers, are neither obvious nor simple. In the following sections, simplifying approximations are made based on the observation and understanding of the physical behavior of aircraft dynamics.

7.4.3 The short-period oscillation mode

Both longitudinal dynamic stability modes are excited whenever the aircraft is disturbed from its equilibrium trim state. A disturbance may be initiated by pilot control inputs, a change in power setting, airframe configuration changes, such as flap deployment, and external atmospheric influences, such as gusts and turbulence.

The short-period mode is typically a damped oscillation in pitch about the y axis. Whenever an aircraft is disturbed from its pitch equilibrium state, the mode is excited and manifests itself as a classical second-order oscillation in which the principal variables are incidence $\alpha(w)$, pitch rate q, and pitch attitude θ. This observation is easily confirmed by reference to the eigenvectors in the solution of the equations of motion; it may be seen figure 7.2. Typically, the undamped natural frequency of the mode ranges from 1 rad/s to 10 rad/s, and the damping is usually stabilizing, although the damping ratio is often lower than desired. A significant feature of the mode is that the speed remains approximately constant ($u = 0$) during a disturbance. As the period of the mode is short, inertia and momentum effects ensure that speed response in the time scale of the mode is negligible.

The physical situation applied can be interpreted by comparison with a torsional mass-spring-damper system. The aircraft behaves as if it were restrained by a torsional spring about the y axis, as indicated in figure 7.3. A pitch disturbance from trim equilibrium causes the "spring" to produce a

Copyright © 2025 Xiaowei He

restoring moment, thereby giving rise to an oscillation in pitch. The oscillation is damped, which can be interpreted as a viscous damper. The spring and viscous damping effects are not mechanical. In reality, they are produced entirely by aerodynamic mechanisms with contributions from all parts of the airframe, not all of which are necessarily stabilizing. However, in the interest of promoting understanding, the stiffness and damping effects are assumed to be dominated by the aerodynamic effects of the tailplane. The spring stiffness arises from the natural weathercock tendency of the tailplane to align with the incident flow. The damping arises from the motion of the tailplane during the oscillation when it behaves as a kind of viscous paddle damper. The total observed mode dynamics depend not only on the tailplane contribution but also on the magnitudes of the additional contributions from other parts of the airframe. When the overall stability is marginal, it is implied that the additional contributions are significant, which makes it much more difficult to identify and quantify the principal aerodynamic mode drivers.

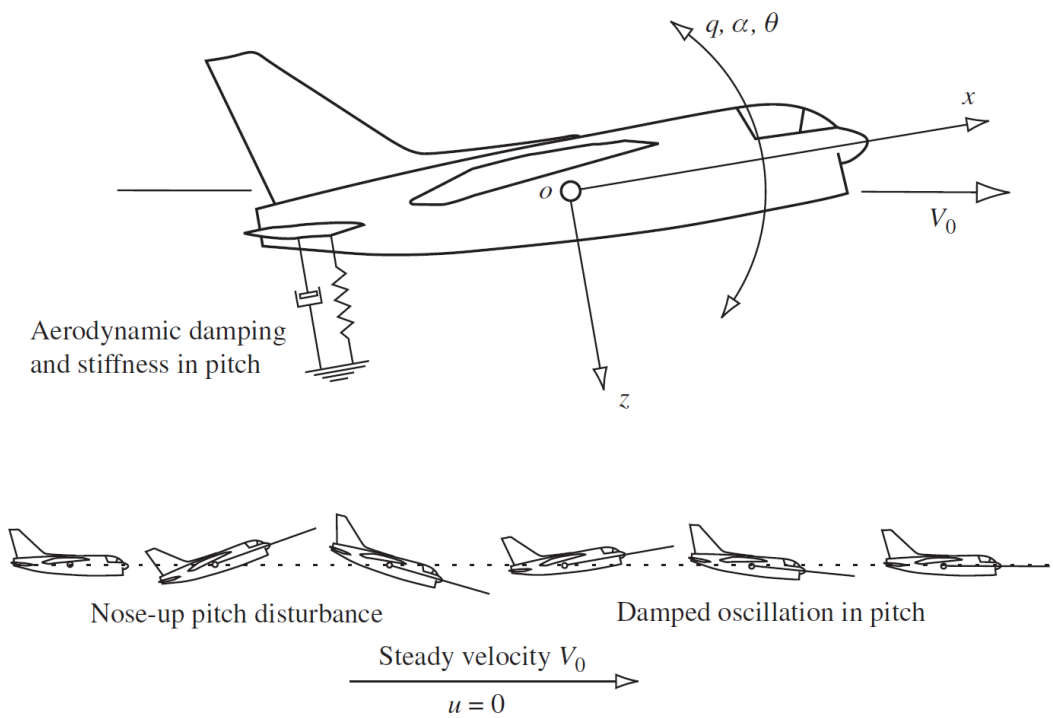

Figure 7.3: Stable short-period pitch oscillation [1].

7.4.4 The phugoid mode

The phugoid mode is most commonly a lightly damped low-frequency oscillation in speed u, which couples into pitch attitude θ and height h. A significant feature of this mode is that the incidence $\alpha(w)$ remains substantially constant during a disturbance. These observations have been confirmed by reference to the eigenvectors in the solution of the equations of motion, which may be seen figure 7.2. However, it is clear that the phugoid appears in all of the longitudinal motion variables while the relative magnitudes of the phugoid components in incidence $\alpha(w)$ and pitch rate q are very small. Typically, the undamped natural frequency of the phugoid is in the range 0.1 rad/s to 1 rad/s, and the damping ratio is very low. However, the apparent damping characteristics of the mode may be substantially influenced by power effects in some aircraft.

Consider the development of classical phugoid motion following a small disturbance in speed, as illustrated in figure 7.4. The aircraft is initially in trimmed level equilibrium flight with a steady velocity

Copyright © 2025 Xiaowei He

V_0, such that the lift L and weight mg are equal. Let the aircraft be disturbed (phase a) such that the velocity is reduced by a small amount u. Since the incidence remains substantially constant, this results in a small reduction in lift such that the aircraft is no longer in vertical equilibrium. It therefore starts to lose height and, since it is flying "downhill", the aircraft starts to accelerate (phase b). The speed continues to build up to a value in excess of V_0, which is accompanied by a build-up in lift that eventually exceeds the weight by a significant margin. The build-up in speed and lift causes the aircraft to pitch up steadily until it starts to climb (phase c). Since it now has an excess of kinetic energy, inertia, and momentum effects cause it to fly up through the nominal trimmed height datum (phase d), losing speed and lift as it goes because it is now flying "uphill". As it decelerates, it pitches down steadily until its lift is significantly less than the weight, and the accelerating descent starts again (phase e). Inertia and momentum effects cause the aircraft to continue flying down through the nominal trimmed height datum (phase f). As speed and lift continue to build up, it pitches up steadily until it starts climbing again to commence the next cycle of oscillation (phase g). As the motion progresses, the effects of drag cause the motion variable maxima and minima at each peak to reduce gradually in magnitude until the motion eventually damps out.

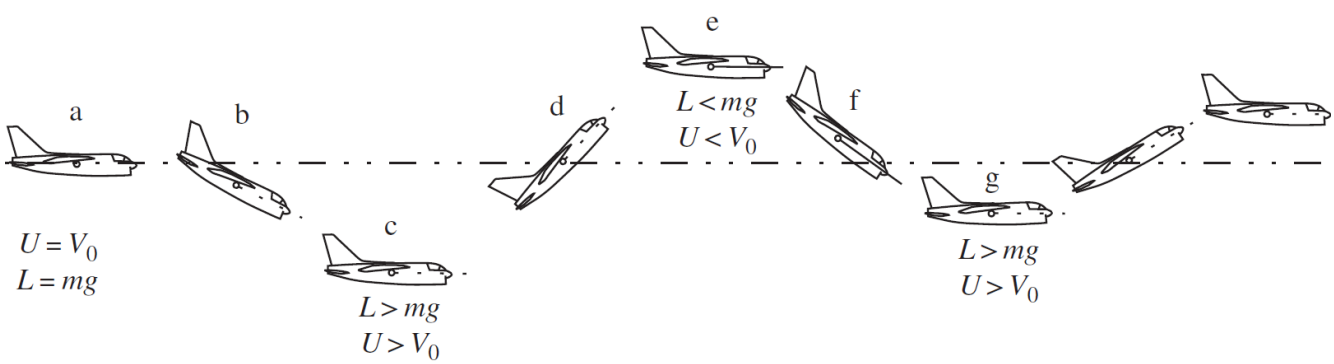

Figure 7.4: Development of a stable phugoid [1].

Thus, the phugoid is classical damped harmonic motion, resulting in the aircraft flying a gentle sinusoidal flight path about the nominal trimmed height datum. As large inertia and momentum effects are involved, the motion is necessarily relatively slow such that the angular accelerations, $\dot{q}$ and $\dot{\alpha}(\dot{w})$, are insignificantly small. Consequently, the natural frequency of the mode is low and, since drag is designed to be low, the damping is also low. Typically, once excited, many cycles of the phugoid may be visible before it eventually damps out. Since the rate of energy loss is low, a consequence of low drag-damping effects, the motion is often approximated by undamped harmonic motion, in which potential and kinetic energy are exchanged as the aircraft flies the sinusoidal flight path.

7.5 Lateral-directional dynamics

The procedures for investigating and interpreting the lateral-directional dynamics of an aircraft are much the same as those used to deal with the longitudinal dynamics. However, some aspects of lateral-directional dynamics and their interpretation differ significantly from those of longitudinal dynamics, and the procedures for interpreting these differences are addressed appropriately. The lateral-directional response transfer functions are obtained in the solution of the lateral equations of motion (equation (6.55) or equation (6.56)). The transfer functions completely describe the linear dynamic asymmetric response in sideslip, roll, and yaw to aileron and rudder inputs. As in the longitudinal solution, implicit in the response are the dynamic properties determined by the lateral-directional stability characteristics of the

Copyright © 2025 Xiaowei He

aircraft. As before, the transfer functions and the response variables described by them are linear since the entire modeling process is based on the assumption that the motion is constrained to small disturbances about an equilibrium trim state. The equilibrium trim state is assumed to mean steady-level flight in the first instance, and the previously stated caution concerning the magnitude of a small lateral-directional perturbation applies.

The most obvious difference between the solutions of the longitudinal equations of motion and the lateral-directional equations of motion is that there is more algebra to deal with. Since two aerodynamic inputs are involved, the ailerons and the rudder, two sets of input-output response transfer functions are produced in the solution of the equations of motion. However, these are no more difficult to deal with than a single input-output set of transfer functions. The most significant difference between the longitudinal and lateral-directional dynamics of the aircraft concerns interpretation. In general, the lateral-directional stability modes are not so distinct and tend to exhibit dynamic coupling to a greater extent. A mitigating observation is that, unlike longitudinal dynamics, lateral-directional dynamics do not change much with flight conditions since most aircraft possess aerodynamic symmetry by design.

7.5.1 Lateral-directional transfer functions and response to controls

Transfer functions. The lateral-directional equations of motion describing small perturbations about an equilibrium trim condition, referenced to wind axes, are given by the state equation (6.56)

$$\begin{bmatrix} \dot{v} \\ \dot{p} \\ \dot{r} \\ \dot{\phi} \end{bmatrix} = \begin{bmatrix} y_v & y_p & y_r & y\phi & y_\psi \\ l_v & l_p & l_r & l\phi & l_\psi \\ n_v & n_p & n_r & n\phi & n_\psi \\ 0 & 1 & 0 & 0 & 0 \end{bmatrix} \begin{bmatrix} v \\ p \\ r \\ \phi \end{bmatrix} + \begin{bmatrix} y_\xi & y_\zeta \\ l_\xi & l_\zeta \\ n_\xi & n_\zeta \\ 0 & 0 \end{bmatrix} \begin{bmatrix} \xi \\ \zeta \end{bmatrix}, \tag{7.55}$$

of which the solution produces two sets of four response transfer functions. One set describes motion in response to aileron input, and a second set describes the response to rudder input. The transfer functions describing the response to the aileron are written as

$$\begin{aligned} \frac{v(s)}{\xi(s)} &\equiv \frac{N_\xi^v(s)}{\Delta(s)} = \frac{k_v(s+1/\tau_{\beta_1})(s+1/\tau_{\beta_2})}{(s+1/\tau_\mathrm{s})(s+1/\tau_\mathrm{r})(s^2+2\zeta_\mathrm{d}\omega_\mathrm{d}s+\omega_\mathrm{d}^2)}, \\ \frac{p(s)}{\xi(s)} &\equiv \frac{N_\xi^p(s)}{\Delta(s)} = \frac{k_p s(s^2+2\zeta_\phi\omega_\phi s+\omega_\phi^2)}{(s+1/\tau_\mathrm{s})(s+1/\tau_\mathrm{r})(s^2+2\zeta_\mathrm{d}\omega_\mathrm{d}s+\omega_\mathrm{d}^2)}, \\ \frac{r(s)}{\xi(s)} &\equiv \frac{N_\xi^r(s)}{\Delta(s)} = \frac{k_r(s+1/\tau_\psi)(s^2+2\zeta_\psi\omega_\psi s+\omega_\psi^2)}{(s+1/\tau_\mathrm{s})(s+1/\tau_\mathrm{r})(s^2+2\zeta_\mathrm{d}\omega_\mathrm{d}s+\omega_\mathrm{d}^2)}, \\ \frac{\phi(s)}{\xi(s)} &\equiv \frac{N_\xi^\phi(s)}{\Delta(s)} = \frac{k_\phi(s^2+2\zeta_\phi\omega_\phi s+\omega_\phi^2)}{(s+1/\tau_\mathrm{s})(s+1/\tau_\mathrm{r})(s^2+2\zeta_\mathrm{d}\omega_\mathrm{d}s+\omega_\mathrm{d}^2)}, \end{aligned} \tag{7.56}$$

Copyright © 2025 Xiaowei He

and the transfer functions describing the response to the rudder are written as

$$
\begin{aligned}
\frac{v(s)}{\zeta(s)} &\equiv \frac{N_\zeta^v(s)}{\Delta(s)} = \frac{k_v(s+1/\tau_{\beta_1})(s+1/\tau_{\beta_2})(s+1/\tau_{\beta_3})}{(s+1/\tau_\mathrm{s})(s+1/\tau_\mathrm{r})(s^2+2\zeta_\mathrm{d}\omega_\mathrm{d}s+\omega_\mathrm{d}^2)}, \\
\frac{p(s)}{\zeta(s)} &\equiv \frac{N_\zeta^p(s)}{\Delta(s)} = \frac{k_p s(s+1/\tau_{\phi_1})(s+1/\tau_{\phi_2})}{(s+1/\tau_\mathrm{s})(s+1/\tau_\mathrm{r})(s^2+2\zeta_\mathrm{d}\omega_\mathrm{d}s+\omega_\mathrm{d}^2)}, \\
\frac{r(s)}{\zeta(s)} &\equiv \frac{N_\zeta^r(s)}{\Delta(s)} = \frac{k_r(s+1/\tau_\psi)(s^2+2\zeta_\psi\omega_\psi s+\omega_\psi^2)}{(s+1/\tau_\mathrm{s})(s+1/\tau_\mathrm{r})(s^2+2\zeta_\mathrm{d}\omega_\mathrm{d}s+\omega_\mathrm{d}^2)}, \\
\frac{\phi(s)}{\zeta(s)} &\equiv \frac{N_\zeta^\phi(s)}{\Delta(s)} = \frac{k_\phi(s+1/\tau_{\phi_1})(s+1/\tau_{\phi_2})}{(s+1/\tau_\mathrm{s})(s+1/\tau_\mathrm{r})(s^2+2\zeta_\mathrm{d}\omega_\mathrm{d}s+\omega_\mathrm{d}^2)}.
\end{aligned}
\tag{7.57}
$$

Similar to the longitudinal transfer functions, the polynomials factorize into real and complex pairs of roots and constant gains ($k_{v,p,r,\phi}$). The roots are interpreted as time constants ($\tau_{\beta_{1,2,3},\phi_{1,2},\psi}$), damping ratios ($\zeta_{\phi,\psi}$), and natural frequencies ($\omega_{\phi,\psi}$). Note that the time constants $\tau_{\mathrm{s,r}}$, the damping ratio ζ_d, and the natural frequency ω_d in the denominators represent the corresponding parameters of different dynamic modes, not to be confused with those of the state variables.

These transfer functions each describe uniquely different, yet related, variables in the motion of the aircraft in response to a control input. However, it will be observed that the notation adopted indicates similar values for some numerator terms in both aileron and rudder response transfer functions. For example, k_r, τ_ψ, ζ_ψ and ω_ψ appear in both $\dfrac{r(s)}{\xi(s)}$ and $\dfrac{r(s)}{\zeta(s)}$. It must be understood that the numerator parameters are context-dependent and usually have a numerical value that is unique to the transfer function in question. To repeat the comment, the notation is a convenience for allocating particular numerator terms, and it serves only to identify the role of each term as a gain, time constant, damping ratio, or frequency.

As before, the denominator of the transfer functions describes the characteristic polynomial, which in turn describes the lateral-directional stability characteristics of the aircraft. The transfer function denominator is therefore common to all response transfer functions. Thus, the response of all variables to an aileron or a rudder input is dominated by the denominator parameters — time constant, damping ratio, and natural frequency. The differences between the individual responses are entirely determined by their respective numerators, and the response shapes of the individual variables are determined by the common denominator and "colored" by their respective numerators.

The responses of the Douglas DC-8 aircraft based on aerodynamic data obtained from Teper [15] to a pulse elevator input and a step rudder input are shown in figures 7.5 and 7.6, respectively. At the flight condition of interest, the aircraft has a total weight of $190,000\,\mathrm{lb}$ ($86,183\,\mathrm{kg}$) and is flying at Mach 0.44 at an altitude of $15,000\,\mathrm{ft}$ ($4,572\,\mathrm{m}$).

Figure 7.5 shows the response of the aircraft to a unit (1°) aileron pulse, held for two seconds and then returned to zero. All of the variables obtained in the solution of the equations of motion are shown, where the individual responses are characterized by the transfer functions. The dynamics associated with the three stability modes are visible in the responses, although at first glance they appear to be dominated by the oscillatory Dutch roll mode since its damping is relatively low. Both the roll and spiral modes appear as exponentially convergent characteristics since they are both stable in this example. The roll mode converges relatively quickly with a time constant of $0.75\,\mathrm{s}$, whereas the spiral mode converges very slowly indeed with a time constant of $154\,\mathrm{s}$. The roll mode is most clearly seen in the roll rate

Copyright © 2025 Xiaowei He

response p, where it determines the exponential rise at 0 s and the exponential recovery when the pulse is removed at 2 s. The spiral mode characteristic is rather more subtle and is most easily seen in the roll attitude response ϕ, where it determines the longer-term convergence to zero and is fully established at 30 s. Once again, all of the response shapes are determined by the common stability mode dynamics, and the obvious differences between them are due to the unique numerators in each transfer function. All of the response variables shown in figure 7.5 eventually decay to zero in the time scale of the spiral mode (about 200 seconds) since the aircraft is stable.

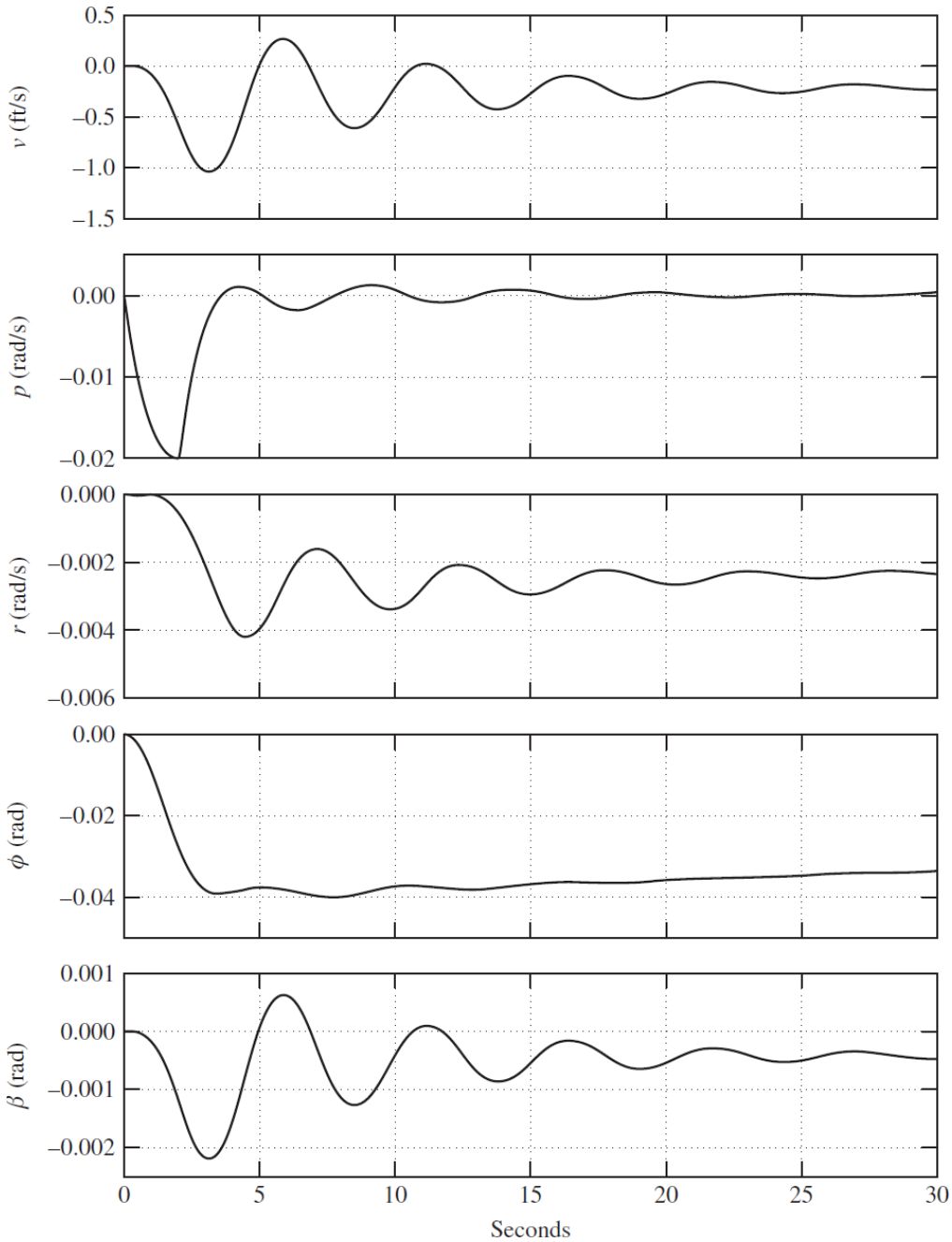

Figure 7.5: Aircraft response to a 1°, 2 sec aileron pulse input [1].

Copyright © 2025 Xiaowei He

The response of the aircraft to a unit (1°) rudder step input is shown in figure 7.6. All of the variables obtained in the solution of the equations of motion are shown. Again, it is very clear that the response is dominated by the oscillatory Dutch roll mode. However, unlike the previous illustration, the roll and spiral modes are not discernible in the response. This is due to the fact that a step was chosen as the input that causes the aircraft to diverge from its initial equilibrium. This motion, together with the Dutch roll oscillation, effectively masks the two non-oscillatory modes.

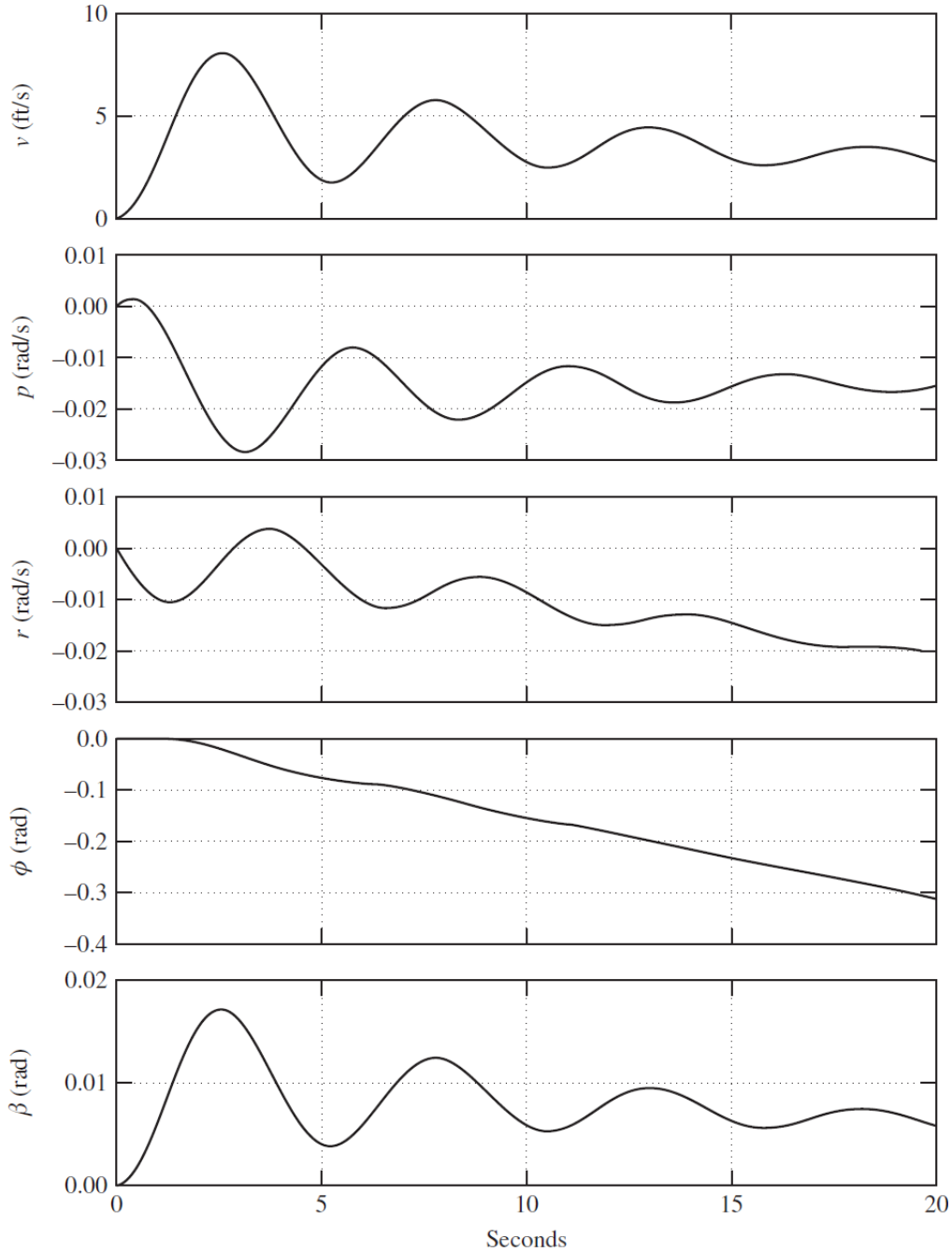

Figure 7.6: Aircraft response to a 1° rudder step input [1].

Copyright © 2025 Xiaowei He

It is possible to observe another interesting phenomenon in the response. The effect of non-minimum phase terms in the transfer function would seem to be insignificantly small since they are not detectable in the responses shown in figures 7.5 and 7.6, with one exception. The roll rate response p to rudder, shown in figure 7.6, exhibits a sign reversal for the first second or so of its response; this is the manifestation of the non-minimum phase effect. In aeronautical parlance, it is referred to as *adverse roll* in response to the rudder.

A positive rudder step input is assumed to cause the aircraft to turn to the left, which is a negative response in accordance with the notation. Once the turn is established, this results in negative yaw and yaw rate together with negative roll and roll rate induced by yaw-roll coupling. These general effects are correctly portrayed in the responses shown in figure 7.6. However, when the rudder is deflected, initially a substantial side force is generated at the center of pressure of the vertical tail, which in turn generates the yaw moment, causing the aircraft to turn. At the same time, the side force acts at some distance above the roll axis and also generates a roll moment, which causes the aircraft to roll in the opposite sense to that induced by the yaw motion. Since inertia in roll is somewhat lower than inertia in yaw, the aircraft responds quicker in roll and starts to roll in the "wrong" direction, but as the yaw motion becomes established, the aerodynamically induced roll moment eventually overcomes the adverse roll moment and the aircraft then rolls in the "correct" sense. A similar characteristic, *adverse yaw* in response to aileron, is caused by the differential drag effects associated with aileron deflection, giving rise to an adverse yaw moment. This characteristic is also commonly observed in many aircraft.

7.5.2 Lateral-directional characteristic equation

The lateral-directional characteristic polynomial for a classical aircraft is fourth order; it determines the common denominator of the lateral and directional response transfer functions and, when equated to zero, defines the characteristic equation, which is written as

$$As^4 + Bs^3 + Cs^2 + Ds + E = 0, \tag{7.58}$$

which is most commonly factorized into two real roots and a pair of complex roots, and is written as

$$\underbrace{(s + 1/\tau_\mathrm{s})}_{\text{spiral mode}}\underbrace{(s + 1/\tau_\mathrm{r})}_{\text{roll mode}}\underbrace{(s^2 + 2\zeta_\mathrm{d}\omega_\mathrm{d}s + \omega_\mathrm{d}^2)}_{\text{Dutch roll mode}} = 0. \tag{7.59}$$

The first real root in equation (7.59) describes the non-oscillatory spiral mode, the second real root describes the non-oscillatory roll subsidence mode, and the pair of complex roots describes the oscillatory Dutch roll mode. Since the equations of motion from which the characteristic equation is derived are referenced to wind axes, the stability modes comprising equation (7.59) provide a complete description of the lateral-directional stability properties of the aircraft with respect to the total steady velocity vector and subject to the constraints of small-perturbation motion.

When the equations of motion are referred to a body axes system, the state equation (6.55) is fifth order, as is the characteristic equation. The solution of the characteristic equation then has the following factors

$$s(s + 1/\tau_\mathrm{s})(s + 1/\tau_\mathrm{r})(s^2 + 2\zeta_\mathrm{d}\omega_\mathrm{d}s + \omega_\mathrm{d}^2) = 0. \tag{7.60}$$

The modes are unchanged except for the addition of a zero root, which indicates neutral stability. The zero root results from the addition of yaw angle to the state equation and indicates neutral stability in yaw or heading. Interpretation of lateral-directional dynamics is unchanged, and the additional information indicates that the aircraft has an indeterminate yaw or heading angle. In other words, lateral-directional

Copyright © 2025 Xiaowei He

dynamics are evaluated with respect to the steady total velocity vector, which assumes an arbitrary direction in azimuth, yaw, or heading. Interpretation of the non-zero roots of the characteristic equation is most easily accomplished if reference is first made to the properties of the classical mass-spring-damper system.

Unlike longitudinal dynamics, the interpretation of lateral-directional dynamics is not so straightforward because the stability modes are not as distinct; there usually exists a significantly greater degree of mode coupling or interaction. This tends to make the necessary simplifying assumptions less appropriate, with a consequent reduction of confidence in the observations. However, an assortment of well-tried procedures for interpreting the dynamic characteristics of well-behaved aircraft exist, and these are discussed in the following sections.

7.5.3 The roll subsidence mode

The *roll subsidence mode*, or simply *roll mode*, is a non-oscillatory lateral characteristic that is usually substantially decoupled from the spiral and Dutch roll modes. Since it is non-oscillatory, it is described by a single real root of the characteristic polynomial and manifests itself as an exponential lag characteristic in rolling motion. The aerodynamic principles governing the behavior of the roll mode are illustrated in figure 7.7.

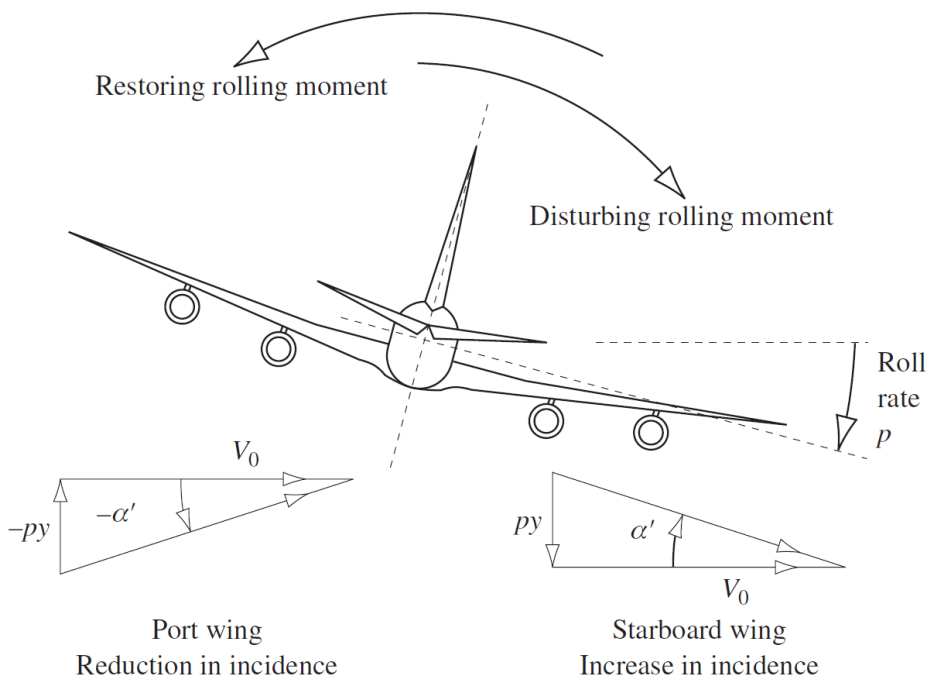

Figure 7.7: Roll subsidence mode [1].

With reference to figure 7.7, the aircraft is viewed from the rear, so the indicated motion is shown in the same sense as experienced by the pilot. Assume that the aircraft is constrained to a single degree of freedom motion in roll about the ox axis only and that it is initially in trimmed wings-level flight. If the aircraft experiences a positive disturbing rolling moment, it commences to roll with an angular acceleration in accordance with Newton's second law of motion. In roll motion, the wing experiences a component of velocity normal to the wing py, where y is the spanwise coordinate measured from the roll axis x. This results in a small increase in incidence on the down-going starboard wing and a small

Copyright © 2025 Xiaowei He

decrease in incidence on the up-going port wing. The resulting differential lift gives rise to a restoring roll moment as indicated. The corresponding resulting differential induced drag also gives rise to a yawing moment, but this is usually small enough to be ignored. Thus, following a disturbance, the roll rate builds up exponentially until the restoring moment balances the disturbing moment, and a steady roll rate is established.

In practice, this kind of behavior would be transient rather than continuous, as implied in this illustration. The physical behavior explained is simple "paddle" damping and is stabilizing in effect in all aircraft operating in normal, aerodynamically linear flight regimes. For this reason, the stability mode is sometimes referred to as *roll damping*.

In some modern combat aircraft designed to operate in seriously nonlinear aerodynamic conditions, for example, at angles of attack approaching 90 deg, it is possible for the physical conditions governing the roll mode to break down completely. The consequent loss of roll stability can result in rapid roll departure followed by complex lateral-directional motion of a hazardous nature. However, in conventional aircraft, the roll mode appears to the pilot as a lag in roll response to controls. The lag time constant is largely dependent on the moment of inertia in roll and the aerodynamic properties of the wing and is typically around 1 s or less.

7.5.4 The spiral mode

The *spiral mode* is also non-oscillatory and is determined by the other real root in the characteristic polynomial. When excited, the mode dynamics are usually slow to develop and involve complex coupled motions in roll, yaw, and sideslip. The dominant aerodynamic principles governing the mode dynamics are illustrated in figure 7.8. The mode characteristics are very dependent on the lateral static stability and the directional static stability of the aircraft, which were discussed in sections 4.3.1 and 4.3.2.

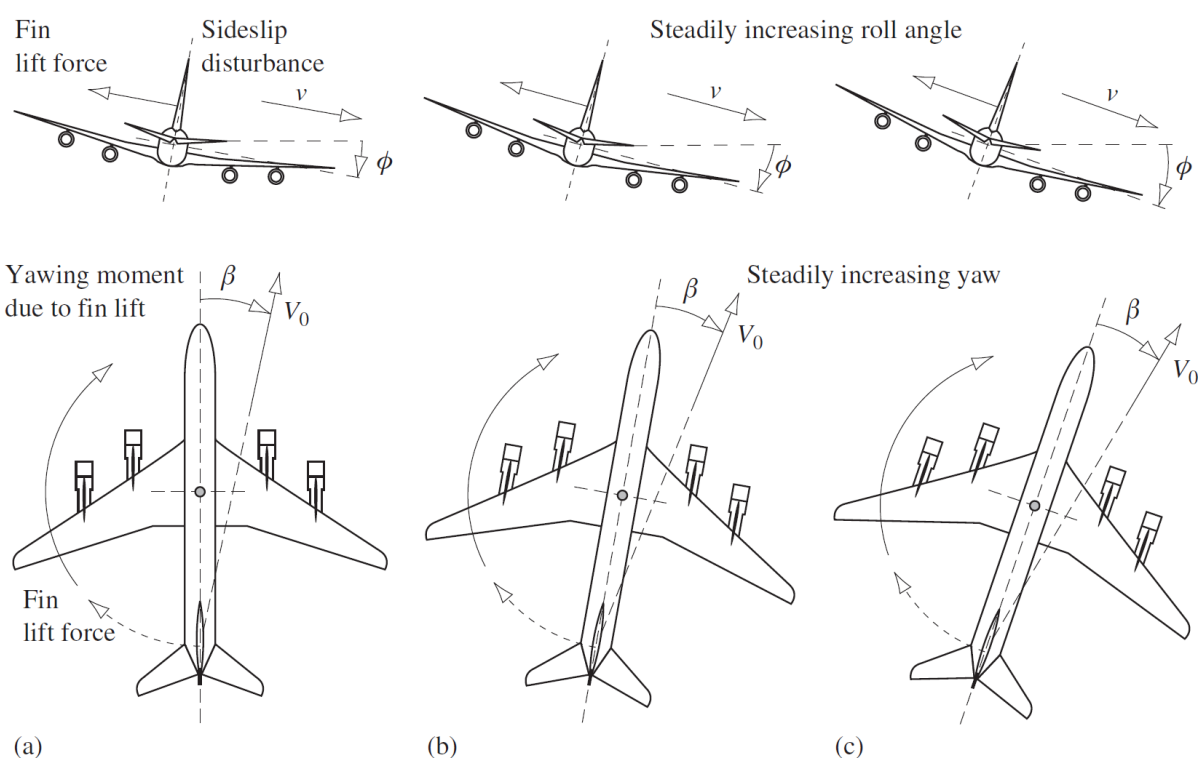

Figure 7.8: Spiral mode development [1].

Copyright © 2025 Xiaowei He

The spiral mode is usually excited by a disturbance in sideslip, which typically follows a disturbance in roll and causes a wing to drop. Assume that the aircraft is initially in trimmed wings-level flight and that a disturbance causes a small positive roll angle ϕ to develop. Left unchecked, this results in a small positive sideslip velocity v as indicated in figure 7.8a. The sideslip puts the fin at incidence β, which produces lift and generates a yaw moment to turn the aircraft into the direction of the sideslip. The yaw motion produces differential lift across the wing span, which in turn results in a roll moment, causing the starboard wing to drop further, thereby exacerbating the situation. This developing divergence is indicated in figure 7.8b and c. Simultaneously, the dihedral effect of the wing generates a negative restoring roll moment due to sideslip, which acts to return the wing to a level attitude. Some additional restoring roll moment is also generated by the fin lift force when it acts at a point above the roll axis x, which is usual.

The situation is thus one in which the fin effect, or directional static stability, and the dihedral effect, or lateral static stability, act in opposition to create this interesting dynamic condition. Typically, the requirements for lateral and directional static stability are such that the opposing effects are very nearly equal. When the dihedral effect is greater, the spiral mode is stable and hence convergent; when the fin effect is greater, the spiral mode is unstable and hence divergent. Since these effects are nearly equal, the spiral mode is nearly neutrally stable, and sometimes it may even be neutrally stable, that is, it is neither convergent nor divergent. Since the mode is non-oscillatory, it manifests itself as a classical exponential convergence or divergence, and, since it is nearly neutral, the time constant is very large, typically 100 s or more. This means that when the mode is stable, the wing is slow to recover a level attitude following a disturbance, and when it is unstable, the rate at which it diverges is also very slow. When it is neutral, the aircraft simply flies a turn at a constant roll attitude.

It is the unstable condition that attracts the most attention. Once the mode is excited, the aircraft flies a slowly diverging path in both roll and yaw, and since the vertical forces are no longer in equilibrium, the aircraft also loses height. Thus, the unstable flight path is a spiral descent which, if left unchecked, ends when the aircraft hits the ground. However, since the rate at which the mode diverges is usually very slow, most pilots can cope with it. For this reason, an unstable spiral mode is permitted provided its time constant is sufficiently large. Because the mode is very slow to develop, the accelerations in the resulting motion are insignificantly small, and the motion cues available to the pilot are almost imperceptible. In a spiral departure, the visual cues become the most important cues to the pilot. It is also important to appreciate that a spiral departure is not the same as a spin. Spinning motion is a fully stalled flight condition, whereas, in a spiral descent, the wing continues to fly in the usual sense.

7.5.5 The Dutch roll mode

The Dutch roll mode is a classical damped oscillation in yaw, about the z axis of the aircraft, which couples into roll and, to a lesser extent, into sideslip. The motion it describes is therefore a complex interaction between all three lateral-directional degrees of freedom. The characteristics of the Dutch roll mode are described by the pair of complex roots in the characteristic polynomial. Fundamentally, the Dutch roll mode is the lateral-directional equivalent of the longitudinal short-period mode. Since the moments of inertia in pitch and yaw are of similar magnitude, the frequency of the Dutch roll mode and the longitudinal short-period mode are of similar order. However, the fin is generally less effective than the tailplane as a damper, and the damping of the Dutch roll mode is often inadequate. The Dutch roll mode is so called because the motion of the aircraft following its excitation is said to resemble the rhythmical flowing motion of a Dutch skater on a frozen canal. One cycle of typical Dutch rolling motion is shown in figure 7.9.

The physical situation applied in a Dutch roll disturbance can be appreciated by imagining that the

Copyright © 2025 Xiaowei He

aircraft is restrained in yaw by a torsional spring acting about the yaw axis z, the spring stiffness being aerodynamic and determined largely by the fin. Thus, when in straight-level trimmed equilibrium flight, a disturbance in yaw causes the "aerodynamic spring" to produce a restoring yaw moment which results in classical oscillatory motion. However, once the yaw oscillation is established, the relative velocity of the air over the port and starboard wings also varies in an oscillatory manner, giving rise to oscillatory differential lift and drag perturbations. This aerodynamic coupling in turn creates an oscillation in roll which lags the oscillation in yaw by approximately 90 deg. This phase difference between yaw and roll motions means that the forward-going wing panel is low and the aft-going wing panel is high, as indicated in figure 7.9. Consequently, the classical manifestation of the Dutch roll mode is given by the path described by the wing tips relative to the horizon and is usually elliptical. The ratio of peak roll to peak yaw is usually less than 1, as indicated, and is usually associated with a stable Dutch roll mode. However, when the ratio is greater than 1, an unstable Dutch roll mode is more likely.

Copyright © 2025 Xiaowei He

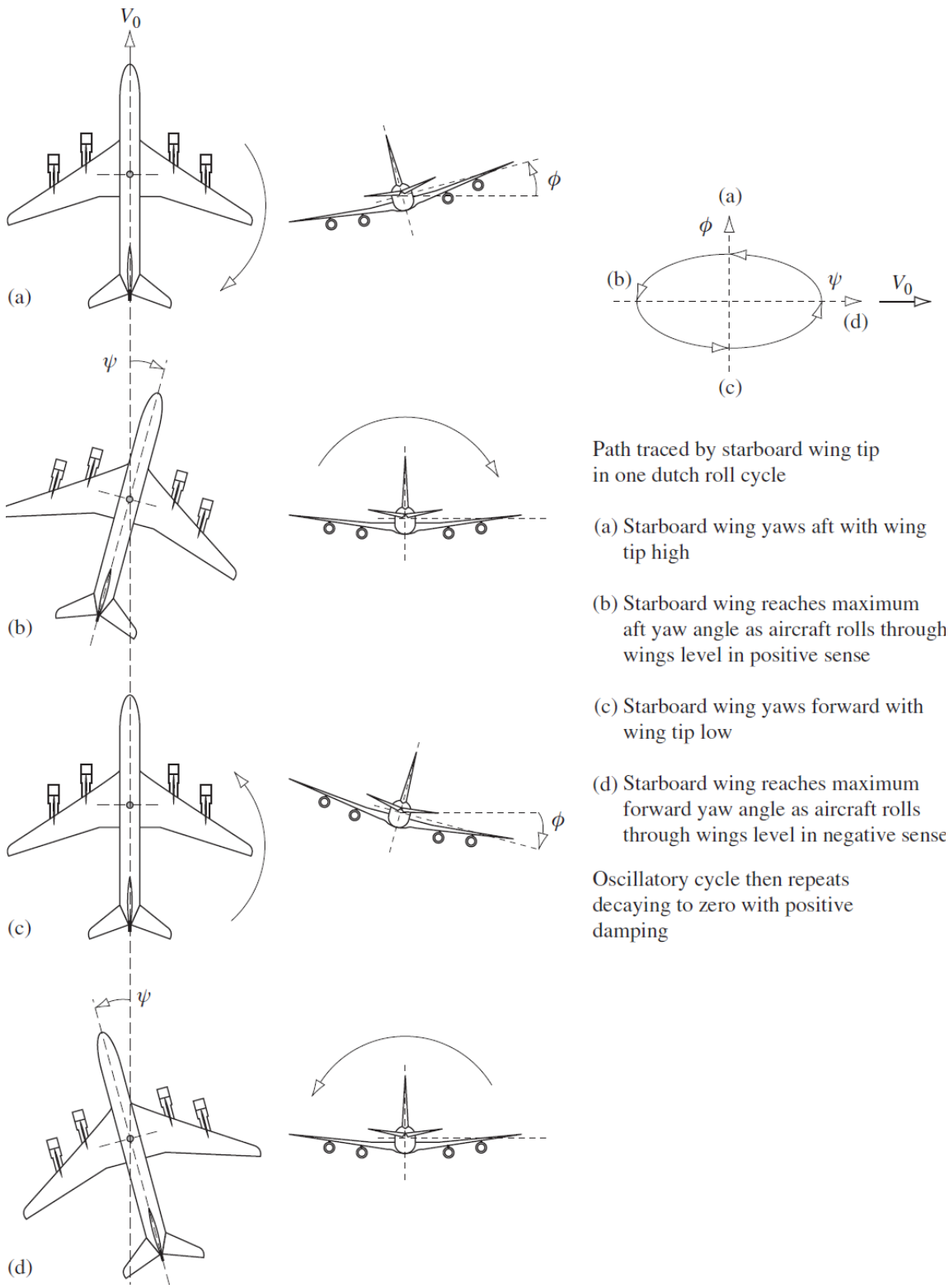

Figure 7.9: Oscillatory Dutch roll mode [1].

Whenever the wing is disturbed from level trim, the aircraft, left to its own devices, starts to slip

Copyright © 2025 Xiaowei He

sideways in the direction of the low wing. Thus, the oscillatory roll motion leads to some oscillatory sideslip motion in Dutch roll motion, although the sideslip velocity is generally small. The motion experienced in a Dutch rolling aircraft seems analogous to that of a ball bearing dropped into an inclined channel having a semicircular cross-section. The ball bearing rolls down the inclined channel whilst oscillating from side to side on the circular surface.

Both the damping and stiffness in yaw, which determine the characteristics of the mode, are largely determined by the aerodynamic properties of the fin, a large fin being desirable for a well-behaved, stable Dutch roll mode. Unfortunately, this contradicts the requirement for a stable spiral mode. The resulting aerodynamic design compromise usually results in aircraft with a mildly unstable spiral mode and a poorly damped Dutch roll mode. The complexity of the dynamics associated with this mode suggests that there must be other aerodynamic contributions to the mode characteristics in addition to the fin. This is generally the case, and it is possible for the additional aerodynamic effects to be as significant as the aerodynamic properties of the fin, if not more so. However, one thing is certain: It is very difficult to quantify all aerodynamic contributions to the Dutch roll mode with any degree of confidence.

7.6 Summary of aircraft dynamic modes

The aircraft dynamic modes are distinguished by their characteristic behaviors and the main states that they excite. We briefly summarize the longitudinal and lateral-directional modes in table 7.1 below.

Table 7.1: Aircraft dynamic modes.

	Mode	States	Characteristics	Damping	Period
longitudinal	short-period	w, q, θ	fast, stable pitch oscillation	heavily damped	a few seconds, usually less
	phugoid	u, θ	slow, stable or unstable altitude oscillation	lightly positive or negative	can be several minutes
lateral-directional	roll	p, ϕ	fast, stable roll motion	always positively damped	non-oscillatory, half-amplitude occurs very fast
	spiral	ϕ, ψ	slow, stable or unstable coupling of roll and yaw	lightly positive or negative	non-oscillatory, half-amplitude can occur in a few minutes
	Dutch roll	v, p, r, ϕ, ψ	oscillatory coupling of sideslip, yaw, and roll	positive or negative	aircraft-size dependent

7.7 Aerodynamic stability and control derivatives

It must be remembered that the aircraft response transfer functions are obtained based on the input-output relations of the linearized aircraft equations of motions — equations (6.53) and (6.56), which trace back to equations (6.27) and (6.32). Therefore, one should always recognize that all coefficients in the transfer functions (k, τ, ζ, ω) are determined by the terms contained in the equations of motion discussed in sections 6.2.2 to 6.2.5 — gravitational, aerodynamic, control, and power terms — along with

Copyright © 2025 Xiaowei He

the moments/products of inertia on the response sides of the equations. The gravitational, inertial, and power terms are straightforward and have been derived in previous discussions. It is a good practice to explicate some of the aerodynamic and aerodynamic control terms to reveal more about the aerodynamic physics carried out in these equations.

Recall that, in sections 6.2.3 and 6.2.4, the aerodynamic and aerodynamic control terms were reduced to first-order *aerodynamic stability derivatives* and *aerodynamic control derivatives* through Taylor expansion. As is usual in aerodynamic analysis, to obtain simple expressions for the stability and control derivatives, a wind axis reference system is assumed throughout. The choice of wind axes is convenient since it reduces the derivatives to their simplest possible description by retaining only the essential contributions and hence maximizes the visibility of the physical phenomena involved. It is therefore very important to remember that if the derivatives thus obtained are required for use in equations of motion referred to an alternative axis system, then the appropriate axis transformation must be applied to the derivatives.

7.7.1 Longitudinal aerodynamic stability derivatives

A number of expressions are required repeatedly in the derivative analysis, so it is convenient to assemble these expressions prior to embarking on the analysis. A longitudinal small perturbation is shown in figure 7.10 in which the aircraft axes are wind axes and the initial condition assumes steady symmetric level flight at velocity V_0. Although not strictly an aerodynamic force, the thrust T is shown since it may behave like an aerodynamic variable in a perturbation. As indicated, the thrust force is tied to the aircraft's x axis and moves with it.

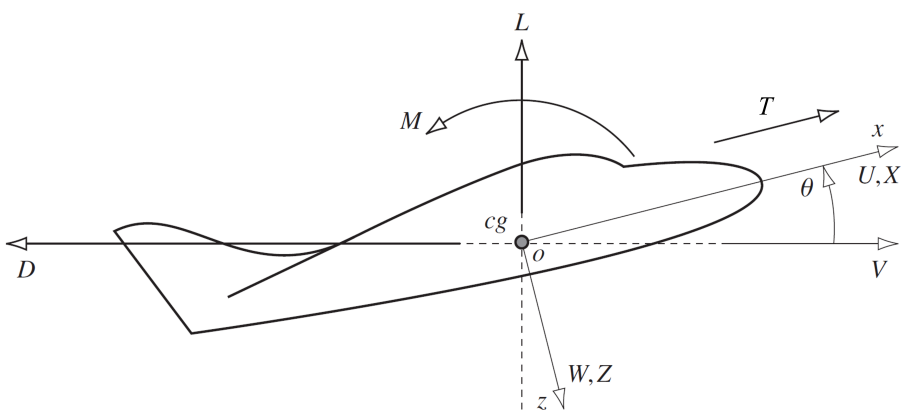

Figure 7.10: Perturbed wind axes [1].

In the perturbation, the total velocity becomes V with components U and W along the x and z axes, respectively. Whence

$$V^2 = U^2 + W^2, \tag{7.61}$$

and

$$\begin{aligned} U &= U_\mathrm{e} + u = V\cos\theta, \\ W &= W_\mathrm{e} + u = V\sin\theta. \end{aligned} \tag{7.62}$$

Since wind axes are assumed, the pitch attitude perturbation θ and the incidence perturbation α are the same and are given by

$$\tan\theta = \tan\alpha = \frac{W}{U}. \tag{7.63}$$

Copyright © 2025 Xiaowei He

Differentiate with respect to U and W

$$\frac{\partial V}{\partial U} = \frac{U}{V}, \qquad \frac{\partial V}{\partial W} = \frac{W}{V}, \tag{7.64}$$

and, by definition, θ is a small angle,

$$\frac{\partial V}{\partial U} = \cos\theta \cong 1, \qquad \frac{\partial V}{\partial W} = \sin\theta \cong 0. \tag{7.65}$$

In a similar way, differentiate the tangential relation with respect to U and W, and by the small angle assumption, we obtain

$$\begin{aligned} \frac{\partial \theta}{\partial U} &= \frac{\partial \alpha}{\partial U} = \frac{-\sin\theta}{V} \cong 0, \\ \frac{\partial \theta}{\partial W} &= \frac{\partial \alpha}{\partial W} = \frac{\cos\theta}{V} \cong \frac{1}{V}. \end{aligned} \tag{7.66}$$

Aerodynamic force and moment components. With reference to figure 7.10, the lift and drag forces may be resolved into the disturbed aircraft axes to give the components of aerodynamic force. The perturbed axial force is

$$X = L\sin\theta - D\cos\theta + T = \frac{1}{2}\rho V^2 S(C_L \sin\theta - C_D\cos\theta) + T, \tag{7.67}$$

and the perturbed normal force is

$$Z = -L\cos\theta - D\sin\theta = -\frac{1}{2}\rho V^2 S(C_L\cos\theta + C_D\sin\theta). \tag{7.68}$$

In the initial steady trim condition, by definition, the pitching moment M is zero. However, in the perturbation, the transient pitch moment is nonzero and is given by

$$M = \frac{1}{2}\rho V^2 S\bar{c}C_m. \tag{7.69}$$

Force derivatives due to velocity perturbations.

- $\mathring{X}_u = \dfrac{\partial X}{\partial u}$ **axial force due to axial velocity.**

  Differentiate equation (7.67) with respect to U to obtain

$$\begin{aligned} \frac{\partial X}{\partial U} =& \frac{1}{2}\rho V^2 S\left(\frac{\partial C_L}{\partial U}\sin\theta + C_L\cos\theta\frac{\partial\theta}{\partial U} - \frac{\partial C_D}{\partial U}\cos\theta + C_D\sin\theta\frac{\partial\theta}{\partial U}\right) \\ &+ \rho V S\frac{\partial V}{\partial U}(C_L\sin\theta - C_D\cos\theta) + \frac{\partial T}{\partial U}. \end{aligned} \tag{7.70}$$

  Substitute for $\partial V/\partial U$ from equation (7.65) and for $\partial\theta/\partial U$ from equation (7.66), it simplifies to

$$\frac{\partial X}{\partial U} = -\frac{1}{2}\rho V^2 S\frac{\partial C_D}{\partial U} - \rho V S C_D + \frac{\partial T}{\partial U}. \tag{7.71}$$

  Apply the chain rule and substitute again

$$\frac{\partial C_D}{\partial U} = \frac{\partial C_D}{\partial V}\frac{\partial V}{\partial U} = \frac{\partial C_D}{\partial V}, \tag{7.72}$$

Copyright © 2025 Xiaowei He

and, similarly,

$$\frac{\partial T}{\partial U} = \frac{\partial T}{\partial V} \tag{7.73}$$

In the limit, the total perturbation velocity tends to the equilibrium value and $V \cong V_0$. Hence,

$$\mathring{X}_u = \frac{\partial X}{\partial U} = -\rho V_0 S C_D - \frac{1}{2}\rho V_0^2 S \frac{\partial C_D}{\partial V} + \frac{\partial T}{\partial V}. \tag{7.74}$$

- $\mathring{Z}_u = \dfrac{\partial Z}{\partial U}$ **normal force due to axial velocity.**

  Differentiating equation (7.68) and using the relations from equations (7.65) and (7.66), we have

$$\frac{\partial Z}{\partial U} = -\rho V S C_L - \frac{1}{2}\rho V^2 S \frac{\partial C_L}{\partial U}. \tag{7.75}$$

  Again, applying the chain rule

$$\frac{\partial C_L}{\partial U} = \frac{\partial C_L}{\partial V}\frac{\partial V}{\partial U} = \frac{\partial C_L}{\partial V}. \tag{7.76}$$

  Thus in the limit $V \cong V_0$ the derivative may be written as

$$\mathring{Z}_u = \frac{\partial Z}{\partial U} = -\rho V_0 S C_L - \frac{1}{2}\rho V_0^2 S \frac{\partial C_L}{\partial V}. \tag{7.77}$$

- $\mathring{X}_w = \dfrac{\partial X}{\partial W}$ **axial force due to normal velocity.**

  Differentiate equation (7.67) with respect to W

$$\frac{\partial X}{\partial W} = \frac{1}{2}\rho V^2 S \left(\frac{1}{V} C_L - \frac{\partial C_D}{\partial W}\right) + \frac{\partial T}{\partial W}. \tag{7.78}$$

  With reference to equation (7.66) and noting that $\alpha = \theta$,

$$\frac{\partial C_D}{\partial W} = \frac{\partial C_D}{\partial \theta}\frac{\partial \theta}{\partial W} = \frac{1}{V}\frac{\partial C_D}{\partial \alpha}. \tag{7.79}$$

  Similarly,

$$\frac{\partial T}{\partial W} = \frac{1}{V}\frac{\partial T}{\partial \alpha} = 0, \tag{7.80}$$

  since it is assumed that thrust variation resulting from small incidence perturbations is negligible. Thus, in the limit $V \cong V_0$, the derivative may be written as

$$\mathring{X}_w = \frac{\partial X}{\partial W} = \frac{1}{2}\rho V_0 S \left(C_L - \frac{\partial C_D}{\partial \alpha}\right). \tag{7.81}$$

- $\mathring{Z}_w = \dfrac{\partial Z}{\partial W}$ **normal force due to normal velocity.**

  As before, differentiate equation (7.68) with respect to W

$$\frac{\partial Z}{\partial W} = -\frac{1}{2}\rho V^2 S \left(\frac{\partial C_L}{\partial W} + \frac{1}{V} C_D\right) = -\frac{1}{2}\rho V S \left(\frac{\partial C_L}{\partial \alpha} + C_D\right). \tag{7.82}$$

  In the limit, the derivative may be rewritten as

$$\mathring{Z}_w = \frac{\partial Z}{\partial W} = -\frac{1}{2}\rho V_0 S \left(\frac{\partial C_L}{\partial \alpha} + C_D\right). \tag{7.83}$$

Copyright © 2025 Xiaowei He

Moment derivatives due to velocity perturbations.

- $\mathring{M}_u = \dfrac{\partial M}{\partial U}$ **pitch moment due to axial velocity.**

  In a perturbation, the pitch moment becomes nonzero and is given by equation (7.69). Differentiating equation (7.69) with respect to U,

$$\frac{\partial M}{\partial U} = \frac{1}{2}\rho V^2 S\bar{c}\frac{\partial C_m}{\partial U} + \rho V S\bar{c}C_m, \tag{7.84}$$

  and with reference to equation (7.65),

$$\frac{\partial C_m}{\partial U} = \frac{\partial}{\partial V}\frac{\partial V}{\partial U} = \frac{\partial C_m}{\partial V}. \tag{7.85}$$

  In the limit, as the perturbation tends to zero, the pitch moment coefficient C_m in the second term tends to the steady equilibrium value, which is zero. Therefore, in the limit, the derivative simplifies to

$$\mathring{M}_u = \frac{\partial M}{\partial U} = \frac{1}{2}\rho V_0^2 S\bar{c}\frac{\partial C_m}{\partial V}. \tag{7.86}$$

  In subsonic flight, the pitch moment coefficient C_m is very nearly independent of velocity; thus, the derivative $\mathring{M}_u$ is often assumed to be negligibly small for those flight conditions.

- $\mathring{M}_w = \dfrac{\partial M}{\partial W}$ **pitch moment due to normal velocity.**

  Differentiating equation (7.69) with respect to W and with reference to equation (7.66) noting $\alpha = \theta$

$$\frac{\partial M}{\partial W} = \frac{1}{2}\rho V^2 S\bar{c}\frac{\partial C_m}{\partial W} = \frac{1}{2}\rho V S\bar{c}\frac{\partial C_m}{\partial \alpha}. \tag{7.87}$$

  In the limit $V \cong V_0$, the derivative may be written as

$$\mathring{M}_w = \frac{\partial M}{\partial W} = \frac{1}{2}\rho V_0 S\bar{c}\frac{\partial C_m}{\partial \alpha}. \tag{7.88}$$

Derivatives due to a pitch velocity perturbation. It is usually assumed that the longitudinal aerodynamic properties of an aircraft are dominated by those of the wing and tailplane. However, when the disturbance is a small perturbation in pitch rate q, it is assumed that the dominating aerodynamic properties are those of the tailplane. Thus, in the first instance, the resulting aerodynamic changes contributing to the stability derivatives are assumed to arise entirely from tailplane effects. By so doing, it is acknowledged that the wing contribution may not necessarily be small and that its omission will reduce the accuracy of the derivative estimates. However, experience has shown that the error incurred by adopting this assumption is usually acceptably small.

An aircraft pitching through its equilibrium attitude with pitch rate perturbation q is shown in figure 7.11. Since the effect of the pitch rate is to cause the tailplane to experience a normal velocity component due to rotation about the cg, the resultant effect is a change in the local incidence α_T of the tailplane. The total perturbation velocity is V, and the tailplane incidence perturbation is given by

$$\alpha_\mathrm{T} \cong \tan\alpha_\mathrm{T} = \frac{ql_\mathrm{T}}{V}, \tag{7.89}$$

since α_T is a small angle by definition. It is important to appreciate that α_T is the change, or increment, in tailplane incidence relative to its equilibrium value and, like the pitch rate perturbation, is transient in nature. It follows that

$$\frac{\partial \alpha_\mathrm{T}}{\partial q} = \frac{l_\mathrm{T}}{V}. \tag{7.90}$$

Copyright © 2025 Xiaowei He

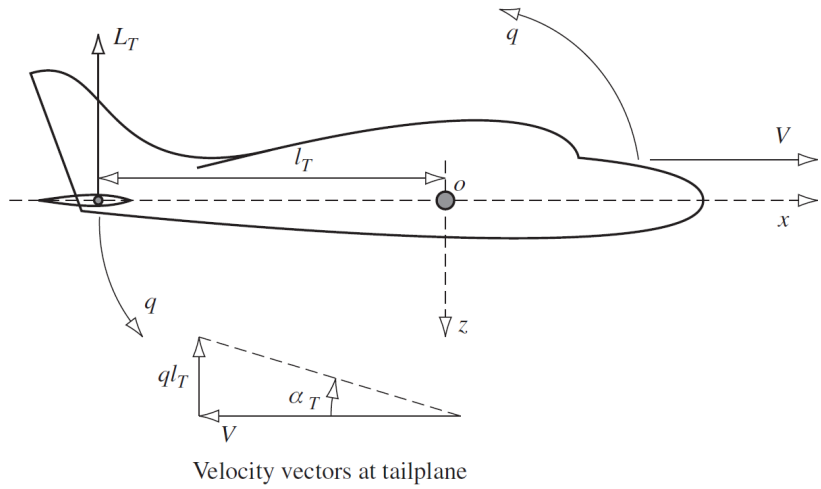

Figure 7.11: Tailplane incidence due to pitch rate [1].

- $\mathring{X}_p = \dfrac{\partial X}{\partial p}$ **axial force due to pitch rate.**

  In this instance, for the reasons given above, it is assumed that the axial force perturbation arises from the tailplane drag perturbation only; thus

$$X = -D_{\mathrm{T}} = -\frac{1}{2}\rho V^2 S_{\mathrm{T}} C_{D_{\mathrm{T}}}. \tag{7.91}$$

  Assuming V to be independent of pitch rate q, differentiate the equation with respect to the perturbation variable q

$$\frac{\partial X}{\partial q} = -\frac{1}{2}\rho V^2 S_{\mathrm{T}} \frac{\partial C_{D_{\mathrm{T}}}}{\partial q}. \tag{7.92}$$

  With reference to equation (7.90),

$$\frac{\partial C_{D_{\mathrm{T}}}}{\partial q} = \frac{\partial C_{D_{\mathrm{T}}}}{\partial \alpha_{\mathrm{T}}} \frac{\partial \alpha_{\mathrm{T}}}{\partial q} = \frac{l_{\mathrm{T}}}{V} \frac{\partial C_{D_{\mathrm{T}}}}{\partial \alpha_{\mathrm{T}}}. \tag{7.93}$$

  In the limit $V \cong V_0$, the derivative may be written as

$$\mathring{X}_q = \frac{\partial X}{\partial q} = -\frac{1}{2}\rho V_0 S_{\mathrm{T}} l_{\mathrm{T}} \frac{\partial C_{D_{\mathrm{T}}}}{\partial \alpha_{\mathrm{T}}}. \tag{7.94}$$

  Since the rate of change of tailplane drag with incidence is usually small, it is customary to assume that the derivative $\mathring{X}_q$ is insignificantly small and it is frequently ignored in aircraft stability and control analysis.

- $\mathring{Z}_q = \dfrac{\partial Z}{\partial q}$ **normal force due to pitch rate.**

  Similarly, it is assumed that in a pitch rate perturbation, the change in normal force arises from tailplane lift only; thus

$$Z = -L_{\mathrm{T}} = -\frac{1}{2}\rho V^2 S_{\mathrm{T}} C_{L_{\mathrm{T}}}. \tag{7.95}$$

  Differentiate the equation with respect to q and with reference to equation (7.90); then

$$\frac{\partial Z}{\partial q} = -\frac{1}{2}\rho V S_{\mathrm{T}} l_{\mathrm{T}} a_1, \tag{7.96}$$

Copyright © 2025 Xiaowei He

where, again, it is assumed that V is independent of pitch rate q and that, additionally, the tailplane lift coefficient is a function of incidence only, with lift curve slope denoted a_1. Hence, in the limit $V \cong V_0$, the derivative may be written as

$$\mathring{Z}_q = \frac{\partial Z}{\partial q} = -\frac{1}{2}\rho V_0 S_\mathrm{T} l_\mathrm{T} a_1. \tag{7.97}$$

- $\mathring{M}_q = \dfrac{\partial M}{\partial q}$ **pitch moment due to pitch rate.**

  Again, in a pitch rate perturbation q, the pitch moment is assumed to arise entirely from the moment of the tailplane normal force perturbation about the cg. Thus,

$$M = Zl_\mathrm{T} = -\frac{1}{2}\rho V^2 S_\mathrm{T} l_\mathrm{T} C_{L_\mathrm{T}}. \tag{7.98}$$

  Differentiate the equation with respect to q and substitute for $\mathring{Z}_q$

$$\frac{\partial M}{\partial q} = l_\mathrm{T}\frac{\partial Z}{\partial q} = l_\mathrm{T}\mathring{Z}_q. \tag{7.99}$$

  Therefore,

$$\mathring{M}_q = \frac{\partial M}{\partial q} = -\frac{1}{2}\rho V_0 S_\mathrm{T} l_\mathrm{T}^2 a_1. \tag{7.100}$$

  $\mathring{M}_q$ is the all-important pitch damping derivative. Although this simple model illustrates the importance of the tailplane in determining the pitch-damping characteristics of the aircraft, wing and body contributions may also be significant. This derivative should therefore be regarded as the first estimate rather than the definitive estimate of the derivative. However, it is often good enough for preliminary analysis of stability and control.

Derivatives due to acceleration perturbations. The derivatives due to the acceleration perturbations $\dot{u}$, $\dot{w}$, and $\dot{q}$ are not commonly encountered in the longitudinal equations of motion since their numerical values are usually insignificantly small. We will not discuss them in detail in this course.

7.7.2 Lateral-directional aerodynamic stability derivatives

Unlike the longitudinal aerodynamic stability derivatives, the lateral-directional derivatives are much more difficult to estimate with any degree of confidence. The problem arises from the mutual aerodynamic interference between the lifting surfaces, fuselage, power plant, undercarriage, and so forth in asymmetric flow conditions, which makes it difficult to identify the most significant contributions to a particular derivative with any degree of certainty. When a derivative cannot be estimated by the simplest analysis of the often complex aerodynamics, then the use of strip theory is resorted to, which is a method of analysis that also tends to oversimplify the aerodynamic conditions in order that progress can be made. Either way, analytical estimates of the lateral-directional derivatives are often of poor accuracy. However, the simple theories used for the purpose do give a useful insight into the physical phenomena involved and, consequently, are a considerable asset to the proper understanding of aircraft dynamics. We will discuss the derivative that closely relates to the roll-damping phenomenon as an example.

- $\mathring{L}_p = \dfrac{\partial L}{\partial p}$ **roll moment due to roll rate.**

  As seen by the pilot, a positive roll is to the right, consistent with a down-going right wing, and the small-perturbation roll rate transient is denoted p. The nature of a free positive roll rate disturbance

Copyright © 2025 Xiaowei He

is such that as the right wing tends to drop, it is accompanied by a tendency for the nose to turn to the right and for the aircraft to sideslip to the right. The reaction to the roll rate disturbance is stabilizing if the aerodynamic forces and moments produced in response tend to restore the aircraft to a wings-level zero sideslip equilibrium state.

Roll moment due to roll rate arises largely from the wing, with smaller contributions from the fuselage, tailplane, and fin. This derivative is most important since it quantifies the damping in roll and is therefore significant in determining the dynamic characteristics of the roll subsidence mode discussed section 7.5.3. The following analysis considers the wing contribution only.

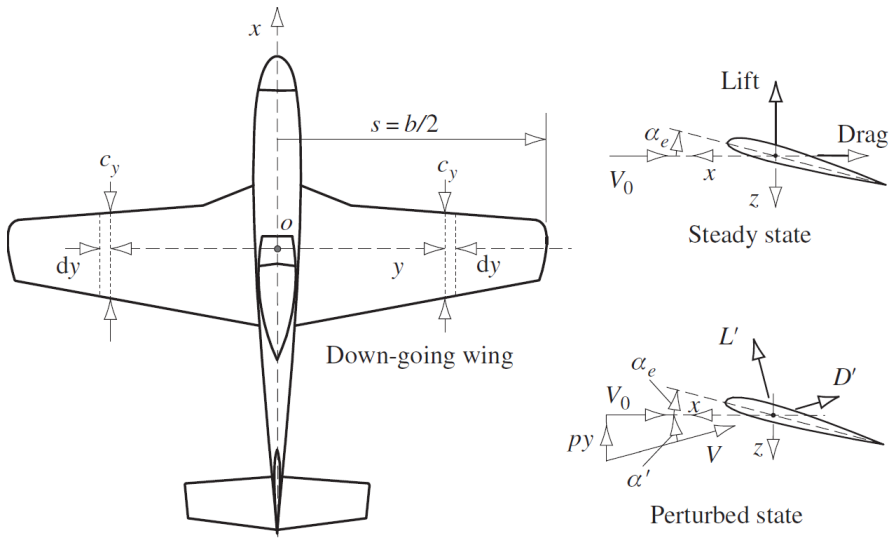

Figure 7.12: Wing incidence in a roll [1].

With reference to figure 7.12, when the right wing experiences a positive perturbation in roll rate p, assuming the aircraft rolls about the x axis, then the small increase in incidence α' at the chordwise strip element is given by

$$\alpha' \cong \tan\alpha' = \frac{py}{V_0}. \tag{7.101}$$

There is a reduction in incidence on the corresponding chordwise strip element on the left wing. Denoting the total lift and drag increments in the disturbance on the chordwise strip element on the right wing L' and D', respectively, then

$$L' = \frac{1}{2}\rho V_0^2 c_y \mathrm{d}y a_y(\alpha_\mathrm{e} + \alpha') \tag{7.102}$$

and

$$D' = \frac{1}{2}\rho V_0^2 C_y \mathrm{d}y C_{D_y}. \tag{7.103}$$

The normal force increment δZ_{right} acting at the chordwise strip element in the roll rate perturbation is given by

$$\delta Z_{\text{right}} = -L'\cos\alpha' - D'\sin\alpha' \cong -L' - D'\alpha', \tag{7.104}$$

since α' is a small angle. Substitute for L', D', and α', respectively, to obtain

$$\delta Z_{\text{right}} = -\frac{1}{2}\rho V_0^2 \left(a_y\alpha_\mathrm{e} + (a_y + C_{D_y})\frac{py}{V_0}\right) c_y \mathrm{d}y. \tag{7.105}$$

Copyright © 2025 Xiaowei He

The resulting increment in roll moment is then given by

$$\delta L_{\text{right}} = y\delta Z_{\text{right}} = -\frac{1}{2}\rho V_0^2 \left(a_y \alpha_{\text{e}} + (a_y + C_{D_y})\frac{py}{V_0} \right) c_y y \mathrm{d}y, \tag{7.106}$$

and the corresponding increment in roll moment arising from the left wing, where the incidence is reduced by α' since the left wing is rising with respect to the incident airflow, is given by

$$\delta L_{\text{left}} = -y\delta Z_{\text{left}} = \frac{1}{2}\rho V_0^2 \left(a_y \alpha_{\text{e}} + (a_y + C_{D_y})\frac{py}{V_0} \right) c_y y \mathrm{d}y. \tag{7.107}$$

The total roll moment due to roll rate is obtained by summing the increments from the right and left chordwise strips and integrating from the root to the tip of the wing,

$$L_{\text{total}} = \int\limits_{\text{span}} (\delta L_{\text{left}} + \delta L_{\text{right}}) = -\rho V_0 p \int_0^s (a_y + C_{D_y}) c_y y^2 \mathrm{d}y, \tag{7.108}$$

and, by definition,

$$p\mathring{L}_p = L_{\text{total}} = -\rho V_0 p \int_0^s (a_y + C_{D_y}) c_y y^2 \mathrm{d}y. \tag{7.109}$$

Hence the dimensional derivative expression is given by

$$\mathring{L}_p = -\rho V_0 \int_0^s (a_y + C_{D_y}) c_y y^2 \mathrm{d}y. \tag{7.110}$$

7.7.3 Aerodynamic control derivatives

Estimates may be made for the aerodynamic control derivatives provided that the controller in question is a simple flap-like device and that its aerodynamic properties can be modeled with a reasonable degree of confidence. However, estimates of the aileron and rudder control derivatives obtained from simple models are unlikely to be accurate since it is very difficult to describe the aerodynamic conditions applied in sufficient detail. Estimates for the lateral-directional aerodynamic control derivatives are best obtained by experimental measurement. However, simple models for the aileron and rudder control derivatives are given here for completeness and in order to illustrate the principles of lateral-directional control.

Derivatives due to elevator. Typically, the lift coefficient for a tailplane with elevator control is given by

$$C_{L_{\text{T}}} = a_0 + a_1 \alpha_{\text{T}} + a_2 \eta, \tag{7.111}$$

where a_1 is the lift curve slope of the tailplane and a_2 is the lift curve slope with respect to elevator angle η. The corresponding drag coefficient may be expressed as

$$C_{D_{\text{T}}} = C_{D_{0_{\text{T}}}} + k_{\text{T}} C_{L_{\text{T}}}^2, \tag{7.112}$$

where all parameters are tailplane-dependent.

- $\mathring{X}_\eta = \dfrac{\partial X}{\partial \eta}$ **axial force due to elevator.**

  It is assumed that for a small elevator deflection, consistent with a small perturbation, the resulting axial force perturbation arises from the drag change associated with the tailplane only. Whence,

$$X = X_{\text{T}} = -D_{\text{T}} = -\frac{1}{2}\rho V^2 S_{\text{T}} C_{D_{\text{T}}}. \tag{7.113}$$

Copyright © 2025 Xiaowei He

Thus,

$$\mathring{X}_\eta = \frac{\partial X_\mathrm{T}}{\partial \eta} = -\frac{1}{2}\rho V^2 S_\mathrm{T} \frac{C_{D_\mathrm{T}}}{\partial \eta}. \tag{7.114}$$

Substitute for C_{D_T} to obtain

$$\mathring{X}_\eta = \frac{\partial X_\mathrm{T}}{\partial \eta} = -\rho V^2 S_\mathrm{T} k_\mathrm{T} C_{L_\mathrm{T}} \frac{\partial C_{L_\mathrm{T}}}{\partial \eta}. \tag{7.115}$$

For a small perturbation,

$$\frac{\partial C_{L_\mathrm{T}}}{\partial \eta} \cong a_2, \tag{7.116}$$

and in the limit $V \cong V_0$, the derivative may be written as

$$\mathring{X}_\eta = -\rho V^2 S_\mathrm{T} k_\mathrm{T} C_{L_\mathrm{T}} a_2. \tag{7.117}$$

- $\mathring{Z}_\eta = \dfrac{\partial Z}{\partial \eta}$ **normal force due to elevator.**

  As before, it is assumed that for a small elevator deflection, the resulting normal force perturbation arises from the lift change associated with the tailplane only. Whence

$$Z = Z_\mathrm{T} = -L_\mathrm{T} = -\frac{1}{2}\rho V^2 S_\mathrm{T} C_{L_\mathrm{T}}. \tag{7.118}$$

  Thus,

$$\mathring{Z}_\eta = \frac{\partial Z_\mathrm{T}}{\partial \eta} = -L_\mathrm{T} = -\frac{1}{2}\rho V^2 S_\mathrm{T} \frac{C_{L_\mathrm{T}}}{\partial \eta}. \tag{7.119}$$

  Substitute for C_{L_T}, and for a small perturbation, in the limit $V \cong V_0$,

$$\mathring{Z}_\eta = \frac{\partial Z_\mathrm{T}}{\partial \eta} = -\frac{1}{2}\rho V_0^2 S_\mathrm{T} a_2 \tag{7.120}$$

- $\mathring{M}_\eta$ **pitch moment due to elevator.**

  It is assumed that the pitch moment resulting from elevator deflection is due entirely to the moment of the tailplane lift about the *cg*. Whence

$$M = M_\mathrm{T} = -L_\mathrm{T} l_\mathrm{T} = -\frac{1}{2}\rho V^2 S_\mathrm{T} l_\mathrm{T} C_{L_\mathrm{T}}. \tag{7.121}$$

  Thus,

$$\mathring{M}_\eta = \frac{\partial M_\mathrm{T}}{\partial \eta} = -\frac{1}{2}\rho V^2 S_\mathrm{T} l_\mathrm{T} \frac{C_{L_\mathrm{T}}}{\partial \eta} = \mathring{Z}_\eta l_\mathrm{T}. \tag{7.122}$$

Derivatives due to aileron. Typical aileron geometry is shown in figure 7.13 and comprises a part-span flap in the outboard sections of both port and starboard wings. Differential deflection of the flaps creates the desired control in roll. As described in figure 2.9, a positive aileron deflection results in the starboard (right) surface deflecting its trailing edge down and the port (left) surface trailing edge up, and aileron angle ξ is taken to be the mean of the two surface angles. Thus, the local lift coefficient at spanwise coordinate y is given by

$$\begin{aligned} \left(C_{L_y}\right)_\mathrm{right} &= a_0 + a_y \alpha + a_{2_\mathrm{A}} \xi, \\ \left(C_{L_y}\right)_\mathrm{left} &= a_0 + a_y \alpha - a_{2_\mathrm{A}} \xi. \end{aligned} \tag{7.123}$$

Copyright © 2025 Xiaowei He

Since it is not practical to define a simple model for the increment in local drag coefficient due to aileron deflection, let it be defined more generally as

$$\begin{aligned}\left(C_{D_y}\right)_{\text{right}} &= \frac{\partial C_{D_y}}{\partial \xi}\xi,\\ \left(C_{D_y}\right)_{\text{left}} &= -\frac{\partial C_{D_y}}{\partial \xi}\xi,\end{aligned} \tag{7.124}$$

where it is assumed that, for small aileron angles, the change in drag $\partial C_{D_y}/\partial \xi$ is dominated by induced drag effects and may vary over the aileron span.

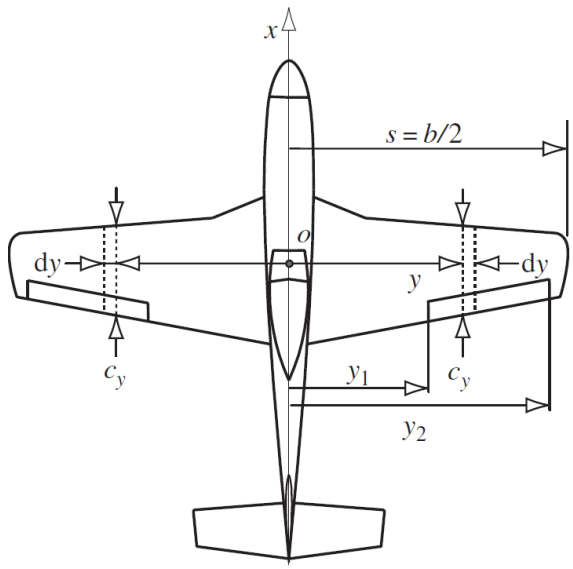

Figure 7.13: Aileron control geometry [1].

- $\mathring{Y}_\xi = \dfrac{\partial Y}{\partial \xi}$ **sideforce due to aileron.**

  For aircraft of conventional layout, the side force due to the aileron is zero or insignificantly small. However, for aircraft of unconventional layout, with highly swept wings or that utilize differential canard surfaces for roll control, this may not be the case. In such cases, simple analytical models would not be the most appropriate means for obtaining an estimate of the derivative value.

- $\mathring{L}_\xi = \dfrac{\partial L}{\partial \xi}$ **roll moment due to aileron.**

  This derivative describes the roll control property of the aircraft, and an accurate estimate of its value is important to flight dynamics analysis. With reference to equation (7.123) and figure 7.13, the application of simple strip theory enables the rolling moment due to starboard aileron deflection to be written as

$$L_{\text{right}} = -\frac{1}{2}\rho V^2 \int_{y_1}^{y_2} \left(C_{L_y}\right)_{\text{right}} c_y y \mathrm{d}y = -\frac{1}{2}\rho V^2 \int_{y_1}^{y_2} (a_0 + a_y\alpha + a_{2_\text{A}}\xi) c_y y \mathrm{d}y, \tag{7.125}$$

  where a_{2_A} is the aileron lift curve slope, which is assumed to be constant over the span of the aileron. Similarly, the roll moment due to the port aileron deflection may be written as

$$L_{\text{left}} = \frac{1}{2}\rho V^2 \int_{y_1}^{y_2} \left(C_{L_y}\right)_{\text{right}} c_y y \mathrm{d}y = \frac{1}{2}\rho V^2 \int_{y_1}^{y_2} (a_0 + a_y\alpha - a_{2_\text{A}}\xi) c_y y \mathrm{d}y. \tag{7.126}$$

Copyright © 2025 Xiaowei He

It follows that the total roll moment may be written as

$$\mathring{L}_\xi \xi = L_{\text{right}} + L_{\text{left}} = -\rho V^2 (a_{2_\text{A}} \xi) \int_{y_1}^{y_2} c_y y \mathrm{d}y. \tag{7.127}$$

Hence, in the limit $V \cong V_0$, the dimensional derivative is given by

$$\mathring{L}_\xi = -\rho V_0^2 a_{2_\text{A}} \int_{y_1}^{y_2} c_y y \mathrm{d}y. \tag{7.128}$$

- $\mathring{N}_\xi = \dfrac{\partial N}{\partial \xi}$ **yaw moment due to aileron.**

  This derivative describes the adverse yaw property of the aircraft in response to aileron roll commands. With reference to equation (7.124) and figure 7.13, the application of simple strip theory enables the yawing moment due to starboard aileron deflection to be written as

$$N_{\text{right}} = \frac{1}{2}\rho V^2 \int_{y_1}^{y_2} \left(C_{D_y}\right)_{\text{right}} c_y y \mathrm{d}y = \frac{1}{2}\rho V^2 \int_{y_1}^{y_2} \left(\frac{\partial C_{D_y}}{\partial \xi}\xi\right) c_y y \mathrm{d}y. \tag{7.129}$$

  Similarly, the yaw moment due to port aileron deflection may be written as

$$N_{\text{left}} = -\frac{1}{2}\rho V^2 \int_{y_1}^{y_2} \left(C_{D_y}\right)_{\text{left}} c_y y \mathrm{d}y = -\frac{1}{2}\rho V^2 \int_{y_1}^{y_2} \left(-\frac{\partial C_{D_y}}{\partial \xi}\xi\right) c_y y \mathrm{d}y. \tag{7.130}$$

  Then the total yaw moment may be written as

$$\mathring{N}_\xi \xi = N_{\text{right}} + N_{\text{left}} = \rho V^2 \int_{y_1}^{y_2} \left(\frac{\partial C_{D_y}}{\partial \xi}\xi\right) c_y y \mathrm{d}y. \tag{7.131}$$

  Thus, the dimensional derivative, in the limit $V \cong V_0$, is given by

$$\mathring{N}_\xi = \rho V_0^2 \int_{y_1}^{y_2} \frac{\partial C_{D_y}}{\partial \xi} c_y y \mathrm{d}y. \tag{7.132}$$

Copyright © 2025 Xiaowei He

8 Introduction to Aircraft Feedback Control

8.1 Time response

As discussed in section 7.2.5, the time response of a system is the time history of the states in response to the system input. It can be obtained by finding the inverse Laplace transform of the multiplication of the system transfer function and the input transfer function, which gives a convolution in the time domain.

8.1.1 Step input

The concept of a step input was first introduced in section 7.2.5. In this case, the step input magnitude is represented by the magnitude k as shown in figure 8.1. A physical approximation of a step input occurs when the pilot quickly moves the stick from the neutral position to another position.

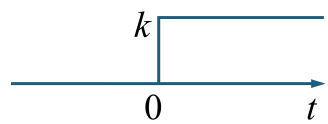

Figure 8.1: Step input of magnitude k.

The time domain representation is

$$r(t) = k\delta(t), \tag{8.1}$$

where $r(t)$ is the output of the step and $\delta(t)$ is the delta function that defines a step change in time. The Laplace transform of a step input with a magnitude of k is

$$R(s) = k\frac{1}{s}. \tag{8.2}$$

When $k = 1$, it becomes a *unit step input*. Now we can use $R(s)$ as input to other given systems to determine their *step-input response*.

8.1.2 Poles and zeros of transfer functions

The output response of a system is the sum of two responses: the forced response (steady-state response or particular solution) and the natural response (homogeneous solution). The use of poles and zeros and their relationship to the time response of a system gives us a qualitative "handle" on problems. The concept of poles and zeros, fundamental to the analysis and design of control systems, simplifies the evaluation of a system's response.

Poles of a transfer function. The *poles* of a transfer function are (1) the values of the Laplace transform variable s that cause the transfer function to become infinite or (2) any roots of the denominator of the transfer function that are common to roots of the numerator.

Strictly speaking, the poles of a transfer function satisfy part (1) of the definition. For example, the roots of the characteristic polynomial in the denominator are values of s that make the transfer function infinite, so they are thus poles. However, if a factor of the denominator can be canceled by the same factor in the numerator, the root of this factor no longer causes the transfer function to become infinite. In control systems, it often refers to the root of the canceled factor in the denominator as a pole even though the transfer function will not be infinite at this value. Hence, part (2) is included in the definition.

Copyright © 2025 Xiaowei He

Zeros of a transfer function. The *zeros* of a transfer function are (1) the values of the Laplace transform variable s that cause the transfer function to become zero, or (2) any roots of the numerator of the transfer function that are common to roots of the denominator.

Strictly speaking, the zeros of a transfer function satisfy part (1) of this definition. For example, the roots of the numerator are values of s that make the transfer function zero and are thus zeros. However, if a factor of the numerator can be canceled by the same factor in the denominator, the root of this factor no longer causes the transfer function to become zero. In control systems, it often refers to the root of the canceled factor in the numerator as a zero even though the transfer function will not be zero at this value. Hence, part (2) is included in the definition.

Poles and zeros of a first-order system. Given the transfer function $G(s)$ in figure 8.2a, a pole exists at $s = -5$, and a zero exists at $s = -2$. These values are plotted on the complex s-plane in figure 8.2b, using an $\times$ for the pole and a $\bigcirc$ for the zero.

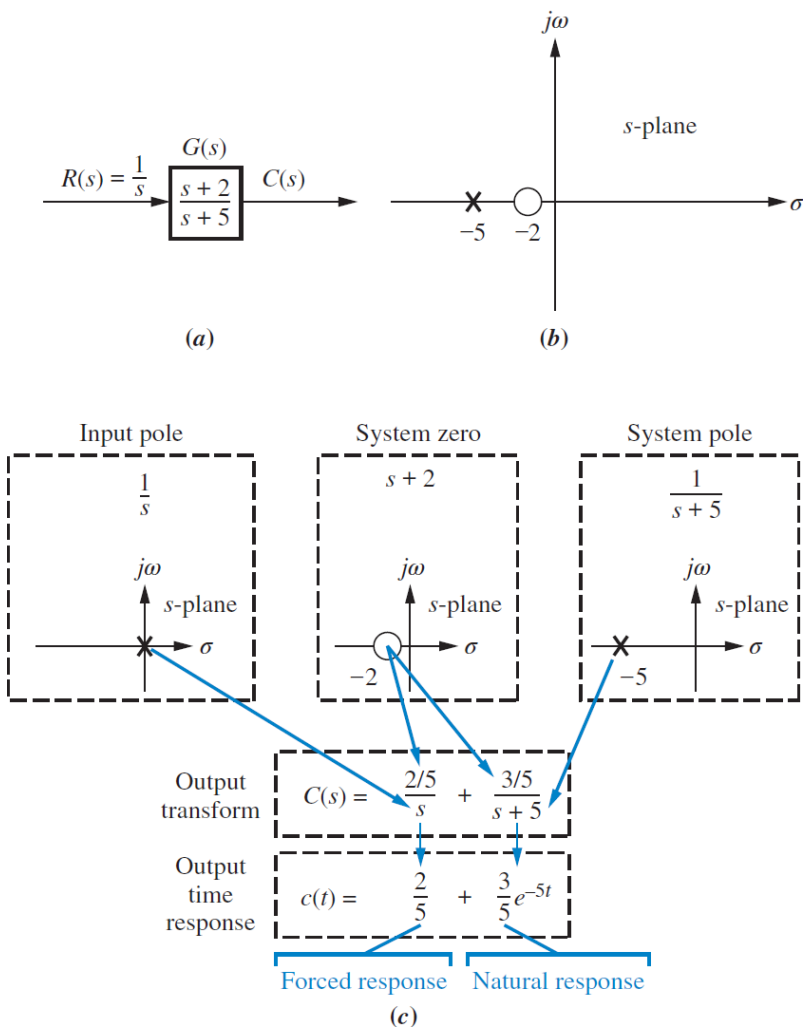

Figure 8.2: Poles and zeros of a first-order system [16].

To show the properties of the poles and zeros, we find the unit step response of the system. Multi-

Copyright © 2025 Xiaowei He

plying the transfer function of figure 8.2a by a step function yields

$$C(s) = G(s)R(s) = \frac{s+2}{s(s+5)} = \frac{A}{s} + \frac{B}{s+5} = \frac{2/5}{s} + \frac{3/5}{s+5}, \tag{8.3}$$

where

$$\begin{aligned} A &= \left.\frac{s+2}{s+5}\right|_{s\to 0} = \frac{2}{5}, \\ B &= \left.\frac{s+2}{s}\right|_{s\to -5} = \frac{3}{5}. \end{aligned} \tag{8.4}$$

Thus,

$$c(t) = \frac{2}{5} + \frac{3}{5}e^{-5t}. \tag{8.5}$$

From the development summarized in figure 8.2c, we draw the following conclusions:

- A pole of the input function generates the form of the forced response (that is, the pole at the origin generated a step function at the output).
- A pole of the transfer function generates the form of the natural response (that is, the pole at $s = -5$ generated e^{-5t}).
- A pole on the real axis generates an exponential response of the form $e^{-\alpha t}$, where $-\alpha$ is the pole location on the real axis. Thus, the farther to the left a pole is on the negative real axis, the faster the exponential transient response will decay to zero (see figure 8.3 for the general case).

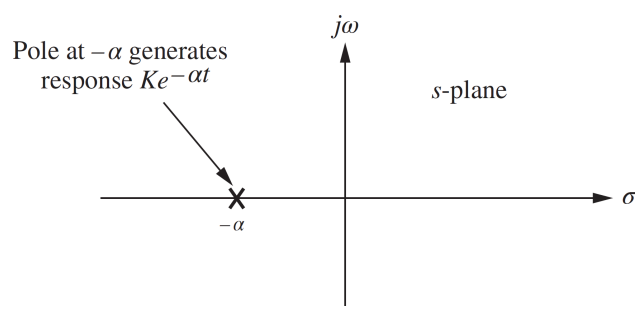

Figure 8.3: Effect of a real-axis pole upon transient response [16].

- The zeros and poles generate the amplitudes for both the forced and natural responses (this can be seen from the calculation of A and B).

Example 8.1

Given the system

$$G(s) = \frac{s+3}{(s+2)(s+4)(s+5)},$$

write the output $c(t)$ undergoes a unit step input $R(s) = 1/s$ in general terms. Specify the forced and natural parts of the solution.

Solution: By inspection, each system pole generates an exponential as part of the natural response,

Copyright © 2025 Xiaowei He

and the input's pole generates the forced response. Thus,

$$C(s) = R(s)G(s) = \underbrace{\frac{K_1}{s}}_{\substack{\text{forced}\\\text{response}}} \underbrace{+\frac{K_2}{s+2} + \frac{K_3}{s+4} + \frac{K_4}{s+5}}_{\text{natural response}}.$$

Taking the inverse Laplace transform,

$$c(t) = \underbrace{K_1}_{\substack{\text{forced}\\\text{response}}} \underbrace{+K_2e^{-2t} + K_3e^{-4t} + K_4e^{-5t}}_{\text{natural response}}.$$

8.1.3 Time response of first-order systems

We now discuss first-order systems without zeros to define a performance specification for such a system. A first-order system without zeros can be described by the transfer function shown in figure 8.4a.

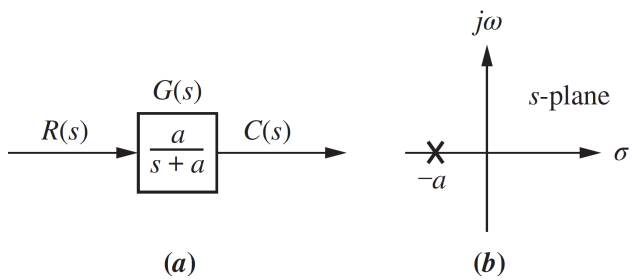

Figure 8.4: A first-order system and its pole plot [16].

If the input is a unit step, where $R(s) = 1/s$, the Laplace transform of the step response is $C(s)$, where

$$C(s) = R(s)G(s) = \frac{a}{s(s+a)}. \tag{8.6}$$

Taking the inverse Laplace transform, the step response is given by

$$c(t) = c_{\mathrm{f}}(t) + c_{\mathrm{n}}(t) = 1 - e^{-at}, \tag{8.7}$$

where the input pole at the origin generated the forced response $c_{\mathrm{f}}(t) = 1$, and the system pole at $-a$, as shown in figure 8.4b, generated the natural response $c_{\mathrm{n}}(t) = -e^{-at}$. The step response is plotted in figure 8.5. We examine the significance of parameter a, the only parameter needed to describe the transient response. When $t = 1/a$,

$$c(t) = 1 - e^{-at}\big|_{t=1/a} = 1 - 0.37 = 0.63. \tag{8.8}$$

Time constant. 1/a the time constant (sometimes referred to as $1/tau$) of the response. The time constant can be described as the time for e^{-at} to decay to 37% of its initial value. Alternately, is is the time it takes for the step response to rise to 63% of its final value (see figure 8.5).

The reciprocal of the time constant has the units [1/seconds], or frequency. Thus, we can call the parameter a the exponential frequency. Since the derivative of e^{-at} is $-a$ when $t = 0$, a is the initial rate of change of the exponential at $t = 0$. Thus, the time constant can be considered a transient response

Copyright © 2025 Xiaowei He

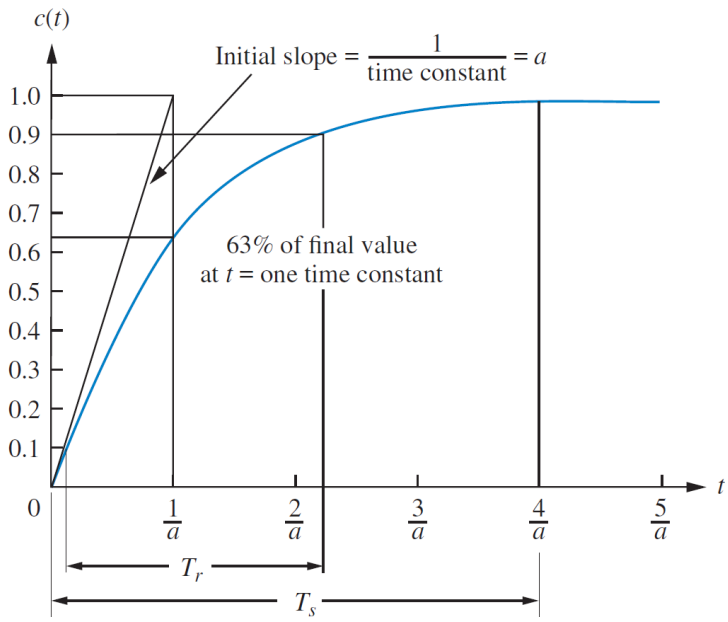

Figure 8.5: First-order system response to a unit step [16].

specification for a first-order system, since it is related to the speed at which the system responds to a step input.

The time constant can also be evaluated from the pole plot (see figure 8.4b). Since the pole of the transfer function is at $s = -a$, the pole is located at the reciprocal of the time constant, and the farther the pole from the imaginary axis, the faster the transient response.

Rise time T_r. Rise time is defined as the time for the waveform to go from 0.1 to 0.9 of its final value. Rise time is found by solving time response equation (8.7) for the difference in time at $c(t) = 0.9$ and $c(t) = 0.1$. Hence,

$$T_\mathrm{r} = \frac{2.31}{a} - \frac{0.11}{a} = \frac{2.2}{a}. \tag{8.9}$$

Settling time T_s. Settling time is defined as the time for the response to reach, and stay within, 2% of its final value. Letting $c(t) = 0.98$ in the time response equation (8.7) and solving for time t, the settling time is

$$T_\mathrm{s} = \frac{4}{a}. \tag{8.10}$$

8.1.4 Time response of second-order systems

Two physically meaningful specifications, natural frequency ω_n and damping ratio ζ, are defined for second-order systems. These quantities can be used to describe the characteristics of the second-order transient response just as time constants describe the first-order system response. As reviewed in section 1.3.1, the general second-order transfer function can be written as

$$G(s) = \frac{\omega_\mathrm{n}}{s^2 + 2\zeta\omega_\mathrm{n}s + \omega_\mathrm{n}}, \tag{8.11}$$

of which the poles are found at

$$p_{1,2} = -\zeta\omega_\mathrm{n} \pm j\omega_\mathrm{n}\sqrt{1-\zeta^2}. \tag{8.12}$$

Copyright © 2025 Xiaowei He

The various cases of second-order response are a function of ζ are summarized in figure 8.6.

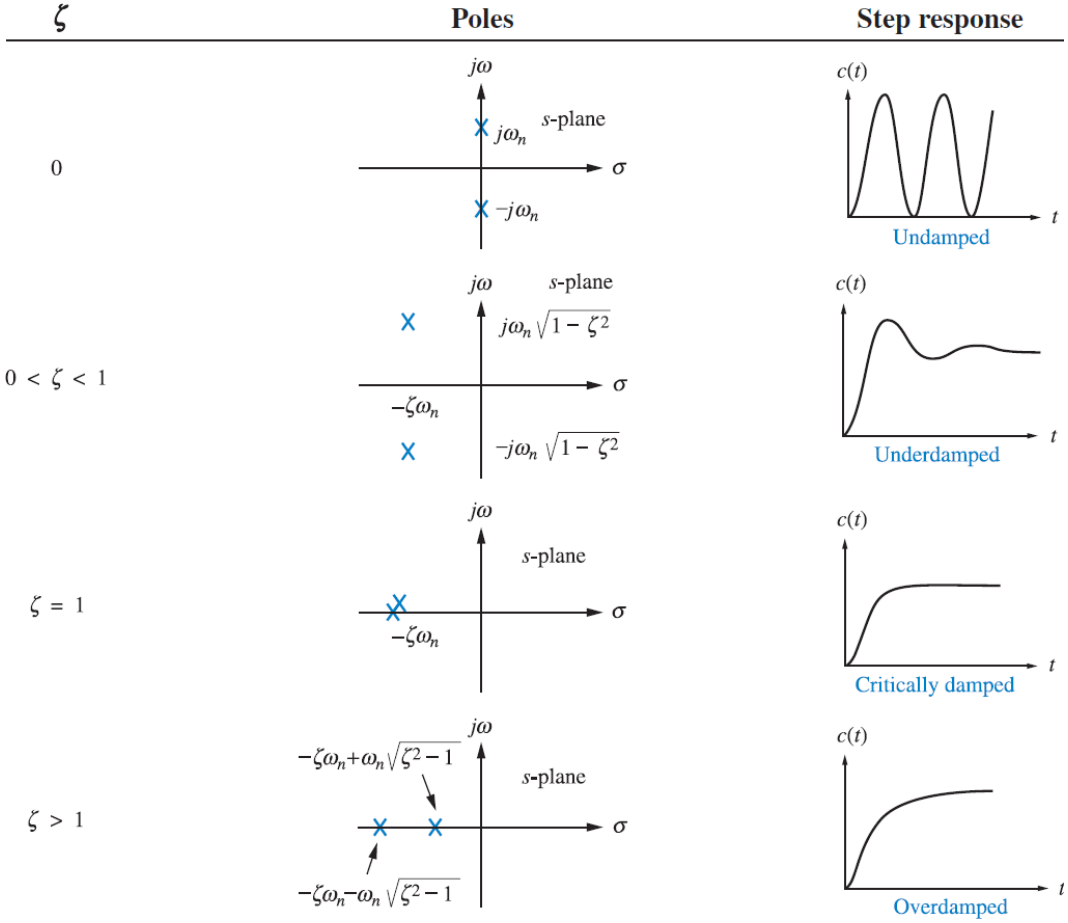

Figure 8.6: Second-order response as a function of damping ratio [16].

We analyze the step response of an underdamped second-order system. Not only will this response be found in terms of ζ and ω_n, but more specifications indigenous to the underdamped case will be defined. The underdamped second-order system, a common model for physical problems, displays unique behavior that must be itemized; a detailed description of the underdamped response is necessary for both analysis and design.

The unit step response of a second-order system is

$$C(s) = R(s)G(s) = \frac{\omega_\mathrm{n}}{s(s^2 + 2\zeta\omega_\mathrm{n}s + \omega_\mathrm{n})} = \frac{K_1}{s} + \frac{K_2 s + K_3}{s^2 + 2\zeta\omega_\mathrm{n}s + \omega_\mathrm{n}}, \tag{8.13}$$

where it is assumed that $\zeta < 1$ (the underdamped case). Expanding by partial fractions and taking the inverse Laplace transform, we have the time response of a second-order system

$$c(t) = 1 - \frac{1}{\sqrt{1-\zeta^2}} e^{-\zeta\omega_\mathrm{n}t} \cos\left(\omega_\mathrm{n}\sqrt{1-\zeta^2}t - \phi\right), \tag{8.14}$$

where

$$\phi = \arctan\frac{\zeta}{\sqrt{1-\zeta^2}}. \tag{8.15}$$

Copyright © 2025 Xiaowei He

A plot of this response appears in figure 8.7 for various values of ζ, plotted along a time axis normalized to the natural frequency. The relationship between the value of ζ and the type of response is obtained: The lower the value of ζ, the more oscillatory the response. The natural frequency is a time-axis scale factor and does not affect the nature of the response other than to scale it in time.

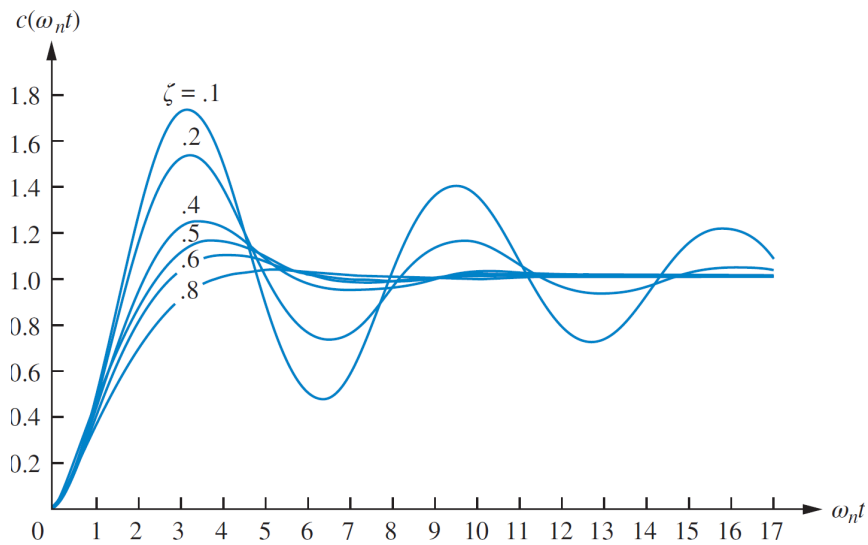

Figure 8.7: Second-order underdamped responses for damping ratio values [16].

Other parameters associated with the underdamped response are rise time, peak time, percent overshoot, and settling time. These specifications are defined as follows (see also Figure 4.14):

- **Rise time** T_r. The time required for the waveform to go from 0.1 of the final value to 0.9 of the final value. It indicate how fast the system responds to a step input. A precise analytical relationship between rise time and damping ratio cannot be found. However, using a computer and equation (8.14), the rise time can be approximated by

$$T_\mathrm{r} \approx \frac{1 + 1.1\zeta + 1.4\zeta^2}{\omega_\mathrm{n}}. \tag{8.16}$$

- **Peak time** Tp. The time required to reach the first, or maximum, peak (overshoot). T_p is found by differentiating $c(t)$ in equation (8.14) and finding the first zero crossing after $t = 0$.

$$T_\mathrm{p} = \frac{\pi}{\omega_\mathrm{n}\sqrt{1-\zeta^2}}. \tag{8.17}$$

- **Percent overshoot** $\%_\mathrm{os}$. The amount that the waveform overshoots the steady-state, or final, value at the peak time, expressed as a percentage of the steady-state value.

$$\%_\mathrm{os} = \frac{c_\mathrm{max} - c_\mathrm{final}}{c_\mathrm{final}} \times 100, \tag{8.18}$$

in which c_max is found by evaluating $c(t)$ at the peak time T_p

$$c_\mathrm{max} = c(T_\mathrm{p}) = 1 + \exp\left(-\frac{\zeta\pi}{\sqrt{1-\zeta^2}}\right). \tag{8.19}$$

Copyright © 2025 Xiaowei He

For the unit step used for equation (8.14), $c_{\text{final}} = 1$. Thus,

$$\%_{\text{os}} = \exp\left(-\frac{\zeta\pi}{\sqrt{1-\zeta^2}}\right) \times 100. \tag{8.20}$$

- **Settling time** Ts. The time required for the transient's damped oscillations to reach and stay within 2% of the steady-state value, which is approximated by

$$T_{\text{s}_{2\%}} \approx \frac{4}{\zeta\omega_{\text{n}}}. \tag{8.21}$$

8.2 Frequency response

For the vast majority of flight dynamics investigations, time domain analysis is usually adequate, especially when the subject is the classical unaugmented aircraft. The principal graphical tool used in time domain analysis is the time history plot showing the response of the aircraft to controls or some external disturbance. However, when the subject aircraft is an advanced modern aircraft fitted with a flight control system, flight dynamics analysis in the frequency domain can provide additional valuable insight into its behavior. In recent years frequency domain analysis has made an important contribution to the understanding of the sometimes unconventional handling qualities of aircraft whose flying qualities are largely shaped by a flight control system. It is for this reason that a brief review of simple frequency response concepts is considered here.

Consider the hypothetical situation in which the elevator of an otherwise trimmed aircraft is operated sinusoidally with constant amplitude k and variable frequency ω. The longitudinal input to the aircraft may therefore be expressed as

$$\eta(t) = k \sin \omega t. \tag{8.22}$$

It is reasonable to expect that each of the output variables describing aircraft motion will respond sinusoidally to the input. However, the amplitudes of the output variables will not necessarily be the same, and they will not necessarily be in phase with one another or with the input. Thus the general expression describing any output response variable may be written as

$$y(t) = K \sin(\omega t + \phi), \tag{8.23}$$

where both output amplitude K and phase shift ϕ are functions of excitation frequency ω. As excitation frequency ω is increased from zero so, initially, at low frequencies, the sinusoidal response is visible in all output variables. As it is increased further, the sinusoidal response starts to diminish in magnitude and eventually becomes imperceptible in the outputs. Simultaneously, phase shift ϕ indicates an increasingly large lag between input and output.

The reason for the observations just given is that, at sufficiently high frequencies, the mass and inertia properties of the aircraft prevent it from responding quickly enough to follow the input. The limiting frequency at which the response commences to diminish rapidly is referred to as the *bandwidth* of the aircraft with respect to the output variable of interest. A more precise definition of bandwidth is given later. Since aircraft respond only to frequencies below the bandwidth frequency, they have the frequency response properties of a low-pass system. At exciting frequencies corresponding to the damped natural frequencies of the phugoid and short-period modes, peaks in output magnitude K are seen together, with significant changes in phase shift ϕ. The mode frequencies are described as resonant,

Copyright © 2025 Xiaowei He

and the magnitudes of the output parameters K and ϕ at resonance are determined by the damping ratios of the modes. The system (or aircraft) gain in any particular response variable is defined as

$$\text{system gain} = \left|\frac{K(\omega)}{k}\right|, \tag{8.24}$$

where it is usually assumed that the input and output variables have the same units in normal control system applications. This is often not the case in aircraft applications, and care must be exercised in the interpretation of gain.

8.2.1 The bode diagram

The intention here is not to describe the construction of a Bode diagram but to describe its application to the aircraft and to explain its correct interpretation. To illustrate the application of the Bode diagram to a typical classical aircraft, consider the transfer function of pitch attitude response to elevators

$$\frac{\theta'(s)}{\eta'(s)} = \frac{k_\theta(s + 1/\tau_{\theta_1})(s + 1/\tau_{\theta_2})}{(s^2 + 2\zeta_\mathrm{p}\omega_\mathrm{p}s + \omega_\mathrm{p}^2)(s^2 + 2\zeta_\mathrm{s}\omega_\mathrm{s}s + \omega_\mathrm{s}^2)}. \tag{8.25}$$

This function is of particular relevance to longitudinal handling studies and has the simplifying advantage that both input and output variables have the same units. In frequency response calculation it is usual to assume a sinusoidal input signal of unit magnitude. Also, it is important that, whenever the response transfer function is negative, which is often the case in aircraft applications, a negative input is assumed which ensures the correct computation of phase. Therefore, in this particular application, since k_θ is usually a negative number, a sinusoidal elevator input of unit magnitude, $\eta'(t) = -1 \sin \omega t$ is assumed. The pitch attitude frequency response is calculated by writing $s = j\omega$ in equation (8.25); the right-hand side then becomes a complex number whose magnitude and phase can be evaluated for a suitable range of frequency ω. Since the input magnitude is unity, the system gain from equation (8.24) is given by the absolute value of the magnitude of the complex number representing the right-hand side of equation (8.25) and is a function of frequency ω.

Because the calculation of gain and phase involves the products of several complex numbers, it is preferred to work in terms of the logarithm of the complex number representing the transfer function. The total gain and phase then become the simple sums of the gain and phase of each transfer function factor. For example, each factor in parentheses on the right-hand side of equation (8.25) may have its gain and phase characteristics calculated separately as a function of frequency; total gain and phase are then given by summing the contributions from each factor. However, the system gain is now expressed as a logarithmic function of the gain ratio from equation (8.24), defined as

$$\text{logarithmic gain} = 20 \log_{10} \left|\frac{K(\omega)}{k}\right| \text{ [dB]} \tag{8.26}$$

with units of decibels [dB].

The Bode diagram comprises the corresponding *gain plot* and *phase plot*. The gain plot shows the logarithmic gain (in decibels), plotted against $\log_1 0(\omega)$, and the phase plot shows the phase (in degrees), also plotted against $\log_1 0(\omega)$. To facilitate interpretation, the two plots are often superimposed on a common frequency axis. The Bode diagram showing the typical pitch attitude frequency response, as given by the transfer function (equation (8.25)), is shown in figure 8.8.

Also shown in figure 8.8 are the asymptotic approximations to the actual gain and phase plots as functions of frequency. The asymptotes can be drawn from inspection of the transfer function, and serve

Copyright © 2025 Xiaowei He

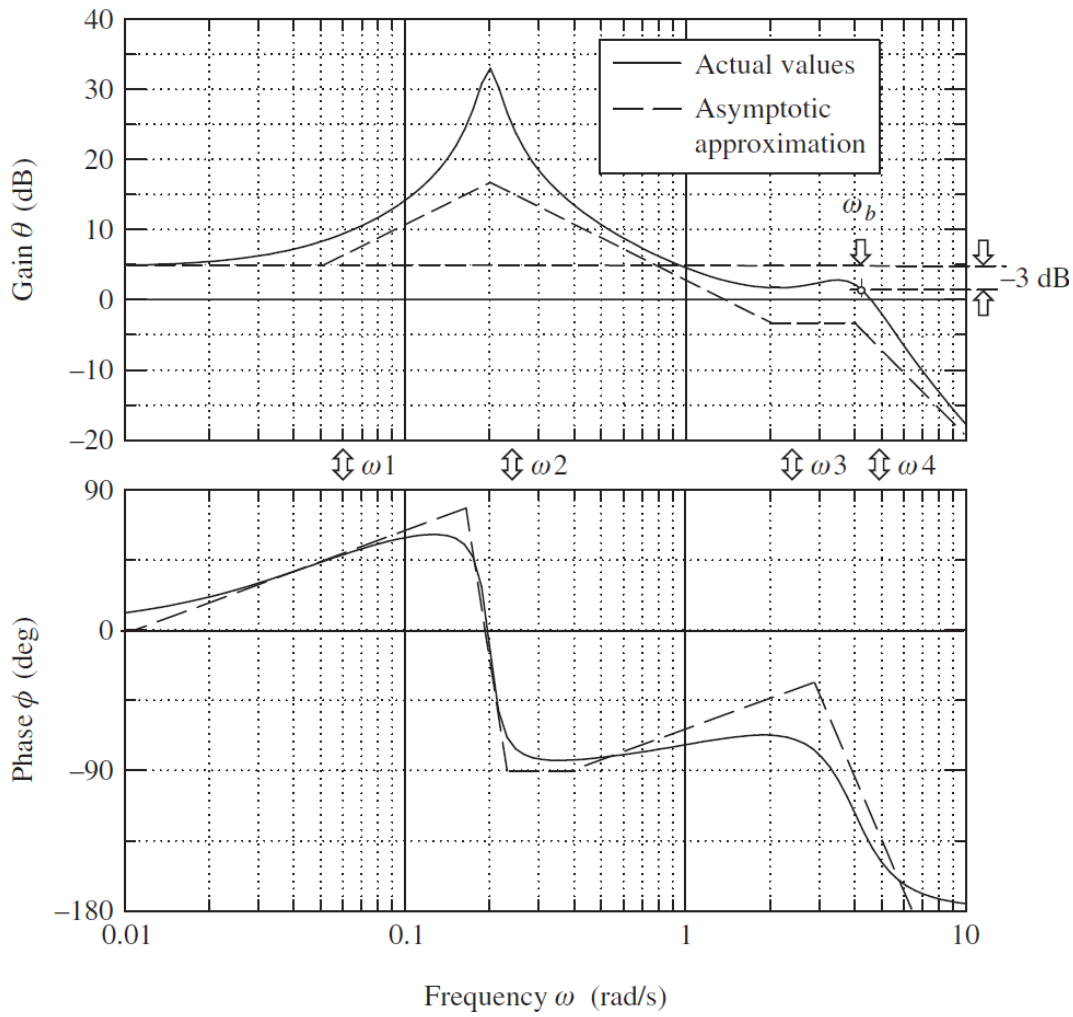

Figure 8.8: Bode diagram showing the classical pitch attitude frequency response [1].

as an aid to interpretation. Quite often the asymptotic approximation is sufficient for the evaluation in hand, thereby dispensing with the need to compute the actual frequency response entirely.

The shape of the gain plot is characterized by the *break frequencies* $\omega 1$ to $\omega 4$, which determine the locations of the discontinuities in the asymptotic gain plot. Each break frequency is defined by a key frequency parameter in the transfer function:

- $\omega 1 = \dfrac{1}{T_{\theta_1}}$ with first-order phase lead ($+45°$);
- $\omega 2 = \omega_{\mathrm{p}}$ with second-order phase lag ($-90°$);
- $\omega 3 = \dfrac{1}{T_{\theta_2}}$ with first-order phase lead ($+45°$);
- $\omega 4 = \omega_{\mathrm{s}}$ with second-order phase lag ($-90°$).

Since the transfer function is classical minimum phase, the corresponding phase shift at each break frequency is either a *lead*, if it arises from a numerator term, or a *lag*, if it arises from a denominator term. If, as is often the case in aircraft studies, non-minimum phase terms appear in the transfer function, their frequency response properties are unchanged except that the sign of the phase is reversed. Further, a

Copyright © 2025 Xiaowei He

first-order term gives rise to a total phase shift of 90 deg, and a second-order term gives rise to a total phase shift of 180 deg. The characteristic phase response is such that half the total phase shift associated with any particular transfer function factor occurs at the corresponding break frequency. Armed with this limited information, a modest interpretation of the pitch attitude frequency response of the aircraft is possible. The frequency response of the other motion variables may be dealt with in a similar way.

8.2.2 Interpretation of the Bode diagram

With reference to figure 8.8, it is seen that at very low frequencies $\omega < 0.01\,\mathrm{rad/s}$, there is no phase shift between the input and output and the gain remains constant — a little below 5 dB in this illustration. In other words, the pitch attitude follows the stick movement more or less precisely. As the input frequency is increased through $\omega 1$, the pitch response leads the input in phase, the output magnitude increases rapidly, and the aircraft appears to behave like an amplifier. At the phugoid frequency, the output reaches a substantial peak, consistent with the low damping, and thereafter the gain drops rapidly, accompanied by a rapid increase in phase lag. As the input frequency is increased further, the gain continues to reduce gently and the phase settles at -90 deg until the influence of break frequency $\omega 3$ comes into play. The reduction in gain is arrested, and the effect of the phase lead may be seen. However, when the input frequency reaches the short-period break frequency, a small peak in gain is seen, consistent with the higher damping ratio, and at higher frequencies the gain continues to reduce steadily. Meanwhile, the phase lag associated with the short-period mode results in a constant total phase lag of -180 deg at higher frequencies.

Once the output-input gain ratio drops below unity (0 dB), the aircraft appears to behave like an attenuator. The frequency at which the gain becomes small enough for the magnitude of the output response to become insignificant is called the *bandwidth frequency*, denoted ω_b. There are various definitions of bandwidth, but the one used here is probably the most common and defines bandwidth frequency as the frequency at which the gain first drops to -3 dB below the zero-frequency, or steady-state, gain. The bandwidth frequency is indicated in figure 8.8, and it is commonly a little higher than the short-period frequency. A gain of -3 dB corresponds with a gain ratio of $1/\sqrt{2} = 0.707$. Thus, by definition, the gain at the bandwidth frequency is 0.707 times the steady-state gain. Since the pitch attitude bandwidth frequency is close to the short-period frequency, the latter may sometimes be substituted for the bandwidth frequency, which is often good enough for most practical purposes.

The peaks in the gain plot are determined by the characteristics of the stability modes. A very pronounced peak indicates low mode damping and vice versa, an infinite peak corresponding with zero damping. The magnitude of the changes in gain and phase occurring in the vicinity of a peak indicates the significance of the mode in the response variable in question. Figure 8.8 indicates that the magnitude of the phugoid is much greater than the magnitude of the short-period mode in the pitch response of the aircraft. This is in fact confirmed by response time histories discussed in section 7.4.

In the classical application of the Bode diagram, as used by the control engineer, inspection of the gain and phase properties in the vicinity of the bandwidth frequency enables conclusions to be made about the stability of the system. Typically, stability is quantified in terms of *gain margin* and *phase margin*. However, such evaluations are only appropriate when the system transfer function is *minimum phase*. Since aircraft transfer functions that are non-minimum phase are frequently encountered, and many also have the added complication that they are negative, it is not usual for aircraft stability to be assessed in the Bode diagram. It is worth noting that, for aircraft augmented with flight control systems, the behavior of the phase plot in the vicinity of the bandwidth frequency is now known to be linked to the susceptibility of the aircraft to pilot-induced oscillations, a handling deficiency.

Copyright © 2025 Xiaowei He

The foregoing summary interpretation of frequency response assumes a sinusoidal elevator input to the aircraft. This is never likely to occur as a result of normal pilot action, but normal pilot actions may be interpreted to comprise a mix of many different frequency components. For example, in gentle maneuvering, the frequency content of the input is generally low whilst in aggressive or high-workload situations the frequency content is higher and may even exceed the bandwidth of the aircraft. In such a limiting condition the pilot is certainly aware that the aircraft cannot follow one's demands quickly enough and, depending in detail on the gain and phase response properties of the aircraft, one may well encounter hazardous handling problems. For this reason, bandwidth is a measure of the *quickness of response* achievable in a given aircraft. As a general rule, it is desirable that flight control system designers seek the highest response bandwidth consistent with the dynamic capabilities of the airframe.

8.3 Closed-loop system analysis

The resultant closed-loop control system is similar in many respects to the classical control systems. A significant advantage of this approach is that the analysis of the augmented, or closed-loop, aircraft makes full use of the control engineering's well-established tools. The systems approach to flight dynamics analysis was introduced in earlier chapters, where, for example, control engineering tools were utilized for solving the equations of motion.

A functional block diagram of a typical flight control system (FCS) is shown in figure 8.9. It is assumed that the primary flying controls are mechanical such that pilot commands drive the control surfaces via control actuators, which augment the available power to levels sufficient to overcome the aerodynamic loads on the surfaces. The electronic flight control system (EFCS) comprises two feedback loops, both of which derive their control signals from motion sensors appropriate to the requirements of the control laws. The outputs from the inner- and outer-loop controllers are summed electronically, and the resultant signal controls the aircraft via a small servo-actuator. Typically, the servo-actuator is an electro-hydraulic device that converts low-power electrical signals to mechanical signals at a power level compatible with those originating at the pilot, to which it is summed mechanically. Although only a single control axis is indicated in figure 8.9, it is important to appreciate that the FCS, in general, includes closed-loop controllers operating simultaneously on the roll, pitch, and yaw control axes of the aircraft and may even extend to include closed-loop engine control as well. Thus multivariable feedback involving many separate control loops is implied, which is typical of many modern FCS.

The *inner loop* provides stability augmentation and is usually regarded as essential for continuous proper operation of the aircraft. The inner-loop control system alone makes up the *stability augmentation system* (SAS); it is usually the first part of the FCS to be designed and, together with the airframe, comprises the *augmented aircraft*.

The *outer loop* provides the *autopilot*, which, as its name suggests, enables the pilot to fly various maneuvers under automatic control. Although necessary for operational reasons, an autopilot is not essential to a safe well-behaved aircraft. The autopilot control modes are designed to function with the augmented aircraft and may be selectively engaged as required to automate the piloting task. Their use is intended to release the pilot from the monotony of flying steady conditions manually and to fly precision maneuvers in adverse conditions which may be at, or beyond, the limits of human capability. Autopilot control modes vary from the very simple (e.g., height hold) to the very complex — such as automatic landing.

Since, typically, for most aircraft the control law gains required to effect good stability, control, and handling vary with operating conditions, it is necessary to make provision for their continuous adjustment. These variations often arise as a result of variations in the aerodynamic properties of the airframe over

Copyright © 2025 Xiaowei He

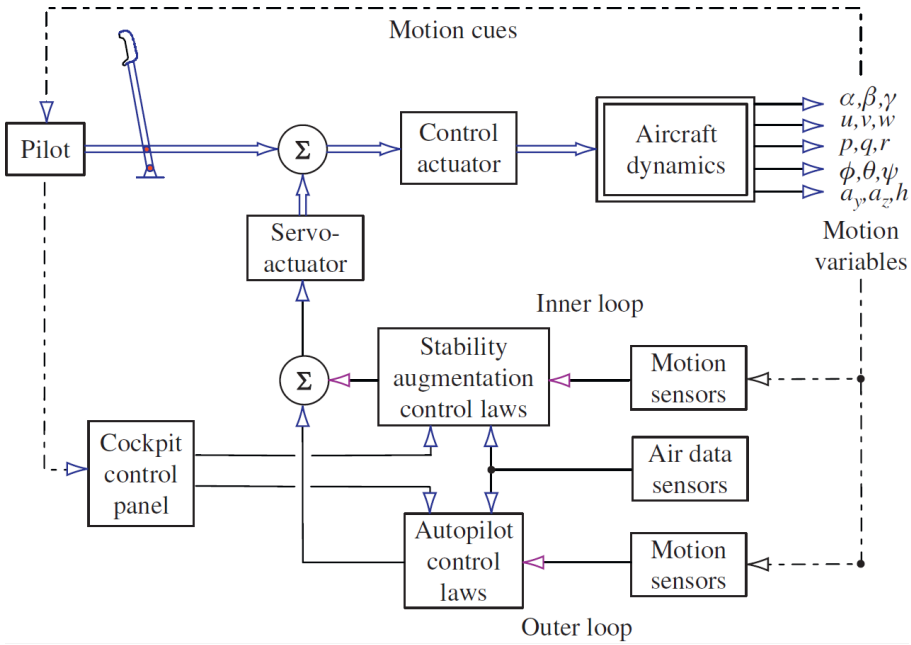

Figure 8.9: Typical flight control system [1].

the flight envelope. For example, at low speed, the aerodynamic effectiveness of the control surfaces is generally less than at high speed. This means that higher control gains are required at low speeds and vice versa. It is therefore common practice to vary, or schedule, gains as a function of flight conditions. Commonly used flight condition variables are dynamic pressure, Mach number, altitude, and so on — information which is grouped under the description of air data. Generally, air data information is available to all control laws in an FCS, as indicated in figure 8.9.

A control panel is provided in the cockpit to enable the pilot to control and monitor the operation of the FCS. SAS controls are usually minimal and enable the pilot to monitor the system for correct, and thus safe, operation. In some cases, the pilot may also be provided with means for selectively isolating parts of the SAS. On the other hand, the autopilot control panel is rather more substantial. Controls are provided to enable the pilot to set up, engage, and disengage the various autopilot mode functions. The control panel also enables him to monitor progress during the automated maneuver selected.

In piloted phases of flight, the autopilot is normally disengaged and, as indicated in figure 8.9, the pilot derives one's perception of flying and handling qualities from the motion cues provided by the augmented aircraft. Thus the inner-loop control system provides the means by which all aspects of stability, control, and handling may be tailored to improve the characteristics of the basic aircraft.

8.3.1 The control law

The control law is a mathematical expression that describes the function implemented by an augmentation or autopilot controller. For example, a very simple and very commonly used control law describing an inner-loop control system for augmenting yaw damping is

$$\zeta(s) = K_\zeta \delta_\zeta(s) - K_r \left(\frac{s}{1 + s\tau} \right) r(s). \tag{8.27}$$

This equation simply states that the control signal applied to the rudder $\zeta(s)$ comprises the sum

Copyright © 2025 Xiaowei He

of the pilot command $\delta_\zeta(s)$ and the yaw rate feedback $r(s)$. The gain K_ζ is the mechanical gearing between rudder pedals and rudder, and the gain K_r is the all-important feedback gain chosen by design to optimize damping in yaw. The second term in the equation is negative since negative feedback is required to increase stability in yaw. The second term also, typically, includes a washout, or high-pass, filter with a time constant of around 1 or 2 seconds. The filter is included to block yaw rate feedback in steady turning flight to prevent the feedback loop from opposing the pilot command once the rudder pedals are returned to the center after maneuver initiation. However, the filter is effectively transparent during transient motion, thereby enabling the full effect of the feedback loop to quickly damp out the yaw oscillation.

8.3.2 Safety

In any aircraft fitted with a flight control system, safety is the most critical issue. Since the FCS has direct "access" to the control surfaces, considerable care must be exercised in the design of the system to ensure that under no circumstances can a maximum instantaneous uncontrolled command be applied to any control surface. For example, a sensor failure might cause its output to saturate at its maximum possible value. This signal, in turn, is conditioned by the control law to apply what could well be a demand of sufficient magnitude to cause a maximum control surface displacement. The resulting failure transient might be some kind of hazardous divergent response. Clearly, steps must be taken in the design of the flight control system architecture to incorporate mechanisms to protect the aircraft from partial or total system malfunction.

The design of safety-critical flight control system architectures, as opposed to the simpler problem of control law design, is a substantial subject in its own right. However, at an introductory level, it is sufficient to appreciate that the requirements for safety can sometimes override the requirements for control, especially when relatively large control system gains are necessary. For simple stability augmentation systems of the kind exemplified by the control law, the problem may be overcome by limiting the maximum values of the control signals, giving rise to what is referred to as a limited-authority control system. In more complex FCS where authority limiting is not acceptable for control reasons, it may be necessary to employ control system redundancy. Redundant FCS comprises two or more systems that are functionally similar and normally operate in parallel. In the event of a system malfunction, the faulty equipment is isolated, leaving the remaining healthy system components to continue the augmentation task. In such systems, automatic fault containment can reduce the failure transient to an imperceptible level. It is then necessary to provide the pilot with information enabling him to continuously monitor the health of the FCS on an appropriate cockpit display.

8.3.3 Augmentation system architecture

The architecture of an inner-loop stability augmentation system is shown in figure 8.10. This classical system description assumes an aircraft with mechanical flying controls to which the EFCS connects via the servo-actuator. The system is typical of those applied to many aircraft of the 1950s and 1960s. For the purpose of discussion, only one control axis is shown in the figure, but it applies equally well to the remaining axes.

As previously stated, the essential element of the SAS is the control law; the remaining components are the necessary by-products of its implementation. Noise filtering is often required to remove unwanted information from sensor outputs. At best, noise can cause unnecessary actuator activity and, at worst, may even give rise to unwanted aircraft motion. Sometimes, when the sensor is located in a region of significant structural flexibility, the "noise" may be due to normal structure distortion. The control demand may then exacerbate structure bending to result in structural divergence. Thus an unwanted unstable

Copyright © 2025 Xiaowei He

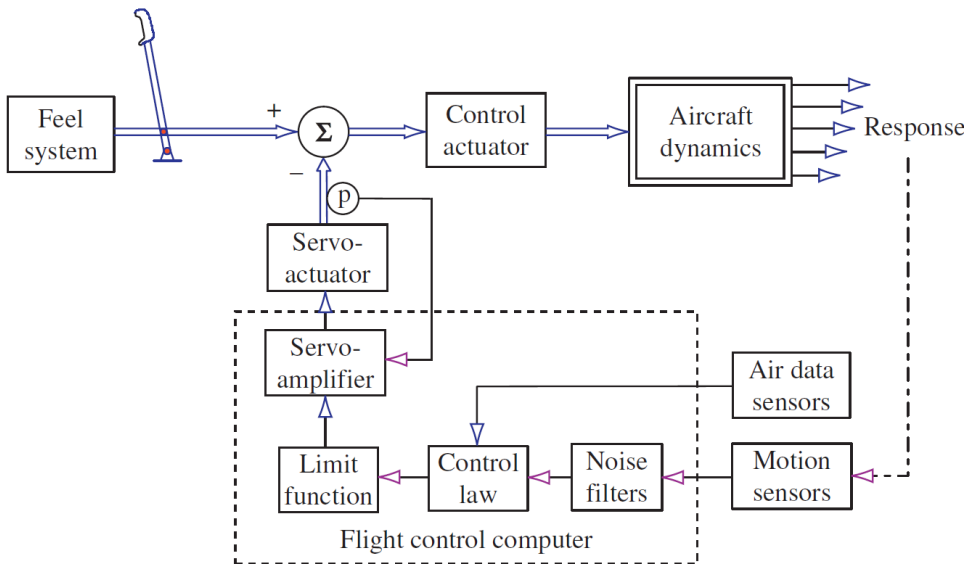

Figure 8.10: Typical stability augmentation system [1].

structural feedback loop can be created inadvertently. The cure usually involves narrow-band filtering to remove information from the sensor output signal at sensitive structural bending mode frequencies.

The fundamental role of the SAS is to minimize response transients following an upset from equilibrium. Therefore, when the system is working correctly in a non-maneuvering flight, the response variables have values at or near zero since the action of the negative feedback loop is to drive the error to zero. Thus an SAS does not normally require large authority control, and the limit function typically limits the amplitude of the control demand to, say, ±10% of the total surface deflection. The limiter may also incorporate a rate limit function to further contain transient response by imposing a maximum actuator slew rate demand. It is important to realize that whenever the control demand exceeds the limit, the system saturates, becoming temporarily open-loop, and the dynamics of the aircraft revert to those of the unaugmented airframe. This is not usually considered a problem because saturation is most likely to occur during maneuvering flight when the pilot has very "tight" manual control of the aircraft and effectively replaces the SAS control function.

The servo-amplifier, together with the servo-actuator, provides the interface between the flight control system and the mechanical flying controls. These two elements make up a classical position servo-mechanism as indicated by the electrical feedback from a position sensor on the output of the servo-actuator. Mechanical amplitude limiting may well be applied to the servo-actuator as well as, or instead of the electronic limits programmed into the flight control computer.

Since the main power control actuator, also a classical mechanical servo-mechanism, breaks the direct mechanical link between the pilot's controller and the control surface, the control feeling may bear little resemblance to the aerodynamic surface loads. The feedback loop around the control actuator is normally mechanical because it may well need to function with the SAS inoperative. It is therefore necessary to augment the controller feeling characteristics as well. The feel system may be a simple non-linear spring but is more commonly an electro-hydraulic device, often referred to as a *Q-feel system* since its characteristics are scheduled with dynamic pressure Q. Careful design of the feel system enables the apparent controls-free maneuver margin of the aircraft to be adjusted independently of the other interrelated stability parameters.

Copyright © 2025 Xiaowei He

When the mechanical flying controls are dispensed with altogether and replaced by an electrical or electronic link, the resultant stability augmentation system is described as a *fly-by-wire* (FBW) system. When the FCS shown in figure 8.10 is implemented as an FBW system, its functional structure is changed to that shown in figure 8.11. The SAS inner control loop remains unchanged; the only changes are related to the primary control path and the actuation systems.

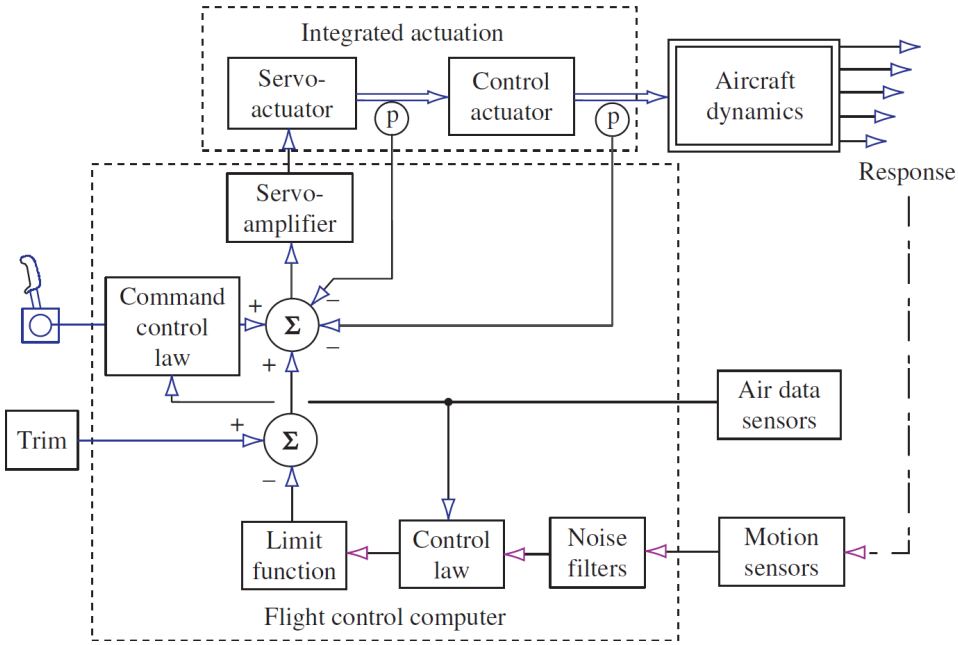

Figure 8.11: Typical fly-by-wire command and stability augmentation system [1].

Since the only mechanical elements in the FCS are the links between the control actuator and the surfaces, it is usual for the servo-actuator and the control actuator to be combined into one unit. Its input is then the electrical control demand from the flight control computer and its output is the control surface deflection. An advantage of an integrated actuation system is the facility for mechanical simplification, since the feedback loops may be closed electrically rather than by a combination of electrical and mechanical feedback. Mechanical feedback is an unnecessary complication because, in the event of a flight control computer failure, the aircraft becomes uncontrollable. This puts a rather more demanding emphasis on the safety of the flight control system.

Primary control originates at the pilot's control inceptors which, since they are not constrained by mechanical control linkages, may now take alternative forms — for example, a side-stick controller. The control command signal is conditioned by a command control law which determines the control and response characteristics of the augmented aircraft. Since the command control law effectively shapes the command signal in order to achieve acceptable response characteristics, its design is a means for augmenting handling qualities independently of stability augmentation. For this reason, an FCS with the addition of command path augmentation is known as a *command and stability augmentation system* (CSAS).

Provision is shown in figure 8.11 for an electrical trim function since not all aircraft with advanced technology FCS employ mechanical trimmers. The role of the trim function is to set the datum control signal value, and thus the control surface angle, to that required to maintain the chosen equilibrium flight condition. The precise trim function utilized is application-dependent, and in some cases, an entirely

Copyright © 2025 Xiaowei He

automatic trim system may be implemented. In this latter case, no pilot trimming facility is required.

The pilot must have full-authority control over the aircraft at all times, so it is implied that the actuation system must also have full-authority control. The implications for safety following a failure in any component in the primary control path are critical. As for the simple SAS, the feedback control signal may be authority-limited prior to summing with the primary control commands; this protects the system against failures within the stability augmentation function. However, this solution cannot be used in the primary control path. Consequently, FBW systems must have reliability of a very high order, which usually means significant levels of redundancy in the control system architecture together with sophisticated mechanisms for identifying and containing the worst effects of system malfunction.

In this brief description of an FBW system, it is assumed that all control signals are electrical and transmitted by normal electrical cables. However, since most modern flight control computers are digital, the transmission of control signals also involves digital technology. Digital signals can be transmitted optically with some advantage, especially in the demanding environment within aircraft. Today it is common for optical signal transmission to be used in FCSs if for no other reason than to maintain electrical isolation between redundant components within the system. There is no reason why optical signaling should not be used for primary flight control, and there are a number of optically signaled systems currently flying. Such a control system is referred to as a *fly-by-light* (FBL) system, and the control function is essentially the same as that of the FBW system or the simple stability augmentation system it replaces. It is most important to recognize that for a given aircraft, the stability augmentation function required of the flight control system is the same irrespective of the architecture adopted for its implementation. In the context of stability augmentation, there is nothing special or different in an FBW or in an FBL system solution.

8.3.4 Longitudinal stability augmentation

The choice of feedback variable is important in determining the nature of the change in the stability characteristics of the aircraft, since each variable results in a unique combination of changes Provided that the aircraft is equipped with the appropriate motion sensors, various feedback control schemes are possible; it then becomes necessary to choose the feedback variable(s) best suited to augment the deficiencies of the basic airframe. It is also useful to appreciate what effect each feedback variable has on the stability modes when assessing a flight control system design. However complex the functional structure of the system, the basic augmentation effect of each feedback variable does not change. Feedback is also used for reasons other than stability augmentation, for example, in autopilot functions. In such cases, augmentation also occurs and may not be desirable. If so, a thorough understanding of the effects of the most commonly used feedback variables is invaluable.

To evaluate the effect of feedback utilizing a particular response variable, it is instructive to conduct a survey of all single-loop feedback options. In every case, the feedback loop is reduced to a simple gain component only. By this means the possible intrusive effects of other loop components, such as noise filters, phase compensation filters, and sensor and actuator dynamics, are prevented from masking the true augmentation effects. The longitudinal stability augmentation options are summarised in figure 8.12, in which it is implied that a negative feedback loop may be closed between any of the motion variables and the elevator. Other loops may be closed between the motion variables and alternative longitudinal control motivators, or engine thrust control, for example, but these are not considered here.

The survey is conducted by taking each motion variable in turn and evaluating its influence on the closed-loop stability characteristics as a function of the loop gain K. The root locus plot is especially useful for this purpose since it enables simultaneous assessment of the relative influence on, and relative

Copyright © 2025 Xiaowei He

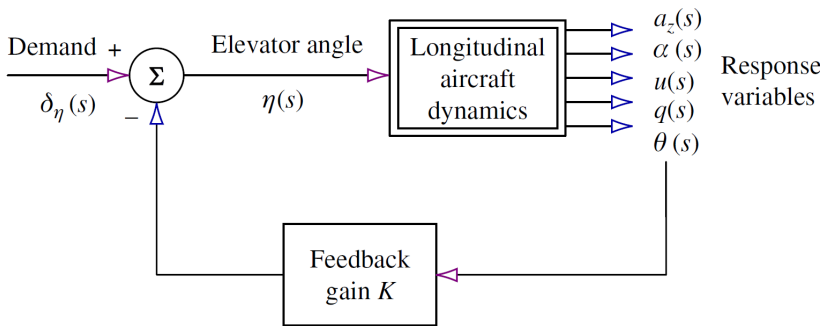

Figure 8.12: Longitudinal feedback options [1].

sensitivity of, each stability mode. As the detailed effect of feedback depends on the aircraft and flight condition of interest, it is not easy to generalize.

8.3.5 Lateral-directional stability augmentation

The lateral-directional stability augmentation options are summarised in figure 8.13, in which it is implied that a negative feedback loop may be closed between any of the motion variables and either the ailerons or the rudder. Other loops can be closed between the motion variables and alternative lateral-directional control motivators, but, again, these are not considered here.

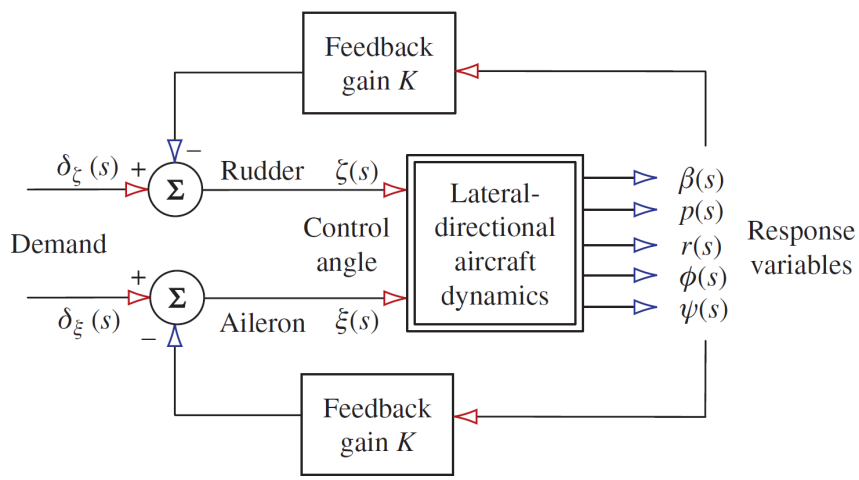

Figure 8.13: Lateral-directional feedback options [1].

The survey is conducted by taking each motion variable in turn and evaluating its influence on the closed-loop stability characteristics as a function of the loop gain K. The detailed effects of the lateral-directional feedback options are much more dependent on the aircraft and the flight condition than the longitudinal feedback options. Therefore, it is more difficult, and probably less appropriate, to generalize.

Copyright © 2025 Xiaowei He

References

[1] Cook, M. V., *Flight Dynamics Principles: A Linear Systems Approach to Aircraft Stability and Control*, 3rd ed., Butterworth-Heinemann, Waltham, MA, 2013.

[2] Meriam, J. L., and Kraige, L. G., *Engineering Mechanics: Dynamics*, 7th ed., Wiley, Hoboken, NJ, 2012.

[3] Smith, H., "Aircraft Flight Mechanics," , 2022. url https://aircraftflightmechanics.com.

[4] Anderson, J. D., *Fundamentals of Aerodynamics*, 6th ed., McGraw-Hill Education, New York, NY, 2017.

[5] Gerhart, A. L., Gerhart, P. M., and Hochstein, J. I., *Munson, Young, Okiishi's Fundamentals of Fluid Mechanics*, 9th ed., Wiley, Hoboken, NJ, 2021.

[6] Yechout, T. R., *Introduction to Aircraft Flight Mechanics*, 2nd ed., AIAA Educational Series, Reston, VA, 2014.

[7] Franklin, G. F., Powell, J. D., and Emami-Naeini, A., *Feedback Control of Dynamic Systems*, 6th ed., Pearson Higher Education, Upper Saddle River, NJ, 2009.

[8] Hopkin, H. R., "A Scheme of Notation and Nomenclature for Aircraft Dynamics and Associated Aerodynamics: Basic notation and nomenclature," Tech. rep., H. M. Stationery Office, 1970. Aeronautical Research Council, Reports and Memoranda No. 3562.

[9] Anderson, J. D., *Aircraft Performance and Design*, 1st ed., McGraw-Hill Education, New York, NY, 1998.

[10] Raymer, D. P., *Aircraft Design: A Conceptual Approach*, 5th ed., AIAA Educational Series, Reston, VA, 2012.

[11] Kermode, A. C., *Mechanics of Flight*, 11th ed., Pearson Education, Essex, England, 2006.

[12] FAA, *Airplane Flying Handbook (FAA-H-8083-3C)*, 1st ed., Skyhorse Publishing, New York, NY, 2021.

[13] Gates, S. B., and Lyon, H. M., "A continuation of longitudinal stability and control analysis: Part 1, general theory," Tech. rep., H. M. Stationery Office, 1944. Aeronautical Research Council, Reports and Memoranda No. 2027.

[14] Bryan, G. D., *Stability in Aviation*, MacMillan, London, 1911.

[15] Teper, G. L., "Aircraft stability and control data," Tech. rep., NASA, 1972. STI-176-1.

[16] Nise, N. S., *Control Systems Engineering*, 7th ed., Wiley, Hoboken, NJ, 2015.

Copyright © 2025 Xiaowei He